KU LEUVEN

ARENBERG DOCTORAL SCHOOL
Faculty of Engineering Science

Cardiorespiratory dynamics: algorithms and application to mental stress monitoring

Devy WIDJAJA

Dissertation presented in partial fulfillment of the requirements for the degree of Doctor in Engineering

April 2015

Cardiorespiratory dynamics: algorithms and application to mental stress monitoring

Devy WIDJAJA

Examination committee:
Prof. dr. ir. P. Van Houtte, chair
Prof. dr. ir. S. Van Huffel, supervisor
Prof. dr. ir. B. Puers
Prof. dr. O. Van den Bergh
Prof. dr. ir. M. Van Hulle
Prof. dr. ir. R. Bailón
(University of Zaragoza)
Dr. ir. L. Faes
(University of Trento)

Dissertation presented in partial fulfillment of the requirements for the degree of Doctor in Engineering

April 2015

© 2015 KU Leuven – Faculty of Engineering Science
Uitgegeven in eigen beheer, Devy WIDJAJA, Kasteelpark Arenberg 10, box 2446, B-3001 Heverlee (Belgium)

Alle rechten voorbehouden. Niets uit deze uitgave mag worden vermenigvuldigd en/of openbaar gemaakt worden door middel van druk, fotokopie, microfilm, elektronisch of op welke andere wijze ook zonder voorafgaande schriftelijke toestemming van de uitgever.

All rights reserved. No part of the publication may be reproduced in any form by print, photoprint, microfilm, electronic or any other means without written permission from the publisher.

Dankwoord

Ik schrijf niet graag dankwoorden. Niet dat ik dat al veel heb moeten doen, maar ik ben er niet zo goed in, denk ik. Het is zo persoonlijk en het valt me dan ook niet makkelijk om dit te schrijven. Maar een dankwoord *hoort* in een thesis - het is wellicht het meest gelezen stuk - dus ben ik maar gauw aan een lijstje met namen begonnen, vooral uit schrik mensen te vergeten. Dat is waarschijnlijk ook gebeurd, en bij deze alvast een sorry voor diegenen die ik over het hoofd zag. Toen ik mijn eerste lijst maakte, met meer dan 80 namen, merkte ik des te meer hoeveel mensen belangrijk zijn geweest om dit doctoraat tot een goed eind te brengen. Eerlijk gezegd, had ik 4,5 jaar geleden niet gedacht dat ik er ooit *klaar* voor zou zijn om mijn doctoraat te verdedigen, maar hier sta ik dan. En dat ik hier sta, is dankzij al die opgelijste namen, want, om het met een cliché te zeggen, een doctoraat schrijf je niet alleen. Niet enkel op wetenschappelijk vlak heb je steun nodig, ook op persoonlijk vlak heb je goede mensen naast je nodig om je te helpen ontspannen, maar ook om je te steunen tijdens moeilijkere tijden. En ik besef nu, hoe belangrijk het voor mezelf is om even de tijd te nemen om enkele mensen te bedanken die me op de een of andere manier hebben geholpen tijdens dit doctoraat.

Vooreerst wil ik mijn promotor, Prof. Sabine Van Huffel, bedanken. In de eerste plaats, bedankt om me warm te maken om aan een doctoraat te beginnen. Ik heb er lang over getwijfeld, maar heb er geen seconde spijt van gehad. Zonder jouw steun en vertrouwen stond ik hier nu niet. De Biomed-groep die je hebt opgebouwd is er één om trots op te zijn, waar er een goede sfeer heerst waar velen jaloers op zijn, mede dankzij de driejaarlijkse Biomed-etentjes bij jouw thuis. Bedankt ook voor de vrijheid die je me gaf om vaak op conferentie te gaan waardoor ik zelf samenwerkingen kon uitbouwen.

Verder wil ik ook graag Prof. Omer Van den Bergh bedanken die een belangrijke rol heeft gespeeld in de keuze van het onderwerp van mijn doctoraat door me wegwijs te maken in het debat rond *respiratory sinus arrhythmia* vlak na mijn master thesis. Ook aan de samenwerking met andere leden van je groep, Prof.

Ilse Van Diest en Dr. Elke Vlemincx, heb ik enorm veel gehad. Bedankt, Ilse en Elke, om zonder problemen jullie data te delen met mij, om steeds klaar te staan om mijn resultaten te bespreken en om zo vaak op het laatste nippertje papers na te lezen voor submissie naar congressen of tijdschriften.

Dank ook aan Prof. Bob Puers en Prof. Marc Van Hulle om in mijn begeleidingscommissie te zetelen doorheen mijn doctoraat alsook deel uit te maken van mijn jury. Prof. Raquel Bailón, though we haven't collaborated, I am very happy you accepted the invitation to be in my examination committee as our fields of research are closely related. I highly appreciate the valuable feedback I received from you during my preliminary defense. Thanks also to Dr. Luca Faes for the nice collaboration we started over one year ago. You have supported me greatly in the last part of my PhD and thanks to your constructive feedback and answers to my many questions, I believe we conducted nice research together. Therefore, I am really happy and grateful that you are also part of my examination committee. Bedankt ook aan Prof. Paul Van Houtte om mijn doctoraatsverdedigingen voor te zitten.

Vervolgens wil ik Prof. André Aubert ook enorm bedanken om me de kans te geven om deel uit te maken van het project rond paraboolvluchten. Dat was werkelijk een unieke ervaring die me altijd zal bijblijven, en ook de reisjes naar Bordeaux zal ik me nog lang herinneren. Ook jouw hulp bij het schrijven van papers heb ik enorm geapprecieerd. Also, Prof. Daniele Marinazzo, Alessandro Montalto and Dr. Michele Orini, deserve a word of gratitude for the nice and fruitful collaborations.

Ook zou ik graag het Agenschap voor Innovatie door Wetenschap en Technology (IWT) bedanken voor de financiële steun gedurende vier jaar. I would also like to thank Zonta International for awarding me the Amelia Earhart Fellowship. Bedankt ook aan Ida, Elsy, John, Wim, Mimi, Liesbeth en Maarten voor de uitstekende administratieve, financiële en ICT omkadering.

Thanks to everyone who ever was or still is part of the Biomed group since I started my PhD: Aileen, Adrian, Alexander, Amir, Anca, Ben, Bharath, Bogdan, Bori, Carolina, Diana, Dzemila, Griet, Ivan, Jan, Joachim, Katrien, Kirsten, Kris, Laure, Lieven, Maarten, Maria Isabel, Milica, Nico, Nicolas, Ninah, Otto, Rob, Rosy, Steven, Thomas, Tim, Vanya, Vladimir, Wang, Wout and Yipeng. Thank you all for making Biomed such a fun place to work at. Thanks to many of you with whom I had the chance to go on conferences; we always made the perfect combination between work and fun. Nogmaals bedankt, Joachim en Steven, voor de goede master thesis begeleiding waardoor ik geïnteresseerd raakte in onderzoek. Ook de samenwerkingen achteraf verliepen steeds vlotjes. Ook bedankt, Katrien, voor de leuke babbels en etentjes. En natuurlijk ook mijn koffiemaatje, Kirsten! Ik moet zeggen dat ik onze koffiepauzes wel enorm

heb gemist de laatste maanden, maar dat hebben we toch al deels goedgemaakt tijdens de etentjes, en die traditie zullen we zeker voortzetten. En nu het doctoraat achter de rug is, zal ik ook eens werk maken van die langbeloofde (2 jaar zeker?) uitnodiging om te komen eten. A special thanks also to Milica, my office mate from the start until the end of my PhD. Milica, thanks for listening, the fun talks in the office (and sorry to our neighbours if we made too much noise) and all the best in the future.

Ook veel van de collega's buiten Biomed verdienen het om in dit lijstje te staan. Hierbij wil ik expliciet Marc, Nico, Arnaud en Wouter bedanken voor de goede samenwerking voor de oefenzittingen van 'Systeemtheorie en Regeltechniek'. Marc, nog een dikke merci om steeds in te springen als ik om de een of andere reden geen oefenzitting kon geven.

Dan zijn er nog alle vrienden en familie die me vooral op persoonlijk vlak hebben gesteund en hebben gezorgd voor de nodige ontspanning, maar ook klaarstonden om mij doctoraatsgerelateerde frustraties te laten ventileren. Daarbij wil ik in de eerste plaats iedereen van de 'bende' bedanken: Elisabeth, Felix, Manu, Heleen, Olivier, Stephanie, Anneke, Siegfried, Thomas, Sophie en Patje. De leuke samenkomsten in de vorm van etentjes, wijnproeverijen, (wijn)reisjes, filmavonden, kwissen (en nog zo veel meer) waren steeds fijne momenten die voor ontspanning zorgden. Stéphane en Katrien, bedankt voor jullie steun en toeverlaat, zeker de laatste maanden. Convento is als een tweede thuis in Leuven geworden. Een aanrader trouwens voor iedereen uit het Leuvense (en ver daarbuiten) die dit leest ;)

Ook mijn dansvrienden zou ik graag bedanken, zowel de danseressen en danser van de 'oude' als 'nieuwe' dansschool. Jullie beseffen niet half hoezeer de danslessen mij hebben geholpen om mijn gedachten te verzetten, zeker na lange dagen op bureau met races tegen de klok. En dat is voor een groot stuk danzij de leuke sfeer die jullie brachten, tijdens en na de lessen. Ik hoop dat we samen nog vele jaren kunnen dansen.

Bedankt ook aan familie De Praetere–De Backere voor de leuke familie-etentjes en -reisjes. Marie-Ange, een hele dikke merci om voor ons te zorgen in drukke tijden.

Tenslotte wil ik dit doctoraat ook opdragen aan mama en papa. Jullie hebben me steeds alle kansen gegeven, gesteund en ook aangemoedigd om aan dit doctoraat te beginnen. De toewijding om ergens ten volle voor te gaan heb ik zeker van jullie geleerd. Jullie onvoorwaardelijk geloof en vertrouwen in mij lijkt zo normaal, maar daarom niet minder gewaardeerd! Het zijn geen makkelijke jaren geweest, maar samen met Marsha en mijn lievelingstantes Ay Ling en Siu Ling hebben we ons er wel doorgeslaan. Dank ook voor jullie steun en

hulp tijdens moeilijkere momenten, maar ook voor de talrijke gezellige en zeer smakelijke etentjes.

En dan rest mij nog maar één iemand te bedanken. Tom, bedankt om er steeds voor mij te zijn, me zo veel vertrouwen te geven, zo goed voor mij te zorgen en me te steunen in alles wat ik doe. Bedankt voor zo veel meer dan ik hier kan opsommen. Ik kijk echt uit naar onze toekomst samen, wat die ook mag brengen!

Devy
Maart 2015

Abstract

The rate at which our heart beats, is a dynamical process enabling adaptive changes according to the demands of our body. These variations in heart rate are widely studied in so-called heart rate variability (HRV) analyses, as they contain much information about the activity of our autonomic nervous system. Variability in the heart rate arises from several processes, such as thermoregulation, hormones, arterial blood pressure, respiration, etc. One of the main short-term modulators of the heart rate is respiration. This phenomenon is called respiratory sinus arrhythmia (RSA) and comprises the rhythmic fluctuation of the heart rate at respiratory frequency. It has also widely been used as an index of vagal outflow. However, this has been widely debated as some studies have shown that the magnitude of RSA changes with respiratory rate and the depth of breathing, independently of parasympathetic activity. It is therefore questioned whether RSA represents a true index of vagal outflow. The lack of consensus on the precise mechanisms that are responsible for this cardiorespiratory interaction, lead to interpretational problems. It is nevertheless apparent that it is important to include information of respiration when interpretations of HRV studies are conducted. Inspired by the polemic nature of this debate on the interpretation of RSA, this dissertation focuses on three topics.

The first part of the thesis deals with the development of a surrogate respiratory signal based on ECG recordings. This is termed ECG-derived respiration (EDR). It is an important topic to cope retrospectively with possible confounding respiratory parameters in HRV studies without separate respiratory recordings. Additionally, with the trend towards less obtrusive and more cost-efficient monitoring, the possibility to obtain reliable EDR signals would discard the need to separately record respiration using specialized equipment, that often also interferes with natural breathing. In this dissertation, a new algorithm is proposed for single lead ECGs and compared with state-of-the-art EDR methods.

The second focus of the thesis is closely related to the interpretational problems concerning RSA and cardiac vagal activity. As such, the aim is to separate the tachogram in two components: one that is strictly related to respiration, and another component that is unrelated to respiration. Several methods to realize this separation have been proposed in the literature, and an extensive comparison is conducted in this thesis. Additionally, a separation method based on partial time-frequency analyses is discussed. It has the advantage over other methods that it can deal with nonstationary signals.

The last part of this dissertation focuses on the characterization of common dynamics in HRV and respiration. It is well-known that the interactions that play in the cardiorespiratory system are complex. Although the common dynamics have been studied in the literature using techniques like synchronization, symbolic dynamics and coupled oscillators, the precise mechanisms are still unclear. Therefore, we aim to characterize the common dynamics in a different way in order to gain more insight in the underlying cardiorespiratory mechanisms and their interpretation. In particular, information-theoretic measures that quantify the information storage and internal information of HRV, and the information transfer and cross information from respiration to HRV are discussed.

Throughout this dissertation, special attention is also paid to the application of mental stress monitoring. It has been found that persons who are chronically stressed, have an increased risk for cardiovascular diseases. Also breathing plays an important role, as research suggests that respiration can be used as an interface to deal with negative effects of mental stress, and thus alter cardiac autonomic activity. This makes mental stress an interesting application on which the impact of the last two topics is evaluated.

Samenvatting

De snelheid waarmee ons hart klopt, is een dynamisch proces dat verandert afhankelijk van de eisen van ons lichaam. Deze variaties in hartritme worden doorgaans onderzocht in zogenaamde analyses van hartritmevariabiliteit (HRV) omdat ze veel informatie over de activiteit van ons autonome zenuwstelsel bevatten. Variabiliteit in het hartritme is het resultaat van verschillende processen zoals thermoregulatie, hormonen, bloeddruk, ademhaling, etc. Eén van de belangrijkste kortetermijnmodulatoren van het hartritme is de ademhaling. Dit verschijnsel heet *respiratory sinus arrhythmia* (RSA) en omvat de ritmische fluctuatie van het hartritme in fase met de ademhaling. RSA wordt vaak gebruikt als een index van vagale controle. Deze notie ligt echter onder vuur aangezien onderzoeken hebben aangetoond dat de mate van RSA afhankelijk is van de frequentie en diepte van ademen, onafhankelijk van parasympathische activiteit. Het is dan ook maar de vraag of RSA een ware index van vagale controle is. Het gebrek aan consensus over de precieze mechanismen die verantwoordelijk zijn voor deze cardiorespiratoire interactie, leiden tot problemen in de interpretatie van RSA. Het is desalniettemin duidelijk dat het belangrijk is om informatie van de ademhaling in rekening te brengen wanneer HRV studies worden geïnterpreteerd. Geïnspireerd door dit debat over de interpretatie van RSA, richt dit proefschrift zich op drie grote onderwerpen.

Het eerste deel van dit proefschrift handelt over de ontwikkeling van een surrogaat ademhalingssignaal op basis van ECG metingen. Dit wordt *ECG-derived respiration* (EDR) genoemd en is een belangrijk onderwerp om retrospectief om te gaan met mogelijke verstorende ademhalingsparameters in HRV studies zonder dat afzonderlijke ademhalingsmetingen beschikbaar zijn. Rekening houdend met de trend naar minder invasieve en meer kostenefficiënte monitoring, zou de mogelijkheid om betrouwbare EDR signalen te verkrijgen, de nood om de ademhaling afzonderlijk te registreren, overbodig maken. Bovendien interfereert de apparatuur om de ademhaling op te meten vaak met de natuurlijke ademhaling. In dit proefschrift wordt een nieuw algoritme voorgesteld voor éénkanaals ECG's en vergeleken met state-of-the-art EDR methoden.

De tweede focus van het proefschrift is nauw gerelateerd aan de polemiek rond de interpretatie van RSA en cardiale vagale activiteit. Als zodanig wordt beoogd het tachogram te scheiden in twee componenten: één die strikt gerelateerd is aan de ademhaling, en een ander die geen verband heeft met ademhaling. Verschillende methoden om deze opsplitsing te realiseren zijn besproken in de literatuur en een uitgebreide vergelijking wordt uitgevoerd in dit proefschrift. Bovendien wordt een opsplitsingsmethode op basis van partiële tijd-frequentieanalyses besproken, die als voordeel heeft dat ze kan omgaan met niet-stationaire signalen.

Het laatste deel van dit proefschrift richt zich op de karakterisering van de gemeenschappelijke dynamica in HRV en de ademhaling. Het is bekend dat de interacties in het cardiorespiratoire systeem complex zijn. Hoewel de gemeenschappelijke dynamica in de literatuur reeds bestudeerd werd aan de hand van technieken zoals synchronisatie, symbolische dynamica en gekoppelde oscillatoren, zijn de precieze mechanismen nog onduidelijk. Daarom streven wij ernaar om de gemeenschappelijke dynamica te karakteriseren op een andere manier om meer inzicht te krijgen in de onderliggende cardiorespiratoire mechanismen en hun interpretatie. Met name informatie-theoretische maten die de informatie-opslag en interne informatie van HRV, en de informatie-overdracht en kruisinformatie van de ademhaling naar HRV kwantificeren, worden besproken.

Doorheen dit proefschrift wordt speciale aandacht besteed aan de toepassing van mentale stress monitoring. Het is gebleken dat personen die chronisch gestresst zijn een verhoogd risico hebben op cardiovasculaire aandoeningen. Ook ademhaling speelt hierbij een belangrijke rol aangezien onderzoek suggereert dat ademhaling kan worden gebruikt als interface om om te gaan met negatieve effecten van stress en dus om de cardiale autonome activiteit te veranderen. Dit maakt mentale stress een interessante toepassing waarop de invloed van de laatste twee onderwerpen wordt geëvalueerd.

Nomenclature

Symbols and basic operations

$a, b, \ldots$	Scalars
$\mathbf{a}, \mathbf{b}, \ldots$	Vectors
$\mathbf{A}, \mathbf{B}, \ldots$	Matrices
$\Im$	Imaginary part
$\Re$	Real part
$\sum$	Sum
$\mathbf{A}^T$	Transpose of matrix $\mathbf{A}$
x^*	Complex conjugate of x
f_s	Sampling frequency
f_{RSP}	Respiratory frequency
V_T	Tidal volume

Metrics

bpm	beats-per-minute
cpm	cycles-per-minute
h	hour
Hz	Hertz
l	liter
m	meter
min	minute
ml	milliliter
mmHg	millimeter mercury
ms	milliseconds
mV	millivolt
s	seconds

Abbreviations

AB	Abdomen
ANCOVA	Analysis of covariance
ANS	Autonomic nervous system
ARD	Automatic relevance determination
ARMAX	Autoregressive moving average with exogenous inputs
AT	Attention task
AUC	Area under the curve
AV	Atrio-ventricular
BPRSA	Bivariate phase-rectified signal averaging
CNS	Central nervous system
CO	Cardiac output

CVD	Cardiovascular disease
CVS	Cardiovascular system
DAP	Diastolic arterial pressure
DRG	Dorsal respiratory group
ECG	Electrocardiogram
EDR	ECG-derived respiration
EDR_{eig}	EDR signal based on the kPCA algorithm, using an RBF kernel, with σ^2 optimized according to the eigenvalue criterion
EDR_{ent}	EDR signal based on the kPCA algorithm, using an RBF kernel, with σ^2 optimized according to the entropy criterion
EDR_{kPCA}	EDR signal based on the kPCA algorithm, using an RBF kernel, with σ^2 optimized according to the entropy criterion
EDR_{PCA}	EDR signal based on the PCA algorithm
EDR_{RA}	EDR signal based on the R peak amplitude
EDR_{RBF}	EDR signal based on the kPCA algorithm, using an RBF kernel, with σ^2 chosen according to a rule-of-thumb
FFT	Fast Fourier transform
FIR	Finite impulse response
HF	High frequencies
HR	Heart rate
HRV	Heart rate variability
ICA	Independent component analysis
kPCA	Kernel principal component analysis
LF	Low frequencies
LMS	Least-mean squares
LS-SVM	Least-squares support vector machines
MAP	Mean arterial pressure

MSE	Mean-squared error
MSPCA	Multiscale principal component analysis
MT1	First mental arithmetic task
MT2	Second mental arithmetic task
NN	normal-to-normal
NPV	Negative predictive value
NRMSE	Normalized root-mean-squared error
nu	Normalized units
OSP	Orthogonal subspace projection
PCA	Principal component analysis
PNS	Peripheral nervous system
PP	Pulse pressure
PPG	Photoplethysmography
PPV	Positive predictive value
PRG	Pontine respiratory group
PRSA	Phase-rectified signal averaging
PSD	Power spectral density
PSG	Polysomnography
RBF	Radial basis function
RC	Ribcage
RD	Relaxing documentary watching
RIP	Respiratory inductive plethysmography
ROC	Receiver operating characteristic
RP	Recovery period
RR	RR interval series
RR_{orig}	Original tachogram

RR_{res}	Residual tachogram
RR_{RSP}	Respiratory component of the tachogram
RSA	Respiratory sinus arrhythmia
RSP	Respiratory signal
RSP_{AB}	Respiratory signal derived from the abdominal effort
RSP_{ref}	Reference respiratory signal
RSP_{TH}	Respiratory signal derived from the thoracic effort
S^{+}	Sensitivity
S^{-}	Specificity
SA	Sino-atrial
SAP	Systolic arterial pressure
SE	Squared error
SNR	Signal-to-noise ratio
SNS	Somatic nervous system
SV	Stroke volume
TF	Time-frequency
TFD	Time-frequency distribution
TFPD	Time-frequency phase difference
TP	Total power
TPR	Total peripheral resistance
ULF	Ultra low frequencies
VAR	Vector autoregressive
VLF	Very low frequencies
VRG	Ventral respiratory group
WHO	World health organization

Contents

Dankwoord i

Abstract v

Samenvatting vii

Nomenclature xiii

Contents xv

List of Figures xxi

1 Introduction 1

1.1 Physiological background 1

1.1.1 Nervous system 2

1.1.2 Cardiovascular system 5

1.1.3 Respiratory system 11

1.1.4 Heart rate variability 12

1.1.5 Respiratory sinus arrhythmia 16

1.2 Aims of the thesis 19

1.3 Application: mental stress monitoring 20

1.3.1 Problem statement 20
1.3.2 Data acquisition and experimental protocol 21
1.3.3 Main findings from previous research 23
1.4 Chapter-by-chapter overview 25
1.5 Collaborations 27
1.6 Personal contributions 28
1.7 Conclusion 31

2 Kernel principal component analysis for single lead ECG-derived respiration 33

2.1 Introduction 34
2.2 Methods 35
2.2.1 Data 35
2.2.2 (Kernel) principal component analysis 36
2.2.3 R peak amplitude 41
2.2.4 Comparison of EDR methods 42
2.2.5 Statistical analysis 43
2.3 Results 43
2.3.1 Comparison of EDR signals using different kernel functions 43
2.3.2 Comparison of EDR signals using kPCA, linear PCA and R peak amplitude 44
2.4 Discussion 46
2.4.1 ECG feature selection 46
2.4.2 Selection of σ^2 48
2.4.3 Performance of kernel PCA as EDR algorithm 48
2.4.4 Computational effort 50
2.4.5 Failure of EDR algorithms 50
2.4.6 Other EDR methods 51

2.5 Conclusion 51

3 Separation of respiratory influences from the tachogram 53

3.1 Introduction 54

3.2 Separation algorithms 55

3.2.1 Adaptive filtering 55

3.2.2 Independent component analysis 57

3.2.3 ARMAX model 57

3.2.4 Multiscale principal component analysis 59

3.2.5 Orthogonal subspace projection 60

3.3 Comparison study 61

3.3.1 Data 61

3.3.2 Simulation study 62

3.3.3 Stability study 65

3.3.4 Discussion 70

3.4 Real-life example: mental stress classification 74

3.4.1 Data aquisition and preprocessing 74

3.4.2 Classifier design 74

3.4.3 Results 75

3.4.4 Discussion 79

3.5 Conclusion 80

4 Separation of the tachogram using partial time-frequency analyses 81

4.1 Introduction 82

4.2 Time-frequency analysis 83

4.2.1 Cross time-frequency analysis 83

4.2.2 Partial time-frequency analysis 84

4.3 Simulation study 84

4.3.1 Setup 84
4.3.2 Results 86
4.3.3 Discussion 87
4.4 Application: mental stress monitoring 88
4.4.1 Data and methods 88
4.4.2 Results 90
4.4.3 Discussion 98
4.5 Methodological comments 101
4.6 Conclusion 101

5 Information dynamics in cardiorespiratory time series 103

5.1 Introduction 103
5.2 Methods 106
5.2.1 Information-theoretic measures 106
5.2.2 Entropy estimation 108
5.3 Comparison of information-theoretic measures during controlled breathing 110
5.3.1 Data acquisition and preprocessing 111
5.3.2 Results 112
5.3.3 Discussion 113
5.4 Application: mental stress monitoring 116
5.4.1 Data and methods 116
5.4.2 Results 117
5.4.3 Discussion 119
5.5 Conclusion 124

6 Separation of the tachogram: sensitivity to the respiratory signal 127

6.1 Introduction 128

6.2 Methodology 129
6.2.1 Data acquisition and preprocessing 129
6.2.2 ECG-derived respiration 129
6.2.3 Separation of the tachogram 130
6.2.4 Sensitivity to the type of respiratory signal 131
6.3 Results and discussion 132
6.4 Conclusion 134

7 Conclusions and future work **137**
7.1 Conclusions of the thesis 137
7.1.1 Mathematical techniques 138
7.1.2 Mental stress monitoring 139
7.2 Future work 141
7.2.1 Surrogate respiratory signals 141
7.2.2 Separation of the tachogram 142
7.2.3 Physiological interpretation 142
7.2.4 Time-varying techniques 143
7.2.5 New applications 143
7.2.6 Heart-respiration-brain interactions 143
7.2.7 Mental stress 144

Bibliography **145**

Curriculum vitae **169**

Publication list **171**

List of Figures

1.1 A lateral view of the brain. From [84]. 3

1.2 A schematic overview of the organization of the nervous system. From [170]. 4

1.3 Sympathetic and parasympathetic pathways of the autonomic nervous system. From [170]. 6

1.4 A schematic overview of the cardiovascular system. Oxygenated blood is given in red, deoxygenated blood in blue. From [83]. . 7

1.5 Electrical activity in the heart that generates an electrocardiogram. From [170]. 9

1.6 Electrocardiogram and its tachogram. 13

1.7 Power spectral density of tachogram of 30 minutes, with indication of VLF, LF and HF bands and their corresponding powers. 16

1.8 Tachogram and simultaneously recorded respiration. 17

1.9 Tachogram and simultaneously recorded respiration of one subject during mental stress monitoring. 24

1.10 Chapter-by-chapter overview. 26

2.1 Toy example showing the idea of kernel PCA. 37

2.2 Structure of input matrix $\mathbf{X}$. 38

2.3 Entropy e of the kernel matrix for two values for σ^2. 40

2.4 Eigenvalues of the kernel matrix for two values for σ^2. 41

2.5 EDR signals of subject `f1y07` ($EDR_{poly(d=2)}$, $EDR_{poly(d=3)}$, EDR_{RBF}), PSD of RSP_{ref} and magnitude squared coherence of the EDR signals and RSP_{ref}. 45

2.6 Correlation and magnitude squared coherence coefficients between $EDR_{poly(d=2)}$, $EDR_{poly(d=3)}$, EDR_{RBF} and RSP_{ref}. . . . 46

2.7 EDR signals of subject `f1y07` (EDR_{eig}, EDR_{ent}, EDR_{PCA}, EDR_{RA}), PSD of RSP_{ref} and magnitude squared coherence of the EDR signals and RSP_{ref}. 47

2.8 Demonstration of the selection criteria for choosing a suitable σ^2 for the RBF kernel. 48

2.9 Correlation and magnitude squared coherence coefficients between EDR_{ent}, EDR_{eig}, EDR_{PCA}, EDR_{RA} and RSP_{ref}. 49

3.1 Scheme of the LMS adaptive filtering to separate respiratory influences from the tachogram. 56

3.2 Application of MSPCA to extract the respiratory component from the tachogram. 60

3.3 Block diagram of the simulation study. 64

3.4 Example of the simulation study of a typical subject using the ARMAX model and OSP. 66

3.5 Boxplots of the normalized root-mean-squared errors (NRMSE) of the simulation study. 67

3.6 Boxplots of the squared errors (SE) in LF and HF power of the simulation study. 67

3.7 Block diagram of the stability study. 69

3.8 Boxplots of the normalized root mean-squared errors (NRMSE), the squared errors (SE) in LF and HF power of the stability study in the residual tachogram. 70

3.9 Example of the stability study using OSP. 71

3.10 Mean ROC of all classifiers. 77

3.11 The importance of $LFnu_{res} = LF_{res}/TP_{res}$ in the classification of rest and stress is shown: LF_{res} versus TP_{res}. 78

3.12 Power spectral densities of the original and residual tachograms during rest and mental stress. 78

4.1 Time-frequency spectra of signals $x_1(t)$, $x_2(t)$ and $x(t)$ of simulation study 1. 85

4.2 Time-frequency spectra of signals $x_1(t)$, $x_2(t)$ and $x(t)$ of simulation study 2. 85

4.3 Averaged results of simulation studies 1 and 2. In the ideal case, the partial spectrum $\overline{S_{xx/2}}(t,f)$ equals $S_{11}(t,f)$. 86

4.4 Averaged instantaneous power of the two spectral components of $x_1(t)$ in simulation study 2 of $S_{11}(t,f)$, $S_{xx}(t,f)$ and $S_{xx/2}(t,f)$. 86

4.5 Example of RR interval series, respiratory signal, their TF spectra $(S_{RR-RR}(t,f), S_{RSP-RSP}(t,f))$, coherence $(\gamma_{RR-RSP}(t,f))$, and partial TF spectra $(S_{RR-RR,RSP}(t,f), S_{RR-RR/RSP}(t,f))$ during documentary watching. 91

4.6 Example of RR interval series, respiratory signal, their TF spectra $(S_{RR-RR}(t,f), S_{RSP-RSP}(t,f))$, coherence $(\gamma_{RR-RSP}(t,f))$, and partial TF spectra $(S_{RR-RR,RSP}(t,f), S_{RR-RR/RSP}(t,f))$ during the first mental stress task. 92

4.7 Median instantaneous respiratory frequency $(f_{RSP}(t))$, heart rate $(HR(t))$, coherence $(\gamma^{\beta_{RSP}}_{RR-RSP}(t))$ and phase difference $(\Theta^{\beta_{RSP}}_{RR-RSP}(t))$ in the time-varying band $\beta_{RSP}(t)$. 94

4.8 Median instantaneous power for TF spectra $S_{RR-RR}(t,f)$, $S_{RR-RR,RSP}(t,f)$ and $S_{RR-RR/RSP}(t,f)$ in the total frequency band. 95

4.9 Median instantaneous power for TF spectra $S_{RR-RR}(t,f)$, $S_{RR-RR,RSP}(t,f)$ and $S_{RR-RR/RSP}(t,f)$ in the LF band. . . . 96

4.10 Median instantaneous power for TF spectra $S_{RR-RR}(t,f)$, $S_{RR-RR,RSP}(t,f)$ and $S_{RR-RR/RSP}(t,f)$ in the HF band. . . . 97

4.11 Median instantaneous frequency for TF spectra $S_{RR-RR}(t,f)$ and $S_{RR-RR,RSP}(t,f)$ in the HF band. 98

5.1 Graphical interpretation of information-theoretic measures. . . 107

5.2 Boxplot of the predictive information P_{RR} during spontaneous breathing, breathing at 12 and 6 cpm with i/e ratios of 0.42 and 2.33. 113

5.3 Boxplot of the transfer entropy $T_{RSP\rightarrow RR}$ and self-entropy S_{RR} during spontaneous breathing and breathing at 12 and 6 cpm with i/e ratios of 0.42 and 2.33. 114

5.4 Boxplot of the cross-entropy $C_{RSP\rightarrow RR}$ and conditional self-entropy $S_{RR|RSP}$ during spontaneous breathing and breathing at 12 and 6 cpm with i/e ratios of 0.42 and 2.33. 114

5.5 Bar graphs indicating the percentage of significant information-theoretic measures and the percentage of significant nonlinearities, during relaxing documentary watching (RD), sustained attention (AT) and the mental stress tasks (MT1 and MT2). 118

5.6 Boxplots of information-theoretic measures P_{RR}, $T_{RSP\rightarrow RR}$, S_{RR}, $C_{RSP\rightarrow RR}$ and $S_{RR|RSP}$, estimated using the nonlinear model-free approach, during relaxing documentary watching (RD), sustained attention (AT) and the mental stress tasks (MT1 and MT2). 120

5.7 Boxplots of mean information-theoretic measures P_{RR}, $T_{RSP\rightarrow RR}$, S_{RR}, $C_{RSP\rightarrow RR}$ and $S_{RR|RSP}$, estimated using the model-free approach using the linear surrogates as input, during relaxing documentary watching (RD), sustained attention (AT) and the mental stress tasks (MT1 and MT2). 120

6.1 Respiratory signals: the reference respiratory signal (RSP_{ref}), thoracic (RSP_{TH}) and abdominal effort (RSP_{AB}), ECG-derived respiratory signals based on the R peak amplitude (EDR_{RA}), PCA (EDR_{PCA}) and kPCA (EDR_{kPCA}). 130

6.2 Boxplots of the results; (a) cross-entropy from RSP_{ref} to RR_{orig}; (b) mean magnitude squared coherence between RSP_{ref} and the other types of respiratory signals; and (c) cross-entropy from RSP_{ref} to RR_{res}^{type} obtained using ARMAX and OSP. 133

Chapter 1

Introduction

This chapter aims to introduce some basic physiological principles of the cardiovascular and respiratory system to the reader. Therefore, in Section 1.1, some background material on the human physiology is given, leading to the aims of this dissertation, which are formulated in Section 1.2. Throughout the thesis, several methodologies are tested on one specific application, i.e. mental stress testing. Information on the interest in this application, the data acquisition and results obtained prior to this thesis, is provided in Section 1.3. The structure of this dissertation is outlined in Section 1.4, and collaborations and personal contributions discussed in respectively Section 1.5 and Section 1.6. Finally, some conclusions are provided in Section 1.7.

1.1 Physiological background

Cardiovascular disease (CVD) is the leading cause of death worldwide. According to the World Health Organization (WHO), 17.3 million people died from CVDs in 2008, corresponding to 30% of all global deaths [222]. In Europe, CVDs are responsible for over 4 million deaths per year, accounting for 42% and 51% of all deaths in respectively men and women. For comparison, all cancers contribute for 23% and 19% to all deaths in men and women [127]. In order to prevent and treat this health concern, it is important to identify and understand the risk factors for CVD [185]. Therefore, in the following paragraphs the basic principles of the human physiology, more specifically of the cardiovascular system (CVS), are discussed. Also, the respiratory system will be addressed as this thesis aims at studying the dynamics between these two interacting

systems. Then, the concepts of heart rate variability (HRV) and respiratory sinus arrhythmia (RSA) are introduced, leading to the aims of this thesis.

The physiological introduction is mainly based on [141] and [170].

1.1.1 Nervous system

The nervous system consists of two closely interacting systems, specialized for the reception, integration and transmission of information. On the one hand, the brain and spinal cord constitute the central nervous system (CNS), and on the other hand, the sensory and motor nerve fibres that enter and leave the CNS or are completely outside the CNS form the peripheral nervous system (PNS). The cells of the nervous system comprise neurons, of which there are 10^{11} that are specialized for the rapid transmission of signals, and glial cells or neuroglia of which there are 10^{12} that nourish and protect the neurons. The nerve fibres of these cells run in the white matter of the CNS or along peripheral nerves. Groups of these nerve fibres that run in a common direction form a compact bundle (nerve, tract, pathway). Neurons can be classified as either motor, sensory, or interneurons. Information is carried from the CNS to organs, glands, and muscles by motor or efferent neurons. Sensory or afferent neurons transmit information from internal organs or from external stimuli to the CNS. Interneurons relay signals between motor and sensory neurons.

Central nervous system

The CNS is the processing unit of the nervous system that receives information from the PNS, processes this and sends information to the PNS. The CNS consists of the brain, which lies within the skull, and the spinal cord, which lies within the vertebral column. Fig. 1.1 shows the brainstem, the cerebellum, the diencephalon and cerebrum, which all together compose the brain. The brainstem links the spinal cord and the cerebrum and is composed of the medulla oblongata, pons and the midbrain. The cerebellum is attached to the brainstem. The diencephalon consists of the thalamus, subthalamus and hypothalamus. The cerebrum comprises the right and left cerebral hemispheres, which are connected by the corpus callosum.

The spinal cord has a segmental structure with dorsal and ventral roots. The dorsal roots carry information into the spinal cord from peripheral receptors, while the ventral roots carry information out to muscles and glands. In cross-section, the spinal cord has a butterfly-shaped area of grey matter and a surrounding zone of white matter. The grey matter comprises sensory and

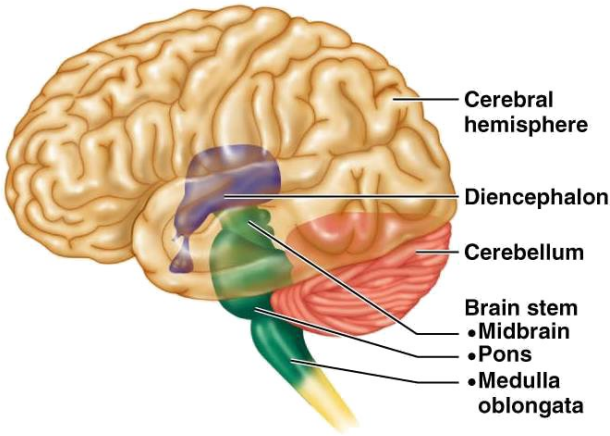


Figure 1.1: A lateral view of the brain. From [84].

motor nuclei. In the ventral horn lie the cell bodies of motor neurons that send efferent signals to muscles and glands; in the dorsal horn lie cell bodies of interneurons dealing with the processing of signals that enter in the dorsal root axons. The white matter of the spinal cord consists of tracts of axons that transmit information to and from the brain. Ascending tracts of white matter carry sensory information from the body to the brain, and descending tracts send efferent signals from the brain to the rest of the body.

Peripheral nervous system

The peripheral nervous system consists of afferent and efferent (motor) neurons. These efferent neurons can further be classified according to their targets; the somatic nervous system (SNS) is responsible for the communication with the environment and controls skeletal muscles, while the autonomic nervous system (ANS) consists of all efferent pathways from the CNS to organs, glands, and various involuntary muscles, such as cardiac and smooth muscles.

The ANS can further be split into the sympathetic and parasympathetic nervous systems. Most of the tissues are innervated by both systems, and usually have opposing effects. In addition, there is a network of nerves in the digestive tract that is controlled by the ANS but can also act independently of the CNS. This is the enteric system.

The cell bodies of the peripheral neurons are grouped to form ganglia. The

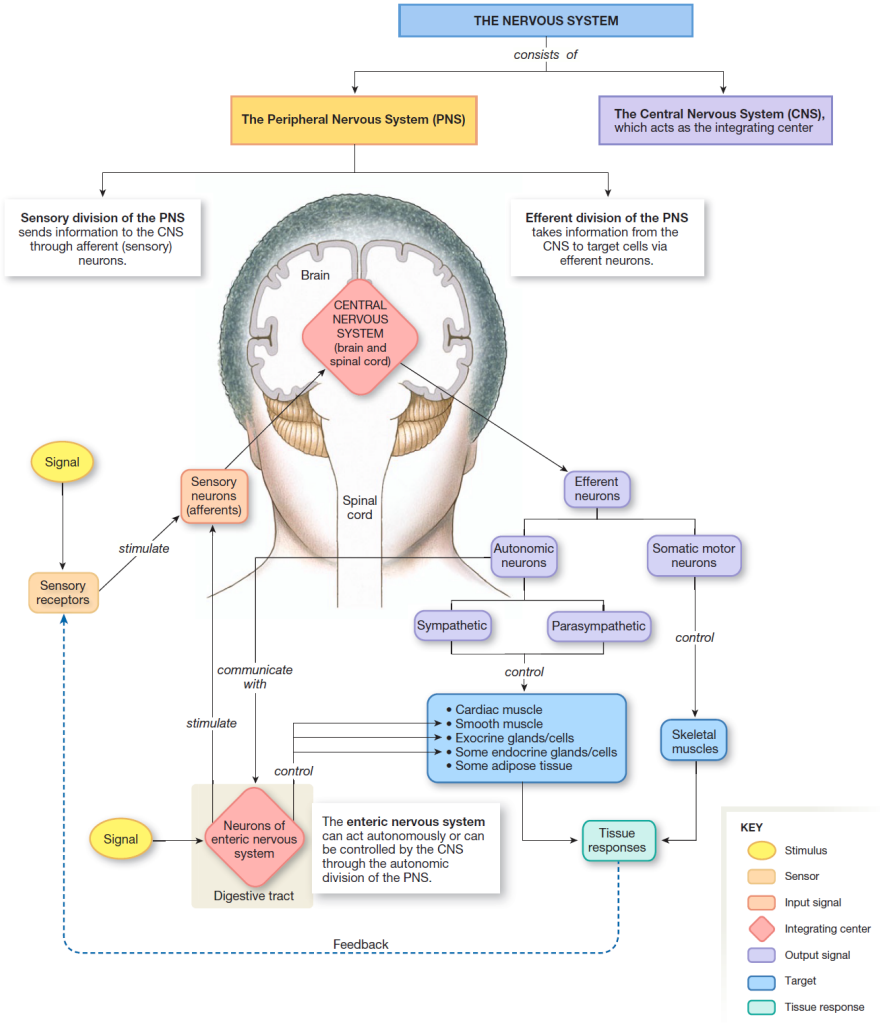


Figure 1.2: A schematic overview of the organization of the nervous system. From [170].

efferent fibres passing from the CNS to the ganglia are preganglionic fibres which release acetylcholine, i.e. they are cholinergic. The final motor neurons from the ganglia to the tissues are postganglionic fibres.

An overview of the organization of the nervous system is given in Fig. 1.2.

Opposing effects of the sympathetic and parasympathetic nervous system

Fig. 1.3 shows the opposing effects and anatomical differences between the sympathetic and parasympathetic nervous systems. Most sympathetic pathways originate in the thoracic and upper lumbar regions of the spinal cord. Sympathetic ganglia are primarily found in two ganglion chains that course along both sides of the vertebral column. The sympathetic preganglionic neurons are short, while the postganglionic neurons are long. The majority of these postganglionic fibres release the neurotransmitter noradrenaline (norepinephrine) and are referred to as adrenergic fibres.

Most of the parasympathetic pathways originate in the brain stem, and some originate in the sacral region. Parasympathetic ganglia are typically located on or near their target organs, and thus the parasympathetic preganglionic fibres are long and the postganglionic fibres are short and release acetylcholine. The major parasympathetic pathway is the vagus nerve (cranial nerve X), which contains about 70% of all parasympathetic fibres. The vagus nerve carries sensory information from organs to the brain as well as parasympathetic output from the brain to internal organs, such as the heart and lungs. The parasympathetic control via the vagus nerve is therefore also called vagal control.

The sympathetic nervous system prepares the body for stress or emergency situations (fight-or-flight response). In these kinds of situations, the sympathetic nervous system causes the heart rate to increase, dilation of the bronchioles of the lungs to increase the oxygen intake, and dilation of the blood vessels to increase the blood supply. The digestion receives a low priority. The sympathetic discharge that occurs in a fight-or-flight situation is mediated by the hypothalamus. However, most sympathetic responses are not the fight-or-flight reflexes to which the whole body responds; often only few sympathetic pathways are activated, without activating all of them.

On the other hand, the parasympathetic nervous system controls the rest-and-digest functions. It reduces blood pressure, breathing and heart rates and stimulates the digestion.

1.1.2 Cardiovascular system

The cardiovascular system (CVS) consists of the heart, which acts as a pump, and blood vessels that are filled with blood. The primary function of the CVS is the transport of oxygen and nutrients to the tissues and removal of waste products from the tissues. In addition, the CVS plays an important role in the cell-to-cell communication and the body's defense to intercept foreign invaders.

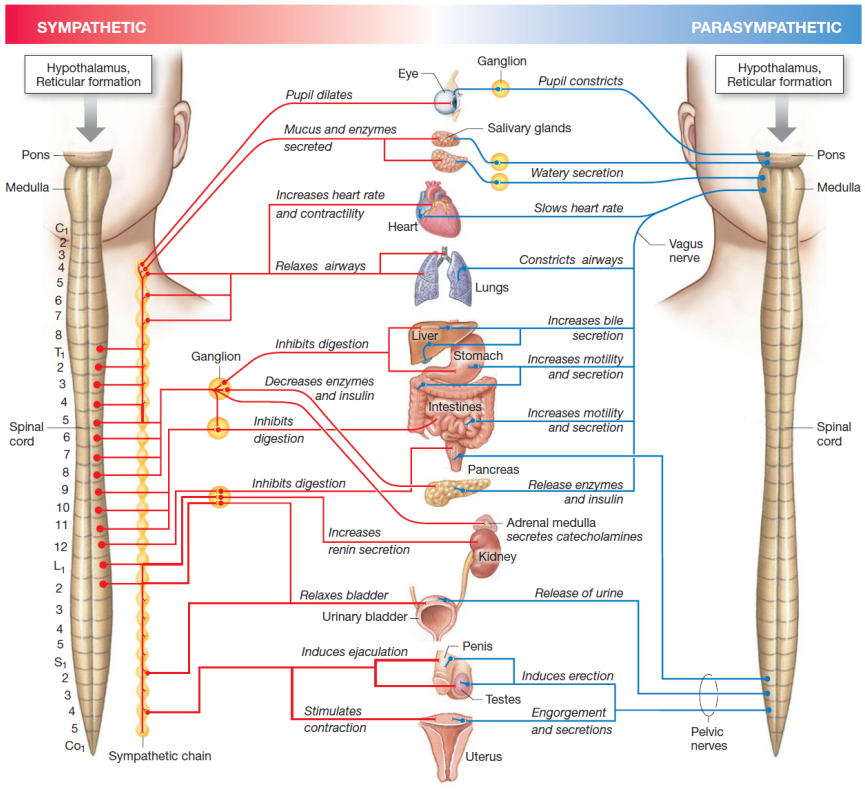


Figure 1.3: Sympathetic and parasympathetic pathways of the autonomic nervous system. From [170].

The cardiovascular system, see Fig. 1.4, is divided in the systemic and the pulmonary circulations, which the heart serves with separate pumps. Deoxygenated blood (given in blue in Fig. 1.4) runs via systemic veins into the right heart and is then pumped into the pulmonary circulation where respiratory gas exchange takes place. Oxygenated blood (given in red in Fig. 1.4) flows via pulmonary veins from the lungs to the left heart, and is then pumped into the aorta to supply the systemic arteries.

Heart

The heart is a muscular organ that has four chambers. Blood from the systemic circulation enters the right atrium of the heart via the inferior and superior

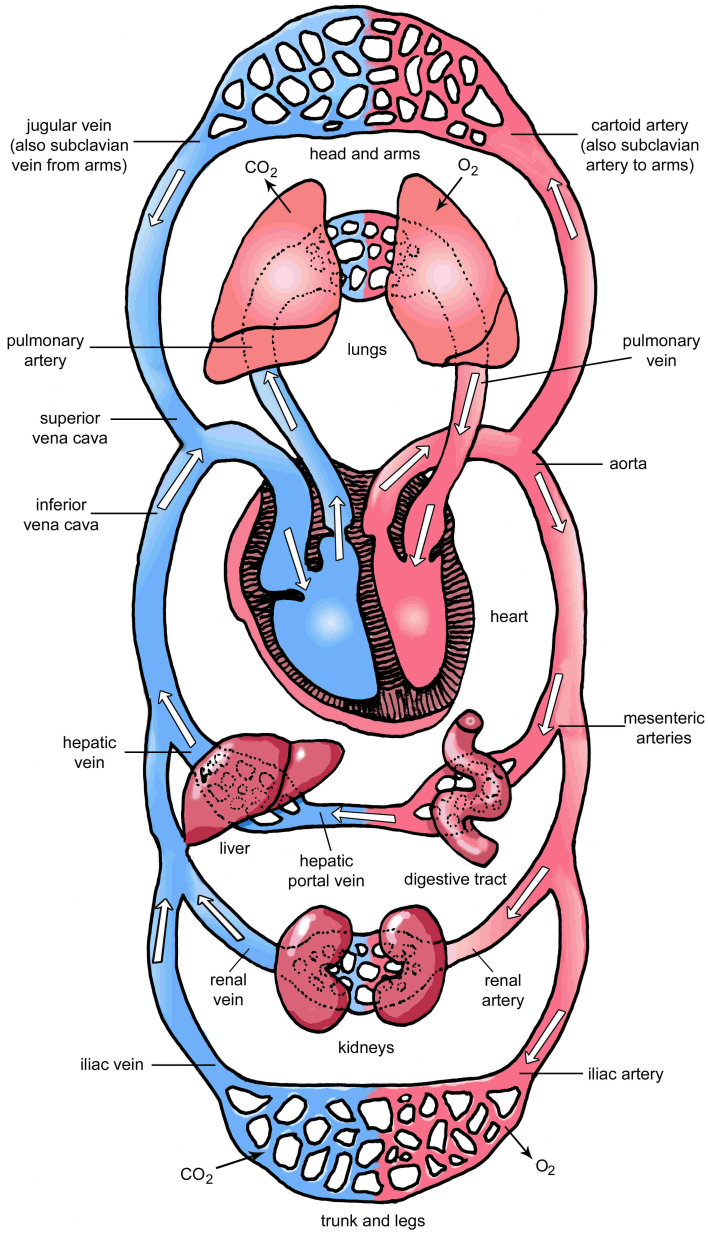


Figure 1.4: A schematic overview of the cardiovascular system. Oxygenated blood is given in red, deoxygenated blood in blue. From [83].

venae cavae and passes into the right ventricle. Similarly, blood that comes from the lungs, enters the left atrium via the pulmonary veins and runs into the left ventricle.

The electrical control of the heart occurs in the heart itself. To this end, the heart has electrically specialized tissue that includes the sino-atrial (SA) node in the dorsal wall of the right atrium, where primary pacemaker cells of the heart are situated; the atrio-ventricular (AV) node, which is the only conducting passage through a tissue layer separating the atria from the ventricles; and additional fast conduction pathways between the AV node and ventricular myocardium to support electrical activation of the ventricular heart muscle.

Electrical properties of the heart

The signal for myocardial contraction does not originate from the nervous system but from specialized myocardial cells known as pacemaker or autorhythmic cells. Myocardial pacemaker cells are anatomically different from contractile cells; they are smaller and contain few contractile fibres as they do not contribute to the contractile force of the heart.

The electrical signal for contraction begins when an action potential is fired by the SA node. Then, the electrical activity goes rapidly via internodal conducting pathways from the SA node to the AV node and the depolarization spreads more slowly to adjacent cells across the atria via gap junctions, causing contraction in the atria. From the AV node, the action potential travels down the ventricular septum in the bundle of His, and then along left and right bundle branches to the Purkinje fibres that spread outward among the contractile cells. The Purkinje network transmits impulses very rapidly (4 m/s), so that all contractile cells in the apex of the ventricle contract almost simultaneously. The conducting system of the heart is displayed in Fig. 1.5.

Each cardiac cycle consists of two phases: diastole and systole. During diastole, the cardiac muscle relaxes, while the muscle contracts during systole. Note that the atria and ventricles do not contract and relax simultaneously, and hence there is a difference between atrial and ventricular systole and diastole.

This synchronized activity of the cardiac chambers results in electrical potential differences that can be recorded from the body surface. Such a signal is called an electrocardiogram (ECG) and provides information on heart rate, electrical conduction and cardiac position, as shown in Fig. 1.5. Three waves can be distinguished on a normal ECG: P wave, QRS complex and T wave. The P wave indicates atrial depolarization. The QRS complex corresponds

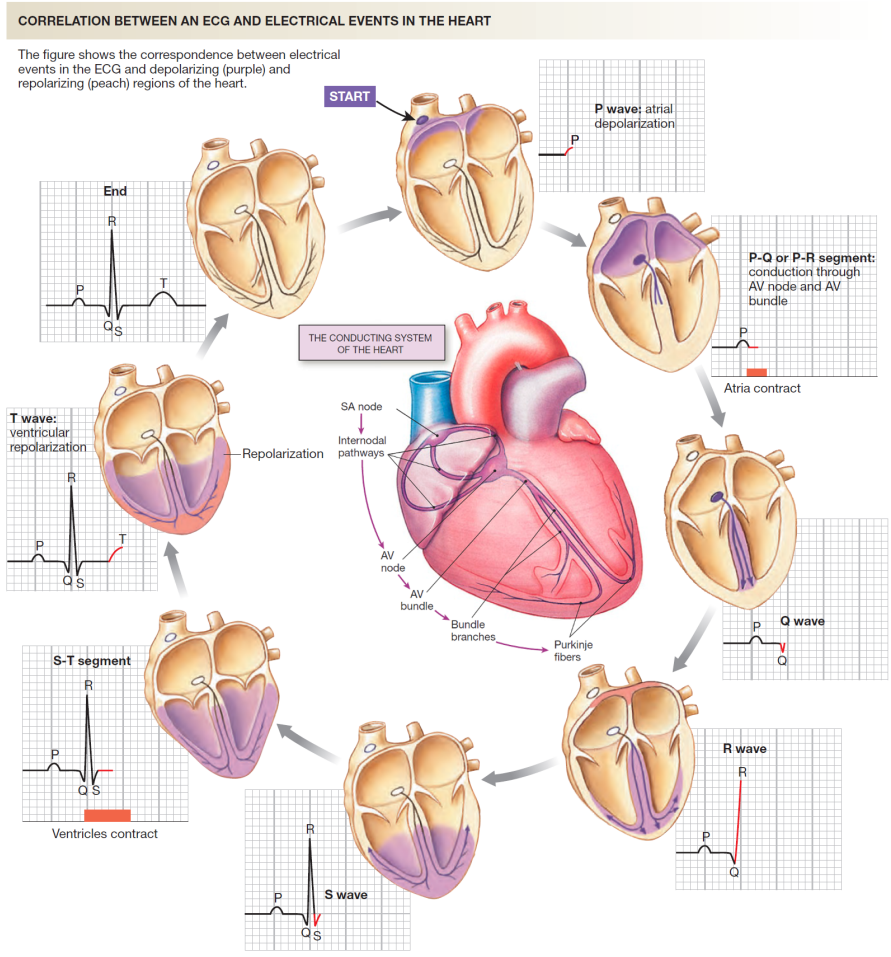


Figure 1.5: Electrical activity in the heart that generates an electrocardiogram. From [170].

to the depolarization of the ventricles, and additionally incorporates atrial repolarization. The T wave originates from the ventricular repolarization.

Vascular system

The vascular system consists of vessels that carry blood throughout the body. These vessels can roughly be split in three categories: arteries that carry blood away from the heart; veins that carry blood to the heart; and capillaries that pass blood from the arteries to the veins. This paragraph will be restricted to the systemic arterial circulation, as this part is responsible for the generation of arterial blood pressure, which is typically measured using a sphygmomanometer.

The aorta and large arteries are highly elastic and their stretching in systole and recoil in diastole results in a pulsatile blood flow from the heart through the vessels. The highest arterial pressure is created by the left ventricle. This is the systolic arterial pressure (SAP) and is around 100-140 mmHg. During ventricular diastole, the pressure falls to values around 50-90 mmHg. This is the diastolic arterial pressure (DAP). The difference between systolic and diastolic pressure is the pulse pressure (PP). The mean arterial pressure (MAP) is calculated by integrating the pressure against time.

Regulation of the cardiovascular system

Short-term regulation of the cardiovascular system is necessary to ensure adequate blood flow to the brain and heart by maintaining sufficient mean arterial pressure. Cardiovascular centres coordinate this regulation and are mainly found in the medulla oblongata and in other areas between the cerebral cortex and spinal cord. Some important concepts for cardiovascular regulation include stroke volume (SV), cardiac output (CO) and total peripheral resistance (TPR). Stroke volume is the amount of blood pumped by one ventricle during a contraction. For an average contraction in a person at rest, the stroke volume is around 70 ml. The cardiac output is a measure of cardiac performance that indicates the total blood flow through the body. CO can be calculated by multiplying the heart rate (in beats-per-minute, bpm) by SV (in ml per beat). For a resting heart rate (HR) of 72 bpm and SV of 70 ml/beat, CO is about 5 l per minute, meaning that at rest, each side of the heart pumps all the blood in the body through it. TPR is the combined resistance to flow of all the parallel vascular beds of the systemic circuit. Note that there is no direct control of MAP; it is determined according to the following relation:

$$\mathrm{MAP} = \mathrm{CO} \times \mathrm{TPR} = (\mathrm{HR} \times \mathrm{SV}) \times \mathrm{TPR}. \tag{1.1}$$

The primary reflex pathway for homeostatic control of mean arterial pressure is the baroreceptor reflex or baroreflex. Baroreceptors, i.e. stretch-sensitive mechanoreceptors, are located in the walls of the carotid arteries and aorta,

where they monitor the pressure of blood flowing to the brain (carotid baroreceptors) and to the body (aortic baroreceptors). The response of the baroreceptor reflex to an increase in MAP is as follows: the baroreceptors increase their firing rate, thereby activating the medullary cardiovascular centre that responds by increasing the parasympathetic activity and decreasing the sympathetic activity. This causes the heart to slow down, and thus CO decreases. Additionally, the arterioles dilate, leading to a decrease in total peripheral resistance. When TPR decreases, there will be more blood flow out of the arteries. This combination of a reduction in CO and TPR lowers, and thus restores, MAP. A decrease in MAP initiates the opposite changes.

There are also peripheral receptors other than the baroreceptors that modulate cardiovascular function. This information is integrated by cardiovascular centres to regulate the CVS. We will not go into detail in all of these receptors and reflexes, but only mention one that is relevant for this thesis, i.e. the Hering-Breuer inflation reflex that is initiated by the lung stretch receptors to prevent over-inflation of the lungs. An increase in tidal volume (V_T) stimulates the lung stretch receptors in the lower airways, causing an increase in HR and decrease in TPR.

1.1.3 Respiratory system

Respiration can be defined as the movement of gases between the environment and the body's cells, and can be divided in four processes: (1) the exchange of air between the atmosphere and the lungs; (2) the exchange of oxygen and carbon dioxide between the lungs and the blood; (3) the transport of oxygen and carbon dioxide by the blood; and (4) the exchange of gases between blood and the cells. The first process is known as ventilation, or breathing, and will also be referred to as respiration throughout the thesis. Inspiration (inhalation) is defined as the movement of air into the lungs. Expiration (exhalation) is the movement of air out of the lungs. A single respiratory cycle consists of an inspiration followed by an expiration.

The respiratory system consists of structures involved in ventilation and gas exchange and can anatomically be divided into the upper respiratory tract (mouth, nasal cavity, pharynx and larynx) and lower respiratory tract (trachea, bronchi and its branches, and lungs). We will not go further into detail in the anatomy of the respiratory system, nor the mechanics of breathing as this is not important for the thesis, but only focus on the regulation of breathing.

Regulation of respiration

Breathing is a rhythmic process that usually occurs unconsciously. However, in contrast to autorhythmic cardiac muscles, skeletal muscles that initiate ventilation are not able to contract spontaneously. Their contraction must be initiated by somatic motor neurons, which are controlled by the CNS.

The rhythmicity of breathing is generated within the respiratory centres which are found in specific areas of the medulla oblongata (dorsal respiratory group (DRG), ventral respiratory group (VRG), and pre Bötzinger complex), and pons (pontine respiratory group (PRG)). The dorsal inspiratory cells of the DRG have an inhibitory effect on the cardiac vagal motor neurons in the nucleus ambiguus. This results in the tachycardia that usually accompanies inspiration. The pre Bötzinger complex contains spontaneously firing neurons that is thought to form the basic respiratory rhythm generator. Some stimuli (e.g. emotion) affect breathing via higher brain centres (hypothalamus and limbic system), which then influence the respiratory centres. Breathing is also under voluntary control from the cerebral cortex, and this pathway bypasses the respiratory centres.

The depth and frequency of the respiratory rhythm are determined by feedback to the respiratory centres from mechano- and chemoreceptors. Carbon dioxide, oxygen, and pH influence respiration via central and peripheral chemoreceptors. Peripheral chemoreceptors are located in the carotid and aortic arteries, and detect changes in the concentration of oxygen, carbon dioxide and pH. Central chemoreceptors are located on the ventral surface of the medulla oblongata and sense changes in the concentration of carbon dioxide in the cerebrospinal fluid. The mechanoreceptors are located in the respiratory tract and include amongst others lung stretch receptors that initiate the Hering-Breuer reflex, lung irritant receptors and pulmonary C receptors.

1.1.4 Heart rate variability

From the physiological background given above, it is clear that our heart does not beat at a fixed rate. The rate at which our heart contracts is in fact determined and continuously modulated by complex interactions between the sympathetic and parasympathetic system in order to properly respond to the demands of our body. These changes in heart rhythm constitute the concept of heart rate variability (HRV). Its easy derivation from non-invasive recordings and its informative value on cardiac autonomic activity, has greatly popularized the study of HRV. Moreover, one of the most important findings of HRV analyses, is that a lack of variability in the HR is related to mortality in patients that

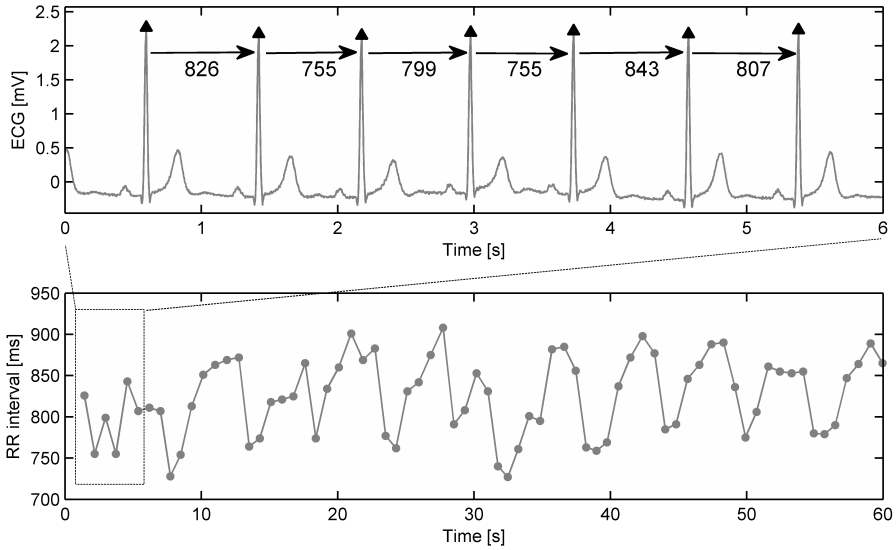


Figure 1.6: Electrocardiogram (top panel) and its tachogram (lower panel). The black triangles indicate the detected R peaks, and the interval (in ms) between two consecutive R peaks is given below each arrow.

suffered from myocardial infarction [190]. Possibly, the decreased HRV is due to a prolonged increased sympathetic or decreased vagal tone [99].

To study HRV, first an ECG is recorded from which the R peaks of the QRS complexes are detected using specialized algorithms. Throughout this dissertation, a real-time QRS detection algorithm based on bandpass filtering, derivative, squaring and integration operations, adaptive thresholding and search procedures, known as the Pan-Tompkins algorithm, is used [136]. In order to deal with possible missing or spurious detections, the estimated R peak locations are additionally processed using an automated procedure that finds the most probable R peak location based on prior heart beats in case of a suspicious location [212]. The time between two consecutive heart beats is an RR interval. Note that an RR interval is related to the heart rate according to HR [bpm]$= \frac{60}{\text{RR [s]}}$. When RR intervals are tracked in time, a tachogram is formed, which constitutes the basic signal for the study of HRV. An example of a tachogram is given in Fig. 1.6. After preprocessing of the RR intervals, they are also called normal-to-normal (NN) intervals.

Based on the tachogram, several measures that characterize heart rate variability

can be deduced [1, 26, 182]. An overview of the most important HRV measures is given in the next paragraph, followed by some important clinical applications of HRV.

Measures of heart rate variability

Linear measures of HRV have been standardized in a Task Force of The European Society of Cardiology and The North American Society of Pacing and Electrophysiology [182]. The most common time domain HRV measures include:

- meanNN [ms]: the mean NN interval;
- diffNN [ms]: the difference between the longest and shortest NN interval;
- SDNN [ms]: the standard deviation of the NN intervals. SDNN reflects all cyclic components responsible for variability and is thus a general measure of HRV;
- RMSSD [ms]: the square root of the mean squared differences of successive NN intervals;
- pNN50 [%]: the percentage of interval differences of successive NN intervals greater than 50 ms;
- SDSD [ms]: the standard deviation of squared differences of successive NN intervals.

The latter three are strongly correlated and related to high frequency spectral power (cfr. infra). These measures are linked to cardiac parasympathetic activity of the ANS.

HRV measures are also commonly deduced from spectral analysis of the tachogram [112]. These frequency domain measures are based on the calculation of the power spectral density (PSD) of the tachogram. To this end, in this thesis, unevenly sampled tachograms are first resampled at 4 Hz using cubic splines [171]. The PSD is then obtained via Welch's method using a 1024 point fast Fourier transform (FFT), a periodic Hamming window, and an overlap of 50%. We can distinguish four frequency bands:

- Ultra low frequencies (ULF): the ULF band is defined from 0 Hz to 0.003 Hz and is only considered in 24 h recordings.

- Very low frequencies (VLF): the VLF band goes from 0.003 Hz to 0.04 Hz.
- Low frequencies (LF): the LF band is defined from 0.04 Hz to 0.15 Hz.
- High frequencies (HF): the HF band goes from 0.15 Hz to 0.40 Hz.

In each frequency band, the power, expressed in ms^2, is computed by integration of the PSD curves. Both LF and HF components are also often expressed in normalized units (nu). This is a relative description of the power in the LF or HF band with respect to the total power (TP). In short-term recordings, TP is determined as the sum of the power in the LF and HF band.

Peak frequencies in the ULF band are related to circadian rhythms, while the physiological meaning of the VLF band is not clear. Possibly, thermoregulation operates in the VLF band. Power in the LF band is reduced by either sympathetic or parasympathetic blockade, and therefore, LF power is believed to reflect both sympathetic and parasympathetic modulations, though this has been debated [66, 152]. Also Mayer waves, i.e. oscillations of arterial pressure with a period of 10 s, affect LF power [90]. The power in the HF band is almost fully eliminated during parasympathetic blockade by atropine, and is therefore often taken as an index of cardiac vagal control. Another commonly used measure is the ratio between LF and HF power (LF/HF), that is considered a measure of sympathovagal balance, though this is also not widely accepted [47, 224].

An example of a PSD is given in Fig. 1.7.

Note that it is important to always compare HRV measures derived from recordings of equal length.

There are also geometric and nonlinear methods to characterize HRV. Although nonlinear methods may account better for the nonlinear processes that are responsible for HRV, their physiological interpretation is not yet clear. Nonlinear HRV measures can roughly be classified in four categories [200]: (1) fractal measures - they assess the self-affinity of heart rate fluctuations over multiple time scales; (2) entropy measures - they determine the (ir)regularity or randomness of heart beat fluctuations; (3) symbolic dynamic measures - they assess the coarse-grained dynamics of heart rate fluctuations based on symbolization; and (4) poincaré plot representations - they assess the heart beat dynamics based on a simplified phase-space embedding. We will not go further into detail in these methods. More information can be found in [113,166,192,200].

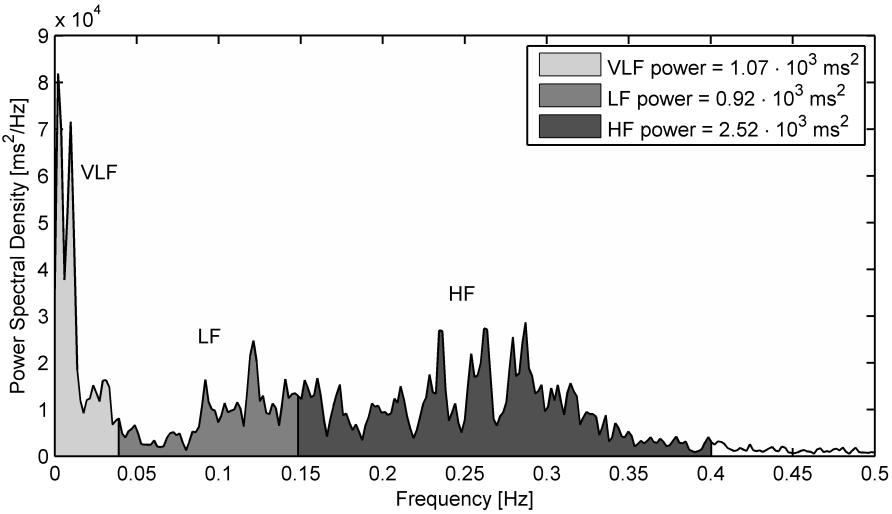


Figure 1.7: Power spectral density of tachogram of 30 minutes, with indication of VLF, LF and HF bands and their corresponding powers.

Clinical importance

As previously mentioned, HRV is related to mortality risk after myocardial infarction. In addition, also links with diseases, including diabetic neuropathy, renal failure and sudden cardiac death, were found [1, 176, 182]. Also in the field of psychophysiology, HRV is commonly used to study among others the influence of mental stress, panic disorders [64], anxiety and depression after myocardial infarction [5].

1.1.5 Respiratory sinus arrhythmia

There is an important relation between respiration and HRV, termed respiratory sinus arrhythmia (RSA). This phenomenon is characterized by an increase in HR during inspiration and a decrease during expiration. RSA is an extra-cardiac modulation of HR, both by higher nervous control and by the mechanical environment. It is estimated that more than 95% of RSA at rest is caused by respiration-related fluctuations in vagal tone. Fig. 1.8 shows a tachogram and a simultaneously recorded respiratory signal. The modulation of the HR, which is inversely related to the RR interval series, clearly modulates in phase with respiration. Some mechanisms responsible for RSA have been described in

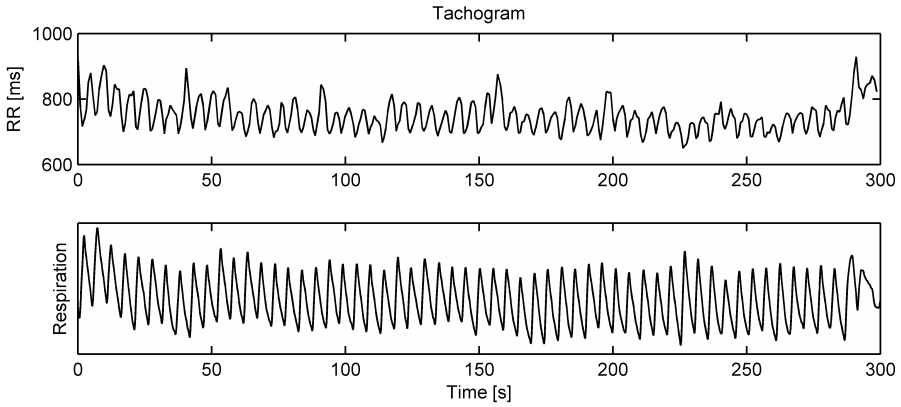


Figure 1.8: Tachogram (top panel) and simultaneously recorded respiration (lower panel). The modulation of the tachogram in phase with respiration, i.e. respiratory sinus arrhythmia, can clearly be observed.

Paragraphs 1.1.2 and 1.1.3, including the Hering-Breuer inflation reflex and the inhibitory effect on cardiac vagal motor neurons by the dorsal inspiratory cells of the dorsal respiratory group.

Studies have shown that RSA is related to cardiac vagal control in anaesthesized dogs under the assumption that cardiac vagal efferent activity stops during inspiration [95, 96]. However, research indicated that in man the inspiratory level of cardiac parasympathetic activity was not reduced to zero [100]. Yet, RSA is often used as an index of vagal control of the heart in behavioural, physiological and clinical studies, including stress, attention, exercise and cardiovascular disease [25]. Moreover, many studies evidenced the dependency of RSA magnitude on respiratory rate and tidal volume when vagal tone remains stable, with an inverse relation with respiratory rate and a direct relation with volume [4,9,30,71,73,80,155,160]. Also the ratio between inspiration/expiration time is suggested to affect RSA [177]. Therefore, it is questioned whether RSA represents a true index of vagal tone. Especially in the field of psychophysiology, this is a largely debated topic that questions which mechanisms are precisely responsible for RSA, how RSA should be quantified and whether it is necessary to correct RSA amplitude for confounding factors that are not related to vagal tone.

Despite many studies, the precise mechanisms that are responsible for the generation of RSA are still largely debated. The mechanisms which have been suggested are not mutually exclusive. The most important ones are the central respiratory rhythm generator in the brain stem that 'gates' vagal

motor neurons [25, 46, 48], the baroreceptors that respond to alterations in intrathoracic pressure [94, 142], the mechanical stretch of the SA node due to changing lung volumes [22], and the inhibition of cardiac vagal efferent activity by activation of the lung stretch receptors [223]. Other studies also relate RSA to the physiological phenomenon to improve the efficiency of pulmonary gas exchange, and save energy by suppressing 'unnecessary' heart beats during expiration [67, 78, 223].

RSA is typically quantified using a time or a frequency domain approach. The time domain approach comprises the peak-valley method that quantifies RSA as the difference between the largest RR interval during expiration and the smallest RR interval during inspiration [26, 107]. Alternatively, in the frequency domain, one can observe that at rest, the respiratory frequency typically lies in the HRV HF band. Therefore, often the power in the HF band is used as alternative measure of RSA amplitude [26]. A comparison between both approaches revealed that they are almost equivalent [43, 70].

However, the debate concerning the underlying mechanisms responsible for RSA, have lead to different strategies as to if and how the possible confounding factors, such as tidal volume and respiratory rate, should be taken into account in the estimation of RSA magnitude. Some of these strategies include statistical correction using analysis of covariance (ANCOVA) with respiratory parameters as covariates [73] and a paced breathing protocol as a calibration procedure for RSA correction [49, 153, 154]. Whether or not these corrections are necessary or appropriate, is questioned due to 'invalid' statistical assumptions and the observation that it does not lead to different interpretations [43, 145]. Additionally, counterarguments are made towards paced breathing as it poses an additional mental load, thereby changing the vagal tone [43]. Research also showed that only the awareness of the recording of respiration prolonged the inspiratory and expiratory time, and thus lowered the respiratory rate [76]. However, also these results are contradicted [9].

It is clear that the mechanisms that generate respiratory sinus arrhythmia are not yet fully understood. Moreover, the use of RSA as a measure of vagal control, and its quantification, is a source of discussion for which no consensus has been reached. It is therefore advised to separately record respiration and analyze RSA with and without taking possible confounding respiratory parameters into account [30, 153].

It is also important to note that RSA does not represent the sole component of cardiac vagal modulation; studies showed that cardiac parasympathetic blockade eliminated HR fluctuations above 0.15 Hz, and about 75 % of those below 0.15 Hz, indicating that HF power reflects vagal activity, but also in the LF band there are significant vagal influences [26]. Moreover, not all vagal activity is

related to respiration, thus one can make the distinction between cardiac vagal activity that is modulated or related to respiration, and vagal activity that is not related to respiration [49, 71, 155].

1.2 Aims of the thesis

Inspired by the debate on the interpretation of RSA, the need to record respiration and the cardiac vagal modulation that can be divided into components related and unrelated to respiration, the aims of this thesis are threefold:

1. Development of a method to derive a surrogate respiratory signal from the electrocardiogram;
2. Separation of the tachogram into a component that is strictly related to respiration, and another component that does not relate to respiration; and
3. Characterization of the common dynamics in the cardiovascular and respiratory system.

The first goal comprises the development of a surrogate respiratory signal based on single lead ECG recordings. This is termed ECG-derived respiration (EDR) and is an important topic to deal retrospectively with possible confounding respiratory parameters in HRV studies without separate respiratory recordings. Additionally, with the trend towards less obtrusive and more cost-efficient monitoring, the possibility to obtain reliable EDR signals would discard the need to separately record respiration using specialized equipment, that often also interferes with natural breathing.

In the second part of the thesis, the goal is to deal in a different way with the respiratory-related heart rate variations and its corresponding interpretational problems concerning RSA and cardiac vagal activity. As such, the aim is to separate the tachogram in two components: one that is strictly related to respiration, and another component that is unrelated to respiration. Next, we aim to conduct HRV analyses on the separate components to investigate whether this approach yields new insights in the mechanisms that generate HRV.

The last goal of this dissertation includes the characterization of common dynamics in HRV and respiration. From the previous paragraphs, it is clear that the interactions that play in the cardiorespiratory system are complex.

Although the common dynamics have been studied in the literature using techniques like synchronization, symbolic dynamics and coupled oscillators, the precise mechanisms are still unclear. Therefore, we aim to characterize the common dynamics in a different way to gain more insight in the underlying cardiorespiratory mechanisms and their interpretation.

The impact of the last two goals will be assessed on one specific application, i.e. during mental stress monitoring. The rationale for this application, and the results that were obtained in previous research is explained in the next section.

1.3 Application: mental stress monitoring

1.3.1 Problem statement

Work-related stress is estimated to cost the US industry yearly over 300 billion USD due to lower productivity, absenteeism, turnover and medical, legal and insurance costs [3, 156]. In Europe, it has been estimated that work-related depression, a possible outcome of prolonged exposure to stress, costs 617 billion EUR annually [50]. Additionally, job stress has been identified as an important risk factor for other mental health problems, musculoskeletal disorders and cardiovascular diseases [36, 45, 51, 79, 81, 98, 159, 162, 185].

When experiencing stress, the fight-or-flight response is activated to enable us to quickly respond to life-threatening situations. This, in turn, stimulates the sympathetic branch of the autonomic nervous system (ANS), acting amongst others on the cardiovascular system [38]. Because HRV can easily be assessed by means of simple ECG recordings, it is a popular tool that has also often been used to study the response of the cardiovascular system to mental stress; typically, the heart rate and sympathovagal balance increase, while the vagal modulation is strongly reduced [24, 81, 134, 144, 172, 180, 197, 201].

Not only the heart rate, but also the breathing frequency increases due to exposure to mental stress [115, 178, 198]. Vlemincx et al. also reported the effect on respiratory variability, and found a reduction in total respiratory variability during sustained nonstressful attention while the opposite occurred during mental load.

Taking into account that the cardiovascular and respiratory system closely interact, a combined cardiorespiratory analysis during mental stress is needed. This has been done in a few studies; Pattyn et al. investigated cardiorespiratory reactivity by means of RSA and separate cardiovascular and respiratory parameters, and found an increase in heart rate and a decreased RSA during

stress [138]. Zhang et al. reported the effects of mental tasks on cardiorespiratory synchronizations and found reduced synchronization epochs during mental arithmetic [225].

Additionally, due to the ability of the human body to also voluntarily control breathing, respiration can also be used as an interface to modulate HRV. The modulation or focus on respiration has especially been used in therapies to reduce the negative effects of stress [29, 35, 39, 77, 139, 174]. Now, HRV biofeedback is an emerging technology to reduce stress [23,75,106,227] that lead to commercially available tools such as the StressEraser (Helicor, NY, USA) and emWave (HeartMath, CA, USA).

Motivated by the above-mentioned arguments, mental stress monitoring forms an interesting application to test the aims of the thesis on. In Paragraph 1.3.2, the data acquisition and experimental protocol are outlined. Paragraph 1.3.3 gives an overview of the most important results that were obtained in [180] and [198] using these data.

1.3.2 Data acquisition and experimental protocol

Participants

A total of 43 healthy students and young people working at the KU Leuven (Leuven, Belgium) participated in the study (21 men and 22 women, age: 18-22 y). Upon arrival, the participants were informed on the course of the experiment and signed the informed consent. The experiment was approved by the Ethics Committees of the Department of Psychology and Educational Sciences and of the Faculty of Medical Sciences. The study was in accordance with the Declaration of Helsinki (2008).

Instrumentation

The respiration (sampling frequency $f_s = 50$ Hz) was measured using the LifeShirt System (Vivometrics Inc., Ventura, CA, USA), which estimates the tidal volume V_T, further used as respiratory signal (RSP), by means of respiratory inductive plethysmography (RIP) around the ribcage and the abdomen. Simultaneously, a single lead ECG ($f_s = 200$ Hz) was recorded.

Protocol

During the experimental protocol, the participants were instructed to conduct two types of tasks. The first type of task was a mental arithmetic task that was designed to induce mental stress. They indicated the correct answer of three solutions using a mouse cursor after which feedback was given. The experimenter was seated next to the participant. A free movie ticket was awarded to the five participants who achieved the most correct answers. Mental arithmetic is widely used to induce stress, as it affects several physiological indices of stress [97, 221]. The second task was a nonstressful attention task where the participants had to indicate the largest number on a computer using a mouse cursor. The attention task required the same motor movement as the mental arithmetic task, but the task difficulty was extremely low; there were no time constraints, nor performance rewards.

The whole protocol consisted of an attention task (AT) and 2 mental stress tasks (MT1 and MT2), each followed by a recovery period (RP). The order of the tasks was randomized. Prior to any task, a resting period was recorded during which the participants watched a relaxing documentary (RD). Each task and RD had a duration of 6 minutes. Prior to the experiment, the participants were instructed not to speak, mumble, or move their lips, to sit comfortably and not to change posture or move the body except for the dominant hand to move the mouse cursor.

Due to missing ECG or respiratory data in 3 subjects, recordings of only 40 students could be analyzed in this thesis.

Data preprocessing

The R peaks in the ECG are detected using the Pan-Tompkins algorithm [136]. Parabolic interpolation using the 5 samples around the detected R peak is conducted to obtain an accuracy of 1 ms when composing the tachogram, in order to prevent coloured noise in the PSD due to the low sampling frequency of the ECG [120]. Unless otherwise stated, the tachogram and respiratory signal are resampled at 4 Hz using cubic spline interpolation. Baseline wander of the respiratory signal is removed using a high-pass filter with a cut-off frequency of 0.05 Hz, while the tachogram is detrended according to [181].

1.3.3 Main findings from previous research

Fig. 1.9 displays the tachogram and respiratory signal of one subject during the full experimental protocol. Taelman and colleagues conducted linear and time-frequency HRV analyses during mental arithmetic and sustained attention [180], while Vlemincx and colleagues studied the respiratory behaviour [198].

From the tachogram displayed in Fig. 1.9, the need for detrending prior to conducting HRV analysis is clear. One can also observe that the RR intervals decrease substantially due to the attention and mental arithmetic tasks. Additionally, the variability of RR intervals is decreased. In terms of HRV measures, Taelman and colleagues found that meanNN, SDNN, pNN50, RMSSD and HF during RD differed significantly from the three tasks. However, apart from meanNN and pNN50, no differences between MT1 and AT were found. SDNN was significantly lower during MT1 and AT, compared to MT2, while vagal HRV measures (pNN50, RMSSD, HF) did not consistently present mutual differences. LF showed significantly lower values during MT1 and AT compared to MT2 and RD. The time-frequency analysis revealed mainly differences between tasks during the first 2-3 min, where especially during MT1, a strong reduction in HF was observed. From these observations, Taelman et al. concluded that only sustained attention already influences ANS activity, as determined by HRV analysis. The addition of mental stress elicited even larger effects (stronger reduction in vagal activity) in HRV measures, yet only during the first minutes of MT1, where the effect of mental stress is superposed to the cardiovascular effect of the attention task. After a few minutes in MT1 and throughout MT2, habituation to the mental arithmetic was noted [180].

The respiratory signal in Fig. 1.9 reveals an increase in respiratory rate during sustained attention and mental arithmetic. Vlemincx et al. studied the respiratory behaviour during these two types of tasks in terms of sigh rate and respiratory variability. Respiratory variability is decomposed in correlated variability, i.e. measures of one breath are correlated with measures of previous and future breaths, and random variability. Spontaneous breathing mainly consists of correlated respiratory variability. During AT, rapid and shallow breathing was noted. Additionally, respiratory variability was reduced compared to RD. The mental stress tasks were also marked by an increase in respiratory rate, yet not as much as during AT. Also an increase in respiratory variability was noted, but the correlated variability was reduced, suggesting the increase of random respiratory variability. The sigh rate was increased during mental arithmetic, fitting the hypothesis that sighing may act as a psychophysiological resetter and that sighing may counteract the increasing random respiratory variability [198].

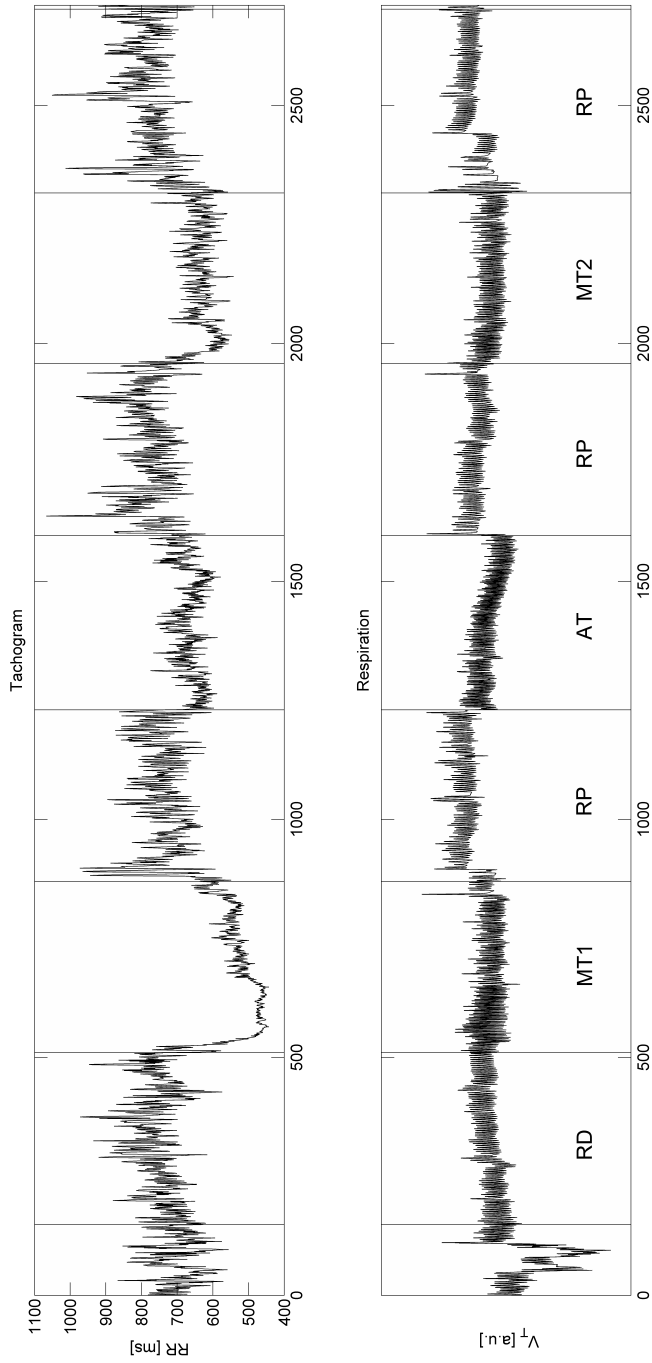


Figure 1.9: Tachogram (top panel) and simultaneously recorded respiration (lower panel, tidal volume V_T) of one subject during mental stress monitoring. (RD = relaxing documentary watching; MT1 = first mental stress task; MT2 = second mental stress task; AT = attention task; RP = resting period).

The studies conducted by Taelman et al. [180] and Vlemincx et al. [198], separately analyzed the tachogram and the respiratory signal. Therefore, we aim to demonstrate the benefit of performing a combined cardiorespiratory analysis in this thesis using these data.

1.4 Chapter-by-chapter overview

In this section, the content of each chapter is briefly outlined. Fig. 1.10 provides a graphical representation of the different chapters, and their mutual relationship.

Chapter 1 provides a general introduction of the thesis. A physiological background on the nervous system, cardiovascular and respiratory systems, and their regulation is given, thereby introducing the concepts of heart rate variability and respiratory sinus arrhythmia. The interpretational problems on the underlying mechanisms that generate RSA, lead to the aims of the thesis. Additionally, the need for mental stress monitoring, which will be used as application throughout the thesis, is explained. Finally, collaborations with other groups and personal contributions are provided.

Chapter 2 deals with the first aim of this dissertation and describes the need for ECG-derived respiration (EDR). In this chapter, the focus lies on single lead EDR methods. An overview of the most important EDR methods is given and a new method based on kernel principal component analysis (kPCA) is proposed. This EDR method is a nonlinear extension of the EDR method based on principal component analysis (PCA). Parameters for kPCA are optimized and a comparison study of the state-of-the-art EDR methods is conducted and discussed in this chapter.

Chapters 3, **4** and **6** are concerned with the second aim of the thesis, i.e. the separation of the tachogram into a component related to respiration and a component unrelated to respiration.

In **Chapter 3**, several methods to conduct this separation are discussed. In order to determine the best method to do so, two comparison studies are performed; a simulation study that determines the efficiency of the different methods in separating the tachogram; and a stability study that tests the robustness of the methods when different window lengths are used. The benefit of this separation is demonstrated on the application of mental stress monitoring, where we aim to classify periods of mental stress and rest.

Chapter 4 conducts the separation of the tachogram in the time-frequency domain. While Chapter 3 is concerned with time domain methods, in this

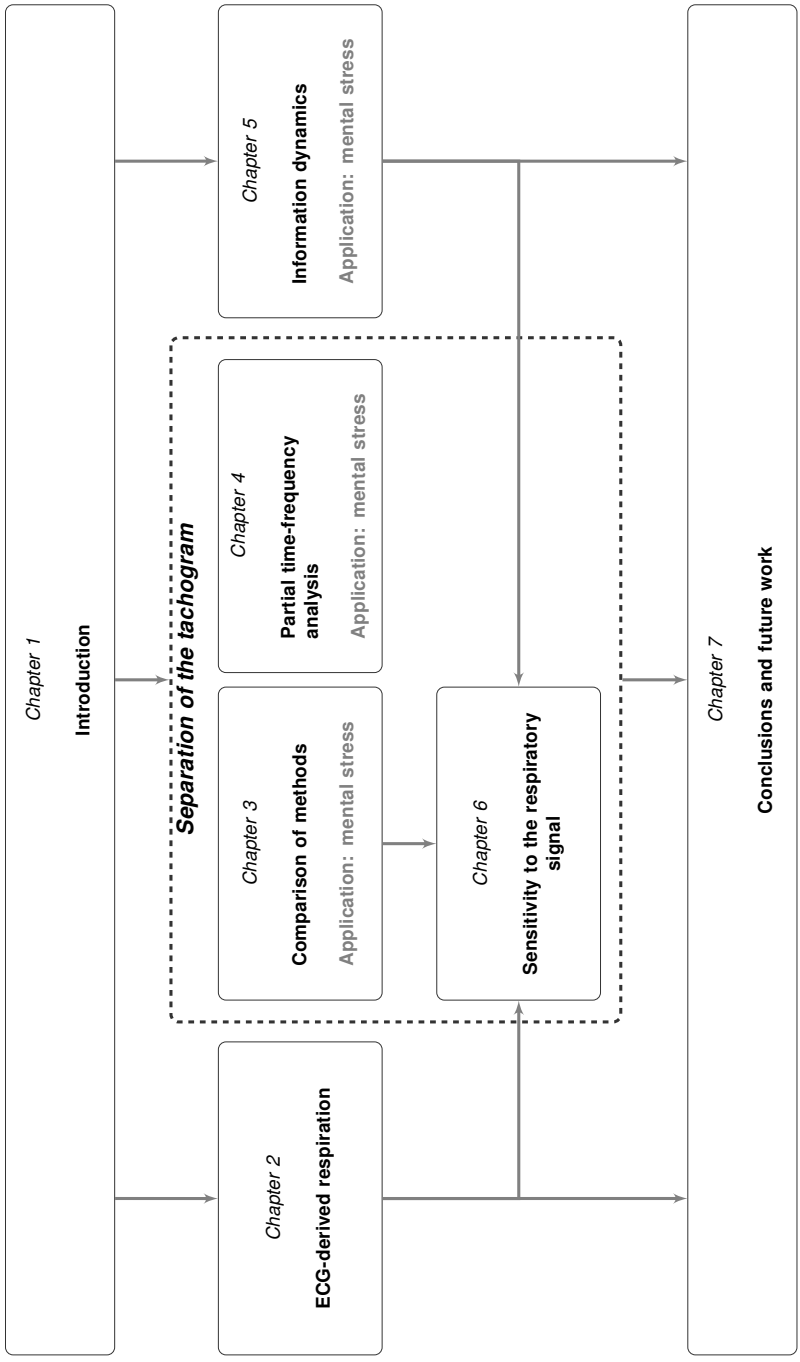


Figure 1.10: Chapter-by-chapter overview.

chapter, the advantages of time and frequency analyses are combined. First, a theoretical framework is given for the partial time-frequency analysis to separate the tachogram. Next, partial time-frequency spectra are studied in the application of mental stress testing.

Chapter 5 deals with the third and last aim of the thesis. Cardiorespiratory dynamics are described by means of information-theoretic measures, such as transfer, cross- and (conditional) self-entropy. Their use for the study of information dynamics in cardiorespiratory data is demonstrated during controlled breathing. Next, these concepts are applied and evaluated during mental stress monitoring.

In **Chapter 6**, the sensitivity of separation methods to the used respiratory signal is discussed. To this end, results from Chapters 2, 3 and 5 are combined; from Chapter 3, the two best separation methods are evaluated. Several respiratory recordings, such as nasal airflow, thoracic and abdominal displacements, as well as some EDR methods from Chapter 2, are used to conduct the separation. The dependency of the separation methods on the respiratory signal is then determined via concepts described in Chapter 5.

Chapter 7 summarizes the work presented in the previous chapters and provides some general conclusions of this thesis. Additionally, some suggestions for future work are given.

1.5 Collaborations

The research conducted throughout my PhD was done in the biomedical data processing research group (BIOMED), STADIUS Center for Dynamical Systems, Signal Processing and Data Analytics, Department of Electrical Engineering (ESAT), KU Leuven, under the supervision of Prof. Sabine Van Huffel. Apart from collaborations within the BIOMED group, several collaborations with other groups were also set up. Their names and affiliations are listed below. Their contributions are described in more detail in Section 1.6.

- *Dr. Elke Vlemincx* and *Prof. Ilse Van Diest*
  Health Psychology, Department of Psychology and Educational Sciences, KU Leuven, Belgium
- *Prof. Johan A.K. Suykens*
  Systems, Models and Control research group (SMC), STADIUS Center for Dynamical Systems, Signal Processing and Data Analytics, Department of Electrical Engineering (ESAT), KU Leuven, Belgium

- *Dr. Michele Orini*
  Institute of Cardiovascular Science, University College of London, UK
- *Dr. Luca Faes*
  IRCS-FBK and BIOtech, Department of Industrial Engineering, University of Trento, Italy
- *Prof. Daniele Marinazzo* and *Alessandro Montalto*
  Department of Data Analysis, Ghent University, Belgium
- *Em. Prof. André E. Aubert*
  Experimental Cardiology, Department of Cardiovascular Sciences, KU Leuven, Belgium
- *Prof. Bea R.H.M. Van Den Bergh*, *Dr. Marijke A.K.A. Braeken* and *Dr. Renée A. Otte*
  Developmental Psychology, Tilburg University, The Netherlands
- *Prof. Bertien Buyse* and *Dr. Dries Testelmans*
  Pneumology, Department of Clinical and Experimental Medicine, KU Leuven, Belgium

1.6 Personal contributions

For each chapter in this thesis, except for Chapter 1, I was the leading researcher who conducted the relevant literature research, study design and experimental set up, algorithm implementation, data analysis, and finally, the interpretation of the obtained results. This is reflected in publications on which I am the first author. It is, however, also important to acknowledge collaborations with colleagues and other groups that lead to the results of this thesis. I will address their contribution and the publications that arose from these collaborations chapter-by-chapter. Additionally, I was involved in several other studies, which are not included in this thesis in order to preserve a certain consistency. These studies will also be listed.

Chapter 2 deals with ECG-derived respiration and uses publicly available data in order for other researchers to compare their method with ours. The development of kPCA as EDR algorithm was done in collaboration with my colleagues Carolina Varon and Dr. Alexander Caicedo Dorado. I acknowledge their valuable help and discussions, especially on the optimization of kPCA for this application. Additionally, Prof. Johan Suykens aided in the interpretation and finetuning of kPCA as EDR method. Preliminary results from this study were presented at the *38th Annual Computing in Cardiology* in Hangzhou, China,

in September 2011 [217]. Later, this was extended to a journal paper which was published in *IEEE Transactions on Biomedical Engineering* [215]. This paper was selected as finalist of the IEEE-EMBS Benelux chapter - Best Paper Award at the *4th Dutch Bio-Medical Engineering Conference 2013*, in Egmond aan Zee, The Netherlands, in January 2013.

In Chapter 3, several methods to separate the tachogram are discussed and compared. The separation method based on multiscale principal component analysis (MSPCA) was proposed by myself and tested using data that were acquired by Prof. Ilse Van Diest. Preliminary results were presented at the *7th International Workshop on Biosignal Interpretation* in Como, Italy, in July 2012 [210], and was also published in a special issue on *Biosignal Processing and Interpretation II* in *International Journal of Bioelectromagnetism* [211]. MSPCA was also used as separation method in the application of mental stress monitoring. The results of this study were presented at the *39th Annual Computing in Cardiology* in Krakow, Poland, in September 2012 [218].

For the comparison of the separation methods, Dr. Elke Vlemincx and Prof. Ilse Van Diest did the data acquisition and provided feedback on the interpretation of the obtained results. I also acknowledge the help of my colleague Dr. Alexander Caicedo Dorado for his contribution on orthogonal subspace projection (OSP) and the comparison studies. For the application of separation methods on stress classification, I designed and conducted the whole study using the mental stress data that Dr. Elke Vlemincx provided. This application was presented at the *35th Annual International Conference of the IEEE Engineering in Medicine and Biology Society* in Osaka, Japan, in July 2013 [219], and was selected at the conference as finalist of the IEEE-EMBC 2013 student paper competition. The comparison of the separation methods and their application to mental stress monitoring were merged into one journal paper that was published in *PLoS ONE* [203].

For the study on partial time-frequency analyses, described in Chapter 4, I collaborated closely with Dr. Michele Orini. As expert in time-frequency analyses, he contributed to the development and interpretation of partial time-frequency spectra as a separation method. Data provided by Dr. Elke Vlemincx were used. The results of this study were presented at the *40th Annual Computing in Cardiology* in Zaragoza, Spain, in September 2013 [207], and later extended to a journal paper that was published in a special issue on *New Trends on Noninvasive Assessment of Autonomic Nervous System through Signal Processing* in *Computational and Mathematical Methods in Medicine* [208].

In Chapter 5 on information dynamics, I collaborated closely with Dr. Luca Faes, Alessandro Montalto and his supervisor Prof. Daniele Marinazzo. The latter two provided Matlab code to compute transfer entropy in a model-free

approach. The extension of this code to new information-theoretic measures (cross-entropy and conditional self-entropy) in cardiorespiratory time series in a model-free approach was done by myself. Dr. Luca Faes provided Matlab code to compute these measures using a model-based approach. In a first study to prove the use of these new measures in cardiorespiratory data, recordings acquired by Prof. Ilse Van Diest were used. The results were interpreted and discussed with all aforementioned parties, especially with Dr. Luca Faes, and were presented at the *36th Annual International Conference of the IEEE Engineering in Medicine and Biology Society* in Chicago, IL, USA in August 2014 [204]. In parallel, Dr. Luca Faes presented the use of these measures in a more theoretical framework using the model-based approach at the same conference [62].

The information-theoretic measures were subsequently evaluated on the application of mental stress testing. To this end, data were provided by Dr. Elke Vlemincx and the obtained results were discussed with Dr. Luca Faes, Alessandro Montalto and Prof. Daniele Marinazzo. This application was presented at the *8th Conference of the European Study Group on Cardiovascular Oscillations* in Trento, Italy, in May 2014 [205]. A journal paper describing an extended analysis during mental stress testing is currently submitted to *PLoS ONE* [206].

For Chapter 6, Prof. Bertien Buyse and Dr. Dries Testelmans provided me with data to conduct the study on the sensitivity of separation methods to the used respiratory signal. I designed, implemented and interpreted the study myself, and discussed the obtained results with my colleague Carolina Varon. This study was presented at the *41st Annual Computing in Cardiology* in Cambridge, MA, USA, in September 2014 [216].

Next to the previously listed studies, I also had the opportunity to work on studies related to space applications. Due to the fact that the influence of respiration on HRV was not taken into account in these analyses, these results are not included in this thesis. A first study, conducted together with Dr. Steven Vandeput and Prof. André Aubert, dealt with the autonomic heart rate regulation in astronauts after spaceflight. Dr. Steven Vandeput designed the experiment, but I aided in the analysis and interpretation of the results. The findings of this study were published in *Medical Science Monitor* [193].

I also had the opportunity to take part in parabolic flight campaigns during which it was the purpose to evaluate the autonomic cardiovascular response to micro- and partial gravity levels. I was involved in the data acquisition and supervised two master students who did preliminary data analyses that were presented at the *Joint Life Science Meeting 'Life in Space for Life on Earth'* in Aberdeen, UK, in June 2012 [2], and at the *39th Annual Computing*

in Cardiology in Krakow, Poland, in September 2012 [89]. I also conducted the final analyses myself and discussed the obtained results with Prof. André Aubert and Dr. Steven Vandeput. A paper containing the most important findings is published in *European Journal of Applied Physiology* [213]. For my work on space-related research, I was awarded the Amelia Earhart Fellowship 2014-2015 by Zonta International. I also acknowledge their financial support for this research.

During my master thesis, I worked on a project of Prof. Bea Van Den Bergh on anxiety in pregnant women and its influence on the development of the fetus. I continued this collaboration with Prof. Bea Van Den Bergh, Dr. Marijke Braeken and Dr. Renée Otte during the supervision of another master student whose results were presented at the *International Conference on Bio-inspired Systems and Signal Processing* in Vilamoura, Portugal, in February 2012 [52].

Lastly, I supervised or participated in other projects in which my contribution was smaller. The results of these studies were presented at the *International Conference on Bio-inspired Systems and Signal Processing* in Barcelona, Spain, in February 2013 [110] and the *41st Annual Computing in Cardiology* in Cambridge, MA, USA, in September 2014 [42]. Additionally, some of the results were published in *Applied Psychophysiology and Biofeedback* [191] and *Advances in Experimental Medicine and Biology* [117].

1.7 Conclusion

In this chapter, background physiology on the nervous system, the cardiovascular and respiratory systems, and their regulation were described. This was necessary to introduce the concepts of heart rate variability and respiratory sinus arrhythmia, as well as their interpretational problems that gave rise to the aims of this dissertation. Specific attention was also paid to mental stress monitoring that will be used throughout the thesis as application on which some of the developed methods will be evaluated to assess the added value on a practical example. The rationale for this application was also discussed, as well as an overview of the main findings, prior to this thesis, of the cardiorespiratory response due to mental stress. A chapter-by-chapter overview was provided, and collaborations with other groups and personal contributions were summarized.

Chapter 2

Kernel principal component analysis for single lead ECG-derived respiration

In this chapter, the first aim is covered. In Section 2.1, an introduction explaining the need for ECG-derived respiration (EDR) and the most important EDR methods, is given. Section 2.2 presents the methodology of the conducted research, starting from the description of the used database. Next, principal component analysis (PCA) as EDR algorithm is explained and a demonstration of how kernel PCA (kPCA) deals with nonlinear data structures is given. Further, kPCA is described in detail and presented as an improved algorithm for deriving surrogate respiratory signals that benefit from the nonlinear relation between the ECG and respiration, including a report on the model selection. The methodology is completed with the description of the R peak amplitude as EDR algorithm and the assessment of the performance of the different EDR methods. In Section 2.3, the results of comparing different kernel functions, and of comparing kPCA, linear PCA and R peak amplitude are evaluated. Section 2.4 comprises a discussion on the obtained results, followed by a conclusion regarding the improvement of our proposed EDR method in Section 2.5. The contents of this chapter is based on [215].

2.1 Introduction

Respiration is an interesting physiological process to monitor as it plays an important role in sleep apnea detection, stress testing and many other applications. A respiratory signal is usually obtained using specialized equipment, like a spirometer, inductive plethysmograph and impedance pneumograph [12]. However, due to increasing costs in the health care industry, there is a growing need to be more cost-effective. This is expressed by a large interest to derive a respiratory signal from another (recorded) physiological signal, which has the additional advantage of being more comfortable for the patient as fewer sensors need to be attached. Moreover, looking for a surrogate respiratory signal has the benefit of not interfering with natural breathing, in contrast to spirometry. One of the most commonly used recordings to derive a respiratory signal from, is the electrocardiogram (ECG). This electrophysiological signal is measured non-invasively via a few electrodes, and is often recorded simultaneously with respiration as it contains much information about the autonomic nervous system, and most importantly, it has a close interaction with respiration.

Respiratory sinus arrhythmia (RSA), a well-known phenomenon in heart rate variability (HRV), describes how respiration modulates the heart rate; during inspiration, the heart rate increases, whereas expiration is coupled with a decrease of the heart rate [25]. This interaction causes respiration to be one of the main modulators of HRV. However, respiration alters the ECG recordings in a different way as well due to the movement of the thorax associated with breathing, the so-called 'mechanical' interaction. This is caused by two factors: (1) the volume changes in the lungs that alter the electrical impedance, and (2) the changing position of the electrodes with respect to the heart, both resulting in modulations in the morphology of the heart beats in the ECG [126,135]. Due to these interactions, it is feasible to derive a surrogate respiratory signal from the ECG, termed ECG-derived respiration (EDR).

EDR algorithms have mainly been used in sleep studies, where the aim is to discard the need for the cumbersome sensors of polysomnography (PSG) to detect sleep apnea. EDR methods have proven to be sufficiently accurate for this purpose [41,65,118,119,125,129]. However, now also stress testing and ambulatory monitoring have received growing interest as EDR applications [11,28,74].

Based on the interactions between respiration and the ECG, a wide range of EDR algorithms have already been developed. Multilead EDR algorithms are typically based on the rotation of the electrical axis of the heart during respiration [11,118,126,226]. In this chapter, we will focus on single lead EDR algorithms.

As described in [12], EDR methods can be divided in three categories: those that are based on changes in the beat-to-beat morphology [40, 41, 102, 116, 119, 129], those that exploit the physiological cardiorespiratory interaction, i.e. based on RSA [28, 40], or those that combine both interactions [28]. Comparison studies of several single lead EDR algorithms have shown that the best methods are based on the changing beat morphology [12]. Most methods filter the ECG in a predefined respiratory frequency band [28, 40], or use the amplitude of the baseline-corrected R peak [40, 129], the R peak amplitude with respect to the S wave [116] or the area under the QRS complex [41, 119]. Another comparison study found the R peak amplitude method to be the most accurate one among those morphology-based EDR algorithms [209].

Recently, Langley et al. introduced the use of principal component analysis (PCA) to look into morphological beat-to-beat variations [102]. Their hypothesis was based on the changing correlation between ECG features, such as the QRS complex, over several heart beats. An EDR signal arises from the coefficients that describe the beat-to-beat variability of the principal components. Langley et al. prove that PCA outperforms the EDR algorithm based on RSA when analyzing beat-to-beat variations. However, using PCA, the relation between respiration and the ECG is assumed to be linear. To tackle this assumption, we propose to use kernel PCA (kPCA) instead of (linear) PCA. Kernel PCA can be seen as a generalization of PCA where nonlinearities in the data are taken into account when the variance is maximized. In this way, nonlinear interactions between respiration and the ECG are included in the construction of a surrogate respiratory signal. KPCA is hypothesized to improve the performance of EDR signals, in particular the EDR signals obtained using PCA and the R peak amplitude.

2.2 Methods

2.2.1 Data

The data from the Fantasia database, available at PhysioNet, are used in this study [68]. This database includes simultaneously recorded lead II ECG and respiratory signals of 20 young (21–34 years old) and 20 elderly (68–85 years old) healthy subjects, with a sampling rate of 250 Hz. Respiration was measured via a belt over the thorax. No respiratory pattern was imposed. All subjects were in supine resting position and watched the movie *Fantasia* (Disney, 1940) to avoid drowsiness. Per subject, 5 minutes of the total recordings were selected in such way that no movement artifacts in the respiratory signal were present.

2.2.2 (Kernel) principal component analysis

Principal component analysis is a method that linearly transforms the input space in such a way that the first principal component accounts for the highest variance of the data. Therefore, PCA is mostly used to reduce the dimensionality of multivariate data. Langley et al. use PCA to find respiratory-induced modulations in ECG features like the QRS complex, P or T wave, by looking for the direction of the highest variance, i.e. the first eigenvector. This eigenvector is used to construct an EDR signal.

However, PCA is restricted to linear transformations. In order to improve the EDR signals, we propose to use kernel PCA, a generalization of linear PCA to a nonlinear setting which was introduced by Schölkopf et al. In kernel PCA, the data are mapped to a possibly higher dimensional feature space F, which is nonlinearly related to the input space. PCA is then performed in F [163]. Fig. 2.1 demonstrates with a toy example how nonlinear data structures benefit from kPCA. KPCA as EDR method is carried out using least-squares support vector machines (LS-SVM) which are implemented in the freely available toolbox LS-SVMlab v1.8 (http://www.esat.kuleuven.be/sista/lssvmlab/, Leuven, Belgium) [179].

Construction of the input matrix

Firstly, an input matrix $\mathbf{X}$ for (kernel) PCA is constructed via the following steps: (a) detection of all R peaks (n) via the Pan-Tompkins algorithm [136] and visual verification of all detections; (b) selection of a fixed window around each R peak (m): 60 ms before and 60 ms after each R peak are selected to capture the QRS complexes; and (c) assembly of all windows in one matrix with aligned R peaks with dimensions $m \times n$ and centering of every column. Fig. 2.2 shows the outline of the resulting input matrix $\mathbf{X}$. Note that ectopic beats are manually excluded from the input matrix.

Principal component analysis

The EDR signals using linear PCA are obtained by calculating the covariance matrix $\mathbf{C}$ of input matrix $\mathbf{X}$: $\mathbf{C} = \frac{1}{m}\sum_{j=1}^{m} \mathbf{x}_j \mathbf{x}_j^T$, leading to an $n \times n$ matrix. Subsequently, the eigenvalue problem $\lambda \mathbf{V} = \mathbf{C}\mathbf{V}$ is solved, resulting in eigenvalues $\lambda \geq 0$ and eigenvectors $\mathbf{v} \in \mathbb{R}^n \backslash \{0\}$. The first eigenvector $\mathbf{v}^1$ is defined as the EDR signal, further denoted as EDR_{PCA} [102].

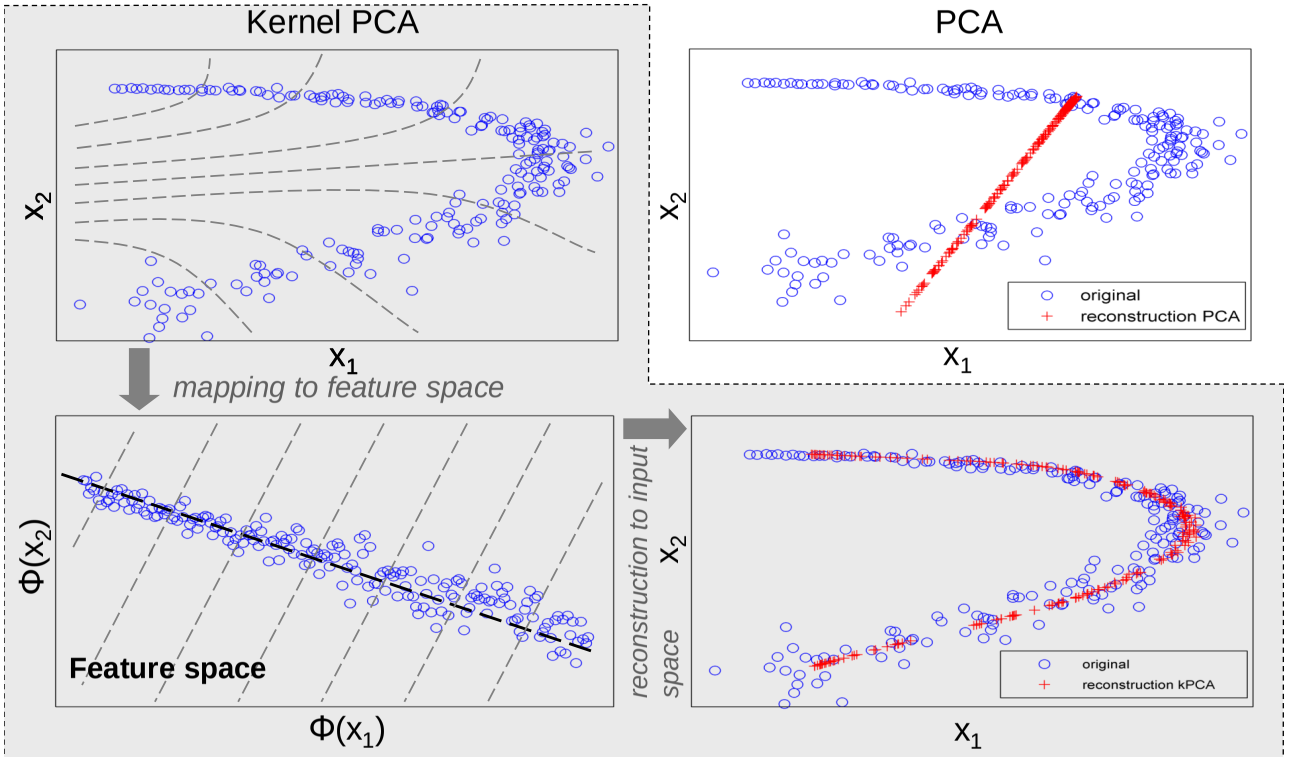


Figure 2.1: Toy example showing the idea of kernel PCA: first, a nonlinear transformation Φ maps the input data to a feature space where PCA is implicitly performed. In this case, the data are denoised using only a few eigenvectors for the reconstruction of the data from the feature space to the input space. Unlike kPCA, PCA fails to detect the nonlinearity of the data.

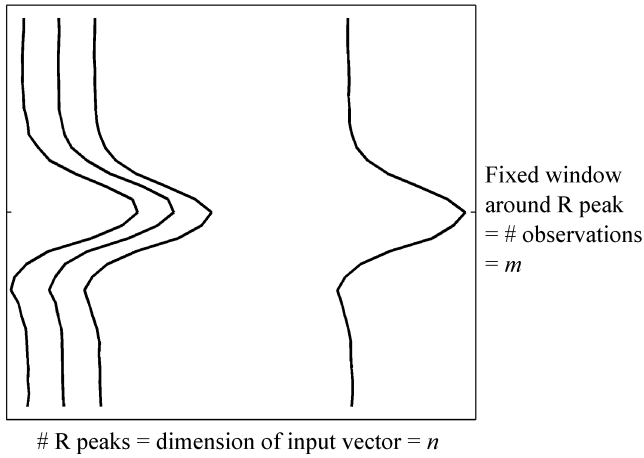


Figure 2.2: Structure of input matrix $\mathbf{X}$.

Kernel principal component analysis

As previously explained, in kPCA, a nonlinear transformation Φ maps the input data into a higher dimensional feature space F and PCA is then carried out in that feature space [163].

For the input data $\{\mathbf{x}_k\}_{k=1}^m$, $\Phi(\mathbf{x}_k)$ represent the mapped data in F. The covariance matrix $\bar{\mathbf{C}}$ of the eigenvalue problem $\lambda\mathbf{V} = \bar{\mathbf{C}}\mathbf{V}$ is

$$\bar{\mathbf{C}} = \frac{1}{m}\sum_{j=1}^{m}\Phi(\mathbf{x}_j)\Phi(\mathbf{x}_j)^T \tag{2.1}$$

with eigenvalues $\lambda \geq 0$ and eigenvectors $\mathbf{v} \in F\backslash\{0\}$. We can write an equivalent system

$$\lambda(\Phi(\mathbf{x}_k)\cdot\mathbf{V}) = (\Phi(\mathbf{x}_k)\cdot\bar{\mathbf{C}}\mathbf{V}) \text{ for } k = 1,\ldots,m. \tag{2.2}$$

Then, consider the coefficients α_i for $i = 1,\ldots,m$ such that

$$\mathbf{V} = \sum_{i=1}^{m}\alpha_i\Phi(\mathbf{x}_i), \tag{2.3}$$

and define an $m \times m$ kernel matrix $\mathbf{K}$ by

$$K_{ij} := (\Phi(\mathbf{x}_i)\cdot\Phi(\mathbf{x}_j)). \tag{2.4}$$

Combining (2.2), (2.3) and (2.4) leads to

$$m\lambda\mathbf{K}\boldsymbol{\alpha} = \mathbf{K}^2\boldsymbol{\alpha}, \tag{2.5}$$

with $\boldsymbol{\alpha}$ a column vector with entries $\alpha_1, \ldots, \alpha_m$. Finding solutions for the eigenvalue problem $m\lambda\boldsymbol{\alpha} = \mathbf{K}\boldsymbol{\alpha}$, solves (2.5). To extract the principal components, the projection of the image of a test point $\Phi(\mathbf{x})$ onto the eigenvectors $\mathbf{v}^k$ in F is computed via

$$(\mathbf{v}^k \cdot \Phi(\mathbf{x})) = \sum_{i=1}^{m} \boldsymbol{\alpha}_i^k (\Phi(\mathbf{x}_i) \cdot \Phi(\mathbf{x})). \tag{2.6}$$

Remark that to solve the equations, the nonlinear transformation Φ is never applied explicitly, only the dot products are required. For that reason, kernel functions $k(\mathbf{x}_i, \mathbf{x}_j)$ can be used [194]. The dot product matrix is then given by $K_{ij} = k(\mathbf{x}_i, \mathbf{x}_j)$.

Applying (2.4), called the kernel trick, implies that it is not needed to construct the nonlinear transformation explicitly and thus results in the fact that the nonlinear transformation is unknown. This poses a problem in this context since the EDR signal is constructed from the first eigenvector in the input space, but kPCA yields eigenvalues and eigenvectors in the feature space F. However, it is possible to find an approximation of the reconstructed data using a limited number of eigenvectors. This process is called pre-imaging and is computed as described in [122] via the function `preimage_rbf` of the LS-SVMlab toolbox. Taking this into account, by reconstructing the input data using the first eigenvector in the feature space, we can get an indication of the direction of the maximal variance in a higher dimensional space. Note that reconstruction using one eigenvector results in projections of the data that are all the same among the rows. The reconstructed observations are thus identical. An EDR signal is then obtained using one row of the reconstructed observations.

Kernel PCA is described in more detail by Schölkopf et al. in [163].

Model selection

The nonlinear transformation Φ is given by kernel functions $k(\mathbf{x}_i, \mathbf{x}_j)$. Two types of kernel functions are evaluated:

- polynomial kernel: $k(\mathbf{x}, \mathbf{y}) = (\mathbf{x}^T\mathbf{y} + t)^d$, with $t \geq 0$ the intercept and d the degree of the polynomial;
- radial basis function (RBF) kernel: $k(\mathbf{x}, \mathbf{y}) = \exp(-\frac{\|\mathbf{x}-\mathbf{y}\|_2^2}{2\sigma^2})$, with σ^2 the variance of the Gaussian kernel.

These kernel functions have specific parameters that need to be tuned. However, as this is a case of unsupervised learning, choosing optimal parameters is

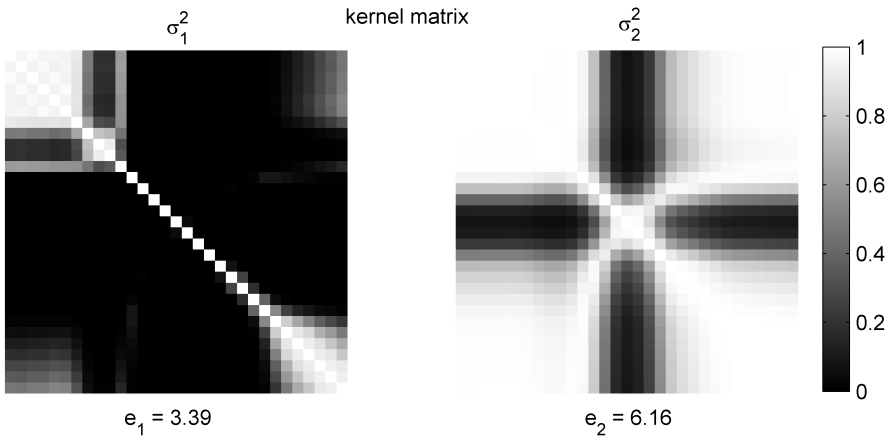


Figure 2.3: Entropy e of the kernel matrix for two values for σ^2, σ_1^2 and σ_2^2.

still an ongoing research topic with no clear solution so far. Therefore, to select a suitable kernel function, they are first evaluated using a fixed set of parameters, after which an optimization of the relevant parameter will take place. In case of the polynomial kernel, t is set to 1[1] and values of $d = 2$ and $d = 3$ are assessed, further noted as $\text{EDR}_{poly(d=2)}$ and $\text{EDR}_{poly(d=3)}$ respectively. Polynomial kernels of higher degrees are not considered as they become too complex. For a first indication of the performance of RBF kernels (EDR_{RBF}), the value for σ^2 is chosen according to a rule-of-thumb: $\widehat{\sigma^2} = m{\cdot}\text{mean}(\text{var}(\mathbf{X}))$.

As will be shown in Section 2.3.1, an RBF kernel produces the best results. In order to further tune the relevant parameter σ^2, we propose two selection criteria. Both options first apply kPCA to a range of 1000 values for σ^2 going from $\widehat{\sigma^2}/100$ to $\widehat{\sigma^2} \cdot 100$. Selection of a value for σ^2 is based on different criteria:

- Entropy (EDR_{ent}): the entropy e of the kernel matrix $\mathbf{K}$ for each σ^2 is calculated according to $e = -\sum(\rho \cdot log_2(\rho))$, where ρ contains the histogram counts of the kernel matrix which is taken as an image. The value for σ^2 with the highest entropy is selected, given that the entropy gives information about diversity of the kernel matrix, and thus the discriminative power of the kernel function. Fig. 2.3 shows the kernel matrices for two values for σ^2, σ_1^2 and σ_2^2, with their corresponding

[1]We tested other values for t as well, but t did not seem to be a critical parameter as all obtained EDR signals appeared to be same.

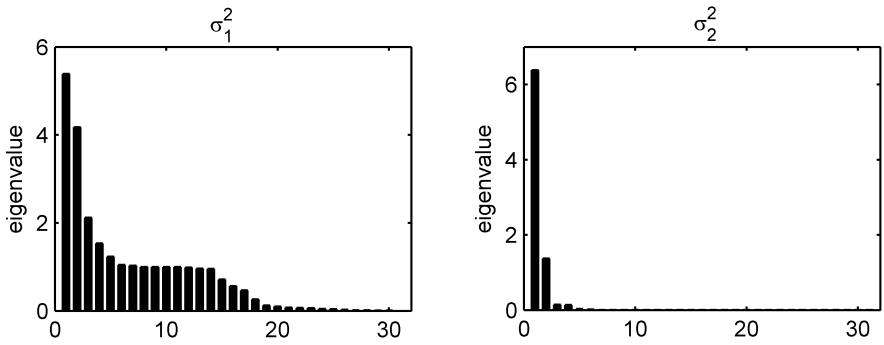


Figure 2.4: Eigenvalues of the kernel matrix for two values for σ^2, σ_1^2 and σ_2^2.

entropies e_1 and e_2. As e_2 is larger than e_1, σ_2^2 is selected for the application of kPCA.

- Eigenvalue (EDR_{eig}): the difference between the first eigenvalue and the sum of the remaining eigenvalues for each σ^2 is evaluated. The value for σ^2 that produces the largest difference, is selected. In this way, the variance represented by the first eigenvector is maximized and the EDR signal will be generated using that eigenvector. Fig. 2.4 displays the eigenvalues of the kernel matrices for two values for σ^2, σ_1^2 and σ_2^2. The plot shows that most of the variance is captured in the first eigenvector in the case that σ_2^2 is used, whereas the eigenvalue distribution when using σ_1^2 indicates that the other eigenvectors account for a large part of the variance as well.

Algorithm 1 summarizes the successive steps of the EDR method based on kPCA described above.

2.2.3 R peak amplitude

In addition to the EDR algorithm using PCA, the algorithm using the amplitude of the R peak (EDR_{RA}) is included in the comparison of EDR algorithms. EDR_{RA} is determined as the amplitude of the R peaks in the baseline-corrected ECG. The baseline wander is removed using 2 median filters, as described by de Chazal et al. [41]. The ECG signal is first filtered with a median filter of 200 ms to remove the QRS complexes and P waves. The filtered signal is then processed using a median filter of 600 ms to remove the T waves. The resulting signal represents the baseline and is subtracted from the original ECG signal.

Algorithm 1 ECG-Derived Respiration using Kernel PCA

Input: single lead ECG.
Output: EDR signal.

1. Construction of the $m \times n$ input matrix $\mathbf{X}$ based on the ECG;
   (a) Detection of the R peaks (n R peaks);
   (b) Selection of a fixed window around each R peak (m samples);
   (c) Assembly of all windows (see Fig. 2.2) in a matrix $\mathbf{X}$ and centering of every column;
2. Definition of a range of values for σ^2 going from $\widehat{\sigma^2}/100$ to $\widehat{\sigma^2} \cdot 100$, with $\widehat{\sigma^2} = m \cdot \text{mean}(\text{var}(\mathbf{X}))$;
3. Application of kPCA using an RBF kernel for every value of σ^2 in the predefined range, yielding a solution for (2.5);
4. Selection of σ^2 (σ^2_{select}) by maximizing:
   (a) the entropy of the kernel matrix; or,
   (b) the difference between the first eigenvalue and the sum of the remaining eigenvalues;
5. Reconstruction (pre-imaging) of the data using the first eigenvector that results from the application of kPCA using an RBF kernel with σ^2_{select}, yielding $\mathbf{X}_{rec}$;
6. Definition of the EDR signal as one row of the reconstructed observations of $\mathbf{X}_{rec}$.

From this baseline-corrected ECG, EDR_{RA} is constructed from the R peaks that are detected as described above.

2.2.4 Comparison of EDR methods

In order to compare the different EDR signals resulting from (k)PCA and the R peak amplitude with the simultaneously recorded reference respiratory signal (RSP_{ref}), the EDR signals are first resampled at 10 Hz by cubic spline interpolation and the reference respiratory signal is downsampled to 10 Hz. The similarity is expressed by means of the correlation coefficient c and the magnitude squared coherence coefficient msc. The correlation coefficient is

determined as the maximum cross-correlation over a lag range of 10 samples such that possible phase delays are taken into account. The magnitude squared coherence $C_{xy}(f)$ is computed via

$$C_{xy}(f) = \frac{|P_{xy}(f)|^2}{P_{xx}(f)P_{yy}(f)} \tag{2.7}$$

with $P_{xx}(f)$ and $P_{yy}(f)$ the power spectral densities of $\mathbf{x}$ and $\mathbf{y}$ respectively, and $P_{xy}(f)$ the cross power spectral density of $\mathbf{x}$ and $\mathbf{y}$. The spectra are calculated via Welch's method using a 1024 point fast Fourier transform (FFT), a periodic Hamming window of a length such that eight equal sections of $\mathbf{x}$ and $\mathbf{y}$ are obtained, and an overlap of 50%.

As no fixed respiratory frequency was imposed, msc is determined as the mean magnitude squared coherence in a range around the fundamental respiratory frequency (f_{RSP}). The range is derived from the power spectrum of the reference respiratory signal and is determined by the frequencies around f_{RSP} which have at least half of the maximum power. In this way, only the frequencies that represent most of the power of the respiratory signal are taken into account in the calculation of msc.

2.2.5 Statistical analysis

The performance of the EDR signals using different types of kernels in kPCA and using PCA and the R peak amplitude are compared using Friedman's test, which is a non-parametric statistical test that is similar to the parametric two-way analysis of variance. Tukey's honestly significant difference criterion is used to take multiple comparisons into account. A $p < 0.05$ is considered statistically significant.

2.3 Results

2.3.1 Comparison of EDR signals using different kernel functions

Fig. 2.5(a) shows the EDR signals and reference respiratory signal of subject `f1y07`. $\text{EDR}_{poly(d=2)}$ ($c = 0.73$, $msc = 0.89$) and $\text{EDR}_{poly(d=3)}$ ($c = 0.73$, $msc = 0.89$) are almost identical. Both signals resemble the reference signal, but visual evaluation of EDR_{RBF} indicates a better performance, which is also represented by a slightly higher correlation and a higher magnitude squared

coherence coefficient ($c = 0.76$, $msc = 0.95$). For comparison, previously proposed EDR methods obtain correlation coefficients of $0.66 - 0.80$ [102]. Fig. 2.5(b) marks the frequency range over which the coherence is averaged. The coherences of the different kernel functions with the reference respiratory signal are given in Fig. 2.5(c), showing a higher coherence when an RBF kernel is used.

The distributions of the correlation and the coherence coefficients of all subjects are shown in Fig. 2.6. Among the correlation coefficients of the different kernel functions, no statistically significant results are obtained. Friedman's test only finds a significant difference in the magnitude squared coherence coefficients ($p = 0.0003$), showing statistically higher coefficients for EDR_{RBF} than $\text{EDR}_{poly(d=2)}$ and $\text{EDR}_{poly(d=3)}$.

2.3.2 Comparison of EDR signals using kPCA, linear PCA and R peak amplitude

As kPCA using an RBF kernel gives promising results for obtaining EDR signals, further 'optimization' of this method is carried out by tuning the parameter σ^2 via a selection criterion based on the entropy and a criterion based on the eigenvalues. Both tuned EDR methods (EDR_{ent} and EDR_{eig}) are compared with the algorithm proposed by Langley et al. using linear PCA (EDR_{PCA}) and with the commonly used algorithm based on the R peak amplitude.

The EDR signals of subject `f1y07` are shown in Fig. 2.7. Both selection criteria for σ^2 yield similar EDR signals; they both resemble the RSP_{ref} ($c = 0.76$ and $msc = 0.96$ for both EDR_{ent} and EDR_{eig}). Fig. 2.8 shows the behaviour of the kernel matrix entropy and the distances of the eigenvalues for different values of σ^2, indicating that both selection criteria lead to similar σ^2-values. Linear PCA and R peak amplitude lead to EDR signals with correlation and coherence coefficients of $c = 0.66$ and $msc = 0.88$, and $c = 0.47$ and $msc = 0.77$ respectively.

When comparing the performances over all subjects, Friedman's test shows significant differences in both the correlation and coherence coefficients of the four EDR methods ($p < 0.0001$ in either case). EDR_{ent} and EDR_{eig} are statistically significantly better than EDR_{PCA} and EDR_{RA}. The algorithm based on linear PCA shows also a significantly better performance over the R peak amplitude in terms of the magnitude squared coherence coefficients. From these results, we can conclude that kPCA using an RBF kernel outperforms PCA and R peak amplitude. However, no difference is found between both

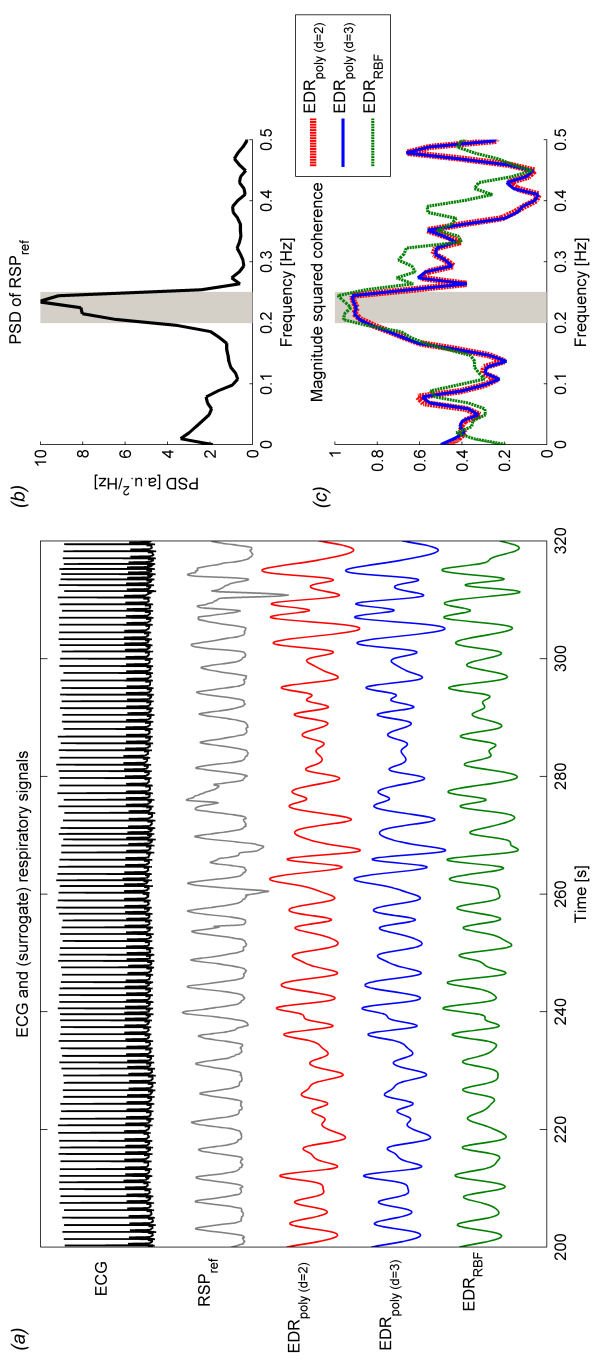


Figure 2.5: EDR signals of subject `f1y07`; (a) EDR signals shown from 200 s to 320 s *(from top to bottom: the ECG signal; the reference respiratory signal (RSP_{ref}); EDR signal using a polynomial kernel of degree 2 ($EDR_{poly(d=2)}$); polynomial kernel of degree 3 ($EDR_{poly(d=3)}$); and RBF kernel (EDR_{RBF}))*; (b) Power spectrum of RSP_{ref}, computed from 200 s to 500 s. The grey area indicates the frequencies around the fundamental respiratory frequency f_{RSP} that contain at least half of the maximum power; (c) Magnitude squared coherence of the EDR signals and RSP_{ref}, computed from 200 s to 500 s.

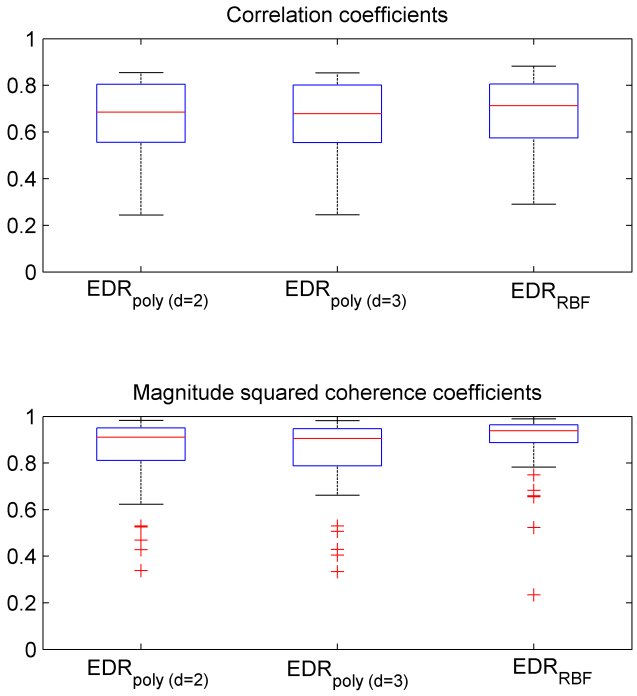


Figure 2.6: Comparison of EDR signals obtained with a polynomial kernel ($d = 2$ and $d = 3$) and an RBF kernel, expressed in terms of the correlation coefficients and the magnitude squared coherence coefficients.

tuning methods for σ^2. Fig. 2.9 shows the distributions of the correlation and coherence coefficients using box plots.

2.4 Discussion

2.4.1 ECG feature selection

In this study, the only selected ECG feature for construction of the input matrix $\mathbf{X}$ is the QRS complex. We tested the selection of the whole beat (WB) as well, given that the performance of this feature in linear PCA is similar to the QRS complex [102]. However, those EDR signals fail to resemble the respiratory

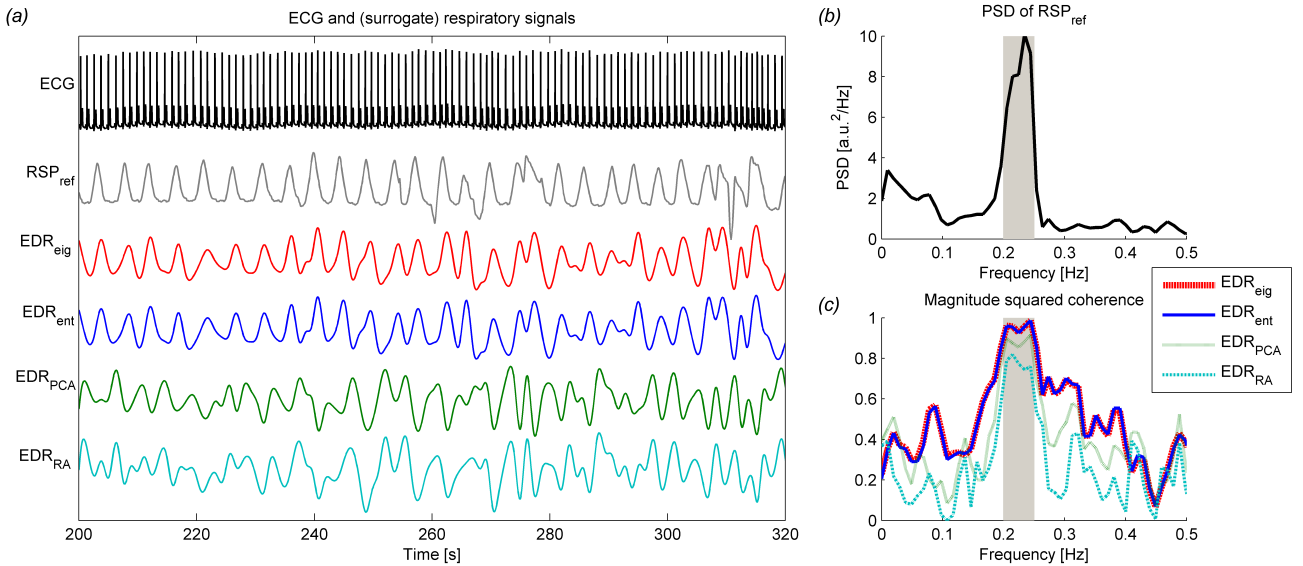


Figure 2.7: EDR signals of subject `f1y07`; (a) EDR signals shown from 200 s to 320 s *(from top to bottom: the ECG signal; the reference respiratory signal (RSP_{ref}); EDR signal using an RBF kernel with σ^2 optimized via the eigenvalue criterion (EDR_{eig}); via the entropy criterion (EDR_{ent}); using linear PCA (EDR_{PCA}); and using the amplitude of the R peak (EDR_{RA})*; (b) Power spectrum of RSP_{ref}, computed from 200 s to 500 s. The grey area indicates the frequencies around the fundamental respiratory frequency f_{RSP} that contain at least half of the maximum power; (c) Magnitude squared coherence of the EDR signals and RSP_{ref}, computed from 200 s to 500 s.

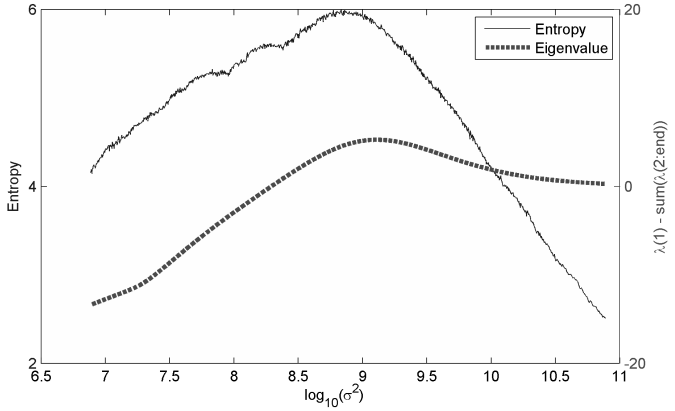


Figure 2.8: Demonstration of the selection criteria for choosing a suitable σ^2 for the RBF kernel. The figure shows the behaviour of the entropy of the kernel matrix (*solid line*) and the difference between the first eigenvalue and the remaining eigenvalues (*thick dashed line*) for several σ^2-values.

signals. The lack of synchronization in samples further away from the R peak seems to play a crucial role as kPCA is more prone to these time alignments.

2.4.2 Selection of σ^2

Two criteria for selecting a suitable σ^2 are proposed, both yielding good EDR signals. However, the chosen σ^2 is not always optimal and better results might be obtained using other values for σ^2. Nevertheless, the obtained respiratory signals outperform EDR signals resulting from algorithms like the amplitude of the R peak and PCA, even though σ^2 is not optimal. Determining this selection criterion in unsupervised learning is thus an important research topic that can greatly influence the performance of this algorithm.

2.4.3 Performance of kernel PCA as EDR algorithm

In order to assess the performance of kPCA as EDR algorithm, the comparison with two frequently used EDR algorithms, linear PCA and R peak amplitude, was made. Kernel PCA showed to outperform both methods. However, many other single lead EDR algorithms exist, such as the algorithms based on the area under the QRS complex [41,119], based on RSA [40] and based on filtering of the ECG [28], which are possibly more robust than the methods evaluated in this

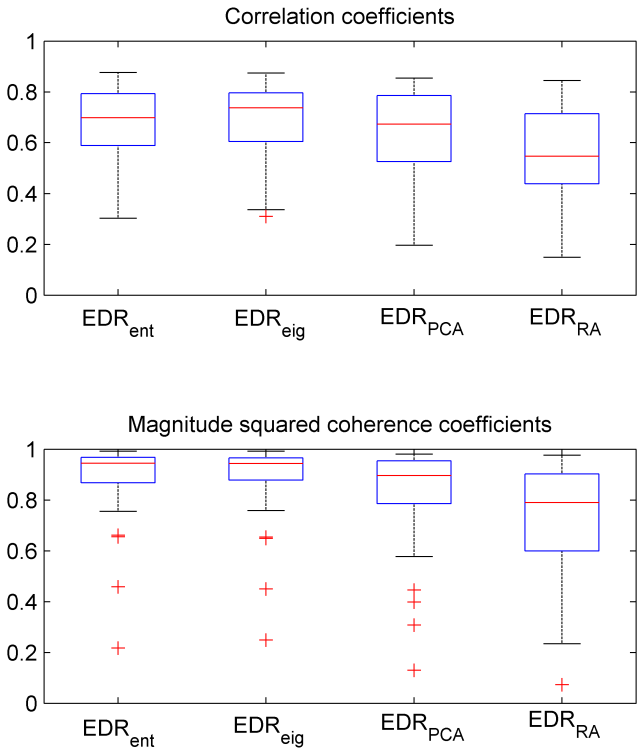


Figure 2.9: Comparison of EDR signals obtained with an RBF kernel with σ^2 tuned according to the entropy and eigenvalue criteria, with linear PCA and with the R peak amplitude, expressed in terms of the correlation coefficients and the magnitude squared coherence coefficients.

chapter. In resting conditions, comparison studies have shown that PCA and the R peak amplitude are better EDR algorithms than the methods mentioned before [102, 209, 214]. However, a validation study that includes all established single lead EDR algorithms is recommended to review the performance of kPCA in a wide range of activities, as in [28], and applications, such as sleep apnea detection.

2.4.4 Computational effort

Kernel PCA as EDR algorithm is computationally more expensive than PCA or R peak amplitude. In order to assess the extra computational effort of kPCA with respect to PCA, we evaluated the computation time of both EDR algorithms. Computations were executed on an Intel(R) Core(TM)2 Quad CPU Q9650 processor with 3 GHz using MATLAB R2010a (MathWorks, NA, USA). The two EDR signals were ten times calculated in every subject, starting from the input matrix $\mathbf{X}$. The overall average computation time of EDR_{ent} and EDR_{eig} are respectively 1.254 s and 0.874 s. The difference in computation time is caused by the calculation of the kernel matrix for every value of σ^2 in the entropy case. This step accounts for over 90% (1.149 s) of the total computation time, whereas iterations based on the eigenvalues cost about 0.724 s. The pre-imaging step takes on average 0.104 s. On the other hand, EDR signals obtained using PCA are acquired in a considerably smaller computation time of 0.007 s.

These results shows that kPCA is less suited for real-time calculation of the surrogate respiratory signal compared to other EDR algorithms. However, for most applications, the higher computational effort is acceptable. To reduce the computation time, we suggest to use the eigenvalue criterion as this is faster and has no disadvantage compared to the entropy criterion.

However, when longer segments are analyzed, kPCA has an advantage over PCA. In this chapter, we only computed the EDR signal of segments of 5 minutes. Longer segments will increase the computation time. In linear PCA, the covariance matrix needs to be calculated, yielding an $n \times n$-matrix. The number of R peaks that can be included is thus subject to the available memory in MATLAB. Kernel PCA on the other hand solves the eigenvalue problem of the kernel matrix $\mathbf{K}$ with dimensions $m \times m$, which is independent of the number of R peaks.

2.4.5 Failure of EDR algorithms

In some cases, kPCA using different values for σ^2 does not succeed in producing a good EDR signal, and both PCA and R peak amplitude fail likewise. This failure might be due to the fact that the orientation of the ECG lead vector and the orientation of the electrical axis of the heart are very close, causing an apparent doubling of the respiratory frequency in the EDR signals. The use of other ECG leads should improve the quality of the EDR signals.

We also hypothesize that the type of breathing influences the performance of the

EDR algorithms; most persons breathe via the chest. However, some persons, such as sportsmen and musicians, are trained to breathe via the abdomen. Both breathing types have other mechanisms to allow filling and emptying of the lungs. The different mechanical movements of chest and abdomen might cause an altered relation between the ECG and the respiratory influence.

The placement of the electrodes, the used ECG leads and the abdominal and thoracic effort during breathing are thus important factors that need to be taken into account. Future studies need to focus on these issues. Additionally, the assumption of ascribing the largest part of variations in QRS complexes to respiration should be verified, especially in ambulatory conditions which are expected to be contaminated by movement artifacts.

2.4.6 Other EDR methods

Since the publication of this study, new methods have been proposed to derive surrogate respiratory signals from single lead ECGs based on the statistical mean shape of QRS complexes [128], homomorphic filtering [169] and QRS slopes [103]. While the former two methods have been evaluated in resting subjects, the latter EDR method also proved to perform well during exercise stress testing. An extensive comparison study of these new EDR methods in resting, sleeping and ambulatory conditions should therefore be set up.

2.5 Conclusion

Kernel principal component analysis proved to be a promising algorithm to obtain single lead ECG-derived respiratory signals. The comparison of different types of kernel functions led to the selection of a radial basis function kernel. However, the parameter σ^2, indicating the variance of the RBF kernel, needed to be optimized, which is a difficulty in unsupervised learning. We proposed two criteria, based on entropy and the difference in eigenvalues, to select a suitable value for σ^2. KPCA using an RBF kernel function and selection of σ^2 according to both criteria showed to outperform linear PCA and R peak amplitude and kPCA using other kernel functions as methods for ECG-derived respiration. These results encourage the use of kernel PCA as improved EDR algorithm in applications like sleep apnea detection or home monitoring.

Chapter 3

Separation of respiratory influences from the tachogram

This chapter deals with the second aim of this dissertation, i.e. the separation of the tachogram in two components: one which is related to breathing and one which contains all heart rate variations that are unrelated to respiration. This goal is driven by the debate on the interpretation of HRV analyses and their interaction with respiration, as discussed in Section 1.1.5 and briefly repeated in this chapter in Section 3.1. We now propose to record respiratory activity and use this information to separate the tachogram. Several algorithms to achieve this have been suggested in the literature, but no comparison between the methods has been performed yet. An overview of these algorithms is given in Section 3.2. Next, two comparison studies are conducted to evaluate the methods' performances to accurately decompose the tachogram in two components and to assess the robustness of the algorithms (Section 3.3). In addition, a real-life example of stress classification is presented in Section 3.4 to demonstrate that this approach to separate respiratory information in HRV studies can reveal changes in the heart rate variations that are otherwise masked by differing respiratory patterns. Finally, some concluding remarks are given in Section 3.5. The contents of this chapter is based on [203].

3.1 Introduction

The rate at which our heart beats, is a dynamical process enabling adaptive changes according to the demands of our body. These variations in heart rate are widely studied in so-called heart rate variability (HRV) analyses, as they contain much information about the activity of our autonomic nervous system (ANS). Furthermore, only the electrocardiogram (ECG) is required, making it a simple, noninvasive and popular tool. From the tachogram, the signal that represents the duration between consecutive heart beats, several HRV measures are defined to characterize ANS activity [182]. These variations in heart rate arise from several processes, such as thermoregulation, hormones, arterial blood pressure, respiration, etc.

One of the main short-term modulators of the heart rate is respiration. This phenomenon is called respiratory sinus arrhythmia (RSA) and comprises the rhythmic fluctuation of the heart rate at respiratory frequency [25]. The precise mechanisms that are responsible for RSA are still questioned, as discussed in Paragraph 1.1.5, and it is largely debated how to deal with possible confounding factors, such as respiratory rate and tidal volume, in the interpretation of RSA measures. No solution has been acknowledged so far, leading to confusion in HRV analyses and questioning its use in practice.

It is, however, apparent that it is important to include information of respiration when interpretations of HRV studies are made [30]. While most current research is focused on this RSA problem, we aim to investigate variations in the heart rate which are unrelated to respiration. More specifically, we propose to separate respiratory influences from the tachogram and thus to obtain a respiratory component of the tachogram and a residual tachogram that only contains variations in the heart rate that are not related to respiration. The goals of this approach are twofold; on the one hand we aim to gain more understanding in the respiratory-related power in HRV analyses. On the other hand, we also believe that this approach might reveal changes in the tachogram that are otherwise dominated by respiratory effects and bring new insights to light.

In the literature, a few methods have been proposed to perform this separation. In this chapter, we aim to conduct an extensive methodological comparison of the proposed methods, such as adaptive filtering [187], independent component analysis [188], system identification [37], multiscale principal component analysis [210] and orthogonal subspace projection [32], to identify the best and most accurate method to perform this separation. An overview of these methods is given in the next section. Then, the comparison is carried out using a simulation study that evaluates the accuracy of the decomposition of the tachogram. In addition, the robustness of each method will be evaluated. Note that in the

literature also several physiology-based mathematical models of cardiorespiratory interactions have been proposed that make it possible to conduct the separation, such as [6,168]. However, these approaches will not be evaluated in this chapter since we focus on data-driven approaches. To conclude the chapter, we will demonstrate that this separation should be considered in future HRV analyses using a real-life example of classifying stress periods based on the residual tachogram.

3.2 Separation algorithms

In this section, we will give a summary of the algorithms that have been proposed in the literature to separate respiratory influences from the tachogram. All algorithms are based on the estimation of the respiratory component of the tachogram (RR_{RSP}) when the original tachogram (RR_{orig}) and a recorded respiratory signal (RSP) are given. The residual tachogram (RR_{res}) is then simply found by:

$$\mathrm{RR}_{res} = \mathrm{RR}_{orig} - \mathrm{RR}_{RSP}. \tag{3.1}$$

All signals are sampled at 4 Hz.

3.2.1 Adaptive filtering

The first method to estimate RR_{RSP} is based on adaptive filtering of the respiratory signal. Adaptive filtering for this application was first proposed by Bianchi et al. in [27] where they used a lattice adaptive filter. In 2008, least-mean squares (LMS) adaptive filtering was introduced to remove respiratory influences from tachogram and blood pressure to estimate the baroreflex sensitivity [187]. A few years later, the authors also applied it to estimate RSA or RR_{RSP} [186]. A scheme of the LMS algorithm is given in Fig. 3.1. Prior to application of the LMS algorithm, the respiratory signal and the tachogram are smoothed using a Savitsky-Golay filter of order 1 in windows of 5 samples, according to [187].

Next, each time sample t of RSP is filtered with a finite impulse response (FIR) filter to estimate RR_{RSP}, according to

$$\mathrm{RR}_{RSP}(t) = \sum_{i=0}^{N_f-1} w_t(i)\mathrm{RSP}(t-i) \tag{3.2}$$

with N_f the number of adjustable filter coefficients $w_t(i)$. The LMS algorithm adapts the filter coefficients by minimizing the mean-squared error (MSE)

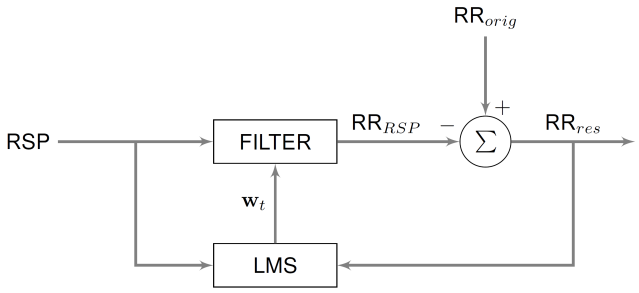


Figure 3.1: Scheme of the LMS adaptive filtering to separate respiratory influences from the tachogram.

between the tachogram and the estimate of the respiration component. A new set of filter coefficients $\mathbf{w}_{t+1}$ is then obtained iteratively by

$$\mathbf{w}_{t+1} = \mathbf{w}_t + 2\mu \mathrm{RR}_{res}(t)\mathrm{RSP}(t) \tag{3.3}$$

where the parameter μ controls the stability and the rate of convergence.

The filter coefficients $\mathbf{w}_t$ are initialized to zero. The entire signal is used to find the coefficients of the converging filter. These coefficients are then used as initial coefficients for the application of the LMS algorithm to the entire signal.

The appropriate selection of μ is important in order for the filter to work properly. The following constraint ensures convergence:

$$0 < \mu < \frac{2}{\sum_{t=1}^{M} \mathrm{RSP}^2(t)} = \mu_{\max}, \tag{3.4}$$

with M the number of samples in RSP.

In [187], a filter length of $N_f = 60$ and convergence parameter $r = 0.08$ ($\mu = r\mu_{\max}$) is chosen for a sampling frequency of 2 Hz. For this case, where a sampling frequency of 4 Hz is used, the parameters are set to $N_f = 120$ and $r = 0.06$.

More details on LMS adaptive filtering to estimate RR_{RSP} can be found in [186, 187].

3.2.2 Independent component analysis

Independent component analysis (ICA) is widely used to decompose observed data into its independent sources. ICA was proposed by Tiinanen et al. to separate respiratory influences from the tachogram [188].

Consider the observation vectors $o_i(t)$ and unknown sources $s_i(t)$, with $i = \{1, \ldots, N\}$ and N the number of sensors, and $t = \{1, \ldots, M\}$ and M the number of samples in each observation vector, then we can write:

$$\mathbf{o}(t) = \mathbf{A}\mathbf{s}(t) \tag{3.5}$$

with $\mathbf{A}$ the mixing matrix. For this purpose, the respiratory signal and tachogram are the observation vectors:

$$\mathbf{o}(t) = [\mathrm{RSP}(t)\ \mathrm{RR}_{orig}(t)]\,. \tag{3.6}$$

The expected independent sources are the respiratory component of the tachogram and the residual component:

$$\mathbf{s}(t) = [\mathrm{RR}_{RSP}(t)\ \mathrm{RR}_{res}(t)]\,. \tag{3.7}$$

Note that the estimated sources are normalized, further annotated with subscript *norm*. Therefore, scaling is needed to process the obtained signals in the correct units. A linear regression model is used to determine the scaling factors α and β:

$$\mathrm{RR}_{orig} = \alpha \mathrm{RR}_{RSP,norm} + \beta \mathrm{RR}_{res,norm} \tag{3.8}$$

$$= \mathrm{RR}_{norm}\phi \tag{3.9}$$

with $\mathrm{RR}_{norm} = [\mathrm{RR}_{RSP,norm}\ \mathrm{RR}_{res,norm}]$ and $\phi = \begin{bmatrix} \alpha \\ \beta \end{bmatrix}$.

Equation (3.9) can be solved via $\hat{\phi} = \mathrm{RR}^{+}_{norm} \cdot \mathrm{RR}_{orig}$ with RR^{+}_{norm} a pseudoinverse.

The FastICA algorithm was used to obtain the sources and mixing matrix [86]. This approach is explained in more detail in [188].

3.2.3 ARMAX model

An autoregressive moving average with exogenous inputs (ARMAX) model was recently proposed to estimate RR_{RSP} [37]. An ARMAX model estimates the

output of the system as a linear combination of previous inputs, outputs and errors. In general, we can write

$$y(t) = \sum_{\tau=1}^{n_a} a(\tau)y(t-\tau) + \sum_{\tau=1}^{n_b} b(\tau)z(t-\tau) + \sum_{\tau=1}^{n_c} c(\tau)e(t-\tau) + e(t) \tag{3.10}$$

with $y(t)$, $z(t)$ and $e(t)$ respectively the outputs, inputs and errors at time t; n_a, n_b, and n_c, and $a(\tau)$, $b(\tau)$ and $c(\tau)$ their respective model orders and predictor coefficients.

In this application, the model is simplified to

$$\mathrm{RR}_{orig}(t) = b(0) + \sum_{\tau=1}^{n_b} b(\tau)\mathrm{RSP}(t-\tau) + \mathrm{RR}_{res}(t) \tag{3.11}$$

with the original tachogram $\mathrm{RR}_{orig}(t)$ $(= y(t))$ that is considered as a linear combination of n_b previous respiratory samples $\mathrm{RSP}(t)$ $(= z(t))$ and a residual signal $\mathrm{RR}_{res}(t)$ which contains all non-respiratory related processes. In [37], the chosen model order n_b was not given. Preliminary experiments using values of 10, 20 and 50 for n_b indicated that the predictor coefficients $b(\tau)$ associated with delays larger than 8 samples are quasi zero. We therefore chose to use a delay (model order) n_b up to 3 seconds (12 samples) to ensure that all possible delayed effects of respiration on the tachogram are captured.

In matrix form, we can write

$$\mathrm{RR}_{orig} = \mathbf{X}_{RSP}\mathbf{b} + \mathrm{RR}_{res} \tag{3.12}$$

with

$$\mathbf{b} = [\ b(0) \quad b(1) \quad \dots \quad b(n_b)\ ]^T \tag{3.13}$$

$$\mathbf{X}_{RSP} = [\ \mathbf{x}_{n_b+1} \quad \mathbf{x}_{n_b+2} \quad \dots\ ]^T \tag{3.14}$$

$$\mathbf{x}_t = [\ 1 \quad \mathrm{RSP}(t-1) \quad \mathrm{RSP}(t-2) \quad \dots \quad \mathrm{RSP}(t-n_b)\ ]^T \tag{3.15}$$

and t starting from sample $n_b + 1$.

The model coefficients $\mathbf{b}$ can be estimated through least-squares via

$$\widehat{\mathbf{b}} = (\mathbf{X}_{RSP}^T\mathbf{X}_{RSP})^{-1}\mathbf{X}_{RSP}^T\mathrm{RR}_{orig} \tag{3.16}$$

The respiratory component of the tachogram RR_{RSP} is computed as $\mathbf{X}_{RSP}\widehat{\mathbf{b}}$. The residual signal RR_{res} is then obtained by subtracting RR_{RSP} from the

original tachogram. An elaborate description of this approach can be found in [37].

A very similar approach is described in [147, 149], where the tachogram is modeled as a sum of autoregressive processes of respiration, systolic blood pressure and other oscillations independent of respiration and blood pressure, in order to find reliable estimates of the baroreflex. When the blood pressure component is combined with the other oscillations, the same set-up as described above is obtained.

3.2.4 Multiscale principal component analysis

Multiscale principal component analysis (MSPCA) was first introduced by B.R. Bakshi in [13]: "[MSPCA] *combines the ability of PCA to decorrelate variables by extracting a linear relationship with that of wavelet analysis to extract deterministic features and approximately decorrelate autocorrelated measurements*" (p.1597).

Fig. 3.2 schematically shows how the MSPCA algorithm is applied to derive the respiratory component from the tachogram, using the following steps:

1. Decomposition of RSP and RR_{orig} using wavelets yielding detail coefficients $\mathbf{cD}_{l,sig}$ and approximation coefficients $\mathbf{cA}_{sig}$, with l the decomposition level, and *sig* the signal (respiration RSP or tachogram RR_{orig}). A Daubechies 4 wavelet is chosen as mother wavelet. The decomposition was performed up to level 5 under the assumption that no interaction between respiration and heart rate exists below frequencies of 0.0625 Hz, i.e. the upper bound of the frequencies contained in $\mathbf{cA}_{sig}$ when a sampling frequency of 4 Hz is used. Note that the maximum level of decomposition also depends on the length of the data.

2. Principal component analysis is applied at each scale except for the approximation coefficients. If the first eigenvector explains over 90% of the variance in the data, the new wavelet coefficients are computed by projecting the coefficients onto the first eigenvector. Otherwise, the wavelet coefficients at that scale are set to 0. This way, only the wavelet coefficients of the tachogram that have an explicit linear relation with those of the respiration are used to construct the respiratory component of the tachogram. The new wavelet coefficients are $\mathbf{c}\hat{\mathbf{D}}_{l,sig}$.

3. The respiratory component of the tachogram can be constructed using $\mathbf{c}\hat{\mathbf{D}}_{l,RR_{orig}}$. The obtained signal RR_{RSP} contains the component of the tachogram which is linearly related to the respiration.

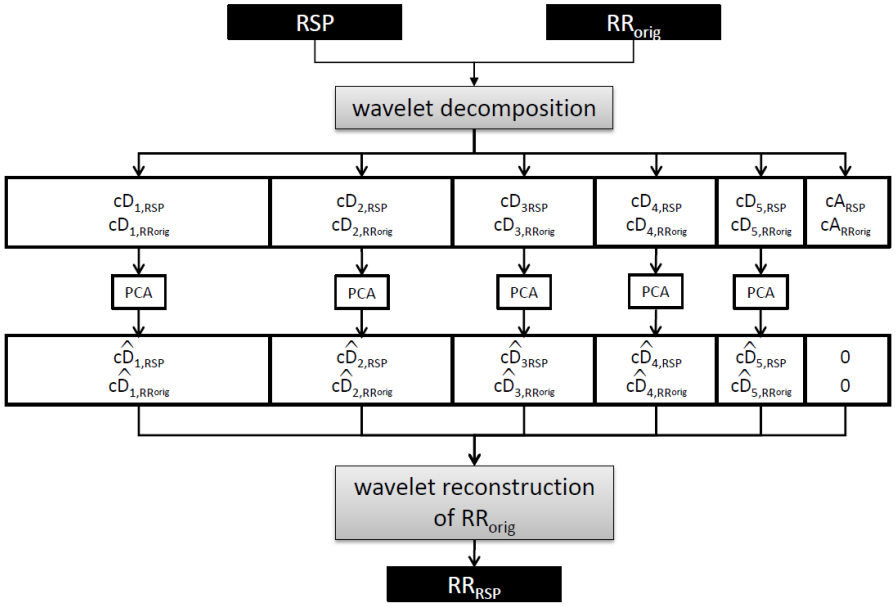


Figure 3.2: Application of MSPCA to extract the respiratory component from the tachogram. First, the tachogram and respiratory signal are separately decomposed in 5 scales using wavelets. Next, PCA is performed on the coefficients of the corresponding scales of both signals. The new wavelet coefficients of the tachogram are then used to reconstruct the respiratory component of the tachogram.

More details can be found in [210].

3.2.5 Orthogonal subspace projection

Orthogonal subspace projection (OSP) is used to decompose a signal in two orthogonal components when a reference, in this case the respiratory signal RSP, is given [32]. First, a subspace that is defined by the basis $\mathbf{X}$ that represents respiratory activity is constructed. Then, the projection matrix $\mathbf{P}$, which projects the original tachogram onto the respiratory subspace, can be computed according to:

$$\mathbf{P} = \mathbf{X}(\mathbf{X}^T\mathbf{X})^{-1}\mathbf{X}^T \tag{3.17}$$

The resulting signal is the respiratory component RR_{RSP} of the tachogram:

$$\mathrm{RR}_{RSP} = \mathbf{P} \cdot \mathrm{RR}_{orig} \tag{3.18}$$

The respiratory basis $\mathbf{X}$ is constructed using the detail signals that are obtained from the wavelet decomposition of RSP using Daubechies 4 wavelet up to level 5. The approximation signal is not included. In addition, a delay n_b up to 3 seconds (12 samples, similar as in the ARMAX model) of each detail signal is included in the basis and the bias is estimated by addition of a column vector of ones in the basis $\mathbf{X}$. Consider the column vector $d_l(t)$, the detail signals of RSP, with l the level and t the samples 12 to M, with M the total number of samples in RSP, then the basis $\mathbf{X}$ consists of 61 components:

$$\mathbf{X} = [\ \mathbf{1}_{(M-n_b+1)\times 1} \quad d_1(t) \quad d_1(t-1) \quad \dots \quad d_1(t-n_b+1) \quad d_2(t) \quad \dots \quad d_5(t-n_b+1)\ ]. \tag{3.19}$$

Note that the proposed OSP combines the strengths of the ARMAX model described in Paragraph 3.2.3 and the multiscale approach in Paragraph 3.2.4. More details about this approach are given in [32].

3.3 Comparison study

The performance of all proposed algorithms to decompose the original tachogram in two components is assessed using two comparison studies. The first study compares the ability of each method to accurately separate two signals using a simulation study. A second study is carried out to evaluate the internal stability or robustness of each algorithm.

3.3.1 Data

Participants

The data used in this study originate from an experiment consisting of baseline recordings (resting sitting position) and conditions of induced worry and mindfulness, and were measured at the Faculty of Psychology and Educational Sciences of the KU Leuven (Leuven, Belgium) [199]. Recordings of 36 subjects (age 18-20) are used, of which one is randomly chosen as reference in the simulation study (cfr. Paragraph 3.3.2). The remaining 35 participants constitute the test subjects. The experiment was approved by the Ethics Committees of the Faculty of Psychology and Educational Sciences and the Faculty of Medical Sciences of the KU Leuven and was in accordance with the

Declaration of Helsinki. All participants were informed on the course of the experiment and provided written consent.

Instrumentation

The electrocardiogram (ECG, sampling frequency $f_s = 200$ Hz) and respiration ($f_s = 50$ Hz) are measured by means of the LifeShirt System (Vivometrics Inc., Ventura, CA). Respiration was recorded using respiratory inductive plethysmography (RIP) around the ribcage (RC) and the abdomen (AB). The sum of RC and AB deflections is taken as an estimate of the tidal volume [72]. This volume will further be considered as the respiratory signal (RSP).

Preprocessing

Only the first 6 minutes of the baseline recordings are used in this study. The tachogram is constructed by detection of the R peaks in the ECG using the Pan-Tompkins algorithm [136]. All detections are manually inspected and corrected where needed. In order to prevent addition of coloured noise in the HRV spectrum due to the low ECG sampling frequency, the R peak locations are enhanced using least-squares parabolic interpolation on five samples surrounding the detected R peaks such that an accuracy of 1 ms is obtained [120]. Next, the respiratory signal and the tachogram are resampled at 4 Hz using cubic spline interpolation. In addition, the respiratory signal is filtered with a high-pass filter with a cut-off frequency of 0.05 Hz in order to remove baseline wander.

All processing steps of the data are performed in MATLAB R2012a (MathWorks, Natick, MA).

3.3.2 Simulation study

Experimental setup

The first experiment is designed to evaluate how well each method can decompose a signal, i.e. a tachogram which is the sum of a respiratory component of the tachogram and a residual component, when the recorded respiratory signal is given. Since no ground truth for the two components is available, a simulation study is set up. In order to have realistic data, we chose to use real tachograms. Let algorithm $A(i)$ be one of the 5 proposed algorithms with i going from 1 to 5, let algorithms $A(k)$ be all of the 5 proposed algorithms except for algorithm $A(i)$, let $S(j)$ be the number of the subject with j going from 1 to 35 and

let $S(ref)$ denote the reference subject with recorded signal $\mathrm{RSP}_{S(ref)}$ and $\mathrm{RR}_{orig,S(ref)}$. Then the experimental procedure is as follows:

1. Apply algorithm $A(i)$ on the data of the reference subject. The respiratory component $\mathrm{RR}^{A(i)}_{RSP,S(ref)}$ is taken as ground truth in the comparison later on.
2. On each of the 35 test subjects $S(j)$ with data $\mathrm{RSP}_{S(j)}$ and $\mathrm{RR}_{orig,S(j)}$, apply the same algorithm $A(i)$ as in step 1 to remove the subjects' own respiratory component and obtain their residual components $\mathrm{RR}^{A(i)}_{res,S(j)}$.
3. Construct for each test subject $S(j)$ a new tachogram: $\mathrm{RR}^{A(i)}_{new,S(j)} = \mathrm{RR}^{A(i)}_{res,S(j)} + \mathrm{RR}^{A(i)}_{RSP,S(ref)}$.
4. Apply all algorithms $A(k)$ to decompose the tachogram in its two components. The inputs for the algorithms are $\mathrm{RR}^{A(i)}_{new,S(j)}$ and $\mathrm{RSP}_{S(ref)}$. The obtained components are $\widehat{\mathrm{RR}}^{A(i),A(k)}_{res,S(j)}$ and $\widehat{\mathrm{RR}}^{A(i),A(k)}_{RSP,S(j)}$.
5. Compare $\widehat{\mathrm{RR}}^{A(i),A(k)}_{res,S(j)}$ and $\widehat{\mathrm{RR}}^{A(i),A(k)}_{RSP,S(j)}$ with $\mathrm{RR}^{A(i)}_{res,S(j)}$ and $\mathrm{RR}^{A(i)}_{RSP,S(ref)}$, respectively using the evaluation measures described in the next paragraph.
6. Repeat steps 1 to 5 using each time a different algorithm $A(i)$ in step 1 and 2.

A block diagram of steps 1 to 4 is shown in Fig. 3.3. This procedure can be seen as a cross-validation over the different algorithms to ensure that the evaluation of the performance is not biased by the use of the same algorithm in steps 1, 2 and 4.

Evaluation measures

The performance of all methods based on the simulation study is evaluated using two criteria of both the residual and respiratory component of the tachogram:

1. The normalized root-mean-squared error (NRMSE) of the time signals, which is defined as the root-mean-squared error divided by the range of the reference signal:
   (a) Residual component: $\widehat{\mathrm{RR}}^{A(i),A(k)}_{res,S(j)}$ versus $\mathrm{RR}^{A(i)}_{res,S(j)}$
   (b) Respiratory component: $\widehat{\mathrm{RR}}^{A(i),A(k)}_{RSP,S(j)}$ versus $\mathrm{RR}^{A(i)}_{RSP,S(ref)}$

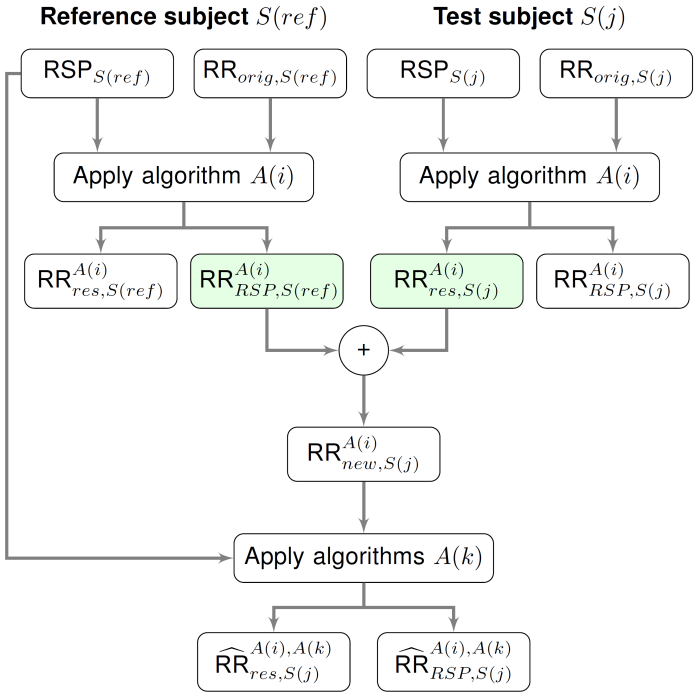


Figure 3.3: Block diagram of the simulation study.

2. The squared errors (SE) of the low-frequency (LF: 0.04-0.15 Hz) and high-frequency (HF: 0.15-0.40 Hz) power:

   (a) Residual component: $\widehat{\mathrm{LF}}^{A(i),A(k)}_{res,S(j)}$ versus $\mathrm{LF}^{A(i)}_{res,S(j)}$, and $\widehat{\mathrm{HF}}^{A(i),A(k)}_{res,S(j)}$ versus $\mathrm{HF}^{A(i)}_{res,S(j)}$

   (b) Respiratory component : $\widehat{\mathrm{LF}}^{A(i),A(k)}_{RSP,S(j)}$ versus $\mathrm{LF}^{A(i)}_{RSP,S(ref)}$, and $\widehat{\mathrm{HF}}^{A(i),A(k)}_{RSP,S(j)}$ versus $\mathrm{HF}^{A(i)}_{RSP,S(ref)}$

The spectra are computed via Welch's method, using a 1024 point fast Fourier transform, a periodic Hamming window of a length such that eight equal sections of the tachogram are obtained, each with an overlap of 50%.

Results

Fig. 3.4 shows an example of the simulation study of a typical subject. The ARMAX model (= $A(i)$) was used in step 1 and 2, and separation of the tachogram was performed using OSP (= $A(k)$). Both in time and in frequency domain, the resemblance between $\mathrm{RR}_{RSP,S(ref)}^{ARMAX}$ and $\widehat{\mathrm{RR}}_{RSP}^{ARMAX,OSP}$, and $\mathrm{RR}_{res}^{ARMAX}$ and $\widehat{\mathrm{RR}}_{res}^{ARMAX,OSP}$ is high.

The overall performance of all algorithms using the simulation study is shown in Figs. 3.5 and 3.6. Fig. 3.5 displays the NRMSE between the reference and the obtained signals. Both in the residual and in the respiratory component of the tachogram, the resulting signals are closest related to the reference signals using orthogonal subspace projection. The ARMAX model, LMS adaptive filter and MSPCA have an average performance while ICA does not show a good correspondence. These conclusions are confirmed when LF and HF power are compared, as in Fig. 3.6. Based on these 4 spectral indices and the NRMSE evaluation measures, OSP had the best overall performance in this simulation study.

When the results are analyzed in more detail, it appears that $\widehat{\mathrm{HF}}_{RSP}^{A(i),A(k)}$ is mostly underestimated and $\widehat{\mathrm{HF}}_{res}^{A(i),A(k)}$ overestimated. Only OSP has a Gaussian distribution of errors around zero. This finding suggests that, except for OSP, the other algorithms might still contain respiratory influences in the residual tachogram. In LF, no consistent over- or underestimation is found.

In order to test the dependency of the results on the chosen reference subject, the analysis is repeated using other randomly chosen subjects as reference. These simulation studies yield similar results, and lead to the same conclusions.

3.3.3 Stability study

Experimental setup

The goal of the second experiment is to assess how sensitive the methods are to the used data lengths by applying the algorithms on several window lengths. Let $A(i)$ be one of the 5 algorithms used for the separation, and let $S(j)$ denote the number of the subject with j going from 1 to 36, then the following procedure is performed:

1. Apply each algorithm $A(i)$ on the 6 minutes data $\mathrm{RSP}_{S(j)}$ and $\mathrm{RR}_{orig,S(j)}$ of every subject $S(j)$. The obtained separated components of the

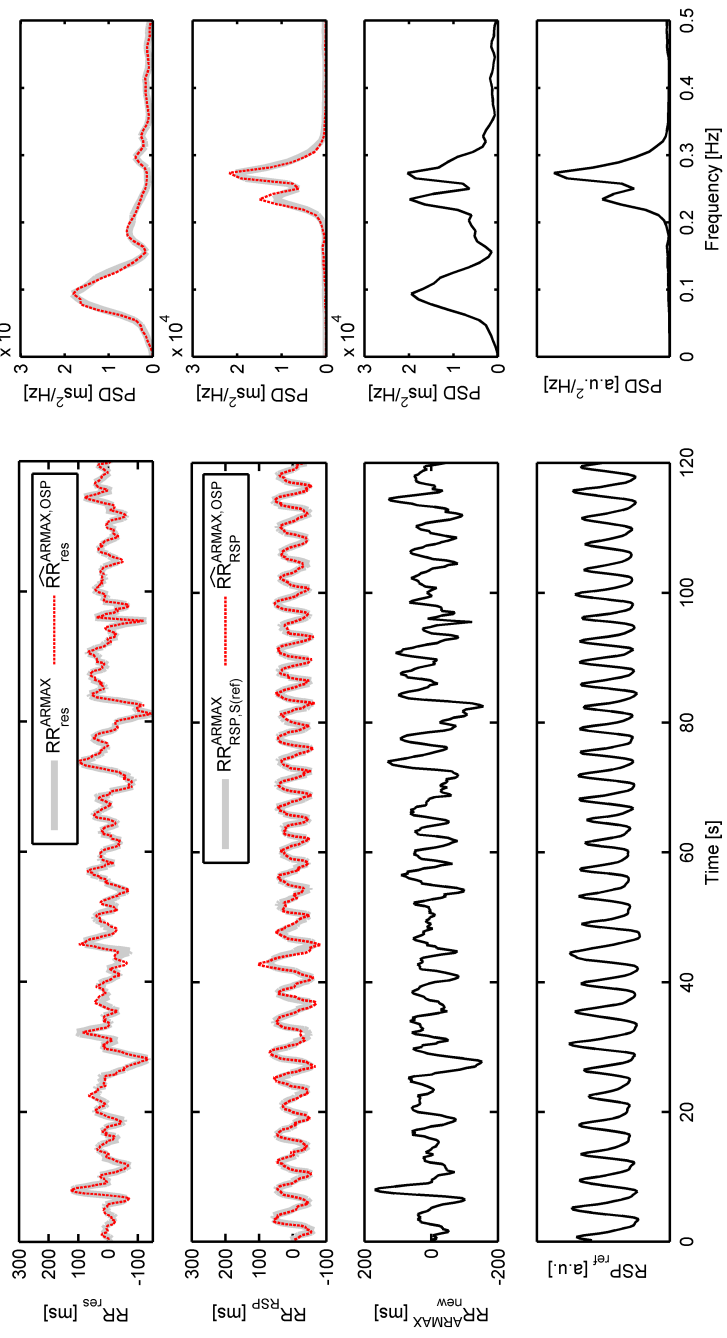


Figure 3.4: Example of the simulation study of a typical subject using the ARMAX model in step 1 and 2. Separation of the tachogram is performed using OSP. The signals are shown in both time (only 120 s are shown here) and frequency domain. From top to bottom: RR_{res}, RR_{RSP}, $\mathrm{RR}_{new}^{ARMAX}$, $\mathrm{RSP}_{S(ref)}$. In dashed red, the estimated components using OSP are displayed.

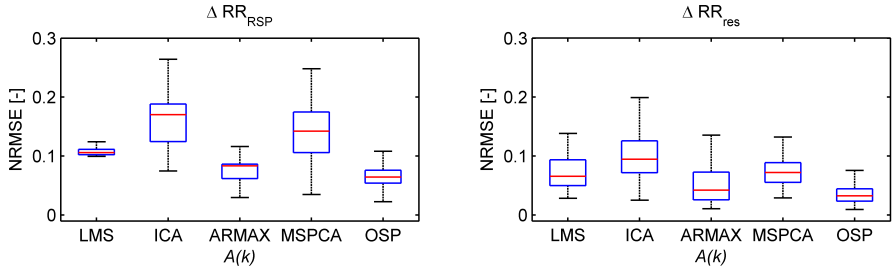


Figure 3.5: Boxplots of the normalized root-mean-squared errors (NRMSE) between $\mathrm{RR}^{A(i)}_{RSP,S(ref)}$ and $\widehat{\mathrm{RR}}^{A(i),A(k)}_{RSP,S(j)}$ (left), and between $\mathrm{RR}^{A(i)}_{res,S(j)}$ and $\widehat{\mathrm{RR}}^{A(i),A(k)}_{res,S(j)}$ (right) obtained using the simulation study. Outliers are not shown.

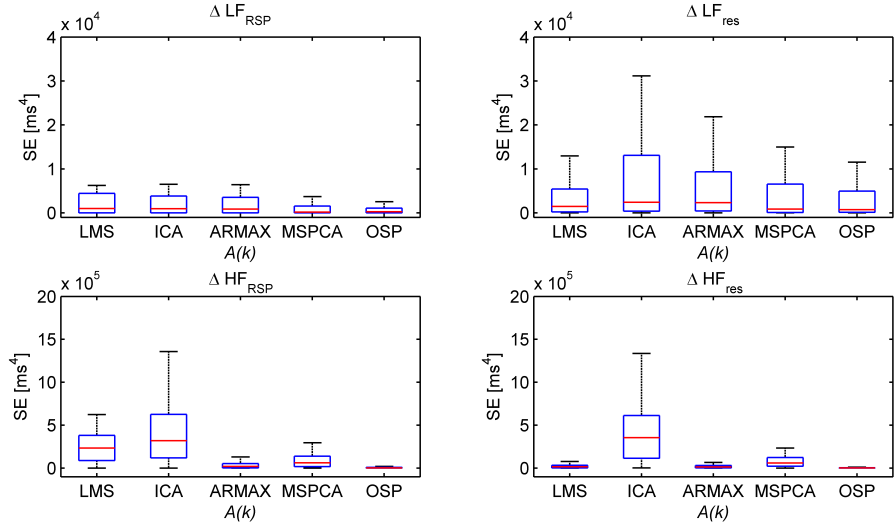


Figure 3.6: Boxplots of the squared errors (SE) in LF power (top) and HF power (bottom) between $\mathrm{RR}^{A(i)}_{RSP,S(ref)}$ and $\widehat{\mathrm{RR}}^{A(i),A(k)}_{RSP,S(j)}$ (left), and between $\mathrm{RR}^{A(i)}_{res,S(j)}$ and $\widehat{\mathrm{RR}}^{A(i),A(k)}_{res,S(j)}$ (right) obtained using the simulation study. Outliers are not shown.

tachogram are the reference for the following steps and denoted as $\mathrm{RR}^{A(i)}_{res,S(j)}$ and $\mathrm{RR}^{A(i)}_{RSP,S(j)}$.

2. Divide each tachogram $\mathrm{RR}_{orig,S(j)}$ and respiratory signal $\mathrm{RSP}_{S(j)}$ in 3 segments of 2 minutes and apply each algorithm $A(i)$ on every segment seg, yielding $\mathrm{RR}^{A(i),seg}_{res,S(j)}$ and $\mathrm{RR}^{A(i),seg}_{RSP,S(j)}$.

3. Concatenate the three 2-minute segments:
$\widehat{\mathrm{RR}}^{A(i)}_{res,S(j)} = [\ \mathrm{RR}^{A(i),seg1}_{res,S(j)} \quad \mathrm{RR}^{A(i),seg2}_{res,S(j)} \quad \mathrm{RR}^{A(i),seg3}_{res,S(j)}\ ]$
$\widehat{\mathrm{RR}}^{A(i)}_{RSP,S(j)} = [\ \mathrm{RR}^{A(i),seg1}_{RSP,S(j)} \quad \mathrm{RR}^{A(i),seg2}_{RSP,S(j)} \quad \mathrm{RR}^{A(i),seg3}_{RSP,S(j)}\ ]$

4. Compare for each algorithm $A(i)$ the acquired $\widehat{\mathrm{RR}}^{A(i)}_{res,S(j)}$ and $\widehat{\mathrm{RR}}^{A(i)}_{RSP,S(j)}$ with the references $\mathrm{RR}^{A(i)}_{res,S(j)}$ and $\mathrm{RR}^{A(i)}_{RSP,S(j)}$ obtained in step 1 using the evaluation measures described in the next section (Paragraph 3.3.3).

In the ideal case, concatenation of the three 2-minute segments yields the same signals as when the full 6 minutes are used. A block diagram of the stability study is given in Fig. 3.7.

Evaluation measures

Similarly as in Paragraph 3.3.2, the performance of all separation methods is evaluated by the NRMSE of the time signals and the SE of the LF and HF powers. The stability of each algorithm is assessed by comparing $\widehat{\mathrm{RR}}^{A(i)}_{res,S(j)}$ with $\mathrm{RR}^{A(i)}_{res,S(j)}$, and $\widehat{\mathrm{RR}}^{A(i)}_{RSP,S(j)}$ with $\mathrm{RR}^{A(i)}_{RSP,S(j)}$.

Results

This second comparison study comprises a stability evaluation of each algorithm by changing the analyzed window size. This comparison is not designed to see how well the methods succeed in separating the tachogram in two components, but is set up to test the robustness of each method. The full window of 6 minutes is taken as reference while 2 minute windows are evaluated. Fig. 3.8 presents the NRMSE and SE of the LF and HF power of the residual tachogram. Comparisons using the respiratory component yield similar results and are not shown here. Based on the NRMSE, ICA shows a low stability. ARMAX has the lowest NRMSE, and surprisingly the performances of LMS, OSP and MSPCA are only average. Close inspection of the time signals, however, indicate that

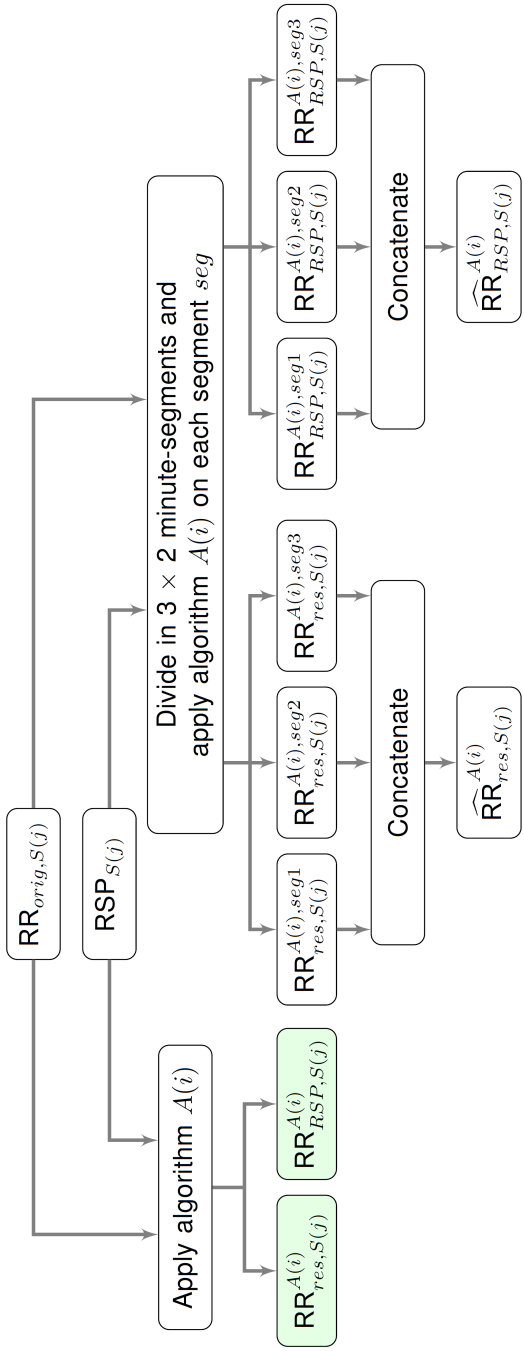


Figure 3.7: Block diagram of the stability study.

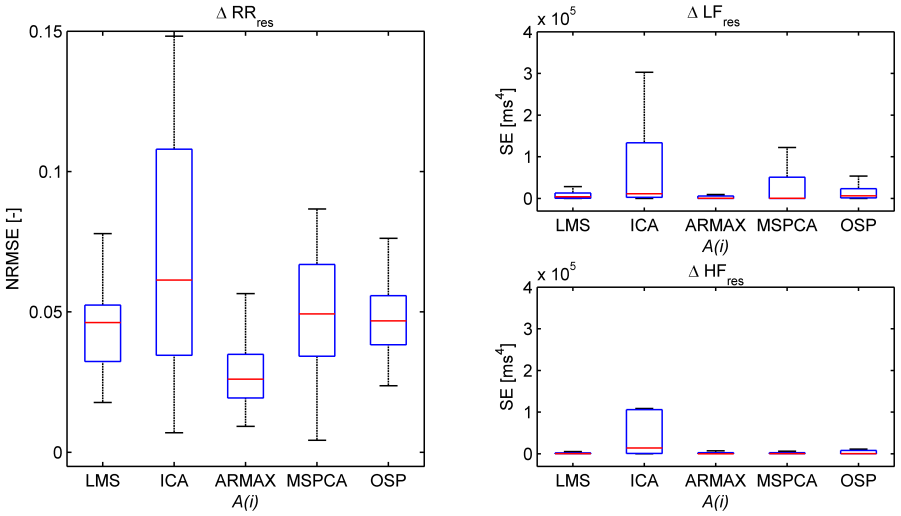


Figure 3.8: Boxplots of the normalized root mean-squared errors (NRMSE) (left), and the squared errors (SE) (right) in LF power (top) and HF power (bottom) between $\widehat{\mathrm{RR}}^{A(i)}_{res,S(j)}$ and $\mathrm{RR}^{A(i)}_{res,S(j)}$ obtained using the stability study. Outliers are not shown.

the low performance of OSP is due to an almost constant bias that is not captured in the smaller windows, as shown in Fig. 3.9. The very low frequency modulations cause a large NRMSE, and are in fact of no importance in most HRV studies as we are only interested in the dynamics in the LF and HF band. It is therefore more interesting to look at the performance based on the LF and HF power. These results indicate that LMS and ARMAX are least sensitive to window sizes when LF and HF power are compared. OSP shows only a moderate performance.

3.3.4 Discussion

In this study, the challenge of respiratory influences in the tachogram is handled by the approach to separate respiratory influences in heart rate variations from non-respiration related changes. In the literature, several methods have been proposed to deal with this problem, but no comparison between the algorithms has been performed. Therefore an extensive comparison using a simulation study and a stability study has been set up. All data-driven algorithms, up to our knowledge, that appeared in the literature to conduct this cardiorespiratory

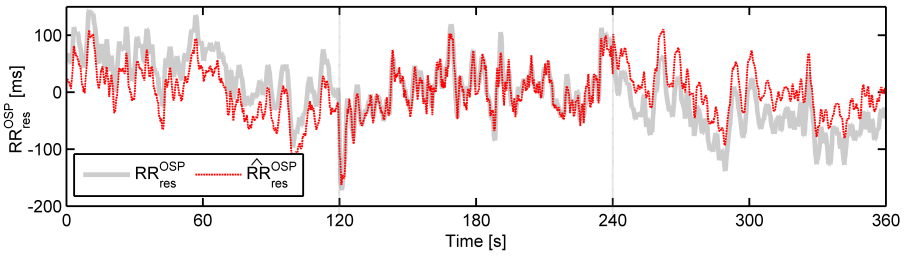


Figure 3.9: Example of the stability study using orthogonal subspace projection. The residual signal of the full 6-minute period (RR_{res}^{OSP}, thick grey) and the three 2-minute segments ($\widehat{\mathrm{RR}}_{res}^{OSP}$, dashed red) are shown.

separation were evaluated. Note that the algorithms were implemented as they appeared in the literature, and thus no further optimisation of parameters was conducted in this comparison study.

The first comparison of algorithms is carried out in a simulation study which was designed to examine which method performs best given two realistic signals of the residual and respiratory component of the tachogram, which are, moreover, also known. We did not use purely simulated signals as they would only provide us a theoretical evaluation of the best method. Moreover, the generation of simulated data requires several preassumptions, such as the extent to which the spectra of the respiratory and residual tachogram overlap, and their relative contributions to the original tachogram. In order to obtain two realistic signals, each of the proposed algorithms was used to estimate a residual tachogram and a respiratory component which has no connection with the residual tachogram as data of another subject were used, and the performance of the remaining algorithms is then evaluated. This cross-validation between the methods ensures a fair comparison and is needed to be implemented as no ground truth of the separated signals is available. It should however be noted that some bias towards OSP might have occurred since this method combines properties of ARMAX and MSPCA. Alternatively, the performance of the separation methods can be evaluated by assessing the absence of coupling between respiration and the residual tachogram, as is also further explained in Chapter 6. The second comparison study is designed to evaluate the robustness of each algorithm as it is important that the algorithm yields similar time signals when a window of 6 minutes is considered than when windows of 2 minutes are used. Without doubt, a good performance in the simulation study is of prime importance; without a correct separation, a good stability is of no use. Conversely, a good separation without a high performance in the stability study should not discard

the use of the algorithm involved, but displays the limitations that should be taken into account.

The simulation study revealed that LMS adaptive filtering has an average performance. Closer inspection of the LMS approach reveals that the use of the Savitsky-Golay filter is an important factor in the performance; when the signals are not smoothed, the performance of adaptive filtering decreases significantly. We should therefore consider including this filter in the other algorithms to further improve the results. Note that the use of a higher order Savitsky-Golay filter will result in limited smoothing, thereby abolishing the beneficial effect of the filter. Although it was expected that adaptive filtering would be least affected by different window sizes, the stability study showed that this method is not as robust as hypothesized.

Both comparison studies indicated that ICA is not a suitable method to separate respiratory influences from the tachogram. Although it was shown in [188] that ICA is a good method to do so, and it does not change the power content, this study shows the inverse. In [188], the simulation study was conducted using LMS adaptive filtering in step 1 and 2, followed by ICA. Our results show that spectral features, especially the HF power, of $\mathrm{RR}_{RSP,S(j)}^{A(i),ICA}$, are largely underestimated using ICA. A possible explanation of the low performance can be found in the presupposition of statistical independency between respiration and heart rate, which can not be assumed. In addition, the stability study showed very low robustness.

MSPCA also shows an average performance. The LF power of the respiratory signal is generally overestimated, while this feature is mostly underestimated in the other algorithms. The main advantage of this method is that several scales are considered, but some arbitrarily chosen parameters largely influence its performance, e.g. the cut-off variance to define when there is a clear relation.

Another method included in our study is the ARMAX model. Generally, this method shows a good performance in the comparison studies. However, the performance can possibly be improved by optimizing the model order. This was fixed at 3 seconds (or 12 samples) to ensure that all possible delayed effects of respiration on the tachogram are taken into account in the model. Nonetheless even without optimization, a satisfactory performance is obtained. In [37] they use this approach to make a model using broadband spectrum. This broadband spectrum was realized using paced breathing. Because it is shown that paced breathing increases the tidal volume [24], they propose a scaling factor to normalize the model for spontaneous breathing. We did not include this procedure as no data were available. In addition, we aim to use this for already analyzed HRV studies, which do not have such broadband breathing spectrum.

Orthogonal subspace projection combines the advantages of MSPCA and ARMAX and also shows to have the best performance. In the simulation study, OSP was the only method of which the difference in spectral features had a distribution around zero. However, similarly as with the ARMAX model, an optimization of the model order might improve the results, as well as the choice of the mother wavelet and its order. The limitation of this method is clear in the stability study; although the spectral features are still reasonably estimated, NRMSE shows that there are discontinuities when the signal is cut in smaller parts. Future research should focus on improving the stability using overlapping windows and subspace tracking to reduce border discontinuities and bias differences, as suggested in [31].

From all the results, we can conclude that OSP and ARMAX are the most reliable methods to separate the tachogram in a respiratory component and a residual tachogram. OSP shows to have the best performance in the simulation study, but the moderate robustness limits its use for longer data. In that case, the ARMAX model should be used.

In future studies, several issues still need to be investigated such as the importance of the measured respiratory signal. In this comparison study, only estimates of the tidal volume are used. The sensitivity to the type of respiratory recording should be examined, as well as the importance of the recording quality. In addition, it should be investigated whether the separation would benefit from nonlinear approaches; in a first study, we only considered linear separation algorithms that were used in the literature. Consequently, possible nonlinear interactions are not taken into account now.

HRV and respiratory oscillations are closely related to blood pressure variations. Indeed, heart rate and blood pressure interact via the feedback (i.e. baroreflex path) and feedforward (i.e. Windkessel effect) mechanisms, and are both influenced by respiration. Hence, many studies have been conducted to model those signals and their interactions, as in [18, 137, 147, 149]. These models could also be used to estimate HRV unrelated to respiration if blood pressure recordings are available. Note however that the present study aimed at investigating the tachogram from which both direct and indirect (via blood pressure) influences of respiration are separated from other sources of HRV, without needing to explicitly define the blood pressure relation to HRV. In this way, HRV analyses can be conducted that are not influenced by the highly debated interaction with respiration. Evidently, one source of the residual tachogram is related to blood pressure and further research is needed to identify other sources of the residual tachogram.

3.4 Real-life example: mental stress classification

The importance of conducting the separation of respiratory influences from the tachogram is demonstrated using the application of stress classification. We aim to show that the classification is enhanced using the residual tachogram instead of the original tachogram.

3.4.1 Data aquisition and preprocessing

The data originate from the mental stress monitoring application as described in Section 1.3. For this real-life example, two randomly chosen resting recovery periods and the two mental stress tasks (MT1 and MT2) of 40 students are used.

The same preprocessing steps of the ECG and respiratory signal as described in Paragraph 3.3.1 are applied. In order to increase the number of signals in the dataset and avoid nonstationarities, each period of 6 minutes is divided in segments of two minutes, with one minute overlap. This procedure results in 10 segments of rest and 10 segments of stress for each subject.

3.4.2 Classifier design

The added value of separating respiratory influences from the tachogram in HRV analyses is assessed by classification of rest and stress segments. A least-squares support vector machines (LS-SVM) classifier is trained using a radial basis function (RBF) kernel and 5-fold cross-validation to avoid overfitting [179]. The data of 32 randomly chosen subjects are used in the training set and the performance is tested on data of the remaining 8 subjects. This setup results in subject-independent classifiers.

Consider stress as the positive class and rest as the negative one, then the performance of each classifier is assessed by means of the sensitivity (S^+), specificity (S^-), positive predictive value (PPV), negative predictive value (NPV), the accuracy (acc) and the area under the ROC (receiver operating characteristic) curve (AUC).

The features used to classify the data segments are spectral indices of the original tachogram RR_{orig}, the residual tachogram RR_{res} and the respiratory component of the tachogram RR_{RSP}, obtained using OSP. The power in the low (LF) and high frequency (HF) band are computed via Welch's method, using a 1024 point fast Fourier transform (FFT), a periodic Hamming window

of a length such that eight equal sections of the tachogram are obtained, and an overlap of 50%. In addition, LFnu $= \frac{\text{LF}}{\text{LF+HF}}$ (normalized units), HFnu $= \frac{\text{HF}}{\text{LF+HF}}$, the ratio LF/HF and the power in the total frequency band TP = LF + HF are considered. These spectral indices are computed for three classifiers using RR_{orig}, RR_{res} and RR_{RSP} separately. Another classifier that combines RR_{res} and RR_{RSP} is constructed.

In addition, a classifier that includes respiratory information in the original tachogram is implemented in order to make a fair comparison with the residual tachogram, because RR_{res} is obtained using additional respiratory information. Therefore, a last classifier that uses the recorded respiratory signal (RSP) is created using three new features: LFnu_{rsp}, HFnu_{rsp} and LFnu/HFnu_{rsp}. These features employ the normalized power as the respiratory signal is in arbitrary units. Typically, the respiratory frequency is narrow banded in the HF band. However, sighs and irregular breathing patterns can lead to power in the LF band, which might contain useful information for the classification.

The following classifiers C are considered:

- $C(\mathbf{RR}_{\text{orig}})$: LF_{orig}, HF_{orig}, LFnu_{orig}, HFnu_{orig}, LF/HF_{orig}, TP_{orig}
- $C(\mathbf{RR}_{\text{orig}}\&\mathbf{RSP})$: LF_{orig}, HF_{orig}, LFnu_{orig}, HFnu_{orig}, LF/HF_{orig}, TP_{orig}, LFnu_{rsp}, HFnu_{rsp}, LFnu/HFnu_{rsp}
- $C(\mathbf{RR}_{\text{res}})$: LF_{res}, HF_{res}, LFnu_{res}, HFnu_{res}, LF/HF_{res}, TP_{res}
- $C(\mathbf{RR}_{\text{RSP}})$: LF_{RSP}, HF_{RSP}, LFnu_{RSP}, HFnu_{RSP}, LF/HF_{RSP}, TP_{RSP}
- $C(\mathbf{RR}_{\text{res}}\&\mathbf{RR}_{\text{RSP}})$: LF_{res}, HF_{res}, LFnu_{res}, HFnu_{res}, LF/HF_{res}, TP_{res}, LF_{RSP}, HF_{RSP}, LFnu_{RSP}, HFnu_{RSP}, LF/HF_{RSP}, TP_{RSP}, $\text{TPnu}_{res} = \text{TP}_{res}/(\text{TP}_{res} + \text{TP}_{RSP})$, $\text{TPnu}_{RSP} = \text{TP}_{RSP}/(\text{TP}_{res} + \text{TP}_{RSP})$, $\text{TP}_{\text{res}}/\text{TP}_{RSP}$.

The most important features of each classifier are determined by 5-fold application of automatic relevance determination (ARD) [179] using different training and test sets. The performance measures of all classifiers are averaged over these 5 runs.

3.4.3 Results

Table 3.1 and Fig. 3.10 show the mean performance of each classifier. We hypothesized that the original tachogram contains modulations from respiration and non-respiration related variations, and that separation of both will reveal

Table 3.1: Performance measures of each classifier (in %)

	$C(\mathrm{RR}_{orig})$	$C(\mathrm{RR}_{orig}$ & RSP)	$C(\mathrm{RR}_{res})$	$C(\mathrm{RR}_{RSP})$	$C(\mathrm{RR}_{res}$ & $\mathrm{RR}_{RSP})$
S^+	63.75	60.75	97.00	75.00	91.00
S^-	50.50	55.00	98.75	57.00	98.25
PPV	56.29	57.45	98.73	63.56	98.11
NPV	58.21	58.36	97.05	69.51	91.61
acc	57.13	57.88	97.88	66.00	94.62
AUC	58.24	60.63	99.89	71.19	99.33

S^+: sensitivity; S^-: specificity; PPV: positive predictive value; NPV: negative predictive value; acc: accuracy; AUC: area under the ROC curve

new information and lead to an increased performance when rest and stress are classified. This study confirms the postulated hypothesis; based on the original tachogram, classification in rest and stress is almost random (accuracy = 57.13%). Even when respiratory information is added, the performance of the classifier does not improve. This indicates that although respiration is influenced by stress, it is not an important marker to classify stress. Possibly, the chosen features to represent the respiratory pattern are too simple. Other features might improve the performance of the classifier. This observation is confirmed when classification is carried out using only RR_{RSP}; the performance is better than with the original tachogram, but the accuracy is barely 66%. An apparent improvement is found when RR_{res} is used, yielding an almost perfect classification (accuracy = 97.88%). Interestingly, combining RR_{res} and RR_{RSP} does not lead to an increased performance, on the contrary.

From these observations we can deduce that respiration not only leads to false interpretations about ANS activity, but the effect of respiration on the tachogram might disguise differences in HRV due to differing respiratory patterns. This study shows that the original tachogram contains HR variations, unrelated to respiration, that seem to be very important to distinguish stress from rest, but these variations are masked by the dominant respiratory influence on the heart rate.

In order to determine the most relevant features for each classifier, automatic relevance determination is applied. The features that are at least three times indicated in the 5-fold iteration are indicated below:

- $C(\mathbf{RR}_{\mathrm{orig}})$: LF_{orig} (3), HFnu_{orig} (3)
- $C(\mathbf{RR}_{\mathrm{orig}}\&\mathbf{RSP})$: LF_{orig} (3), HF_{orig}(3), TP_{orig} (5), LFnu_{rsp} (4)

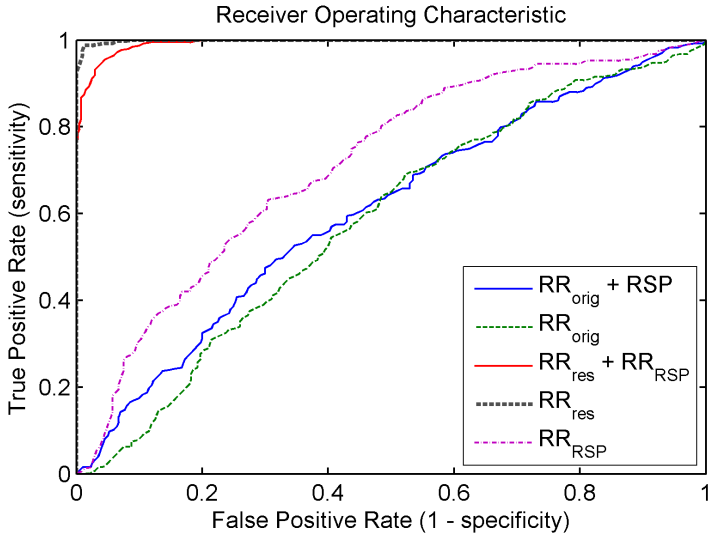


Figure 3.10: Mean ROC of all classifiers.

- $C(\mathbf{RR}_{\text{res}})$: LFnu_{res} (5), HFnu_{res} (5)
- $C(\mathbf{RR}_{\text{RSP}})$: HF_{RSP} (5), LF/HF_{RSP} (3), TP_{RSP} (4)
- $C(\mathbf{RR}_{\text{res}}\&\mathbf{RR}_{\mathbf{RSP}})$: LF_{res} (4), HF_{res} (4), LFnu_{res} (5), HFnu_{res} (5), TP_{res} (5), LF_{RSP} (5), HF_{RSP} (5), LFnu_{RSP} (4), HFnu_{RSP} (4), LF/HF_{RSP} (4), TP_{RSP} (5).

A resemblance between the selected relevant features and the performance of each classifier can be observed as the inferior performing classifiers do not have consistently important features. $C(\text{RR}_{res})$ on the other hand has two key features while the remaining features are never selected by ARD. Fig. 3.11 demonstrates the importance of $\text{LFnu}_{res} = \text{LF}_{res}/\text{TP}_{res}$ in the classification of rest and stress. An almost perfect separation is obtained. Moreover, the results indicate that for the same LF_{res}, HF_{res} is lower during stress than during rest as TP_{res} is higher in rest. This means that the parasympathetic activity that is expected to be represented in HF_{res} is reduced during stress.

Fig. 3.12 displays the PSDs of the original and residual tachograms of one subject during rest and another subject during mental arithmetic. From PSDs of the original tachograms, given in the top panels, no differences in LF_{orig}, HF_{orig}, LFnu_{orig} or HFnu_{orig} can be observed when comparing rest and stress. However, after removal of respiratory influences from the tachogram, differences

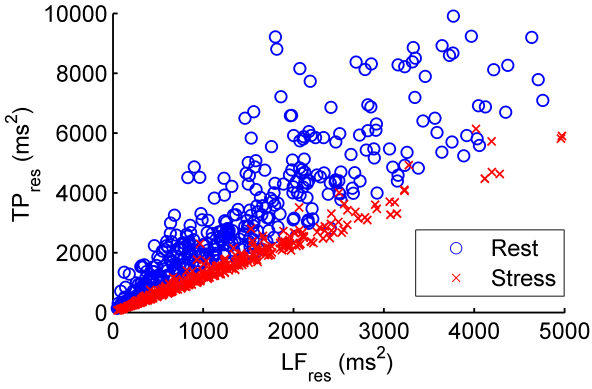


Figure 3.11: The importance of $\mathrm{LFnu}_{res} = \mathrm{LF}_{res}/\mathrm{TP}_{res}$ in the classification of rest and stress is shown: LF_{res} versus TP_{res}.

in LF_{res} and HF_{res} can be noted with a lower LF_{res} and higher HF_{res} during rest than stress (see lower panels of Fig. 3.12). These differences are more apparent when looking at LFnu_{res} and HFnu_{res}, which are exactly those features that appeared to be important in the classification of rest and stress.

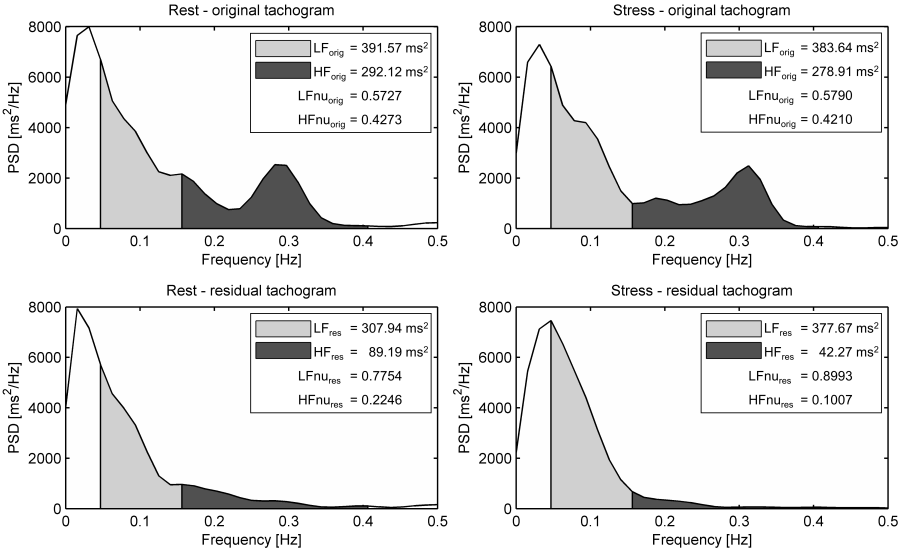


Figure 3.12: Power spectral densities of the original (top panels) and residual (lower panels) tachograms during rest (left) and mental stress (right).

3.4.4 Discussion

The importance of separation of the original tachogram was demonstrated using a real-life example of mental stress classification. The results show that classification using RR_{orig}, with and without additional respiratory information, is almost random. We hypothesized that the original tachogram contains HR modulations of respiration and non-respiration related variations, and that separation of both will lead to an increased performance when rest and stress are classified. This study confirms this; a slightly better performance is obtained when spectral features of RR_{RSP} were used for the classification, but an almost perfect classification was obtained using the residual tachogram. These findings demonstrate that the original tachogram contains HR variations, unrelated to respiration, that seem to be very important to distinguish stress from rest, but these variations might be dominated by the strong respiratory influence on the heart rate.

An important advantage of the followed methodology is the subject-independent classification. In most cases, stress has been considered as a subject-dependent phenomenon and classification was performed in a subject-specific manner, as in [37]. The use of subject-independent classifiers might also explain why inclusion of respiratory information does not lead to an improvement of the performance of the classifier. It has been demonstrated that stress influences the respiratory pattern, but these conclusions are deduced from within-subject comparisons [198, 218]. On a subject-independent level, this information seems to be insignificant.

In this application, OSP was chosen to separate respiratory influences from the tachogram as the data segments have a length of only two minutes. However, in a preliminary study, we also conducted the same stress classification using the ARMAX method, from which we can conclude that similar classification results can be obtained. Possibly, due to the quasi-constant breathing frequency during those two minutes, the strength of the wavelet decomposition in OSP did not need to be exploited, leading to comparable results. Note that we did not conduct stress classification using the other algorithms as they did not provide a reliable separation of respiratory influences from the tachogram. Even if they would obtain good classification results, we would not know whether respiratory or other influences are removed or not, which would lead to problematic interpretations of the results.

However, from these observations we can deduce that the influence of respiration on HRV might not only complicate interpretations regarding ANS activity, it might actually disguise valuable information in the tachogram on efferent ANS activity. These results motivate the conducted comparison study and

demonstrate the importance of the separation in stress classification. However, further studies should confirm the added value of the separation of the tachogram in other cardiorespiratory applications such as analyses of coupling; i.e. this approach might complement analyses of cardiorespiratory coupling by means of phase synchronization between the heart rate and respiration [16]. In addition, future research is needed to determine the physiological meaning of the residual tachogram.

3.5 Conclusion

Cardiorespiratory interactions, such as RSA, are widely studied as they contain information about our autonomic nervous system and cardiac vagal outflow. Whereas most research focuses on finding the correct interpretation of RSA, the research presented in this chapter aimed at separating variations in the heart rate that are related to respiration from HR variations that are not related to respiration. Five algorithms have been proposed in the literature to conduct this separation and are now extensively compared to determine which method is the best to accurately decompose the tachogram in two components. In addition, the robustness of the algorithms is evaluated. The results show that the algorithms based on orthogonal subspace projection and on the ARMAX model yield the best performances, and are therefore advised to be used in future studies.

The importance of separating respiratory influences from the tachogram is demonstrated in the application of stress classification where we showed that the HR variations unrelated to respiration yield almost perfect classification whereas the use of the original tachogram fails. These results prove that the separation of the tachogram can be a very useful tool to investigate changes in the heart rate that are otherwise masked by the dominant effect of respiration.

Chapter 4

Separation of the tachogram using partial time-frequency analyses

In the previous chapter we have evaluated several methods to separate the tachogram into a component that is strictly related to respiration, and another component that is unrelated to respiration. Additionally, we have demonstrated that this approach greatly helps in the application of mental stress classification. In this chapter, we aim to conduct this separation using a time-frequency (TF) approach, that has the advantage over the previously proposed methods that it can deal with nonstationary signals. This is especially interesting in the application of mental stress monitoring, where the physiological signals are more likely to be nonstationary due to the dynamic response to specific mental tasks. After a short introduction with the motivation of this study in Section 4.1, a theoretical framework on cross and partial time-frequency analyses is provided in Section 4.2. The performance of partial TF spectra is evaluated in two simulation studies, as discussed in Section 4.3. Next, Section 4.4 comprises the application of the time-frequency approach to mental stress monitoring. Finally, some concluding remarks are given in Section 4.6. The contents of this chapter is based on [208].

4.1 Introduction

The autonomic nervous system (ANS) dynamically coordinates, among others, cardiovascular variables (such as heart rate and contractility, blood pressure, peripheral resistance), respiration, and the complex interactions between them, of which respiratory sinus arrhythmia (RSA) is probably one of the best known cardiorespiratory interaction. RSA comprises the changes in heart rate in synchrony with respiration, and has been used as a marker that reflects cardiac vagal activity [25]. However, as explained in detail in Chapter 1, the interpretation of RSA has been largely contested [46, 94], driving us to not only study heart rate variations, but to conduct a combined analysis of the cardiac and respiratory system. More specifically, in Chapter 3, we have proposed several methods to separate the tachogram such that we can separately study HR variations that are related to respiration and HR variations that are unrelated to respiration. Additionally, we have demonstrated that with this approach, almost perfect classification of periods of rest and stress was possible using only information derived from the tachogram which was unrelated to respiration. However, due to the nonstationary nature of physiological signals during mental stress testing, the cardiorespiratory data we used, were divided in segments of two minutes. In order to better describe the dynamic interactions between the heart rate and respiration, time-frequency (TF) methods can be used.

In this chapter, we will focus on the changes in cardiorespiratory interactions during mental stress monitoring using time-frequency analyses. Spectral analysis has the advantage of having a clear link with physiology, but has the limitation that it requires stationary signals. The benefit of time domain analyses lies in the dynamic response of the cardiorespiratory coupling to mental stress that is obtained. Time-frequency analyses combine the advantages of time and frequency domain analyses, and thus can be used to analyze nonstationary signals, and in particular to quantify the temporal variations of their spectral content [132, 133].

In addition, we aim to conduct partial TF analyses where influences of respiration on HRV are separated. Partial spectral analysis is a well established, model-free and fully data-driven technique used to modify the spectrum of a signal based on the information carried by another one [21]. A partial TF spectrum represents a modified version of the TF spectrum of signal $x(t)$, from which the magnitude of the components linearly related to signal $y(t)$ have been reduced in a way which is proportional to the coherence between $x(t)$ and $y(t)$. This technique was previously used by Badra et al. to assess the partial coherence between HRV and systolic pressure by removing the influence that respiration exerts on both signals [9]. In this study, we will consider one partial spectrum that

contains HRV related to respiration, and one that is unrelated to respiration. Prior to the application of TF spectra on mental stress monitoring, a simulation study is given in Section 4.3 to assess the performance of partial TF spectra.

In Section 4.4, we will conduct (cross) TF analyses of RR interval series and respiration, and assess their coherence during two similar mental stress tasks and a sustained attention task. We hypothesize to find a strong cardiorespiratory response during the first stress task and also a clear, but reduced, coupling during the second task due to habituation. The attention task is nonstressful and is hypothesized to only induce a small reaction. As the interaction between HRV and respiration is vagally mediated and stress is linked to a reduced vagal control, the strength of the cardiorespiratory coupling is expected to decrease as a response to stress. The partial TF spectrum related to respiration is hypothesized to mainly have HF power, while it is expected that the partial spectrum unrelated to respiration will primarily contain LF power, and only little HF power.

4.2 Time-frequency analysis

4.2.1 Cross time-frequency analysis

The cross time-frequency spectrum $S_{xy}(t,f)$ of signals $x(t)$ and $y(t)$ is estimated using a time-frequency distribution (TFD) [130]:

$$S_{xy}(t,f) = \int\int_{-\infty}^{+\infty} \Phi(\tau,\nu) A_{xy}(\tau,\nu) e^{j2\pi(t\nu-\tau f)} d\nu d\tau \tag{4.1}$$

$$A_{xy}(\tau,\nu) = \int_{-\infty}^{+\infty} x\left(t+\frac{\tau}{2}\right) y^*\left(t-\frac{\tau}{2}\right) e^{-j2\pi\nu t} dt \tag{4.2}$$

where $A_{xy}(\tau,\nu)$ is the cross-ambiguity function. Smoothing is performed by an exponential kernel; in the ambiguity domain, defined as:

$$\Phi(\tau,\nu) = \exp\left\{-\pi\left[\left(\frac{\nu}{\nu_0}\right)^2 + \left(\frac{\tau}{\tau_0}\right)^2\right]^{2\lambda}\right\}. \tag{4.3}$$

In this study, values of τ_0, ν_0 and λ are set to 0.050, 0.046 and 0.3 respectively, leading to a kernel function with a TF resolution of $\{\Delta_t, \Delta_f\} = \{10.9\text{ s}, 0.039\text{ Hz}\}$, where Δ_t and Δ_f quantify the spreading introduced by the kernel [130, 132].

Time-frequency coherence is an estimate of the strength of the local coupling between two signals and is determined by:

$$\gamma_{xy}(t,f) = \frac{|S_{xy}(t,f)|}{\sqrt{S_{xx}(t,f)S_{yy}(t,f)}} \; ; \gamma_{xy}(t,f) \in [0,1]. \tag{4.4}$$

Time-frequency phase difference (TFPD) is given by:

$$\Theta_{xy}(t,f) = \arctan\left[\frac{\Im[S_{xy}(t,f)]}{\Re[S_{xy}(t,f)]}\right] \; ; \Theta_{xy}(t,f) \in [-\pi,\pi]. \tag{4.5}$$

4.2.2 Partial time-frequency analysis

The partial TF spectrum of $x(t)$ from which influences of signal $y(t)$ are removed, can be defined as:

$$\begin{aligned} S_{xx/y}(t,f) &= S_{xx}(t,f) - \frac{S_{xy}(t,f)S_{yx}(t,f)}{S_{yy}(t,f)} \\ &= (1-\gamma^2_{xy}(t,f))S_{xx}(t,f). \end{aligned} \tag{4.6}$$

Its complement, i.e. the partial TF spectrum of $x(t)$ that expresses the coupling with $y(t)$ is determined by:

$$S_{xx,y}(t,f) = \gamma^2_{xy}(t,f)S_{xx}(t,f). \tag{4.7}$$

4.3 Simulation study

4.3.1 Setup

In order to evaluate the performance of partial TF spectra, a simulation study is set up. Let $x_1(t)$ and $x_2(t)$ be two nonstationary signals, each one composed by one or two different complex exponentials showing both amplitude ($A_k(t)$) and frequency ($f_k(t)$) modulations:

$$x_i(t) = \sum_{k=1}^{M_i} A_k(t) exp(j(\phi_k(t) + \theta_k)) \tag{4.8}$$

with $f_k(t) = \frac{1}{2\pi}\frac{d\phi_k(t)}{dt}$, $i = \{1,2\}$ and M_i is the number of spectral components. Let $x(t)$ be:

$$x(t) = x_1(t) + x_2(t) + \xi(t) \tag{4.9}$$

where $\xi(t)$ is complex zero-mean white Gaussian noise, whose standard deviation is adjusted to obtain a SNR equal to 20 dB. In a first simulation study, M_1 and M_2 are respectively 2 and 1. The TF spectra $S_{11}(t,f)$ and $S_{22}(t,f)$ are given in Fig. 4.1. In a second simulation study, an extra component is added to $x_2(t)$, yielding signals with TF spectra shown in Fig. 4.2.

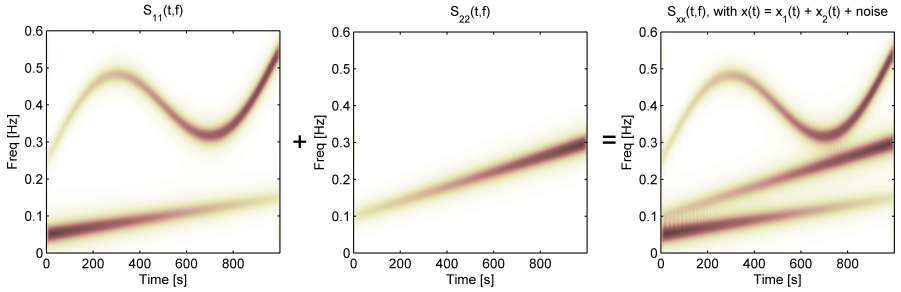


Figure 4.1: Time-frequency spectra of signals $x_1(t)$, $x_2(t)$ and $x(t)$, see Eqs. (4.8)-(4.9), of simulation study 1. Note that $x_1(t)$ and $x_2(t)$ do not share a spectral component.

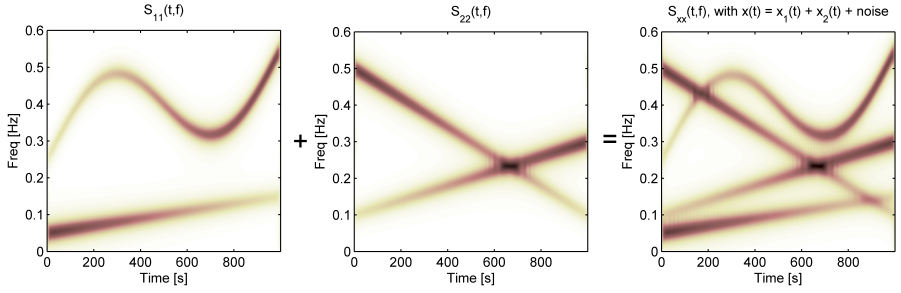


Figure 4.2: Time-frequency spectra of signals $x_1(t)$, $x_2(t)$ and $x(t)$, see Eqs. (4.8)-(4.9), of simulation study 2. Note that spectral components of $x_1(t)$ and $x_2(t)$ intersect in the TF domain.

In the next step of the simulation study, the partial spectrum $S_{xx/2}(t,f)$ is computed. The performance of partial TF spectra is evaluated based on the agreement between $S_{xx/2}(t,f)$ and $S_{11}(t,f)$. This agreement is quantified by the spectral distance d between both TF spectra [131]:

$$d = \frac{\left\| \overline{S_{xx/2}}(t,f) - S_{11}(t,f) \right\|_{l_1}}{\left\| S_{11}(t,f) \right\|_{l_1}} \tag{4.10}$$

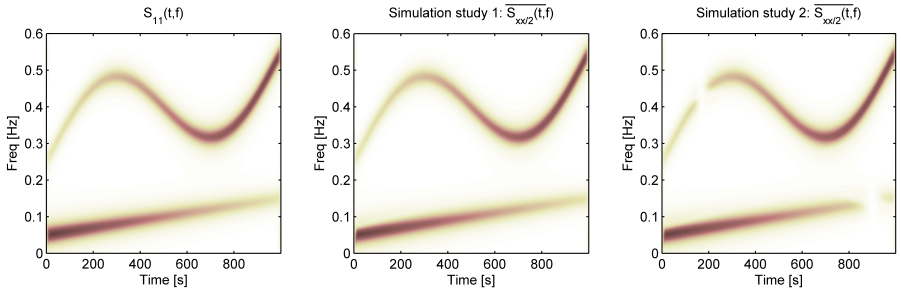


Figure 4.3: Averaged results of the simulation study: (left) TF spectrum $S_{11}(t,f)$; (middle) Partial TF spectrum $\overline{S_{xx/2}}(t,f)$ of simulation study 1; (right) Partial TF spectrum $\overline{S_{xx/2}}(t,f)$ of simulation study 2. In the ideal case, the partial spectrum $\overline{S_{xx/2}}(t,f)$ equals $S_{11}(t,f)$.

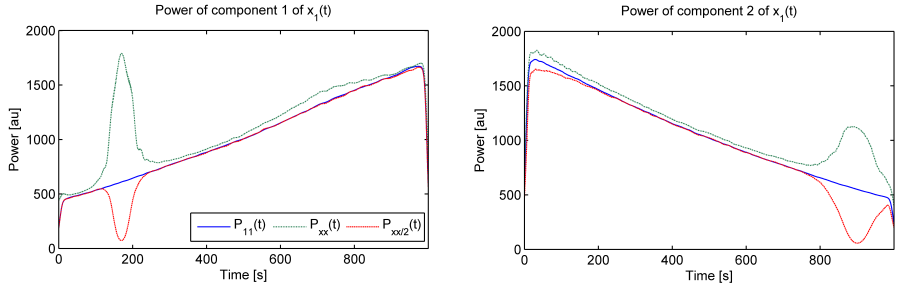


Figure 4.4: Averaged instantaneous power of the two spectral components of $x_1(t)$ in simulation study 2 of $S_{11}(t,f)$, $S_{xx}(t,f)$ and $S_{xx/2}(t,f)$. (left) component 1 of $x_1(t)$, which corresponds to the sinusoidal component; (right) component 2 of $x_1(t)$, which corresponds to the linear component.

with $\overline{S_{xx/2}}(t,f)$ the mean partial TF spectrum estimated over all the realizations of each simulation study and $\|\mathbf{A}\|_{l_1}$ the L1-norm of matrix $\mathbf{A}$.

4.3.2 Results

Each simulation study is performed using 50 different realizations of noise and phases θ_k, derived from a uniform random distribution between $-\pi$ and π. The presented results arise from averaging over these realizations. Fig. 4.3 shows the averaged results of the simulation studies. In the left plot, the TF spectrum $S_{11}(t,f)$ is given. The middle figure displays the partial TF spectrum $\overline{S_{xx/2}}(t,f)$

of the first simulation. A high similarity ($d = 0.20$) between $\overline{S_{xx/2}}(t, f)$ and $S_{11}(t, f)$ is found in the first simulation.

The result of the second simulation study is shown in Fig. 4.3 (right). We can observe 'missing' parts around $t = 170$ s and $t = 900$ s, precisely for those portions of the TF domain in which spectral components of $x_1(t)$ and $x_2(t)$ intersect. A higher spectral distance $d = 0.22$ is found, indicating a slightly lower agreement between $\overline{S_{xx/2}}(t, f)$ and $S_{11}(t, f)$. Fig. 4.4 shows the instantaneous power of the spectral components of $x_1(t)$ in simulation study 2 of $S_{11}(t, f)$, $S_{xx}(t, f)$ and $S_{xx/2}(t, f)$, computed as the mean power in a window Δ_f around the frequency modulation $f_k(t)$ from Eq. (4.8). Components 1 and 2 correspond respectively to the sinusoidal and linear components of $x_1(t)$ with a linear increasing and decreasing power (see $P_{11}(t)$). Remark that the instantaneous power of $S_{xx}(t, f)$ significantly increased around $t = 170$ s and $t = 900$ s, precisely when the instantaneous frequencies of $x_1(t)$ and $x_2(t)$ intersect. The instantaneous power of $S_{xx/2}(t, f)$ decreased in correspondence to these intersections.

4.3.3 Discussion

The use of partial TF analyses was evaluated in two simulation studies, where the performance was assessed by the similarity between $S_{11}(t, f)$ and $\overline{S_{xx/2}}(t, f)$. In simulation study 1, none of the signal spectral components intersect, i.e. they have no overlapping instantaneous frequencies. As shown in the left and middle panels of Fig. 4.3 there is a high correspondence between $S_{11}(t, f)$ and $\overline{S_{xx/2}}(t, f)$, which demonstrates that a good performance is obtained in the case that two signals do not share a spectral component.

In simulation study 2, the instantaneous frequencies of $x_1(t)$ and $x_2(t)$ overlap twice, around $t = 170$ s and $t = 900$ s, where $P_{xx}(t)$ increases and $\overline{S_{xx/2}}(t, f)$ is lower than $S_{11}(t, f)$. A strong reduction in $\overline{S_{xx/2}}(t, f)$ is expected because in these portions of the TF domain, $\gamma^2_{xx}(t, f) \sim 1$ and, by definition, partialization is achieved by removing $\gamma^2_{xx}(t, f)S_{xx}(t, f)$ from $S_{xx}(t, f)$. From this second simulation study, we can conclude that partial TF spectra cannot be used to separate the contribution of two spectral components which are simultaneously oscillating at the same instantaneous frequency. However, this limitation is expected to have little impact on the analysis of cardiorespiratory interactions for the following reasons: (1) RR oscillations locally coupled to and synchronous with respiration are assumed to come from respiration itself; (2) the hypothetical overlapping between HRV oscillations related to and not related to respiration is expected to be low, because the respiratory signal is relatively narrow banded; and (3) as long as the difference between the instantaneous frequencies of the

spectral components of different signals is lower than the frequency resolution (Δ_f), the partial spectrum correctly separates them. A critical evaluation on partial spectral analysis can be found in [8].

In addition, Eq. (4.6) shows that the amount of power in the partial TF spectrum $S_{xx/y}(t, f)$ which is removed from $x(t)$ around (t_0, f_0) is proportional to the coherence between $x(t)$ and $y(t)$ around (t_0, f_0). If at time t_0 $x(t)$ and $y(t)$ share a spectral component with the same instantaneous frequency f_0, their coherence at (t_0, f_0) will be close to 1 and thus the component will be removed, regardless of the amplitude modulation of both components.

Finally, it is important to note that the use of partial TF spectra is motivated by the fact that this approach is (1) non-parametric, i.e. it does not rely on any model, and (2) it is fully data-driven, in contrast to other techniques such as TF filtering; (1) model-based approaches, such as the IPFM model, MVAR models or multivariate point process models offer the opportunity to estimate hidden variables and the strength of directional couplings, but their outcomes strongly depend on the goodness-of-fit of the model. For this reason, we opted for a methodology which, in our view, is more robust to evaluate changes in HRV linearly related and unrelated to respiration. (2) TF filtering requires the use of a TF mask or a smoothing function, where it is necessary to decide on the geometry of the mask, its values and, more importantly, its functioning. This makes the algorithm specific to a given set of signals in a given condition. Our approach, on the contrary, being data-driven, can be generalized to any kind of signal in any possible situation, and provides an easier interpretation of the results as the magnitudes of the partial spectra are proportional to the coherence between HRV and respiration.

4.4 Application: mental stress monitoring

4.4.1 Data and methods

Data acquisition and preprocessing

The data originate from the mental stress monitoring application as described in Section 1.3. The respiratory signal and the RR interval series are resampled at 4 Hz using cubic spline interpolation. Both signals are high-pass filtered at 0.003 Hz to remove very slow oscillations. Differences between the attention task (AT), the two mental stress tasks (MT1 and MT2), and the relaxing documentary watching (RD) are studied.

Derivation of time-varying parameters

In this study, we consider the TF spectrum of the RR interval series ($S_{RR-RR}(t,f)$), and the partial spectrum from which the respiratory influences are removed ($S_{RR-RR/RSP}(t,f)$), and its complement, i.e. the partial TF spectrum which contains RR changes related to respiration ($S_{RR-RR,RSP}(t,f)$).

The time courses of several indices that characterize the interactions between HRV and respiration are derived. We compute the following time-varying parameters for TF spectrum $S_\alpha(t,f) \in [S_{RR-RR}(t,f),\ S_{RR-RR/RSP}(t,f),\ S_{RR-RR,RSP}(t,f)]$ in specific frequency bands β, with f_β the frequencies in β:

- Instantaneous power $P_\alpha^\beta(t) = \sum_\beta S_\alpha(t,f_\beta)\delta_f$ with δ_f the frequency step in the spectrum;
- Instantaneous frequency $f_\alpha^\beta(t)$ is estimated as the frequency of the spectral peak in frequency band β.

The considered bands β are based on the traditional HRV frequency bands:

- $\beta_{LF} = [0.04\text{ Hz}, 0.15\text{ Hz}]$;
- $\beta_{HF} = [0.15\text{ Hz}, 0.40\text{ Hz}]$;
- $\beta_{TOT} = [0.04\text{ Hz}, 0.40\text{ Hz}]$.

In addition, two parameters that describe the local coupling between HRV and respiration in a specific frequency band β_{RSP} around respiration are computed:

- Coherence $\gamma_{RR-RSP}^{\beta_{RSP}}(t) = \text{mean}_{f\in\beta_{RSP}}[\gamma_{RR-RSP}(t,f)]$;
- Phase difference $\Theta_{RR-RSP}^{\beta_{RSP}}(t) = \text{mean}_{f\in\beta_{RSP}}[\Theta_{RR-RSP}(t,f)]$;

where $\beta_{RSP}(t)$ is a time-varying band defined as $f_{RSP}(t) \pm \frac{\Delta_f}{2}$ with $f_{RSP}(t)$ the respiratory frequency. This frequency band is centered around the breathing frequency and lies generally within the traditional HF band.

The last two time-varying parameters that are considered are the instantaneous respiratory frequency, $f_{RSP}(t)$, and heart rate, $HR(t)$, expressed in beats per minute [bpm].

Statistical analysis

The Wilcoxon signed rank test is used to assess statistical differences between the 4 conditions (AT, MT1, MT2 and RD). Because we are interested in the dynamic response to each task, statistical analysis was conducted sample by sample to track the p-values in time. Statistical significance is obtained when $p < 0.05$.

In the case of the instantaneous frequency and power, we are only interested in the relative changes, regardless of the subject's general condition or prior influences. Therefore, a correction was applied at the onset of each task prior to application of the Wilcoxon signed rank test to study only the relative response. The reference is taken as the mean value of each parameter in a window Δ_t around the onset of each task. No correction is applied for the coherence and phase difference.

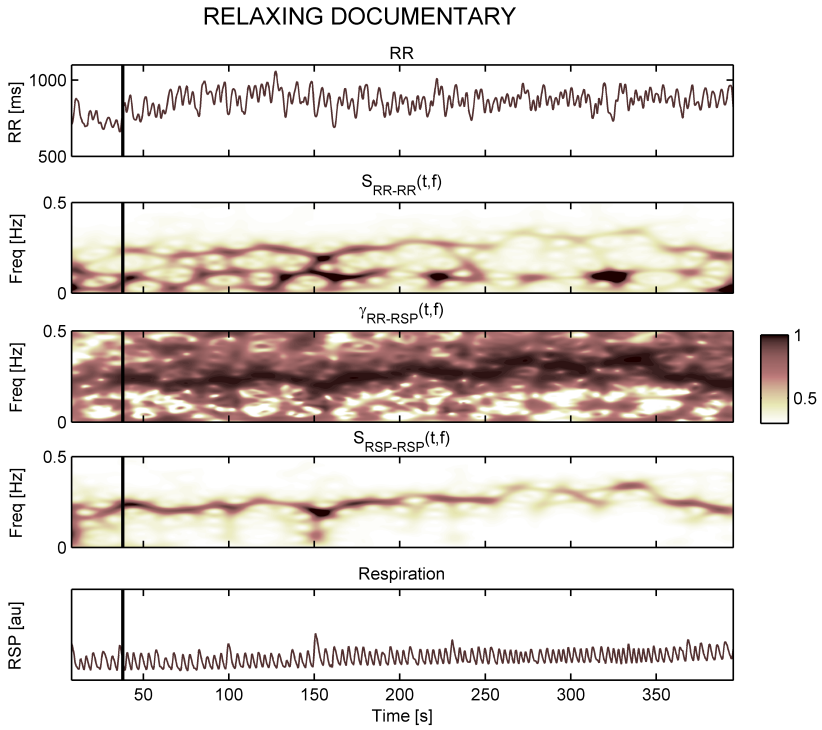
4.4.2 Results

Figs. 4.5(a) and 4.6(a) show the RR interval series, respiratory signal, and TF spectra and coherence of one typical subject during documentary watching (RD) and the first mental stress task (MT1). In the top 2 panels it is shown that both RR and HRV decrease when MT1 is compared with RD for this subject. An increase in the respiratory rate as well as an increased number of sighs are noted during mental stress. A high coherence around respiratory frequency is found during RD, while a reduction in coherence is noticed during stress for this subject.

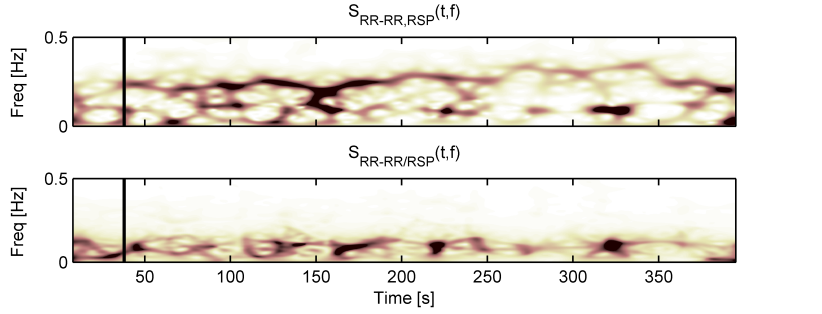
Figs. 4.5(b) and 4.6(b) show the partial TF spectra for the same subject during RD and MT1. During RD, we observe that $S_{RR-RR,RSP}(t,f)$ contains power both in the LF as HF band. On the other hand, $S_{RR-RR/RSP}(t,f)$ includes most power in the LF band. However, note that the HF band still comprises some power, though strongly reduced. $P_{RR-RR,RSP}(t)$ and $P_{RR-RR/RSP}(t)$ decreased during MT1 in comparison to RD.

Time-Varying Parameters

Fig. 4.7 shows the median instantaneous respiratory frequency ($f_{RSP}(t)$), heart rate ($HR(t)$), coherence ($\gamma^{\beta_{RSP}}_{RR-RSP}(t)$) and phase difference ($\Theta^{\beta_{RSP}}_{RR-RSP}(t)$). In addition, the time instances of statistically significant differences between RD and the other tasks are indicated by bars below each subplot. Both $f_{RSP}(t)$ and $HR(t)$ increase during AT, MT1 and MT2, while they slightly decrease

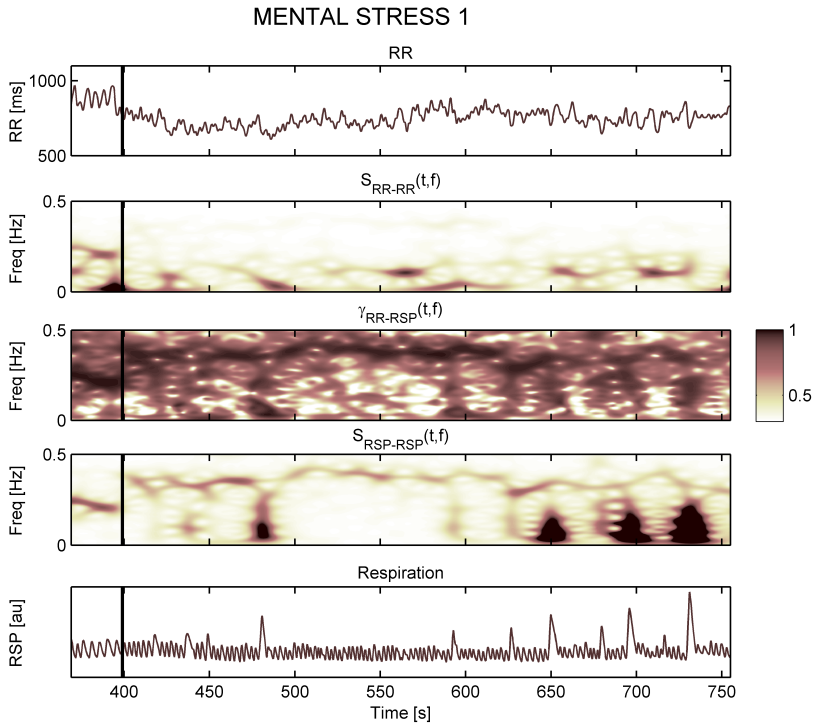


(a)

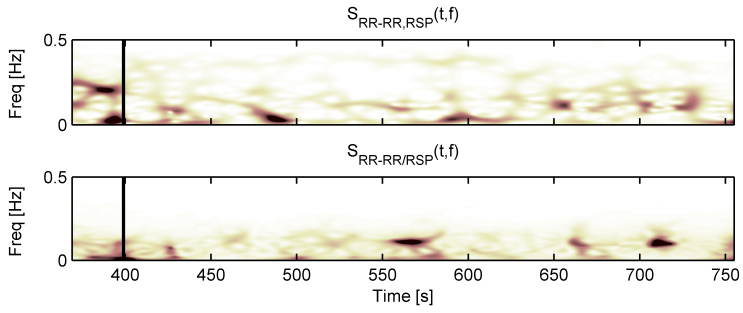


(b)

Figure 4.5: Example of *(a)* RR interval series (RR) and respiratory (RSP) signal, and their TF spectra ($S_{RR-RR}(t,f), S_{RSP-RSP}(t,f)$) and coherence ($\gamma_{RR-RSP}(t,f)$); and *(b)* partial TF spectra ($S_{RR-RR,RSP}(t,f), S_{RR-RR/RSP}(t,f)$) during documentary watching. Vertical lines indicate the onset of RD.



(a)



(b)

Figure 4.6: Example of *(a)* RR interval series (RR) and respiratory (RSP) signal, and their TF spectra $(S_{RR-RR}(t,f), S_{RSP-RSP}(t,f))$ and coherence $(\gamma_{RR-RSP}(t,f))$; and *(b)* partial TF spectra $(S_{RR-RR,RSP}(t,f), S_{RR-RR/RSP}(t,f))$ during the first mental stress task. Vertical lines indicate the onset of MT1.

during RD. Significant differences between RD and the other conditions are observed within 10 s after onset of each task, throughout the whole task for $f_{RSP}(t)$. No differences are found between AT, MT1 and MT2. In the heart rate, significant differences are found a few seconds after onset of each task, between all conditions, except between AT and MT2. The heart rates differ maximally after 30 s from the onset of the task. After 100 s, no consistent differences between the 4 conditions are observed.

Mental stress exhibits a reduction in cardiorespiratory coherence compared to RD and AT. This is only significant for MT1. No other differences in coherence between all conditions can be observed. The phase difference does not show any consistent difference as a result of mental stress or attention.

Fig. 4.8 shows the median instantaneous power in the total frequency band. $P^{TOT}_{RR-RR}(t)$ decreases during mental stress. This reduction is statistically significant already 10 s after onset of the mental task. Also a significant, but smaller, reduction is found during AT after 20 s. When considering the partial spectra, we observe a similar pattern in $P^{TOT}_{RR-RR,RSP}(t)$. $P^{TOT}_{RR-RR/RSP}(t)$ shows statistically significant differences between RD and MT1 from 40 s till 100 s, between RD and MT2 from 30 s till 120 s, and between RD and AT from 45 s till 80 s.

Fig. 4.9 shows the median instantaneous power for TF spectra $S_{RR-RR}(t,f)$, $S_{RR-RR,RSP}(t,f)$ and $S_{RR-RR/RSP}(t,f)$ in the LF band. Interestingly, $P^{LF}_{RR-RR}(t)$ displays a significant reduction during MT2. This reduction is also found during MT1 and AT compared to RD, but to a lesser extent. A similar pattern is observed in $P^{LF}_{RR-RR,RSP}(t)$, suggesting that this reduction may be related to respiration; $P^{LF}_{RR-RR/RSP}(t)$ shows only a significant reduction during MT1 and AT, but not during MT2.

Fig. 4.10 displays the median instantaneous power for TF spectra $S_{RR-RR}(t,f)$, $S_{RR-RR,RSP}(t,f)$ and $S_{RR-RR/RSP}(t,f)$ in the HF band. In the HF band of $S_{RR-RR}(t,f)$, we observe significant differences between 20 s and 50 s when comparing MT1 and AT with RD. This reduction is also found in $P^{HF}_{RR-RR,RSP}(t)$ and to a lesser, but still significant, extent in $P^{HF}_{RR-RR/RSP}(t)$ (only for MT1), showing that the differences that appear in the HF band can be attributed to both HRV related and unrelated to respiration. In contrast with the findings in the LF band, MT2 shows no significant difference with any of the other conditions.

The median instantaneous frequencies in the HF band for TF spectra $S_{RR-RR}(t,f)$ and $S_{RR-RR,RSP}(t,f)$ are given in Fig. 4.11. The instantaneous frequencies in the LF band are not shown as they do not exhibit significant differences between the conditions. The top figure shows $f^{HF}_{RR-RR}(t)$, which is

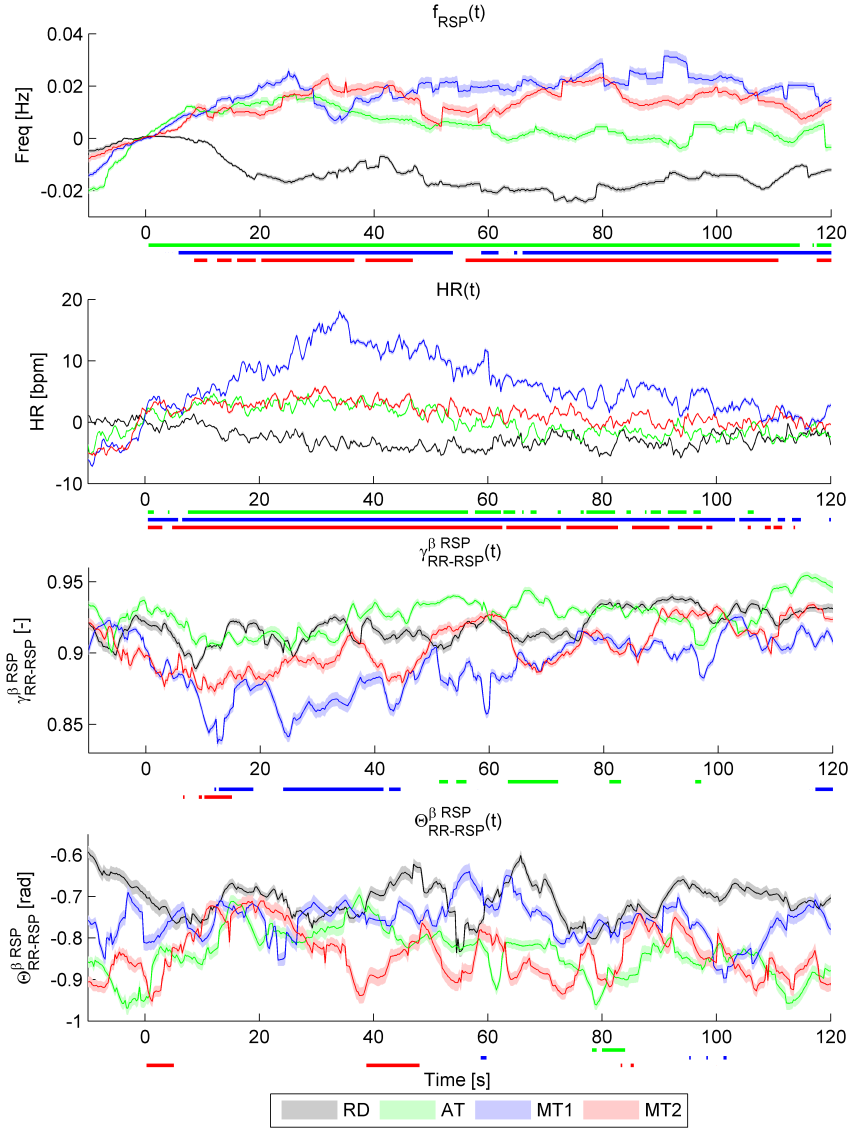


Figure 4.7: Median instantaneous respiratory frequency ($f_{RSP}(t)$), heart rate ($HR(t)$), coherence ($\gamma^{\beta_{RSP}}_{RR-RSP}(t)$) and phase difference ($\Theta^{\beta_{RSP}}_{RR-RSP}(t)$) in the time-varying band $\beta_{RSP}(t)$. The standard error is shaded. The bars below each subplot indicate the time instances of significant differences between RD and the tasks.

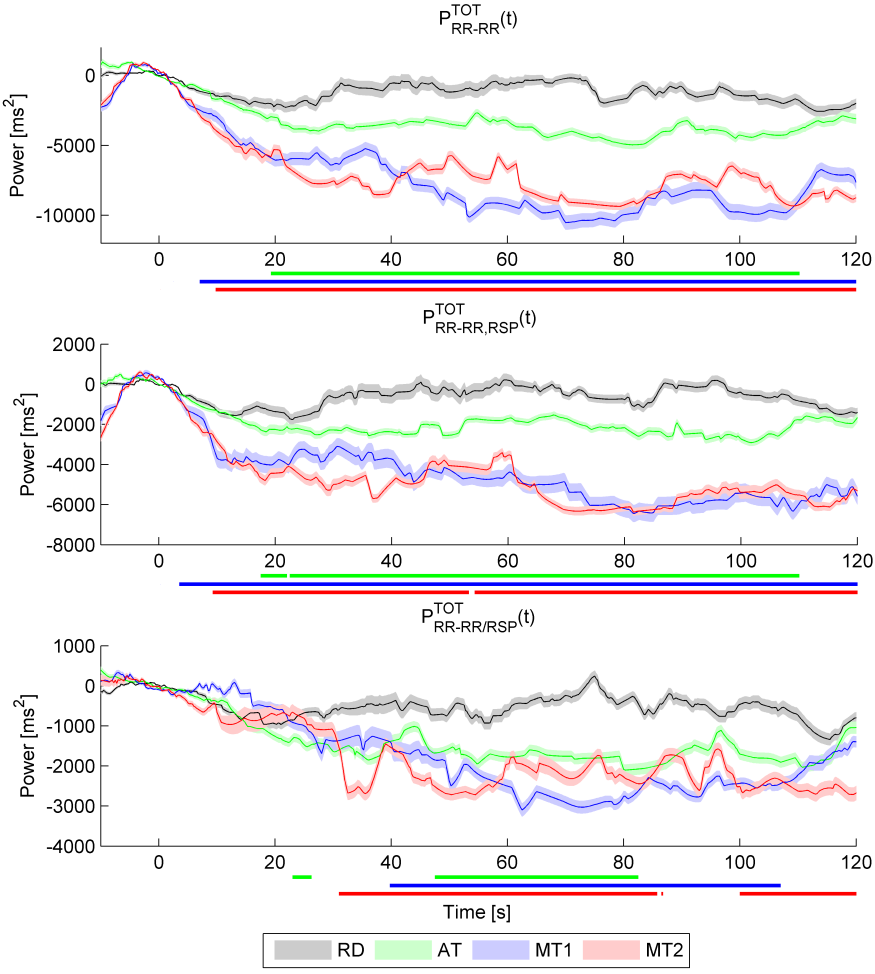


Figure 4.8: Median instantaneous power for TF spectra $S_{RR-RR}(t,f)$, $S_{RR-RR,RSP}(t,f)$ and $S_{RR-RR/RSP}(t,f)$ in the total frequency band. The standard error is shaded. The bars below each subplot indicate the time instances of significant differences between RD and the tasks.

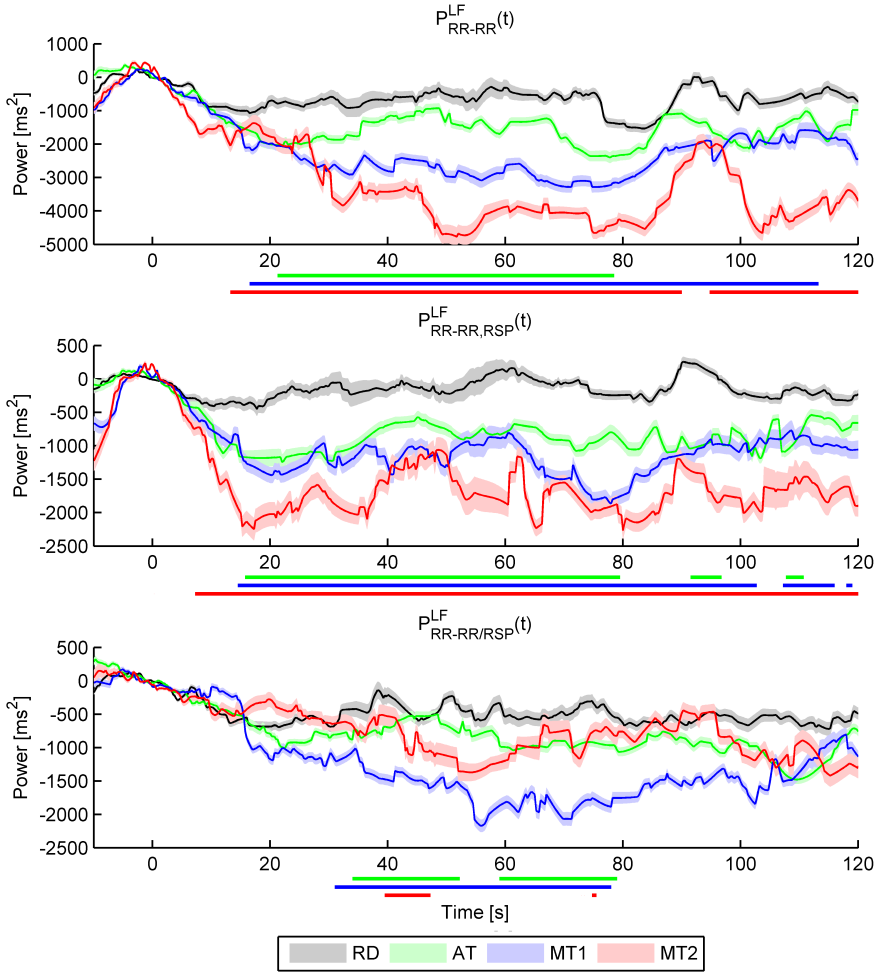


Figure 4.9: Median instantaneous power for TF spectra $S_{RR-RR}(t,f)$, $S_{RR-RR,RSP}(t,f)$ and $S_{RR-RR/RSP}(t,f)$ in the LF band. The standard error is shaded. The bars below each subplot indicate the time instances of significant differences between RD and the tasks.

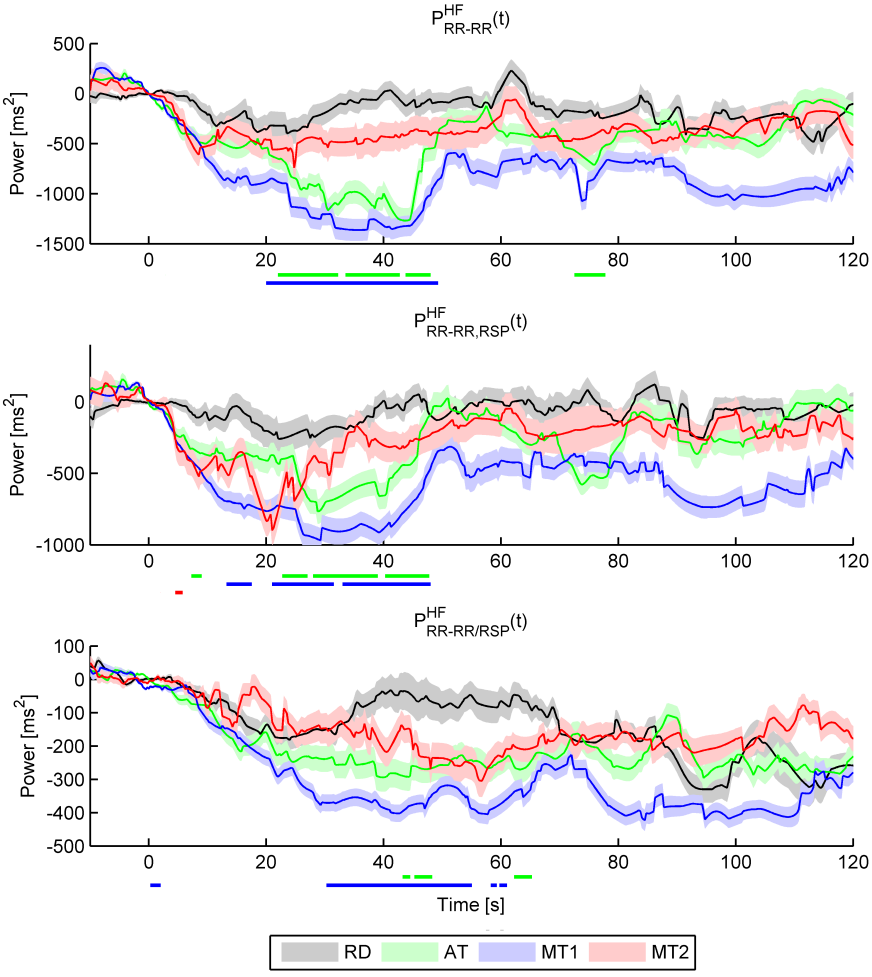


Figure 4.10: Median instantaneous power for TF spectra $S_{RR-RR}(t,f)$, $S_{RR-RR,RSP}(t,f)$ and $S_{RR-RR/RSP}(t,f)$ in the HF band. The standard error is shaded. The bars below each subplot indicate the time instances of significant differences between RD and the tasks.

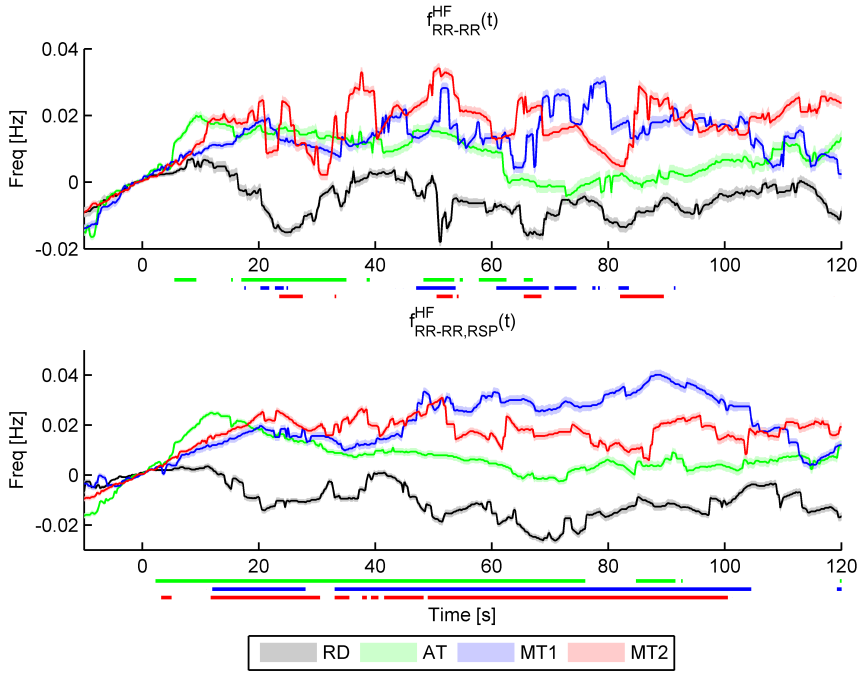


Figure 4.11: Median instantaneous frequency for TF spectra $S_{RR-RR}(t,f)$ and $S_{RR-RR,RSP}(t,f)$ in the HF band. The standard error is shaded. The bars below each subplot indicate the time instances of significant differences between RD and the tasks.

expected to be highly coupled to respiration. This is confirmed when looking at $f^{HF}_{RR-RR,RSP}(t)$, which shows a highly similar pattern as $f_{RSP}(t)$ in Fig. 4.7. Also here, significant differences between AT, MT1 and MT2, and RD are found. Note that we have chosen to not display the instantaneous frequencies in the HF band for $S_{RR-RR/RSP}(t,f)$ since these spectra are not narrow banded, and thus have no clear physiological meaning.

4.4.3 Discussion

Time-frequency analyses were conducted as they provide the time course of spectral indices which have an established physiological interpretation. The proposed TFD was used in previous research [130,132,133] and proved to provide

a better TF resolution and localization than spectrogram and continuous wavelet transform of the local coupling between two signals.

The heart rate shows a clear increase due to mental stress and sustained attention. These findings are in agreement with those reported in [24,138,180,201]. In line with the hypothesis, the largest increase is found during MT1, while a smaller increase is observed during MT2 and AT, suggesting a positive correlation between HR and mental load.

Also in line with our hypothesis is the decrease in the total power of HRV that is more pronounced during the mental tasks than during the attention task. Watching the documentary also gives rise to a brief reduction in total power immediately after onset of the task. These results suggest that mental stress causes vagal withdrawal, and sustained attention also a small reduction in vagal activity.

As previously reported in [180], the strongest reduction of HF power corresponds to MT1. Moreover, this study reveals that the reduction during AT is mainly due to the initial drop in HF between 20 and 50 s. The effect of MT1 is also strongest during this interval, but a small reduction persists throughout the whole task. In contrast to what was found in [180], no significant difference between MT2 and RD was observed, indicating that habituation might have occurred during MT2. The influence of the second mental stress task is only seen in the LF band, which corresponds to both sympathetic and vagal influences. A small reduction is found during AT and MT1. These results are in contrast with the findings by Taelman et al. using the original RR interval series [180]. They found a strong reduction in LF power during MT1 and AT, but MT2 did not differ significantly from RD. When conducting TF analyses, they did report significant differences between AT and MT2, but no differences between AT and MT1. We can observe a similar pattern, i.e. the largest difference is between AT and MT2. However, these differences are not significant in this study. The differing results might arise from the applied correction to study only relative changes, thereby discarding possible effects from prior tasks. This was not implemented in [180].

The respiratory frequency increases during AT and MT, which was also reported in [198]. This is an important parameter to take into account as many authors suggest that an inverse relationship between RSA magnitude and respiratory rate exists, which is independent of vagal activity [43,73,153,154]. Seeing that HF power is often taken as a measure of RSA, it is of utmost importance to be able to distinguish changes in HF due to vagal control or due to changes in respiratory rate. The same reasoning holds for the depth of breathing, as it is also shown that this influences RSA magnitude independently of vagal outflow. In this TF framework, information on the depth of breathing can be obtained

in $P_{RSP-RSP}^{\beta_{RSP}}(t)$. We found, however, that in this study, the depth of breathing did not differ significantly among the tasks or compared to RD.

We observed that the coherence slightly decreases during stress. This effect as a result to mental stress was hypothesized, due to vagal withdrawal and sympathetic activation [48]. The phase difference remains constant during the different conditions and is thus not affected by stress nor attention.

Partial TF Analysis

Figs. 4.9 and 4.10 show that there are similar time courses in the 4 conditions between $P_{RR-RR}(t)$ and $P_{RR-RR,RSP}(t)$ in the LF and HF band. This indicates that both the RR interval variations in the LF and HF band are highly coupled to respiration and demonstrates the dominant effect of respiration on HRV, as can also be observed in the instantaneous high frequency in Fig. 4.11. However, the question rises what the physiological interpretation is of this cardiorespiratory coupling in the LF band. Note that during the computation of indices from the LF band, we verified that the respiratory frequency did not fall within this band. If we did encounter slow respiratory rates, we did not compute the indices at those time instances. Possibly, the respiratory influences in the LF band can be explained by the baroreflex feedback theory or irregular breathing patterns, as was suggested by Yildiz and Ider [224].

Also in the total band, the effect of respiration is apparent. Moreover, the effects of stress in $P_{RR-RR,RSP}^{TOT}(t)$ are already pronounced after 3-7 s, while in $P_{RR-RR}^{TOT}(t)$ a significant difference was only found after 10 s. Both in $P_{RR-RR}^{TOT}(t)$ and $P_{RR-RR,RSP}^{TOT}(t)$ the effect of sustained attention is detected after 20 s.

As expected, most of the power in the HF band is related to respiration. However, there is still some HF power in $S_{RR-RR/RSP}(t, f)$, that furthermore shows effects related to stress. Opposed to what we hypothesized, $P_{RR-RR/RSP}^{LF}(t)$ does not show a clear discrimination between the conditions. Only a slight reduction is found during MT1 and AT. The analysis of $P_{RR-RR/RSP}^{TOT}(t)$ exhibits differences between RD and the other tasks; the effects of sustained attention appear only for a short interval, from 45 s to 80 s, while the influence of stress on physiological processes, other than respiration, is observed after 30 s and lasts till 100 s.

The results from partial TF analysis suggest that the effects of stress are mainly related to respiration. Although it was hypothesized that HRV unrelated to respiration would show enhanced stress influences, as was found during classification of rest and stress [219], we found only small differences between the active tasks and RD. The partial TF analyses revealed different temporal

patterns as a result of stress; a fast response (within 7 s) is observed in HRV related to respiration, as shown in Fig. 4.8, while RR interval variations unrelated to respiration are only apparent after 30 s.

Finally, it is important to note that the results not only display different responses to mental stress and attention; also differences between MT1 and MT2 can be observed. Although both tasks are the same, they present a different response, in terms of magnitude and latency. We hypothesized that the response to stress would be faster and stronger during MT1, while during MT2 the effect of stress would be reduced due to habituation, as was also observed by Taelman et al. [180]. This hypothesis is confirmed in terms of heart rate, coherence, HF and total power.

4.5 Methodological comments

As given in Eqs. (4.6) and (4.7), the computation of partial time-frequency spectra relies on the TF coherence, which is defined according to Eq. (4.4). The time-frequency coherence estimates the local coupling between two signals and though we have shown in the simulation study of Section 4.3 that this approach of partial TF spectra is able to correctly separate different components, the TF coherence has a limitation which was not taken into account; the coherence estimate of two uncorrelated signals is not null due to the local averaging of the smoothing function (Eq. (4.3)), causing an uncertainty in the interpretation of coherence estimates [132]. To mitigate this limitation, we can assess the significance of the estimated coherence based on the relative power of the (t, f) point in the autospectra, or based on a statistical threshold [132]. The lack of significant coherences might explain the large portion of LF power in the partial spectrum related to respiration in Fig. 4.9 and it is to be tested how the results would change and possibly correspond more to the results obtained in Chapter 3 if we implement this constraint for TF coherence in the computation of partial TF spectra.

4.6 Conclusion

The goal of this study was to characterize the dynamic interactions in the cardiorespiratory regulation. As such, a time-frequency approach was chosen, which is able to deal with the nonstationary data recorded during mental stress monitoring. To study cardiorespiratory interactions, cross time-frequency analyses were conducted. In addition, partial TF spectra were computed to

evaluate separately the response of RR interval variations linearly related to respiration, and variations that are not linked to respiration.

Sustained attention was adopted as a nonstressful task during which we observed an increased heart and respiratory rate, and a slightly increased coherence. A transitory reduction of HF power suggests a vagal withdrawal during the first minute. Partial TF analyses showed that the response to sustained attention of RR interval variations related to respiration differs from documentary watching after 20 s, while HRV unrelated to respiration exhibits a significant response after 45 s. After 80 s there is no effect detected of this attention task.

We found that mental stress causes an increase in heart rate and respiratory rate. Also a reduction in cardiorespiratory coherence, HF power and LF power was found, indicating vagal withdrawal. The partial TF analysis revealed that the response to stress of RR interval variations related to respiration appears very fast (3 s), while the variations unrelated to respiration react with a slower temporal pattern (30 s).

Chapter 5

Information dynamics in cardiorespiratory time series

In this chapter, we deal with the third and last aim of the thesis, i.e. the characterization of cardiorespiratory dynamics. First, a short overview of methods that are often used to quantify the cardiorespiratory coupling is given in Section 5.1. Our focus lies on information theory to quantify the amount of information that is present in cardiorespiratory data and determine directional interactions. A theoretical framework in which several information-theoretic measures are introduced, is provided in Section 5.2. Additionally, methods to estimate the entropies are discussed. In Section 5.3, these measures are evaluated during a controlled breathing protocol. Finally, the information-theoretic measures are analyzed during mental stress monitoring in Section 5.4, followed by some concluding remarks in Section 5.5. The contents of this chapter is based on [204, 206].

5.1 Introduction

The cardiorespiratory system plays an important role in human physiology. Therefore, it has been studied extensively in the past decades. Most approaches cover monovariate analyses of cardiac or respiratory time series to study e.g. time domain or spectral heart rate variability [182] or correlation properties [140, 198], or employ the recently developed phase-rectified signal averaging (PRSA) [19, 93]. However, as established in Chapter 1, the cardiac and respiratory systems strongly interact, with respiratory sinus arrhythmia one of the best

known cardiorespiratory interaction. Though RSA has been studied widely, no consensus has been reached so far on the interpretation and quantification of RSA. Nevertheless, several methods have been developed to analyze the couplings in dynamical systems, such as the cardiac and respiratory systems. The simplest methods include cross-correlation and coherence analyses, but they might be insufficient to study complex physiological systems and their interactions. In particular, there is a growing interest to detect and quantify the strength and direction of couplings in the cardiorespiratory system to acquire more insight in the physiological regulatory mechanisms. A detailed review of cardiorespiratory coupling methods is provided by Schulz and colleagues in [165] and is briefly summarized below.

One class of coupling methods comprises the symbolization of bivariate time series. In joint symbolic dynamics, the time series are transformed into a bivariate symbol vector, based on increased, decreased or unchanged values in the time series. Some detailed information is lost in this transformation, but the invariant, robust properties of the dynamics are kept. The probabilities of symbol occurrences are then used as measures to assess bivariate couplings [20, 92]. Another related method, yet not based on symbolization, is bivariate phase-rectified signal averaging (BPRSA). BPRSA firstly defines anchor points in one signal based on properties from the other signal. Next, windows around these anchor points are selected, and aligned. Lastly, the windows are averaged, to obtain a BPRSA curve, in which non-periodic components that are not phase synchronized with the anchor points, are cancelled out, and only events that have a fixed phase relationship with the anchor points are kept. The BPRSA curve is then used to study quasi-periodic oscillations and causality in the bivariate time series [167]. Related to the latter method, is another class of coupling methods that is based on phase synchronization [157]. The idea behind this approach originates from coupled oscillators that have a certain relation between the phases of interacting signals, but their amplitudes remain chaotic and nearly uncorrelated. This approach reveals whether the interaction is bi- or unidirectional and also quantifies the degree of asymmetry of the bidirectional coupling [158]. Phase synchronization is also used with the synchrogram to detect phase and frequency locking ($n : m$) [15, 91, 109, 161, 189].

Another popular approach to study couplings between time series comprises Granger causality that assesses whether one time series has a causal influence on another time series if the past of one time series is useful to predict the future of the other time series. Granger causality can be determined via linear and nonlinear methods. Linear methods model the data as a parametric multivariate autoregressive process, and direct causal couplings are assessed based on the predictability improvement. An important extension was proposed by Porta et al. to account for respiration when Granger causality is studied in

cardiovascular time series [148]. Linear approaches to compute Granger causality in the frequency domain have also been often used and include partial directed coherence [7, 55, 123] and directed transfer function [165]. These linear methods to assess Granger causality assume linearity and depend on the goodness-of-fit of the chosen model. As such, methods have been developed to quantify causality in nonlinear signals [56, 114].

The last class of coupling methods comprises methods based on entropy, in which the uncertainty or predictability between time series is determined. Mutual information is used to determine the shared information in multivariate time series [143], while the cross-conditional entropy measures the amount of information that is included in one time series given the past samples of another series [146, 151]. Lastly, transfer entropy was proposed to quantify to which extent the dynamics of one signal influences the conditioned transition probabilities of another signal, and is able to distinguish effectively driving and responding elements and to detect asymmetry in multivariate signals [164]. It has been shown that for Gaussian stochastic processes, Granger causality and transfer entropy are equivalent [14]. In principal, transfer entropy is a model-free approach. However, due to bias in the estimation of the probability distributions of the Shannon entropy, often multivariate autoregressive models are used to determine the conditional entropy. Yet, these models assume that the multivariate process has a joint Gaussian distribution, and only linear interactions are taken into account. Therefore, improved estimations for the conditional entropy have been proposed using a model-free approach with non-uniform embedding [58, 60].

In this chapter, we will focus on the latter coupling approach based on entropy. Information theory has proven to be useful to evaluate directional interactions in cardiorespiratory data [59], and gives other insights than the traditional HRV analyses and analyses of cardiorespiratory coupling by means of e.g. correlation, coherence and synchronization methods. Additionally, based on the results of the separation of the tachogram from Chapters 3 and 4, we aim to separately study dynamics in the tachogram that are related to respiration and dynamics which are unrelated to respiration. Therefore, we aim to quantify cardiorespiratory data in terms of information storage and internal information in the tachogram and information transfer and cross information from respiration to HRV [61].

This chapter is organized as follows: Section 5.2 provides a theoretical framework in which measures of information transfer and storage, as well as cross and internal information are introduced. Also, methods to estimate the entropies are discussed. Next, Section 5.3 presents a real-life example in which these information-theoretic measures are evaluated during a controlled breathing protocol. In Section 5.4, these measures are analyzed during mental stress monitoring, followed by some concluding remarks in Section 5.5.

5.2 Methods

5.2.1 Information-theoretic measures

Consider a system that consists of two interacting subsystems X and Y, and we are interested in the information contained in the present sample y_n. Let $\mathbf{v}_n^X$ and $\mathbf{v}_n^Y$ be the past states of X and Y respectively, then we can define the predictive information P_Y of our target process Y as

$$P_Y = H(y_n) - H(y_n|\mathbf{v}_n^{X,Y}), \tag{5.1}$$

where $H(y_n)$ is the Shannon entropy that measures the amount of information that is carried by the present sample n of the process Y and that can be determined by $H(y_n) = -\sum p(\mathrm{y}_n)\ln p(\mathrm{y}_n)$. $H(y_n|\mathbf{v}_n^{X,Y})$ is the conditional entropy with $\mathbf{v}_n^{X,Y}$ the past states of both X and Y. The predictive information P_Y, then, determines how much of the information carried by y_n can be predicted by the knowledge of the past of X and Y. A graphical interpretation of P_Y can be found in Fig. 5.1a.

Let X, the driver signal, be the respiratory signal and Y, the target signal, the RR interval series, then we can decompose the predictive information P_Y in one term that describes the information transfer going from the respiratory signal X to the RR interval series Y, and another term that contains the information storage of Y, according to

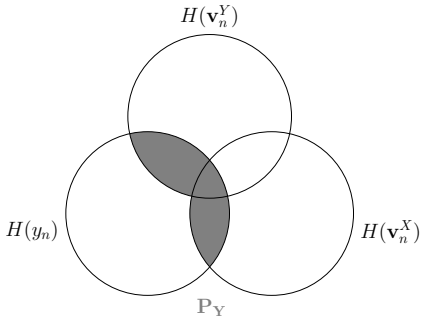
$$P_Y = \underbrace{H(y_n) - H(y_n|\mathbf{v}_n^Y)}_{S_Y} + \underbrace{H(y_n|\mathbf{v}_n^Y) - H(y_n|\mathbf{v}_n^{X,Y})}_{T_{X\to Y}}, \tag{5.2}$$

with S_Y the self-entropy, a measure of information storage that quantifies how much of the information that is carried by y_n can be predicted by the knowledge of its own past [108], and $T_{X\to Y}$ the well-known transfer entropy, a measure of information transfer that quantifies how much of the information carried by y_n that can be predicted by the past of X, conditioned to the knowledge of the past of Y [164]. As such, $T_{X\to Y}$ describes the additional predictability that the past of X brings about the present of Y that was not brought already by the past of Y [61]. $T_{X\to Y}$ and S_Y are graphically represented in Fig. 5.1b.

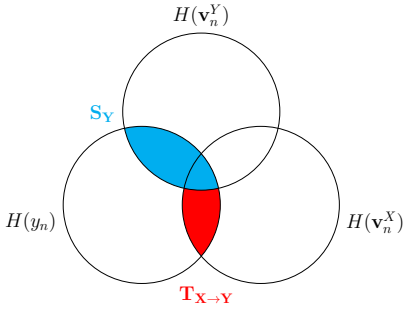
Alternatively, the predictive information of Y can be decomposed by first considering the past of driver X, leading to

$$P_Y = \underbrace{H(y_n) - H(y_n|\mathbf{v}_n^X)}_{C_{X\to Y}} + \underbrace{H(y_n|\mathbf{v}_n^X) - H(y_n|\mathbf{v}_n^{X,Y})}_{S_{Y|X}}, \tag{5.3}$$

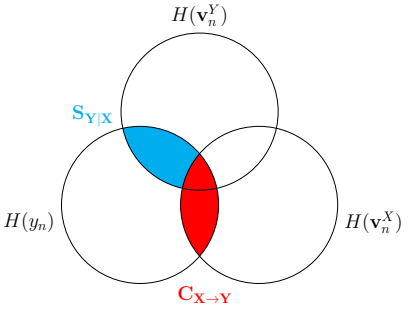
with $C_{X\to Y}$ the cross-entropy from X to Y and $S_{Y|X}$ the conditional self-entropy. $C_{X\to Y}$ is a measure of cross information that quantifies how much



(a) Predictive information P_Y



(b) Transfer entropy $T_{X\to Y}$ and self-entropy S_Y



(c) Cross-entropy $C_{X\to Y}$ and conditional self-entropy $S_{Y|X}$

Figure 5.1: Graphical interpretation of information-theoretic measures.

information carried by y_n can be predicted by the knowledge of the past of X. $S_{Y|X}$ constitutes a measure of internal information that describes how much information carried by y_n can be predicted by its own past, conditioned to the past of X, and thus $S_{Y|X}$ describes the additional predictability that the past of Y brings about its present that was not brought already by the past of X [61]. A graphical interpretation of $C_{X\to Y}$ and $S_{Y|X}$ can be found in Fig. 5.1c.

With X = RSP, the respiratory signal, and Y = RR, the RR interval series, we then have P_{RR} as the predictive information of the RR interval series. $T_{RSP\to RR}$ and $C_{RSP\to RR}$ are measures of respectively information transfer and cross information that can be considered as indices of cardiorespiratory coupling. S_{RR} and $S_{RR|RSP}$ are information-theoretic measures of respectively information storage and internal information in the RR interval series.

5.2.2 Entropy estimation

In order to determine the entropies, the probability function $p(\cdot)$ needs to be estimated. To this end, a linear model-based approach and a nonlinear model-free approach can be used. In the model-based approach, the dynamics of the time series are represented using a bivariate vector autoregressive (VAR) model. In this way, one can easily translate the information-theoretic measures in spectral representations, which, in turn, can be coupled to particular rhythms such as Mayer waves or respiratory frequency in cardiorespiratory time series [59]. However, this model assumes a joint Gaussian distribution which might not always be a valid hypothesis and which only takes linear cardiorespiratory interactions into account. Alternatively, a model-free approach can be used that does not make any prior assumptions about the probability distribution.

Model-based approach

Consider the stationary bivariate process $\mathbf{U}$ that is composed of two zero-mean discrete processes X and Y, and at time n, we have the stochastic variables $\mathbf{u_n} = [x_n, y_n]^T$. Assuming that the bivariate process has a joint Gaussian distribution, then all dynamics in $\mathbf{U}$ can be represented using a bivariate vector autoregressive (VAR) model

$$\mathbf{u_n} = \sum_{k=1}^{P} \mathbf{A}_k \mathbf{u}_{n-k} + \mathbf{e_n} \tag{5.4}$$

with P the model order, $\mathbf{A}_k$ a 2×2 coefficient matrix and $\mathbf{e_n}$ a vector of two white, uncorrelated noise processes with variances σ_X^2 and σ_Y^2. Via the least-squares method, the parameters of the autoregressive model can be estimated. The model order P can be determined via the minimum description length method or the Akaike information criterion. The maximum number of lags taken in this chapter is 5 s (= 10 samples using a sampling frequency of 2 Hz).

Under the assumption of a joint Gaussian distribution, we can then quantify the entropies as:

$$H(y_n) = \frac{1}{2}\ln\, \sigma_Y^2 + \frac{1}{2}\ln\, (2\pi e) \tag{5.5}$$

$$H(y_n|\mathbf{v}_n) = \frac{1}{2}\ln\, \sigma_{Y|\mathbf{v}_n}^2 + \frac{1}{2}\ln\, (2\pi e) \tag{5.6}$$

where the partial variance $\sigma_{Y|\mathbf{v}_n}^2$ of y_n given $\mathbf{v}_n$ can be computed as the variance of the residuals of a linear regression of y_n on $\mathbf{v}_n$ [54]. The statistical significance

of the information-theoretic measures can be assessed by an F-test checking whether the past states of X and/or Y explain a significant portion of the variance of Y.

Model-free approach

In the model-free estimation approach, the conditional entropy is computed according to a procedure for nonuniform conditioning, designed to select - among all possible lagged components forming the past of X and Y - only those components which contribute significantly to the description of the present of the target y_n. This is essential to counteract the curse of dimensionality and provide reliable estimates of information dynamics in short data sets [53, 101, 124]. In essence, the procedure for nonuniform conditioning builds iteratively the vector $\mathbf{v}_n^{X,Y}$ selecting terms from a set of candidate components $\Omega = \{x_{n-1}, \ldots, x_{n-L}, y_{n-1}, \ldots, y_{n-L}\}$. Starting from an empty vector $\mathbf{v}_n^{X,Y} = [\cdot]$, the procedure tests at each step all the candidate components of Ω, computing for each candidate the mutual information between the set of components selected up to that step, $\mathbf{v}_n^{X,Y}$, incremented with the test candidate, and the present of the target; the candidate leading to the maximum mutual information is selected and included in $\mathbf{v}_n^{X,Y}$. This achieves a criterion for maximum relevance and minimum redundancy in the selection of components. Finally, the selection is terminated by means of a randomization test which generates surrogates of the selected component and uses them to set a significance threshold for the mutual information. This allows to include in the final conditioning vector $\mathbf{v}_n^{X,Y}$ only the components that bring statistically significant information to the present of the target. After termination of the procedure, the subvectors $\mathbf{v}_n^X$ and $\mathbf{v}_n^Y$ are deduced from $\mathbf{v}_n^{X,Y}$ by simply taking the terms that belong respectively to the past of X and the past of Y. Finally, the information measures P_Y, S_Y, $S_{Y|X}$, $C_{X\to Y}$, and $T_{X\to Y}$ are estimated from the embedding vectors $\mathbf{v}_n^{X,Y}$, $\mathbf{v}_n^X$ and $\mathbf{v}_n^Y$ as indicated in Eqs. (5.1)-(5.3). The computation of all conditional entropy and mutual information terms is based on coarse-grained quantization using Q quantization levels, followed by approximation of the probability distributions with the frequencies of occurrence of the quantized values. In this chapter, lags up to 5 s ($L = 10$) were considered to cover the past of the respiratory series X and the RR interval series Y, and $Q = 8$ quantization levels were adopted for entropy estimation. All entropies are computed using the MuTE toolbox [124].

The computation of the measures of information dynamics described above is complemented with statistical tests aimed at assessing the significance of each measure. The information about the statistical significance is extracted from the randomization test employed by the procedure for candidate selection. Indeed, as a result of the selection procedure and the exploitation of the full and

reduced vectors $\mathbf{v}_n^{X,Y}$, $\mathbf{v}_n^X$ and $\mathbf{v}_n^Y$, the estimated information measures P_Y, S_Y, $S_{Y|X}$, $C_{X\to Y}$, and $T_{X\to Y}$ result as strictly positive when at least one relevant candidate component is selected from the past of X or Y according to the definitions in Eqs. (5.1)-(5.3), thus yielding statistically significant predictive information, information storage, internal information, cross information or information transfer, and are exactly zero otherwise. Therefore, we considered as statistically significant the information measures when they are larger than zero, and nonsignificant when they are exactly zero.

5.3 Comparison of information-theoretic measures during controlled breathing

In order to diminish the negative effects of stress-related disorders, people have been trying to cope with this, often by voluntarily adjusting the breathing pattern [34]. Most breathing instructions aim to acquire a shift towards a reduction in sympathetic activation and an increase in vagal activity by reducing the breathing frequency and increasing the tidal volume. It is however unclear to which extent other features of the breathing pattern, such as the ratio between the duration of the inspiratory and expiratory phase (i/e ratio), contribute to the beneficial effects of slow breathing. It is therefore interesting to investigate the effects of controlled breathing on the autonomic balance, manipulating both breathing frequency and i/e ratio.

Analyses of these manipulations already revealed that slow breathing is accompanied by higher tidal volumes and that a lower i/e ratio results in a higher heart rate, but that the heart rate is not influenced by the breathing frequency, as reported in [191]. In addition, as expected, RSA is higher when breathing at 6 compared to 12 breathing cycles-per-minute (cpm). An increased RSA is also found in a low compared to high i/e ratio, yet only when breathing at 6 cpm.

The goal of this study is to assess the effects of controlled breathing on the autonomic balance in terms of information dynamics, thereby also comparing the two decompositions of predictive information, as described in Eqs. (5.2) and (5.3).

5.3.1 Data acquisition and preprocessing

Participants

In the context of a study concerning the effects of respiratory rate and i/e ratios on self-reported relaxation states, and on RSA and HRV, 30 students (18–22 years; 2 men) have been selected to participate in the experiment [191]. The data are collected at the Faculty of Psychology and Educational Sciences of the KU Leuven (Leuven, Belgium). The study is approved by the local ethical committee. All participants provided written informed consent.

Instrumentation

The LifeShirt System (Vivometrics Inc., Ventura, CA) is used to measure the electrocardiogram (ECG, sampling frequency $f_s = 200$ Hz) and respiration ($f_s = 50$ Hz). Respiration is recorded by means of inductive plethysmography around the abdomen and ribcage. Based on those two displacements, an estimation of the tidal volume is made, which is further used as respiratory signal. In order to take possible delays between respiratory drive and the recorded tidal volume into account, thereby affecting the causality relation, a time lag of 0.5 s is included in the recorded respiratory signal [160].

Experimental protocol

First, baseline recordings are measured for 7 minutes while sitting quietly and breathing spontaneously. Next, the participants practiced four different breathing patterns, each for 45 s; at first, a pattern of 12 cpm is instructed with an inspiratory time of 1.5 s and an expiratory period of 3.5 s (i/e ratio = 0.42). The second breathing pattern is also at 12 cpm, but with a reversed i/e ratio (= 2.33; 3.5 s in- and 1.5 s exhalation time). In the third case, a respiratory rate of 6 cpm is imposed, again with an i/e ratio of 0.42 (3 s in- and 7 s exhalation time). The last pattern comprises a rate of 6 cpm with an i/e ratio of 2.33 (7 s in- and 3 s exhalation time). These four patterns will further be referred to by their breathing frequency of 6 (slow) or 12 cpm (fast breathing), and a low or high i/e ratio. After this practice period, the recordings during the various breathing patterns started. The participants are asked to follow each breathing pattern during 5 minutes, while being assisted by breathing videos. Both visual stimuli, via a vertical bar that is filling up and emptying when respectively inspiration and expiration is expected, and auditive stimuli to indicate the start of inspiration and expiration with respectively a high and low

pitch, are given. The 24 possible presentation orders of the breathing patterns are counterbalanced across the participants.

Preprocessing

The tachogram is constructed after R peak detection using the Pan-Tompkins algorithm. In order to obtain an accuracy of 1 ms when constructing the tachogram, parabolic interpolation using 5 samples around the detected peak is performed. Next, both tachogram and respiratory signal are resampled at 2 Hz using cubic spline interpolation and both signals are high-pass filtered with a cut-off frequency of 0.05 Hz in order to remove baseline wander. Additionally, the first 10 s of each breathing pattern are removed to reduce transient behaviour. From the baseline period of spontaneous breathing, a 5 minute segment is randomly selected to match the data size of the controlled breathing periods.

Information-theoretic measures

After preprocessing of the tachogram RR and respiratory signal RSP, the predictive information of the RR interval series is computed (P_{RR}). Additionally, both decompositions of predictive information as given in Eqs. (5.2) and (5.3) are used to determine the information-theoretic measures $T_{RSP\to RR}$, $C_{RSP\to RR}$, S_{RR} and $S_{RR|RSP}$. The model-free approach is used to estimate the entropies.

Statistical analysis

After testing for normality and equal variances, a two-way within-subject ANOVA is conducted on the four controlled respiratory patterns, with breathing frequency, i.e. 6 or 12 cpm, and i/e ratio, i.e. low or high as factors. A $p < 0.05$ is considered statistically significant.

5.3.2 Results

Fig. 5.2 displays the predictive information during spontaneous breathing and the four controlled breathing patterns. There is a significant effect of breathing frequency, where slow breathing is accompanied by an increase in P_{RR}. No effect of i/e ratio is found, but a significant interaction effect indicates that only at 12 cpm, a low i/e ratio results in a higher P_{RR} than a high i/e ratio. It is also interesting to note that P_{RR} is lower during spontaneous breathing than during controlled breathing at 6 cpm.

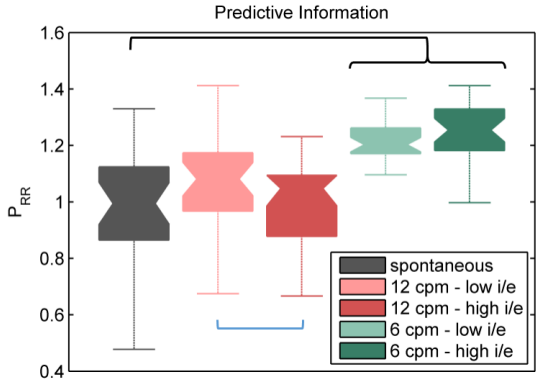


Figure 5.2: Boxplot of the predictive information P_{RR} during spontaneous breathing, breathing at 12 and 6 cpm with i/e ratios of 0.42 (low) and 2.33 (high). The blue square bracket indicates significant differences between a low and high i/e ratio. The black square bracket indicates significant differences between spontaneous breathing and the controlled breathing conditions included in the curly bracket.

The decomposition of predictive information in transfer and self-entropy is given in Fig. 5.3. $T_{RSP\to RR}$ and S_{RR} exhibit significant effects of breathing frequency, with a higher $T_{RSP\to RR}$ and lower S_{RR} during fast compared to slow breathing. Although both in $T_{RSP\to RR}$ and S_{RR}, no effect of i/e ratio is found, a significant interaction effect is observed in S_{RR}, showing also that at 12 cpm, a low i/e ratio results in a higher self-entropy than a high i/e ratio.

The alternative decomposition of predictive information using cross- and conditional self-entropy is given in Fig. 5.4. $C_{RSP\to RR}$ is significantly lower at 12 cpm than at 6 cpm, while $S_{RR|RSP}$ is higher during fast than slow breathing. The i/e ratio does not alter $C_{RSP\to RR}$ or $S_{RR|RSP}$. Spontaneous breathing results in a lower $C_{RSP\to RR}$ than controlled breathing, while the conditional self-entropy exhibits the opposite.

5.3.3 Discussion

Comparison of information-theoretic measures

The two different decompositions of predictive information describing on the one hand the predictability of RR given its own past, whether or not conditioned to the past of RSP, and on the other hand, the predictability of RR given

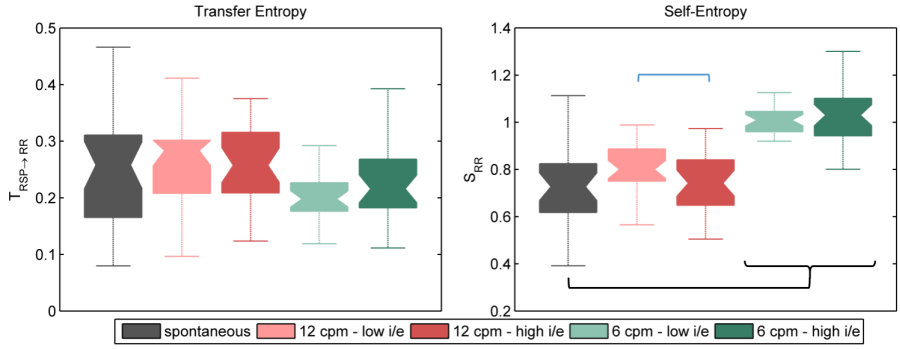


Figure 5.3: Boxplot of the transfer entropy $T_{RSP\to RR}$ (left) and self-entropy S_{RR} (right) during spontaneous breathing and breathing at 12 and 6 cpm with i/e ratios of 0.42 (low) and 2.33 (high). The blue square bracket indicates significant differences between a low and high i/e ratio. The black square bracket indicates significant differences between spontaneous breathing and the controlled breathing conditions included in the curly bracket.

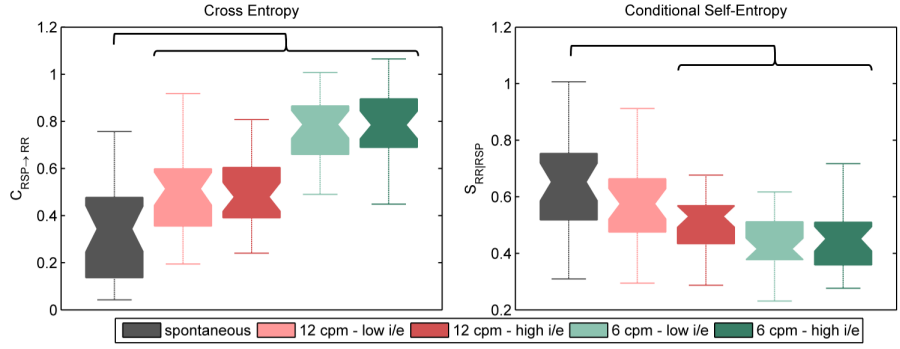


Figure 5.4: Boxplot of the cross-entropy $C_{RSP\to RR}$ (left) and conditional self-entropy $S_{RR|RSP}$ (right) during spontaneous breathing and breathing at 12 and 6 cpm with i/e ratios of 0.42 (low) and 2.33 (high). The black square bracket indicates significant differences between spontaneous breathing and the controlled breathing conditions included in the curly bracket.

the past of RSP, whether or not conditioned to its own past, lead to entirely opposite results; while $S_{RR|RSP}$ and $T_{RSP\to RR}$ are higher during fast than slow breathing, S_{RR} and $C_{RSP\to RR}$ are precisely lower when breathing at 12 cpm.

The opposing results can be explained by the different definitions to determine the predictability of RR based on its own past; the information storage as defined

by S_{RR} not only includes internal memory mechanisms in the target process RR, but also memory in the target process that originates from the driving process RSP [202]. In this traditional decomposition of P_{RR}, the information storage is in fact favoured at the expense of the information transfer, because we first condition on the past of the target series. However in doing so, the measured storage may also reflect some transfer of information. The alternative decomposition does not have this problem because we first condition on the past of the driving respiratory process, but it has the limitation that $C_{RSP\to RR}$ is not a measure of causality in the Granger sense since it can be nonzero, even in the absence of any causal link from driver to target, i.e. if there is a causal link from target to driver. Transfer entropy, on the other hand, will always be zero in the absence of a causal link from driver to target [61]. However, by exploiting the highly unidirectional relation between respiration and HRV [158, 175], this limitation of cross-entropy is mitigated. Moreover, in accordance to the reduction in RSA during fast breathing that was reported in [191], the predictability of RR based on RSP as quantified by $C_{RSP\to RR}$ is lower compared to slow breathing. Note however that the cross-entropy is a measure of cardiorespiratory coupling, but is not necessarily correlated to RSA amplitude.

The information storage as quantified by S_{RR} might also contain some information from the driver RSP that is captured in the past of RR. $S_{RR|RSP}$, on the other hand, proves internal information of the RR interval series since it will be zero in the absence of internal dynamics in the target series [61]. Both S_{RR} and $S_{RR|RSP}$ are related to the self-predictability of the tachogram. Self-predictability is typically associated with an unhealthier cardiovascular system as this indicates a reduced flexibility to respond to bodily demands [200]. Again, $S_{RR|RSP}$, which we can consider as the residual (free from respiration) self-predictability, seems more suitable as its reduction, in contrast to the increase of S_{RR}, during slow breathing also corresponds to the expected shift in autonomic balance.

These results demonstrate that it makes sense to use the alternative decomposition of P_{RR} in $C_{RSP\to RR}$ and $S_{RR|RSP}$ for cardiorespiratory time series. However, though the highly unidirectional relation between respiration and HRV can be exploited, $C_{RSP\to RR}$ does not measure causality, as opposed to $T_{RSP\to RR}$. Therefore, due to their complementary information, it is useful to consider both decompositions in future analyses.

Breathing patterns

The cross-entropy is higher during slow than fast breathing, indicating an increased cardiorespiratory coupling, which is probably related to the shift in autonomic balance towards vagal activity as previous findings reported. Although RSA significantly differed between a high and low i/e ratio during slow breathing [191], this was not perceived in $C_{RSP \to RR}$, demonstrating that the cross-entropy is related to cardiorespiratory coupling, but not as such RSA amplitude. It is also interesting to note that during spontaneous breathing the cross-entropy is significantly lower than during all controlled breathing patterns. This suggests that only the imposition of following a certain breathing pattern, already results in an increase in cardiorespiratory coupling, and possibly RSA, and thus shows the potential of instructed breathing to cope with stress-related conditions.

As already mentioned, the conditional self-entropy can be associated with the ability of the autonomic nervous system to quickly respond to bodily demands [200]. Fast and spontaneous breathing both result in increased values for $S_{RR|RSP}$, suggesting again the beneficial effects of slow breathing; not only the cardiorespiratory coupling increases during slow breathing, the low values for $S_{RR|RSP}$ also indicate a state of more flexibility in autonomic modulation.

5.4 Application: mental stress monitoring

5.4.1 Data and methods

Data acquisition and preprocessing

The data originate from the mental stress monitoring application as described in Section 1.3. In this study, the tachogram and respiratory signal are resampled at 2 Hz using cubic spline interpolation. Baseline wander of the respiratory signal is removed using a high-pass filter with a cut-off frequency of 0.05 Hz, while the tachogram is detrended according to [181]. In order to reduce the transient behaviour, present mainly in the first minute of each task [208], and obtain stationary conditions, only the last 5 minutes of each period are selected for the analysis of information dynamics. Possible delays between the respiratory drive and the recorded tidal volume that might affect the driver-response relation, are taken into account by including a time lag of 0.5 s in the respiratory signal [160]. In order to obtain a more robust estimation using the binning approach, ordinal sampling of the cardiorespiratory time series was

conducted, thereby transforming the signal into its ranks, as is done in most nonparametric statistical tests [105]. Next, stationarity was tested according to the test described in [111]. Signals that failed the stationarity test are discarded from the analysis.

Statistical analysis

After computation of P_{RR}, $T_{RSP\to RR}$, S_{RR}, $C_{RSP\to RR}$ and $S_{RR|RSP}$ using the model-free approach, differences in cardiorespiratory information dynamics between the relaxing documentary watching (RD), attention (AT), and two mental stress (MT1 and MT2) conditions are assessed by means of the Friedman test. Tukey's honestly significant difference criterion is used to take multiple comparisons into account. A significance level of $\alpha = 0.05$ was used.

Testing nonlinearity

In order to determine the significance of the contribution of nonlinear dynamics on the predictive information and on the measures of its decomposition, a test was set up to estimate the information dynamics of 'linearized' versions of each observed bivariate time series. For this purpose, firstly, 100 linearized surrogates of the cardiorespiratory time series are constructed for each bivariate time series. These surrogates are created from a vector autoregressive (VAR) model that is estimated on the bivariate process [54], and is then fed with independent realizations of pairs of white uncorrelated Gaussian noises with the same variance as the residuals of the estimated VAR model. This yields several realizations of linear Gaussian processes sharing the same linear structure of the original observed bivariate process. The optimal model order is determined via the minimum description length method. Next, P_Y, S_Y, $S_{Y|X}$, $C_{X\to Y}$, and $T_{X\to Y}$ of the 100 surrogates are computed using the model-free approach, giving rise to the distribution of these measures under the null hypothesis of linear Gaussian cardiorespiratory time series. The null hypothesis is rejected when the original value obtained using the model-free approach falls outside the 95% confidence interval of the null distribution, thus indicating the presence of nonlinear dynamics.

5.4.2 Results

For the study of information dynamics, data of 5 subjects were discarded due to the lack of stationarity.

Significance and nonlinearity

Fig. 5.5 shows the percentage of subjects that have strictly positive information-theoretic measures (given in plain coloured bars). While for P_{RR}, S_{RR} and $S_{RR|RSP}$, almost all subjects have strictly positive values, not even half of the subjects have any information transfer or cross information, indicating that in the conditioning vector, in many subjects, no candidate of the driver process was selected.

The procedure to test the presence of nonlinearities was followed for each information-theoretic measure, each subject and each experimental condition. The percentage of rejected null hypotheses is given in the hatched coloured bars in Fig. 5.5, indicating that for P_{RR}, S_{RR} and $S_{RR|RSP}$, in the majority of the subjects and in all experimental conditions, the null hypothesis was rejected, and thus significant nonlinearities were observed. In fact, during MT1, the null hypothesis for $S_{RR|RSP}$ was rejected in all subjects except for the one which also did not have a significant $S_{RR|RSP}$. For $T_{RSP\to RR}$ and $C_{RSP\to RR}$, the null hypothesis was rejected in not even half of the subjects, which is evident, given the percentage of significant transfer and cross-entropies. Interestingly, nonlinearities contributed to the transfer entropy $T_{RSP\to RR}$ only in a small subset of the significant measures in the relaxing documentary condition, and in almost all cases during MT1.

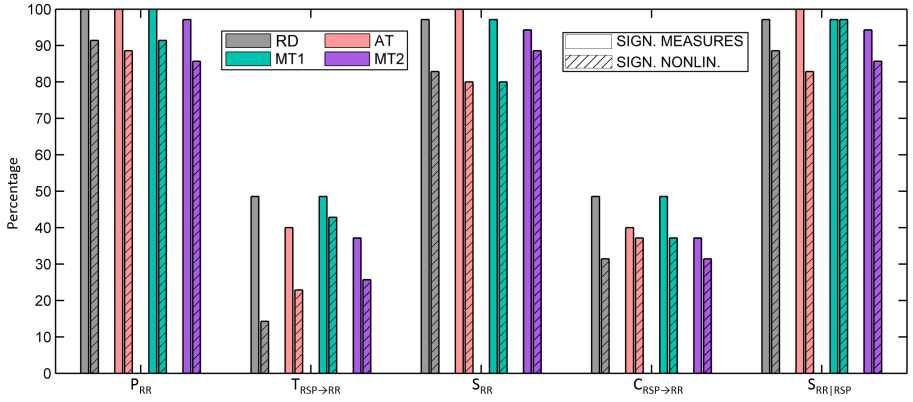


Figure 5.5: Bar graphs indicating the percentage of significant information-theoretic measures (plain) and the percentage of significant nonlinearities (hatched), during relaxing documentary watching (RD), sustained attention (AT) and the mental stress tasks (MT1 and MT2).

Information dynamics

Fig. 5.6 displays boxplots of P_{RR}, $T_{RSP\to RR}$, S_{RR}, $C_{RSP\to RR}$ and $S_{RR|RSP}$ during RD, AT, MT1 and MT2, estimated using the nonlinear model-free approach. The post hoc contrasts reveal that RD and MT2 are significantly different from MT1 in terms of P_{RR} ($p < 0.01$). $T_{RSP\to RR}$, S_{RR} and $C_{RSP\to RR}$ present no differences between experimental conditions, while $S_{RR|RSP}$ is significantly larger during the first mental task than during the other conditions ($p < 0.0001$).

In order to determine the importance of nonlinear cardiorespiratory dynamics, boxplots of P_{RR}, $T_{RSP\to RR}$, S_{RR}, $C_{RSP\to RR}$ and $S_{RR|RSP}$ for the linear surrogates are displayed in Fig. 5.7. For each subject and each experimental condition, the mean of the 100 surrogates was taken as input for the boxplots. Comparing these boxplots to the ones of Fig. 5.6 obtained using the real cardiorespiratory time series and the model-free approach, several differences can be observed; P_{RR} and S_{RR} differ significantly between AT and MT1, whereas when nonlinear interactions are taken into account, no differences between those two conditions for these measures could be observed. Additionally, S_{RR} is also significantly different between MT1 and MT2, while for $S_{RR|RSP}$ there is no difference between RD and MT1 when the linear surrogates are used.

5.4.3 Discussion

Mental arithmetic and sustained attention

In a previous study using these data, traditional time and frequency domain HRV measures were computed to study the effect of mental arithmetic and sustained attention [180]. Almost all measures showed significant differences between RD and the tasks, with increased heart and respiratory rates, and reduced HRV during the tasks. The strongest effect was observed during MT1, then during AT. A habituation effect was noted in the HRV measures during the second mental task. Between the tasks, differences were found between MT2 and the other tasks, but only few measures were able to prove the additional mental load of MT1 compared to AT. Thus, in terms of discrimination of different experimental conditions, no new differences could be found with the analysis of information dynamics that could not be observed with the traditional HRV analysis. The added value lies in the type of information that we can acquire using information dynamics. With the results of these analyses, we can gain more insight in the complex, underlying behaviour of the cardiorespiratory

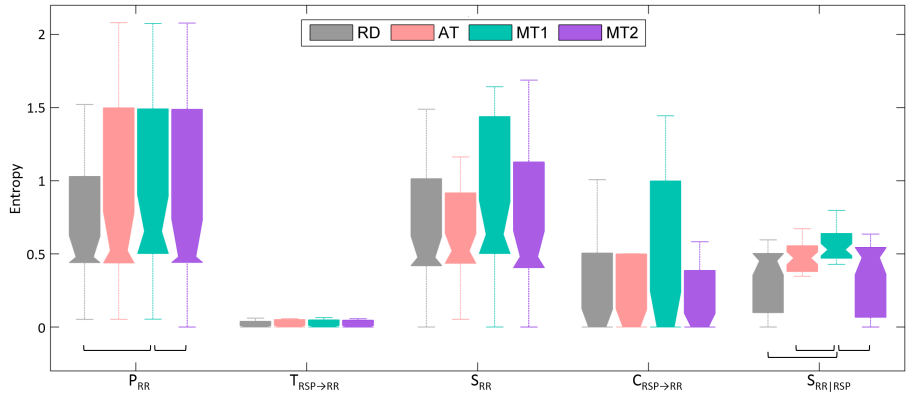


Figure 5.6: Boxplots of information-theoretic measures P_{RR} ($p < 0.01$), $T_{RSP\to RR}$ ($p > 0.05$), S_{RR} ($p > 0.05$), $C_{RSP\to RR}$ ($p > 0.05$) and $S_{RR|RSP}$ ($p < 0.0001$), estimated using the nonlinear model-free approach, during relaxing documentary watching (RD), sustained attention (AT) and the mental stress tasks (MT1 and MT2). The square brackets indicate significant differences between those two experimental conditions as determined by the Friedman test and post hoc contrasts.

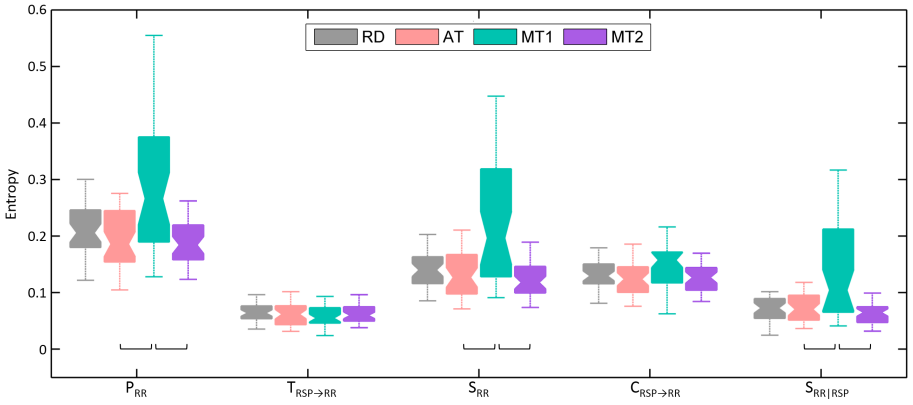


Figure 5.7: Boxplots of mean information-theoretic measures P_{RR} ($p < 0.01$), $T_{RSP\to RR}$ ($p > 0.05$), S_{RR} ($p < 0.001$), $C_{RSP\to RR}$ ($p > 0.05$) and $S_{RR|RSP}$ ($p < 0.01$), estimated using the model-free approach using the linear surrogates as input, during relaxing documentary watching (RD), sustained attention (AT) and the mental stress tasks (MT1 and MT2). The square brackets indicate significant differences between those two experimental conditions as determined by the Friedman test and post hoc contrasts.

system during these different experimental conditions in terms of entropy, and thus predictability of the RR interval time series.

From Fig. 5.6, we could only observe differences between experimental conditions for P_{RR} and $S_{RR|RSP}$. Though transfer $T_{RSP\to RR}$ and cross-entropy $C_{RSP\to RR}$ are both measures of cardiorespiratory coupling and were expected to decrease during mental stress, we could not witness any task effect. It is, however, important to note that RSA is in essence a measure of gain of the cardiorespiratory interaction and not of cardiorespiratory coupling; one could have differences in gain, but with a preserved coupling. In this analysis, we already found a low coupling during RD, which stayed low during other experimental conditions. This suggests that the reduction in RSA amplitude during mental stress, as found in [180], is not accompanied by a reduction in cardiorespiratory coupling. Nevertheless, our results document an increased contribution of nonlinear dynamics to the transfer entropy $T_{RSP\to RR}$ during MT1 compared to RD (Fig. 5.5), thus suggesting that mental stress may induce an alteration in the nature of cardiorespiratory interactions, although this alteration seems not to have an impact on the magnitude of the coupling.

We also observed in Fig. 5.6 that the differences in P_{RR} emanate from the internal information as determined by $S_{RR|RSP}$. This conditional self-entropy indicates how well the RR interval series can be predicted based on information of its own past, taking at first the information of respiration into account. The higher values of $S_{RR|RSP}$ during MT1 indicate that the RR intervals can be better predicted than during the other conditions and thus reveals that the cardiac system is more predictable when experiencing mental stress. The finding of higher predictability of RR confirms previous findings suggesting a reduction of HRV complexity during stress [197]. Taking into account that predictability of the heart rate is typically related to an unhealthier cardiovascular system that shows a reduced rapidity to respond to bodily demands [200], the difference in conditional self-entropy is in accordance with our hypothesis. Additionally, $S_{RR|RSP}$ is not only able to distinguish MT1 from a relaxing documentary watching condition, but also from a lower level of mental load, i.e. during AT. $S_{RR|RSP}$ is also able to describe the habituation effect during MT2 compared to MT1, and as such seems a valuable measure to reflect different levels of sympathetic activation.

It is also interesting to note here that the predictive information already gave a hint about the changes in HRV complexity during mental stress; however, these changes are statistically more evident after accounting for respiration, i.e. by computing the conditional self-entropy rather than the predictive information. Additionally, the conditional self-entropy can also be seen as the internal memory of the tachogram, which appears to be stronger during mental stress, and thus points to reduced flexibility and reactivity of the heart. This has been related

to an increase in sympathovagal balance, which is indeed expected to occur during mental stress [63].

Information decomposition

Two decompositions of the predictive information have been proposed, each with their own advantages and disadvantages. The information transfer as quantified by $T_{RSP\to RR}$ proves real transfer of information, but might underestimate it, especially when the interactions are highly unidirectional [61]. In contrast to what we hypothesized, neither $T_{RSP\to RR}$ nor $C_{RSP\to RR}$ are affected by the experimental condition. These measures of information transfer and cross information are indices of the cardiorespiratory coupling, but in a different way than RSA, as mentioned before. In addition, the low values for $T_{RSP\to RR}$ indicate that the additional predictability of the RR interval series based on RSP given the past of RR is very limited. This can be explained by the fact that in the traditional decomposition of P_{RR}, we first consider the past of the target process, thereby favouring the information storage.

However, the information storage as quantified by S_{RR} might also contain some information from the driver that is captured in the past of RR. $S_{RR|RSP}$, on the other hand, proves internal information of the RR interval series since it will be zero in the absence of internal dynamics in the target series [61]. Using the linear surrogates, no differences between S_{RR} and $S_{RR|RSP}$ can be noted, apart from a constant bias. However, when nonlinear interactions are taken into account, the conditional self-entropy has more discriminative power, whereas the self-entropy has none. It is thus important for cardiorespiratory time series to condition first on the past of RSP to determine the information carried by RR that is unrelated to respiration. The obtained results confirm previous HRV studies in which the effect of respiration was taken into account by separating the tachogram into a component that is strictly related to respiration, and a component that contains all residual heart rate variations [203]. We found that the residual component of the tachogram is highly informative to classify periods of rest and mental stress, while the component related to respiration does not have discriminative power. The latter can be associated to the self-, cross- and transfer entropy while the residual component can be linked to the conditional self-entropy.

Linear versus Nonlinear Information Dynamics

From Figs. 5.6 and 5.7, it can be observed that P_{RR}, S_{RR} and $S_{RR|RSP}$ differ significantly when assessed on the original data and on their linear counterparts.

The higher magnitudes that are observed, are in large part determined by the significant contribution of nonlinear dynamics when the real data were used (cfr. Fig. 5.5). It is, however, also important to add that when we look at the candidates that were selected for the conditioning vector, we can notice a difference in the number of candidates that were chosen using the real cardiorespiratory time series and using the linear surrogates; on average, 2.8 candidates were selected with the real data, whereas 2.25 candidates were chosen with the linear surrogates. A higher number of candidates in the conditioning vector may create some bias towards zero in the conditional entropy, and thus some bias towards higher values in the information-theoretic measures we consider. This bias may partly explain the differences in entropy magnitudes between the real data and the linear surrogates. No differences could be noted between the number of candidates that were selected in several experimental conditions.

When further comparing the information-theoretic measures of the real data and their linear surrogates, other differences between experimental conditions were found for P_{RR}, S_{RR} and $S_{RR|RSP}$. These differences could possibly originate from a larger nonlinear predictability during MT1 and AT. In the traditional decomposition of P_{RR}, the increased nonlinearities in MT1 and AT seem to be distributed over both $T_{RSP\to RR}$ and S_{RR}, thereby abolishing the differences in experimental conditions that were seen in S_{RR} when the linear surrogates were used. On the other hand, in the alternative decomposition of P_{RR}, the nonlinear dynamics seem to contribute substantially to the internal information of RR during the first mental task, leading to significantly larger values during MT1 for $S_{RR|RSP}$ compared to all other experimental conditions. The increase of the impact of nonlinear dynamics on RR during AT seems to be distributed over $C_{RSP\to RR}$ and $S_{RR|RSP}$. It appears thus important to include nonlinear interactions. In fact, seeing that other differences are found using the real cardiorespiratory data and the linear surrogates, it might be interesting for future studies to consider both computations, as information on linear and nonlinear interactions can be deduced separately.

Methodological comments and future work

In cardiorespiratory time series, information dynamics are typically determined using a beat-to-beat approach, and thus not by resampling of the time series. However, taking into account that there are substantial differences between the heart rates during rest (typically around 60 bpm) and stress (up to 120 bpm), we chose to resample the tachogram such that lags up to 5 s can be taken into account in the conditioning vector.

A last remark concerns the need for stationary data segments to assess the information dynamics. For this purpose, the data were high-pass filtered and the transient behaviour at the start of a mental task was discarded by excluding the first minute of each task. Additionally, ordinal sampling was used for the cardiorespiratory time series and their stationarity was tested, resulting in exclusion of data of 5 subjects due to nonstationary behaviour. However, time-frequency analyses showed that the strongest effect of mental stress occurs in the first two minutes of the task [208]. Therefore, there is need for a time-varying approach to capture the information dynamics in fastly varying physiological conditions.

5.5 Conclusion

The goal of this chapter was to characterize the dynamics in cardiorespiratory time series. As such, we have exploited the framework of information theory to quantify the amount of information that is present in cardiorespiratory data. In particular, measures of information storage and internal information of HRV and information transfer and cross information from respiration to HRV have been described and evaluated during a controlled breathing protocol. The results suggested that opposed to the traditionally used transfer entropy, in cardiorespiratory applications, the cross-entropy might also be a useful measure as it does not condition on the past of the heart rate, thereby exploiting the causal relation between respiration and heart rate. In addition, we have found that slow breathing can be associated with an increased cardiorespiratory coupling and reduced residual self-predictability of the tachogram, suggesting why slow breathing is an effective method to enhance vagal activation. Additionally, beneficial effects of controlled breathing could already be observed compared to spontaneous breathing.

Additionally, the cardiorespiratory dynamics during mental arithmetic and sustained attention have been determined. The results suggest that many nonlinearities are present in the cardiorespiratory time series. Also, the comparison between the linear and nonlinear analyses revealed other differences between experimental conditions, motivating not only the use of the nonlinear model-free approach for future studies, but also the approach using the linear surrogates. Additionally, it was shown that, in contrast to the hypothesized reduction in cardiorespiratory coupling, the information transfer and cross information from respiration to HRV were not influenced by the experimental condition. Likewise, the information storage of HRV seemed to substantially incorporate possible influences from respiration, thus exhibiting no differences between experimental conditions. On the other hand, the internal information

measured by the conditional self-entropy of HRV given respiration showed higher predictability during mental stress compared to sustained attention or rest, thus appearing as a very informative quantity for reflecting different levels of activation of the sympathetic nervous system evoked by graded levels of stress.

Chapter 6

Separation of the tachogram: methods and their sensitivity to the respiratory signal

The previous chapter dealt with the last aim of the thesis, as described in Section 1.2. The goal of the current chapter is to link all chapters by building further upon the separation discussed in Chapter 3 using the results of Chapters 2 and 5. In particular, we aim to investigate how sensitive the separation methods are to the type of respiratory signal that is used to estimate the respiratory component of the tachogram. Not only several recorded respiratory signals are evaluated, also several ECG-derived respiratory (EDR) signals, as described in Chapter 2, are considered. The sensitivity of separation methods to the respiratory signals is determined by the lack of cross information, as defined by the cross-entropy in Chapter 5, from the reference respiratory signal to the residual tachogram, i.e. the component that is unrelated to respiration. After a brief introduction in Section 6.1, the methodology of separation algorithms, EDR methods and information transfer is summarized in Section 6.2. The results and a discussion is provided in Section 6.3, followed by some concluding remarks in Section 6.4. The contents of this chapter is based on [216].

6.1 Introduction

Our heart is beating at a rate such that it can properly respond to the needs of our body. This creates continuous variations over time in our heart rate, termed heart rate variability (HRV). One of the main modulators of our heart rate is linked to our breathing; this is called respiratory sinus arrhythmia (RSA) and represents the fluctuation of the heart rate with respiration. These respiratory-related heart rate variations have been associated with vagal activation. However, this has been highly debated as several publications reported that measures of RSA are dependent of tidal volume and respiratory rate, independent of cardiac vagal tone [154]. The lack of consensus on this interpretation, and consequently on certain HRV features, motivated the use of a different approach: the separation of the tachogram in a part related to respiration and a part unrelated to respiration, the so-called residual tachogram. This approach has been dealt with in Chapter 3, in which we have shown that inclusion of respiratory information yields almost perfect classification in periods of rest and stress when spectral HRV features from the residual tachogram are used [203]. That study showed that it is interesting to investigate these residual heart rate variations as they might be masked by the dominant influence of respiration onto the tachogram.

Two separation methods, one based on an ARMAX model [37] and one based on orthogonal subspace projection (OSP) [32], have shown a good performance to conduct this separation of the tachogram. However, these methods require the recording of a respiratory signal. It is well-known that different modalities to record the breathing also yield respiratory signals with diverse morphologies. In this chapter, we aim to investigate how sensitive these separation methods are towards different types of respiratory signals, by comparison of their performance when nasal airflow, and thoracic and abdominal displacements are used. Additionally, we aim to investigate whether the separate recording of respiration is really necessary by evaluating the performance when several ECG-derived respiratory (EDR) signals, discussed in Chapter 2, are used as surrogate respiratory signal.

The sensitivity of separation methods to the used respiratory signal is determined by means of the cross-entropy, a measure of cross information that has been described in Chapter 5. As such, this chapter builds further upon Chapter 3 using the results of Chapters 2 and 5.

Imam et al. recently published a similar study in which they investigated the importance of including respiration in linear parametric modeling of ventricular repolarization variability [87]. Not only the need to include respiratory information was emphasized, also the use of EDR signals instead of directly

recorded respiratory signals was evaluated. They found that EDR signals based on the R peak amplitude yield similar results in the parametric modeling as the recorded respiration.

6.2 Methodology

6.2.1 Data acquisition and preprocessing

The first dataset used in this study originates from the PhysioNet database [68] on the Computing in Cardiology Challenge 2000 for ECG-based apnea detection (Apnea-ECG). Eight records (age: 43.3 yr ± 8.3) contain single-lead ECG recordings and multiple respiratory recordings: nasal airflow recorded with a thermistor (RSP_{ref}), thoracic (RSP_{TH}) and abdominal effort (RSP_{AB}). All signals are sampled at 100 Hz.

The second dataset is recorded in the University Hospital Leuven (UZ Leuven, Belgium), and consists of polysomnography data of 10 patients (age 48.8 yr ± 11.8) with habitual snoring, witnessed apneas and hypersomnolence. Different signals are extracted from this dataset, namely, single lead ECG (lead II), respiratory effort measured around the thorax (RSP_{TH}) and the abdomen (RSP_{AB}), and nasal airflow (RSP_{ref}) recorded with an oronasal thermistor (Braebon, NY, USA). The sampling frequency is 200 Hz.

From all 18 recordings, 5 minutes without apneic events are selected. All ECGs are upsampled to 500 Hz using cubic spline interpolation to obtain tachograms with an accuracy of 2 ms. The nasal airflow signals are always used as the reference respiratory signal (RSP_{ref}). All respiratory signals, including the EDR signals as computed below, and tachogram are resampled at 4 Hz, and high-pass filtered at 0.05 Hz to remove baseline wander.

6.2.2 ECG-derived respiration

Apart from the separately recorded respiratory signals, the performance of the separation methods will also be evaluated when several ECG-derived respiratory signals are used. The goal is to test whether the recording of only ECG is sufficient to reliably separate the tachogram. We will consider three EDR methods:

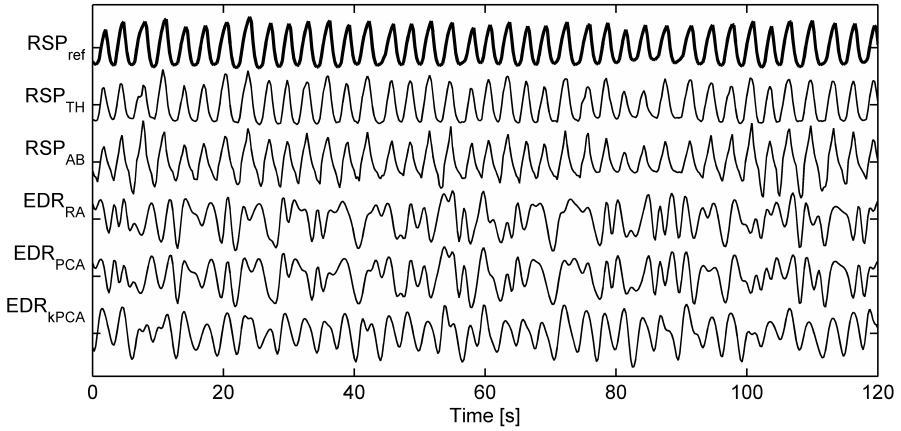


Figure 6.1: Respiratory signals: the reference respiratory signal (RSP_{ref}), thoracic (RSP_{TH}) and abdominal effort (RSP_{AB}), ECG-derived respiratory signals based on the R peak amplitude (EDR_{RA}), PCA (EDR_{PCA}) and kPCA (EDR_{kPCA}).

- **EDR**$_{RA}$: This EDR signal is determined by the amplitude of the R peaks in the baseline-corrected ECG, where the baseline wander is removed using 2 median filters of 200 ms and 600 ms.
- **EDR**$_{PCA}$: The EDR signal based on principal component analysis (PCA) relies on the changing correlation between the QRS complexes over several heart beats, where it is assumed that the largest variations between the QRS complexes are caused by respiration [102].
- **EDR**$_{kPCA}$: This EDR signal is based on the approach using PCA, but exploits nonlinear interactions between the ECG and respiration by the use of the nonlinear kernel PCA (kPCA) instead of the linear PCA [215].

Fig. 6.1 displays several recorded respiratory signals, and EDR signals. Note differences in morphology between the (surrogate) respiratory signals.

6.2.3 Separation of the tachogram

Several methods have been proposed in the literature to separate respiratory variations from the tachogram such that we have two components: one that is strictly related to respiration (RR_{RSP}), and one that contains all heart rate variations that are unrelated to respiration, i.e. the so-called residual tachogram

(RR_{res}). We will evaluate the sensitivity to the type of respiratory signal of two methods that proved to be successful in conducting this separation [203]. Both methods are based on the estimation of the respiratory component of the tachogram (RR_{RSP}) when the original tachogram (RR_{orig}) and a recorded respiratory signal (RSP) are given:

- **ARMAX**: This separation approach was proposed by Choi et al. and estimates RR_{RSP} as a linear combination of past respiratory inputs [37]. Delays up to 3 s are taken into account.
- **OSP**: In this approach, the tachogram is projected onto a respiratory subspace to obtain RR_{RSP}. The respiratory subspace is constructed from delayed detail signals from the wavelet decomposition of the respiratory signal using a Daubechies 4 wavelet, up to level 5. Also here, delays up to 3 s are included [32].

After computation of the respiratory component of the tachogram, the residual component RR_{res} can simply be found by $\mathrm{RR}_{res} = \mathrm{RR}_{orig} - \mathrm{RR}_{RSP}$.

6.2.4 Sensitivity to the type of respiratory signal

In the first stage, the similarity between all 'indirect' respiratory recordings, including the thoracic and abdominal efforts as well as the three computed EDR signals, and the nasal airflow RSP_{ref} is assessed via their coherence. As similarity measure, the mean magnitude squared coherence between the respiratory signals in a range of the full width at half maximum of the fundamental respiratory frequency is computed [215].

Secondly, the sensitivities of ARMAX and OSP to the type of respiratory signal are evaluated by testing whether they succeed in separating the respiratory-related heart rate variations from residual variations when respiratory signals other than RSP_{ref} are used to conduct the separation:

1. Computation of RR_{res} using all six types of respiratory signals and both separation methods, resulting in 12 residual tachograms $\mathrm{RR}^{type}_{res,OSP/ARMAX}$.
2. Assessment of the cross-entropy from the reference respiratory signal RSP_{ref} to all residual tachograms RR_{res}.

For the computation of the cross-entropy, consider the bivariate process $\{X, Y\}$, where x_n and y_n are the processes sampled at the present time n. Then the

cross-entropy, which is defined as the cross information that quantifies how much of the information carried by y_n can be predicted by the past of X, can be computed as $\mathrm{CE}_{X\to Y} = H(y_n) - H(y_n|\mathbf{v}_n^X)$, with $\mathbf{v}_n^X = [\ x_{n-1} \quad x_{n-2} \quad \cdots\ ]$ and $H(.)$ the Shannon entropy. The (conditional) entropies are then estimated via a model-based approach, described in Chapter 5, where the processes are represented by a vector autoregressive model with order p, as optimized by the Akaike information criterion, and delays up to 3 s [54]. Based on this parametric representation, the statistical significance of the cross-entropy from X to Y can be assessed by an F-test checking whether the past of X explains a significant portion of the variance of Y.

For a correct separation of respiratory-related and residual variations, the cross-entropy from the reference respiratory signal $X = \mathrm{RSP}_{ref}$ to the residual tachograms $Y = \mathrm{RR}_{res}$ should be quasi-zero, or non-significant. Instead of the cross-entropy, the transfer entropy can also be employed since the lack of information transfer corresponds to the absence of causal interactions from respiration to the residual tachogram. However, in this case, the non-significance of the cross-entropy is a stricter condition than that of the transfer entropy, and the use of the cross-entropy, thus, will ensure that the residual tachogram is unrelated to respiration.

6.3 Results and discussion

Fig. 6.2 shows the results of the above described analyses. In Fig. 6.2(a) the cross-entropy from the reference respiratory signal to the original tachogram is given. We can observe that 15 out of 18 recordings have a significant cross information.

Next, a comparison between the different types of respiratory signals is conducted via the mean magnitude squared coherence with the reference nasal airflow. These results are displayed in Fig. 6.2(b), where we can see that, as one could expect, both recorded respiratory efforts RSP_{TH} and RSP_{AB} yield high coherences. From the three EDR signals, the algorithm based on the R peak amplitude performs the worst. As described in [215], EDR_{PCA} yields better EDR signals, but the best resemblance to the nasal airflow is for EDR_{kPCA} with coherences around 90%, which are similar as the recorded RSP_{AB}.

In Fig. 6.2(c), the cross-entropies from RSP_{ref} to residual tachograms obtained with the other types of respiratory signals are displayed. When looking at $\mathrm{CE}_{RSP_{ref}\to RR_{res}^{RSP_{ref}}}$ obtained both using ARMAX and OSP, we can observe that the cross-entropies are very small and none of them even exhibit a significant cross information. This indicates that both separation methods successfully

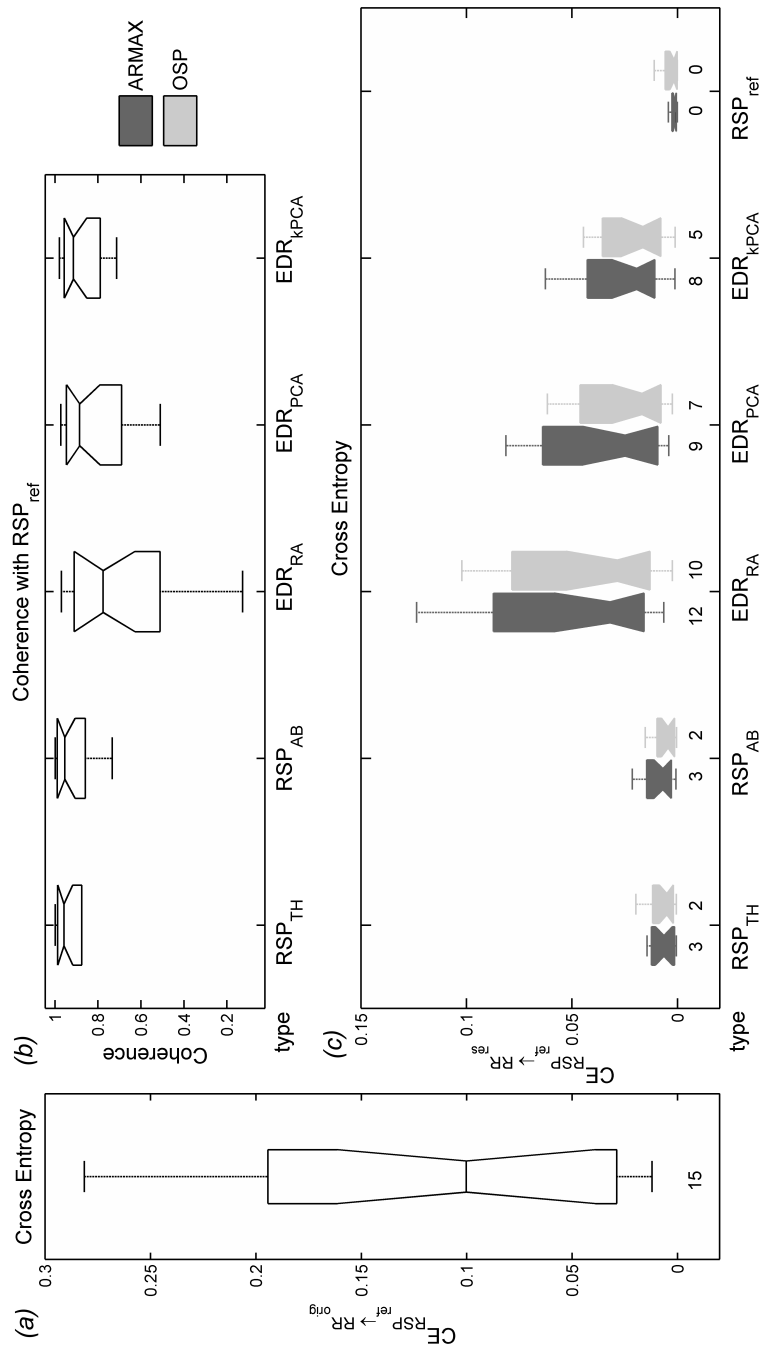


Figure 6.2: Boxplots of the results; (a) cross-entropy from RSP_{ref} to RR_{orig}; (b) mean magnitude squared coherence between RSP_{ref} and the other types of respiratory signals; and (c) cross-entropy from RSP_{ref} to RR_{res}^{type} obtained using ARMAX and OSP. The number below each boxplot indicates the number of significant cross-entropies.

separate the respiratory influences from the tachogram. Also, the cross-entropies from RSP_{ref} to the residual tachograms obtained using RSP_{TH} and RSP_{AB} are quasi-zero. However, both signals yield respectively 3 and 2 significant cross-entropies when ARMAX and OSP are used, indicating that in some cases, the separation methods do not fully succeed to separate respiratory-related heart rate variations and residual variations when 'indirect' recordings of respiration are used. When EDR_{RA} is used to compute the residual tachogram, either using ARMAX or OSP, there are still many significant cross-entropies, showing that the R peak amplitude method can not be used as surrogate respiratory signal to conduct the separation. The results improve, but are still not perfect, when PCA and kPCA are used to compute the EDR signals. Note here that the mechanical interaction between respiration and ECG is used to compose the three EDR signals, causing that the information contained in these signals might be different than in the recorded respiratory signals. The best results with surrogate respiratory signals are obtained when EDR_{kPCA} is combined with OSP. Although there are still 5 out of 18 significant cross-entropies, the cross-entropies are significantly reduced when we compare this with $\text{CE}_{RSP_{ref} \rightarrow RR_{orig}}$. These results indicate that OSP is a solid technique, that might also be useful in several home monitoring applications, such as sleep apnea detection or epilepsy monitoring, where it is desired to use only few sensors. We have shown here that in most cases, enough respiratory-related information can be extracted from the ECG to reliably conduct the separation, and that it might not be needed to separately record the respiration. However, it should be investigated whether e.g. the results for stress classification can be reproduced when EDR_{kPCA} is used [203].

From all these results, we can observe that OSP has always fewer significant cross-entropies than ARMAX, indicating that OSP is less sensitive to the type of respiratory signal. We hypothesize that this is due to the inclusion of the wavelet transform in OSP that reduces the impact of artifacts and different signal morphologies.

6.4 Conclusion

The two methods that we evaluated to separate respiratory influences from the tachogram perform well as demonstrated by the lack of cross information from the reference respiratory signal to the residual tachogram obtained using that reference signal. When other recorded respiratory signals are used, such as abdominal or thoracic displacements, the separation is also good. The ECG-derived respiratory signals on the other hand, do not manage to completely separate the respiratory influences from the tachogram. However, the separation

method based on OSP successfully separates 13 out of 18 recordings when the EDR method based on kPCA is used. We can conclude that OSP is less sensitive than ARMAX to the different morphologies of several respiratory signal types. Additionally, the reported results indicate that the separation of the tachogram is feasible even if only the ECG signal is available.

Chapter 7

Conclusions and future work

In this final chapter, the main conclusions of the thesis are summarized in Section 7.1. Additionally, suggestions for future research directions are provided in Section 7.2.

7.1 Conclusions of the thesis

The cardiac and respiratory systems closely interact, as we have extensively described in Chapter 1. The study of their interaction is interesting as it provides information on cardiac autonomic control, though we have seen that many interpretational problems arise due to the lack of consensus on the precise mechanisms that are responsible for the cardiorespiratory interaction. Thus, we have identified a need to include respiratory information in HRV and RSA analyses. Inspired by this problem, we have focused this dissertation on three topics:

1. ECG-derived respiration;
2. Separation of the tachogram; and
3. Information dynamics in the cardiorespiratory system.

The mathematical approaches that have been followed in this thesis and the main results are summarized in Paragraph 7.1.1. Furthermore, we have paid special attention to mental stress monitoring. The main conclusions of the

developed methodologies performed on this application are given in Paragraph 7.1.2.

7.1.1 Mathematical techniques

ECG-derived respiration

For the first aim on deriving a surrogate respiratory signal from single lead ECGs, kernel principal component analysis was proposed as a nonlinear extension of the PCA approach that was published in the literature as EDR method. In Chapter 2 a framework was given to use kPCA as EDR algorithm. As such, different types of kernel functions were evaluated, with the radial basis function as best kernel option. With this, the parameter σ^2, indicating the variance of the RBF kernel, needed to be optimized, which is a difficulty in unsupervised learning. We proposed two criteria, based on entropy and the difference in eigenvalues, to select a suitable value for σ^2. KPCA as EDR method using an RBF kernel function and selection of σ^2 according to both criteria showed to outperform EDR algorithms based on linear PCA, the R peak amplitude and kPCA using other kernel functions.

Furthermore, in the study described in Chapter 6 on the sensitivity of separation methods for the tachogram, the EDR algorithm based on kPCA also proved to yield the best surrogate respiratory signal to conduct the separation in case a directly recorded respiratory signal was not available. However, EDR signals based on kPCA appeared not to be accurate enough in all situations as transfer of information from the respiratory signal to the residual tachogram was noted in 5 out of 18 recordings.

Separation of the tachogram

The second aim was focused on separating variations in the heart rate that are related to respiration from HR variations that are not related to respiration. The data-driven algorithms that have been proposed in the literature to conduct this separation have extensively been compared in Chapter 3. A simulation study using several test signals, and a stability study evaluating the robustness of the separation methods revealed that the algorithms based on orthogonal subspace projection and on the ARMAX model yield the best performances.

Additionally, the sensitivity of OSP and ARMAX to the type of respiratory signal was evaluated in Chapter 6. In these analyses, we found that when abdominal or thoracic displacements were used, the separation was performed

correctly in 15 (ARMAX) and 16 (OSP) out of 18 recordings. For comparison, when EDR signals were used, 13 (OSP) and 10 (ARMAX) out of 18 recordings were correctly separated. From these analyses, we concluded that OSP is less sensitive than ARMAX to the different morphologies of several respiratory signal types.

The separation of the tachogram was also conducted in a time-frequency framework in Chapter 4 in order to study the dynamic response in nonstationary cardiorespiratory data. As such, the separation was proposed via partial TF spectra in which the response of RR interval variations linearly related to respiration, and variations that are not linked to respiration, were separated. In order to assess the performance of partial TF spectra to correctly separate the tachogram, a simulation study was conducted which revealed that the separation can be conducted reliably, unless two spectral components oscillate simultaneously at the same instantaneous frequency. However, this is assumed to have little impact in cardiorespiratory analyses.

Information dynamics

The last aim of the thesis was concerned with the characterization of information dynamics in cardiorespiratory time series. Accordingly, an information-theoretic framework was introduced in Chapter 5 to quantify the amount of information that is present in cardiorespiratory data. In particular, the predictive information carried in cardiorespiratory data was decomposed in two ways, resulting in the transfer and cross-entropy from respiration to HRV and the self- and conditional self-entropy of HRV. These concepts have been evaluated during a controlled breathing protocol. The results suggested that, in addition to the traditionally used transfer entropy, in cardiorespiratory applications, the cross-entropy might be an interesting way to quantify transfer of information as it does not condition on the past of the heart rate, thereby exploiting the highly unidirectional relation between respiration and heart rate.

7.1.2 Mental stress monitoring

Throughout the thesis, special attention was paid to the application of mental stress monitoring. It has been found that persons who are chronically stressed, have an increased risk for cardiovascular diseases. Also breathing plays an important role, as research suggests that respiration can be used as an interface to deal with negative effects of mental stress, and thus alter cardiac autonomic activity. This made mental stress an interesting application to study in this dissertation.

In a first study on mental stress monitoring, the impact of the separation of the tachogram was evaluated in Chapter 3. At first, several spectral features of the original tachogram and respiratory signal were used to distinguish periods of mental stress and rest, resulting in almost arbitrary classifications. However, when spectral features of the tachogram that is unrelated to respiration were used, an almost perfect classification was obtained. These results demonstrated the importance of including respiratory information in HRV analyses, and moreover proved that the separation of the tachogram can be a very useful tool to investigate changes in the heart rate that are otherwise masked by the dominant effect of respiration onto HRV.

In order to study the dynamic response of the cardiorespiratory system to mental arithmetic and sustained attention, also cross and partial time-frequency analyses were carried out in Chapter 4. During sustained attention and mental arithmetic, increased heart and respiratory rates were found, and vagal withdrawal was suggested mainly during the first minute of the tasks. Both cross and partial TF analyses showed a slower and less pronounced response to sustained attention than to mental arithmetic. Additionally, the response of RR interval variations related to respiration appeared to be faster than the response of variations unrelated to respiration. These results demonstrated that the separation in the time-frequency domain revealed important time information that could not be deduced from the results in Chapter 3.

Finally, the cardiorespiratory dynamics during mental arithmetic and sustained attention have been determined in Chapter 5. The results from these analyses showed that many nonlinearities are present in the cardiorespiratory time series. In addition, it was shown that, in contrast to the hypothesized reduction in cardiorespiratory coupling, the information transfer and cross information from respiration to HRV were not influenced by the mental tasks. Similarly, the self-entropy of HRV seemed to be confounded by respiration, thus exhibiting no differences between experimental conditions. On the other hand, the conditional self-entropy of HRV that takes information of respiration into account, appeared to be very informative to study the predictability of RR interval series during mental tasks, and showed higher predictability during mental stress compared to sustained attention or relaxing documentary watching.

For all these analyses, data recorded during mental arithmetic were used to assess the response to mental stress. Though it has been shown that mental arithmetic affects several physiological indices of stress [97, 221], we have no guarantee that the participants were actually stressed. Additionally, it is important to keep in mind that the experiments were carried out in a controlled, laboratory setting; the obtained results cannot simply be translated into a real-life situation.

7.2 Future work

7.2.1 Surrogate respiratory signals

In this thesis, we have only considered single lead ECG-derived respiratory signals based on morphological changes in the ECG related to respiration. The results we have obtained using kPCA showed to outperform other state-of-the-art single lead EDR algorithms. However, the resemblance with a recorded respiratory signal was not good enough to always correctly separate the tachogram, as mathematically determined in Chapter 6. Whether the proposed EDR algorithm meets the required performance, should, however, be tested in several applications. For example, the stress classification experiment described in Chapter 3 can be repeated using the EDR signal; though the separation might not be perfect, it could be that it is good enough to still have a reliable stress classification. Similarly, EDR signals are used to detect sleep apnea without polysomnography or to analyze cardiorespiratory changes during epileptic seizures [195, 196]. Its performance in these and other applications should be evaluated as a trade-off between the accuracy and the cost-efficiency of ECG-derived respiration. This balance will be different for each application. Furthermore, the EDR algorithm based on kPCA should also be tested in ambulatory settings.

Apart from new applications in which kPCA as EDR algorithm should be tested, future research should also focus on improving its performance by combining it with physiological information that can be derived from the ECG, i.e. RSA; Boyle et al. have shown that a combination of both types of respiratory-related information in the ECG yields the best performance in ambulatory conditions [28].

In addition, it is important to note that recently, new modalities have been proposed to derive the respiratory signal from, such as continuous blood pressure recordings and photoplethysmographic (PPG) signals [104]. Especially PPG-derived respiratory signals have received more and more attention due to the cheap and comfortable acquisition. By combining ECG and PPG, the pulse transit time, has been determined which is also used as surrogate respiratory signal. However, future work should also focus on combining different modalities that are simultaneously recorded in certain applications.

7.2.2 Separation of the tachogram

The tachogram has been separated such that all respiratory-related heart rate variations were clustered in one component, and all other variations in another component. To this end, only linear data-driven techniques have been considered. Though some studies have shown that cardiorespiratory interactions are mainly linear [17], we know that the interactions could be nonlinear, and that the extent of nonlinearity could also depend on the physiological state of the person [82,88]. Therefore, the separation of the tachogram needs a nonlinear extension, such as the one proposed in [33], in which the amount of nonlinear interactions can be assessed as well.

7.2.3 Physiological interpretation

We have shown that the separation of the tachogram reveals valuable information, especially on heart rate variations unrelated to respiration, to classify periods of rest and mental stress. It is however not yet clear how to interpret both components of the tachogram from a physiological point of view. This is an important issue to tackle for the acceptance of the proposed technique in practice. Studies using autonomic blockade could be used for this purpose, though only information on sympathetic and parasympathetic activity can be obtained. The discussion on the interpretation of LF and HF power in HRV have proven that this might not be sufficient. Ultimately, studies identifying the underlying regulation mechanisms responsible for these results are needed. Similarly, the physiological interpretation on the proposed information-theoretic measures for cardiorespiratory data, i.e. transfer entropy, self-entropy, cross-entropy and conditional self-entropy, needs to be determined.

An important determinant that will play a role in the physiological interpretation is the blood pressure. It is known that respiration exerts an influence on both HR and BP, however, in this dissertation, we have focused on the strong interaction between respiration and the heart rate, as RSA has been identified as a marker that contains a lot of information on the autonomic nervous system. Though it is currently debated whether this comes from a central oscillator, the baroreflex, another mechanism or a combination of them, we have opted to leave the complex interaction between HR and BP aside, and study only the relation between respiration and the heart rate, thereby including both direct and indirect influences. However, now that we have demonstrated that valuable information can be extracted from the separated tachogram, future studies should include blood pressure recordings to gain more information on the physiological interpretation. Closed-loop models that describe the interactions between respiration, heart rate and blood pressure have been proposed in the

literature [18, 149]. Yet, these models strongly depend on the goodness-of-fit of the model and the validity of their underlying assumptions.

7.2.4 Time-varying techniques

The methods proposed in this thesis, except for the (partial) time-frequency methods, require quasi-stationary data and are not suitable for online monitoring. We have used short data segments and/or preprocessed the data to mitigate the effects of possible nonstationarities. However, in real-life conditions, such as long-term stress testing or ambulatory monitoring, the data have to be split in smaller segments to ensure stationarity before application of the proposed EDR, separation or information-theoretic methods. This segmentation process creates discontinuities between consecutive parts, which could be dealt with as in [31]. Alternatively, time-varying techniques could be developed to deal with changing conditions and have more reliable results [10, 121]. Indeed, as was shown in Chapter 4 using (partial) time-frequency methods, the response to mental arithmetic and sustained attention varies in time. In order to gain more information on the temporal response, the proposed methods should be modified to be used online or in nonstationary conditions. To this end, adaptive techniques like Kalman or recursive least-squares filtering could be used.

7.2.5 New applications

This dissertation was only focused on mental stress monitoring as representative application in which cardiorespiratory analyses are important. However, as previously mentioned, also sleep and epilepsy studies make up interesting applications for cardiorespiratory studies [195,196,220]. The proposed techniques can also be applied to analyze the cardiorespiratory system of newborn babies; abnormalities in their cardiorespiratory control are believed to contribute to sudden infant death [85]. Additionally, it has been observed that babies up to 6 months have bidirectional interactions between the cardiac and respiratory system, making them a unique group to study [158].

7.2.6 Heart-respiration-brain interactions

In the last decades, the study of heart-brain interactions has gained increasing attention to get more insight in the control mechanisms of the heart [57,150,184]. Also the integrated control of the brain to the heart in response to stress has already been studied [173, 183]. Given that the cardiac and respiratory systems

strongly interact, we propose to extend the study on heart-brain interactions by including their interactions with respiration as well.

7.2.7 Mental stress

Mental stress is a complex phenomenon that results in numerous responses in the human body. We have studied the cardiorespiratory response to stress, but stress is also known to induce among other muscle tension and hormonal changes [44, 162]. Also psychological problems such as depression and chronic fatigue syndrome, have been linked to mental stress [69]. As mental stress is a growing problem in today's society, it is a hot topic in current research, in various disciplines. As this thesis has shown that, instead of separately studying the response of the cardiac and respiratory systems to mental stress, a combined investigation of the cardiorespiratory system lead to more valuable information, a multidisciplinary approach is needed in which physiologists, biomedical engineers and psychologists combine their expertises and integrate their knowledge to get a more complete understanding of mental stress and its impact on several (sub)systems of the human body.

Bibliography

[1] Acharya, U. R., Joseph, K. P., Kannathal, N., Lim, C. M., and Suri, J. S. Heart rate variability: a review. *Medical and Biological Engineering and Computing 44*, 12 (2006), 1031–1051.

[2] Aerts, W., Joosen, P., Widjaja, D., Varon, C., Vandeput, S., Van Huffel, S., and Aubert, A. E. Heart rate and blood pressure variability under moon, mars and zero gravity conditions during parabolic flights. In *Proc. of the Joint Life Science Meeting 'Life in Space for Life on Earth'* (June 2012).

[3] American Psychological Association Practice Organization. Psychologically healthy workplace program fact sheet: By the numbers, 2010.

[4] Angelone, A., and Coulter, N. A. Respiratory sinus arrhythmia: a frequency dependent phenomenon. *Journal of Applied Physiology 19*, 3 (1964), 479–482.

[5] Appelhans, B. M., and Luecken, L. J. Heart rate variability as an index of regulated emotional responding. *Review of General Psychology 10*, 3 (2006), 229–240.

[6] Ataee, P., Belingard, L., Dumont, G. A., Noubari, H. A., and Boyce, W. T. Autonomic-cardiorespiratory regulation: A physiology-based mathematical model. In *Proc. of the 34th Annual International Conference of the IEEE Engineering in Medicine and Biology Society* (2012), pp. 3805–3808.

[7] Baccalá, L. A., and Sameshima, K. Partial directed coherence: a new concept in neural structure determination. *Biological Cybernetics 84*, 6 (2001), 463–474.

[8] Baccalá, L. A., and Sameshima, K. Comments on 'Is partial coherence a viable technique for identifying generators of neural oscillations?'. *Biological Cybernetics 95*, 2 (2006), 135–141.

[9] Badra, L., Cooke, W., Hoag, J., Crossman, A., Kuusela, T., Tahvanainen, K., and Eckberg, D. Respiratory modulation of human autonomic rhythms. *American Journal of Physiology - Heart and Circulatory Physiology 280*, 6 (2001), H2674–H2688.

[10] Bailón, R., Laouini, G., Grao, C., Orini, M., Laguna, P., and Meste, O. The integral pulse frequency modulation model with time-varying threshold: application to heart rate variability analysis during exercise stress testing. *IEEE Transactions on Biomedical Engineering 58*, 3 (2011), 642–652.

[11] Bailón, R., Sornmo, L., and Laguna, P. A robust method for ECG-based estimation of the respiratory frequency during stress testing. *IEEE Transactions on Biomedical Engineering 53*, 7 (2006), 1273–1285.

[12] Bailón, R., Sörnmo, L., and Laguna, P. *Advanced methods and tools for ECG data analysis*. Artech House, 2006, ch. ECG-derived respiratory frequency estimation, pp. 215–244.

[13] Bakshi, B. Multiscale PCA with application to multivariate statistical process monitoring. *AIChE Journal 44*, 7 (1998), 1596–1610.

[14] Barnett, L., Barrett, A. B., and Seth, A. K. Granger causality and transfer entropy are equivalent for Gaussian variables. *Physical Review Letters 103*, 23 (2009), 238701.

[15] Bartsch, R., Kantelhardt, J. W., Penzel, T., and Havlin, S. Experimental evidence for phase synchronization transitions in the human cardiorespiratory system. *Physical Review Letters 98*, 5 (2007), 054102.

[16] Bartsch, R. P., Schumann, A. Y., Kantelhardt, J. W., Penzel, T., and Ivanov, P. C. Phase transitions in physiologic coupling. *Proc. of the National Academy of Sciences 109*, 26 (2012), 10181–10186.

[17] Baselli, G., Cerutti, S., Badilini, F., Biancardi, L., Porta, A., Pagani, M., Lombardi, F., Rimoldi, O., Furlan, R., and Malliani, A. Model for the assessment of heart period and arterial pressure variability interactions and of respiration influences. *Medical and Biological Engineering and Computing 32*, 2 (1994), 143–152.

[18] Baselli, G., Cerutti, S., Civardi, S., Malliani, A., and Pagani, M. Cardiovascular variability signals: towards the identification of a

closed-loop model of the neural control mechanisms. *IEEE Transactions on Biomedical Engineering 35*, 12 (1988), 1033–1046.

[19] Bauer, A., Kantelhardt, J. W., Bunde, A., Barthel, P., Schneider, R., Malik, M., and Schmidt, G. Phase-rectified signal averaging detects quasi-periodicities in non-stationary data. *Physica A: Statistical Mechanics and its Applications 364* (2006), 423–434.

[20] Baumert, M., Walther, T., Hopfe, J., Stepan, H., Faber, R., and Voss, A. Joint symbolic dynamic analysis of beat-to-beat interactions of heart rate and systolic blood pressure in normal pregnancy. *Medical and Biological Engineering and Computing 40*, 2 (2002), 241–245.

[21] Bendat, J. S., and Piersol, A. G. *Random Data: Analysis and Measurement Procedures*. John Wiley & Sons, 2010.

[22] Bernardi, L., Keller, F., Sanders, M., Reddy, P., Griffith, B., Meno, F., and Pinsky, M. R. Respiratory sinus arrhythmia in the denervated human heart. *Journal of Applied Physiology 67*, 4 (1989), 1447–1455.

[23] Bernardi, L., Porta, C., Gabutti, A., Spicuzza, L., and Sleight, P. Modulatory effects of respiration. *Autonomic Neuroscience 90*, 1 (2001), 47–56.

[24] Bernardi, L., Wdowczyk-Szulc, J., Valenti, C., Castoldi, S., Passino, C., Spadacini, G., and Sleight, P. Effects of controlled breathing, mental activity and mental stress with or without verbalization on heart rate variability. *Journal of the American College of Cardiology 35*, 6 (2000), 1462–1469.

[25] Berntson, G., Cacioppo, J., and Quigley, K. Respiratory sinus arrhythmia: Autonomic origins, physiological mechanisms, and psychophysiological implications. *Psychophysiology 30*, 2 (1993), 183–196.

[26] Berntson, G. G., Bigger Jr, J. T., Eckberg, D. L., Grossman, P., Kaufmann, P. G., Malik, M., Nagaraja, H. N., Porges, S. W., Saul, J. P., Stone, P. H., and Van Der Molen, M. W. Heart rate variability: Origins, methods, and interpretive caveats. *Psychophysiology 34*, 6 (1997), 623–648.

[27] Bianchi, A., Scholz, U., Mainardi, L., Orlandini, P., Pozza, G., and Cerutti, S. Extraction of the respiration influence from the heart rate variability signal by means of lattice adaptive filter. In *Proc. of the 16th Annual International Conference of the IEEE Engineering in Medicine and Biology Society* (1994), pp. 121–122.

[28] Boyle, J., Bidargaddi, N., Sarela, A., and Karunanithi, M. Automatic detection of respiration rate from ambulatory single-lead ECG. *IEEE Transactions on Information Technology in Biomedicine 13*, 6 (2009), 890–896.

[29] Brown, R. P., and Gerbarg, P. L. Sudarshan Kriya yogic breathing in the treatment of stress, anxiety, and depression: part I-neurophysiologic model. *Journal of Alternative and Complementary Medicine 11*, 1 (2005), 189–201.

[30] Brown, T. E., Beightol, L. A., Koh, J., and Eckberg, D. L. Important influence of respiration on human RR interval power spectra is largely ignored. *Journal of Applied Physiology 75*, 5 (1993), 2310–2317.

[31] Caicedo, A., Naulaers, G., and Van Huffel, S. Preprocessing by means of subspace projections for continuous cerebral autoregulation assessment using NIRS. In *Proc. of the 35th Annual International Conference of the IEEE Engineering in Medicine and Biology Society* (2013), pp. 2032–2035.

[32] Caicedo, A., Tachtsidis, I., Papademetriou, M., and Van Huffel, S. Decoupling the influence of systemic variables in the peripheral and cerebral haemodynamics during ECMO procedure by means of oblique and orthogonal subspace projections. In *Proc. of the 34th Annual International Conference of the IEEE Engineering in Medicine and Biology Society* (2012), pp. 6153–6156.

[33] Caicedo, A., Varon, C., and Van Huffel, S. Analysis of non-linear respiratory influences on sleep apnea classification. In *Proc. of the 41st Annual Computing in Cardiology* (2014), pp. 593–596.

[34] Cappo, B. M., and Holmes, D. S. The utility of prolonged respiratory exhalation for reducing physiological and psychological arousal in non-threatening and threatening situations. *Journal of Psychosomatic Research 28*, 4 (1984), 265–273.

[35] Carrington, P., Collings Jr, G. H., Benson, H., Robinson, H., Wood, L. W., Lehrer, P. M., Woolfolk, R. L., and Cole, J. W. The use of meditation-relaxation techniques for the management of stress in a working population. *Journal of Occupational and Environmental Medicine 22*, 4 (1980), 221–231.

[36] Chandola, T., Britton, A., Brunner, E., Hemingway, H., Malik, M., Kumari, M., Badrick, E., Kivimaki, M., and Marmot, M. Work stress and coronary heart disease: what are the mechanisms? *European Heart Journal 29*, 5 (2008), 640–648.

[37] Choi, J., and Gutierrez-Osuna, R. Removal of respiratory influences from heart rate variability in stress monitoring. *IEEE Sensors Journal 11*, 11 (2011), 2649–2656.

[38] Chrousos, G., and Gold, P. The concepts of stress and stress system disorders: overview of physical and behavioral homeostasis. *Journal of the American Medical Association 267*, 9 (1992), 1244–1252.

[39] Clark, M., and Hirschman, R. Effects of paced respiration on anxiety reduction in a clinical population. *Biofeedback and Self-regulation 15*, 3 (1990), 273–284.

[40] Cysarz, D., Zerm, R., Bettermann, H., Frühwirth, M., Moser, M., and Kröz, M. Comparison of respiratory rates derived from heart rate variability, ECG amplitude, and nasal/oral airflow. *Annals of Biomedical Engineering 36*, 12 (2008), 2085–2094.

[41] De Chazal, P., Heneghan, C., Sheridan, E., Reilly, R., Nolan, P., and O'Malley, M. Automated processing of the single-lead electrocardiogram for the detection of obstructive sleep apnoea. *IEEE Transactions on Biomedical Engineering 50*, 6 (2003), 686–696.

[42] De Cooman, T., Goovaerts, G., Varon, C., Widjaja, D., and Van Huffel, S. Heart beat detection in multimodal data using signal recognition and beat location estimation. In *Proc. of the 41th Annual Computing in Cardiology* (2014), pp. 257–260.

[43] Denver, J. W., Reed, S. F., and Porges, S. W. Methodological issues in the quantification of respiratory sinus arrhythmia. *Biological Psychology 74*, 2 (2007), 286–294.

[44] Dickerson, S. S., and Kemeny, M. E. Acute stressors and cortisol responses: a theoretical integration and synthesis of laboratory research. *Psychological Bulletin 130*, 3 (2004), 355–391.

[45] Dimsdale, J. E. Psychological stress and cardiovascular disease. *Journal of the American College of Cardiology 51*, 13 (2008), 1237–1246.

[46] Eckberg, D. Point: Counterpoint: Respiratory sinus arrhythmia is due to a central mechanism vs. respiratory sinus arrhythmia is due to the baroreflex mechanism. *Journal of Applied Physiology 106*, 5 (2009), 1740–1742.

[47] Eckberg, D. L. Sympathovagal balance: a critical appraisal. *Circulation 96*, 9 (1997), 3224–3232.

[48] Eckberg, D. L. The human respiratory gate. *The Journal of Physiology 548*, 2 (2003), 339–352.

[49] Egizio, V. B., Eddy, M., Robinson, M., and Jennings, J. R. Efficient and cost-effective estimation of the influence of respiratory variables on respiratory sinus arrhythmia. *Psychophysiology 48*, 4 (2011), 488–494.

[50] European Agency for Safety and Health at Work. Calculating the costs of work-related stress and psychosocial risks. Tech. rep., June 2014.

[51] European Commission. Commission asks workers and employers what action should be taken to combat musculoskeletal disorders, November 2004. IP/04/1358, Brussels.

[52] Eykens, H., Widjaja, D., Vanderperren, K., Taelman, J., Braeken, M. A. K. A., Otte, R. A., Van den Bergh, B. R. H., and Van Huffel, S. Phase-rectified signal averaging for the quantification of the influence of prenatal anxiety on heart rate variability of babies. In *Proc. of the International Conference on Bio-inspired Systems and Signal Processing* (2012), pp. 163–168.

[53] Faes, L., Marinazzo, D., Montalto, A., and Nollo, G. Lag-specific transfer entropy as a tool to assess cardiovascular and cardiorespiratory information transfer. *IEEE Transactions on Biomedical Engineering 61*, 10 (2014), 2556–2568.

[54] Faes, L., Montalto, A., Nollo, G., and Marinazzo, D. Information decomposition of short-term cardiovascular and cardiorespiratory variability. In *Proc. of the 40th Annual Computing in Cardiology* (2013), pp. 113–116.

[55] Faes, L., and Nollo, G. Extended causal modeling to assess partial directed coherence in multiple time series with significant instantaneous interactions. *Biological Cybernetics 103*, 5 (2010), 387–400.

[56] Faes, L., Nollo, G., and Chon, K. H. Assessment of Granger causality by nonlinear model identification: application to short-term cardiovascular variability. *Annals of Biomedical Engineering 36*, 3 (2008), 381–395.

[57] Faes, L., Nollo, G., Jurysta, F., and Marinazzo, D. Information dynamics of brain–heart physiological networks during sleep. *New Journal of Physics 16*, 10 (2014), 105005.

[58] Faes, L., Nollo, G., and Porta, A. Information-based detection of nonlinear Granger causality in multivariate processes via a nonuniform embedding technique. *Physical Review E 83* (2011), 051112.

[59] Faes, L., Nollo, G., and Porta, A. Information domain approach to the investigation of cardio-vascular, cardio-pulmonary, and vasculo-pulmonary causal couplings. *Frontiers in Physiology 2* (2011), 80.

[60] Faes, L., Nollo, G., and Porta, A. Non-uniform multivariate embedding to assess the information transfer in cardiovascular and cardiorespiratory variability series. *Computers in Biology and Medicine 42*, 3 (2012), 290–297.

[61] Faes, L., Porta, A., and Nollo, G. Information decomposition in bivariate systems: Theory and application to cardiorespiratory dynamics. *Entropy 17*, 1 (2015), 277–303.

[62] Faes, L., Widjaja, D., Van Huffel, S., and Nollo, G. Investigating cardiac and respiratory determinants of heart rate variability in an information-theoretic framework. In *Proc. of the 36th Annual International Conference of the IEEE Engineering in Medicine and Biology Society* (2014), pp. 6020–6023.

[63] Friedman, B. H., and Thayer, J. F. Anxiety and autonomic flexibility: a cardiovascular approach. *Biological Psychology 47*, 3 (1998), 243–263.

[64] Friedman, B. H., and Thayer, J. F. Autonomic balance revisited: panic anxiety and heart rate variability. *Journal of Psychosomatic Research 44*, 1 (1998), 133–151.

[65] Furman, G., Shinar, Z., Baharav, A., and Akselrod, S. Electrocardiogram derived respiration during sleep. In *Proc. of the 32nd Annual Computers in Cardiology* (2005), pp. 351–354.

[66] García-González, M., Vázquez-Seisdedos, C., and Pallàs-Areny, R. Variations in breathing patterns increase low frequency contents in HRV spectra. *Physiological Measurement 21*, 3 (2000), 417–423.

[67] Giardino, N., Glenny, R., Borson, S., and Chan, L. Respiratory sinus arrhythmia is associated with efficiency of pulmonary gas exchange in healthy humans. *American Journal of Physiology - Heart and Circulatory Physiology 284*, 5 (2003), H1585–H1591.

[68] Goldberger, A. L., Amaral, L. A. N., Glass, L., Hausdorff, J. M., Ivanov, P. C., Mark, R. G., Mietus, J. E., Moody, G. B.,

Peng, C.-K., and Stanley, H. E. Physiobank, physiotoolkit, and physionet: Components of a new research resource for complex physiologic signals. *Circulation 101*, 23 (2000), e215–e220.

[69] Grippo, A. J., and Johnson, A. K. Stress, depression and cardiovascular dysregulation: A review of neurobiological mechanisms and the integration of research from preclinical disease models: Review. *Stress 12*, 1 (2009), 1–21.

[70] Grossman, P., Beek, J. v., and Wientjes, C. A comparison of three quantification methods for estimation of respiratory sinus arrhythmia. *Psychophysiology 27*, 6 (1990), 702–714.

[71] Grossman, P., Karemaker, J., and Wieling, W. Prediction of tonic parasympathetic cardiac control using respiratory sinus arrhythmia: the need for respiratory control. *Psychophysiology 28*, 2 (1991), 201–216.

[72] Grossman, P., Spoerle, M., and Wilhelm, F. H. Reliability of respiratory tidal volume estimation by means of ambulatory inductive plethysmography. *Biomedical Sciences Instrumentation 42* (2006), 193–198.

[73] Grossman, P., and Taylor, E. W. Toward understanding respiratory sinus arrhythmia: Relations to cardiac vagal tone, evolution and biobehavioral functions. *Biological Psychology 74*, 2 (2007), 263–285.

[74] Grossman, P., Wilhelm, F., and Spoerle, M. Respiratory sinus arrhythmia, cardiac vagal control, and daily activity. *American Journal of Physiology - Heart and Circulatory Physiology 287*, 2 (2004), H728–H734.

[75] Hallman, D. M., Olsson, E. M., Von Schéele, B., Melin, L., and Lyskov, E. Effects of heart rate variability biofeedback in subjects with stress-related chronic neck pain: A pilot study. *Applied Psychophysiology and Biofeedback 36*, 2 (2011), 71–80.

[76] Han, J., Stegen, K., Cauberghs, M., and Van de Woestijne, K. Influence of awareness of the recording of breathing on respiratory pattern in healthy humans. *European Respiratory Journal 10*, 1 (1997), 161–166.

[77] Harris, V. A., Katkin, E. S., Lick, J. R., and Habberfield, T. Paced respiration as a technique for the modification of autonomic response to stress. *Psychophysiology 13*, 5 (1976), 386–391.

[78] Hayano, J., Yasuma, F., Okada, A., Mukai, S., and Fujinami, T. Respiratory sinus arrhythmia: a phenomenon improving pulmonary gas exchange and circulatory efficiency. *Circulation 94*, 4 (1996), 842–847.

[79] Heidt, T., Sager, H. B., Courties, G., Dutta, P., Iwamoto, Y., Zaltsman, A., von zur Muhlen, C., Bode, C., Fricchione, G. L., Denninger, J., et al. Chronic variable stress activates hematopoietic stem cells. *Nature Medicine 20*, 7 (2014), 754–758.

[80] Hirsch, J., and Bishop, B. Respiratory sinus arrhythmia in humans: how breathing pattern modulates heart rate. *American Journal of Physiology - Heart and Circulatory Physiology 241*, 4 (1981), H620–H629.

[81] Hjortskov, N., Rissen, D., Blangsted, A., Fallentin, N., Lundberg, U., and Søgaard, K. The effect of mental stress on heart rate variability and blood pressure during computer work. *European Journal of Applied Physiology 92*, 1 (2004), 84–89.

[82] Hoyer, D., Leder, U., Hoyer, H., Pompe, B., Sommer, M., and Zwiener, U. Mutual information and phase dependencies: measures of reduced nonlinear cardiorespiratory interactions after myocardial infarction. *Medical Engineering & Physics 24*, 1 (2002), 33–43.

[83] http://captainwonder.com/wp-content/uploads/2012/05/circ system.jpg, Oct. 2014.

[84] http://www.edoctoronline.com/medical atlas.asp?, Oct. 2014.

[85] Hunt, C. The cardiorespiratory control hypothesis for sudden infant death syndrome. *Clinics in Perinatology 19*, 4 (1992), 757–771.

[86] Hyvarinen, A. Fast and robust fixed-point algorithms for independent component analysis. *IEEE Transactions on Neural Networks 10*, 3 (1999), 626–634.

[87] Imam, M., Karmakar, C., Khandoker, A., and Palaniswami, M. Effect of ECG-derived respiration (EDR) on modeling ventricular repolarization dynamics in different physiological and psychological conditions. *Medical and Biological Engineering and Computing 52*, 10 (2014), 851–860.

[88] Jamšek, J., Stefanovska, A., and McClintock, P. V. Nonlinear cardio-respiratory interactions revealed by time-phase bispectral analysis. *Physics in Medicine and Biology 49*, 18 (2004), 4407–4425.

[89] Joosen, P., Aerts, W., Varon, C., Widjaja, D., Vandeput, S., Aubert, A. E., and Van Huffel, S. Effect of posture on the cardiorespiratory system using canonical correlation analysis. In *Proc. of the 39th Annual Computing in Cardiology* (2012), pp. 269–272.

[90] Julien, C. The enigma of Mayer waves: facts and models. *Cardiovascular Research 70*, 1 (2006), 12–21.

[91] Kabir, M. M., Saint, D. A., Nalivaiko, E., Abbott, D., and Baumert, M. Time delay correction of the synchrogram for optimized detection of cardiorespiratory coordination. *Medical and Biological Engineering and Computing 49*, 11 (2011), 1249–1259.

[92] Kabir, M. M., Saint, D. A., Nalivaiko, E., Abbott, D., Voss, A., and Baumert, M. Quantification of cardiorespiratory interactions based on joint symbolic dynamics. *Annals of Biomedical Engineering 39*, 10 (2011), 2604–2614.

[93] Kantelhardt, J. W., Bauer, A., Schumann, A. Y., Barthel, P., Schneider, R., Malik, M., and Schmidt, G. Phase-rectified signal averaging for the detection of quasi-periodicities and the prediction of cardiovascular risk. *Chaos 17*, 1 (2007), 015112.

[94] Karemaker, J. Counterpoint: Respiratory sinus arrhythmia is due to the baroreflex mechanism. *Journal of Applied Physiology 106*, 5 (2009), 1742–1743.

[95] Katona, P., and Jih, F. Respiratory sinus arrhythmia: noninvasive measure of parasympathetic cardiac control. *Journal of Applied Physiology 39*, 5 (1975), 801–805.

[96] Katona, P., Poitras, J., Barnett, G., and Terry, B. Cardiac vagal efferent activity and heart period in the carotid sinus reflex. *American Journal of Physiology 218*, 4 (1970), 1030–1037.

[97] Kelsey, R. M., Blascovich, J., Leitten, C. L., Schneider, T. R., Tomaka, J., and Wiens, S. Cardiovascular reactivity and adaptation to recurrent psychological stress: The moderating effects of evaluative observation. *Psychophysiology 37*, 6 (2000), 748–756.

[98] Kivimäki, M., Leino-Arjas, P., Luukkonen, R., Riihimäki, H., Vahtera, J., and Kirjonen, J. Work stress and risk of cardiovascular mortality: prospective cohort study of industrial employees. *British Medical Journal 325*, 7369 (2002), 857.

[99] Kleiger, R. E., Miller, J. P., Bigger Jr, J. T., and Moss, A. J. Decreased heart rate variability and its association with increased mortality after acute myocardial infarction. *The American Journal of Cardiology 59*, 4 (1987), 256–262.

[100] Kollai, M., and Mizsei, G. Respiratory sinus arrhythmia is a limited measure of cardiac parasympathetic control in man. *The Journal of Physiology 424*, 1 (1990), 329–342.

[101] Kugiumtzis, D. Direct-coupling information measure from nonuniform embedding. *Physical Review E 87*, 6 (2013), 062918.

[102] Langley, P., Bowers, E. J., and Murray, A. Principal component analysis as a tool for analysing beat-to-beat changes in electrocardiogram features: Application to ECG-derived respiration. *IEEE Transactions on Biomedical Engineering 57*, 4 (2010), 821–829.

[103] Lázaro, J., Alcaine, A., Romero, D., Gil, E., Laguna, P., Pueyo, E., and Bailón, R. Electrocardiogram derived respiratory rate from QRS Slopes and R-wave angle. *Annals of Biomedical Engineering 42*, 10 (2014), 2072–2083.

[104] Lázaro, J., Gil, E., Bailón, R., Mincholé, A., and Laguna, P. Deriving respiration from photoplethysmographic pulse width. *Medical and Biological Engineering and Computing 51*, 1-2 (2013), 233–242.

[105] Lee, J., Nemati, S., Silva, I., Edwards, B. A., Butler, J. P., and Malhotra, A. Transfer entropy estimation and directional coupling change detection in biomedical time series. *BioMedical Engineering OnLine 11*, 1 (2012), 19.

[106] Lehrer, P. M., Vaschillo, E., and Vaschillo, B. Resonant frequency biofeedback training to increase cardiac variability: Rationale and manual for training. *Applied Psychophysiology and Biofeedback 25*, 3 (2000), 177–191.

[107] Lewis, G. F., Furman, S. A., McCool, M. F., and Porges, S. W. Statistical strategies to quantify respiratory sinus arrhythmia: Are commonly used metrics equivalent? *Biological Psychology 89*, 2 (2012), 349–364.

[108] Lizier, J. T., Prokopenko, M., and Zomaya, A. Y. Local measures of information storage in complex distributed computation. *Information Sciences 208* (2012), 39–54.

[109] Lotrič, M. B., and Stefanovska, A. Synchronization and modulation in the human cardiorespiratory system. *Physica A: Statistical Mechanics and its Applications 283*, 3 (2000), 451–461.

[110] Lucchini, M., Widjaja, D., Varon, C., Jansen, K., and Van Huffel, S. Phase-rectified signal averaging to evaluate ANS

development in premature infants. In *Proc. of the International Conference on Bio-inspired Systems and Signal Processing* (2013), pp. 203–208.

[111] Magagnin, V., Bassani, T., Bari, V., Turiel, M., Maestri, R., Pinna, G. D., and Porta, A. Non-stationarities significantly distort short-term spectral, symbolic and entropy heart rate variability indices. *Physiological Measurement 32*, 11 (2011), 1775–1786.

[112] Malliani, A., Pagani, M., Lombardi, F., and Cerutti, S. Cardiovascular neural regulation explored in the frequency domain. *Circulation 84*, 2 (1991), 482–492.

[113] Mansier, P., Clairambault, J., Charlotte, N., Médigue, C., Vermeiren, C., and LePape, G. C. Linear and non-linear analyses of heart rate variability: a minireview. *Cardiovascular Research 31*, 3 (1996), 371–379.

[114] Marinazzo, D., Pellicoro, M., and Stramaglia, S. Nonlinear parametric model for Granger causality of time series. *Physical Review E 73*, 6 (2006), 066216.

[115] Masaoka, Y., and Homma, I. Anxiety and respiratory patterns: their relationship during mental stress and physical load. *International Journal of Psychophysiology 27*, 2 (1997), 153–159.

[116] Mason, C., and Tarassenko, L. Quantitative assessment of respiratory derivation algorithms. In *Proc. of the 23rd Annual International Conference of the IEEE Engineering in Medicine and Biology Society* (2001), pp. 1998–2001.

[117] Matic, V., Perumpillichira, J. C., Widjaja, D., Jansen, K., Naulaers, G., Van Huffel, S., and De Vos, M. Heart rate variability in newborns with hypoxic brain injury. *Advances in Experimental Medicine and Biology 789* (2013), 43–48.

[118] Mazzanti, B., Lamberti, C., and de Bie, J. Validation of an ECG-derived respiration monitoring method. In *Proc. of the 30th Computers in Cardiology* (2003), pp. 613–616.

[119] Mendez, M., Corthout, J., Van Huffel, S., Matteucci, M., Penzel, T., Cerutti, S., and Bianchi, A. Automatic screening of obstructive sleep apnea from the ECG based on empirical mode decomposition and wavelet analysis. *Physiological Measurement 31*, 3 (2010), 273–289.

[120] Merri, M., Farden, D. C., Mottley, J. G., and Titlebaum, E. L. Sampling frequency of the electrocardiogram for spectral analysis of the heart rate variability. *IEEE Transactions on Biomedical Engineering 37*, 1 (1990), 99–106.

[121] Meste, O., Khaddoumi, B., Blain, G., and Bermon, S. Time-varying analysis methods and models for the respiratory and cardiac system coupling in graded exercise. *IEEE Transactions on Biomedical Engineering 52*, 11 (2005), 1921–1930.

[122] Mika, S., Schölkopf, B., Smola, A., Müller, K., Scholz, M., and Rätsch, G. Kernel PCA and de-noising in feature spaces. *Advances in Neural Information Processing Systems 11*, 1 (1999), 536–542.

[123] Milde, T., Schwab, K., Walther, M., Eiselt, M., Schelenz, C., Voss, A., and Witte, H. Time-variant partial directed coherence in analysis of the cardiovascular system. a methodological study. *Physiological Measurement 32*, 11 (2011), 1787–1805.

[124] Montalto, A., Faes, L., and Marinazzo, D. Mute: A matlab toolbox to compare established and novel estimators of the multivariate transfer entropy. *PLoS ONE 9*, 10 (2014), e109462.

[125] Moody, G., Mark, R., Bump, M., Weinstein, J., Berman, A., Mietus, J., and Goldberger, A. Clinical validation of the ECG-derived respiration (EDR) technique. In *Proc. of the 13th Annual Computers in Cardiology* (1986), pp. 507–510.

[126] Moody, G., Mark, R., Zoccola, A., and Mantero, S. Derivation of respiratory signals from multi-lead ECGs. In *Proc. of the 12th Annual Computers in Cardiology* (1985), pp. 113–116.

[127] Nichols, M., Townsend, N., Scarborough, P., and Rayner, M. Cardiovascular disease in europe 2014: epidemiological update. *European Heart Journal 35*, 42 (2014), 2950–2959.

[128] Noponen, K., Tiinanen, S., and Seppänen, T. Deriving respiration from the electrocardiogram by serial comparison with statistical mean shape. In *Proc. of the 39th Annual Computing in Cardiology* (2012), pp. 809–812.

[129] O'Brien, C., and Heneghan, C. A comparison of algorithms for estimation of a respiratory signal from the surface electrocardiogram. *Computers in Biology and Medicine 37*, 3 (2007), 305–314.

[130] Orini, M., Bailón, R., Laguna, P., Mainardi, L. T., and Barbieri, R. A multivariate time-frequency method to characterize the influence of respiration over heart period and arterial pressure. *EURASIP Journal on Advances in Signal Processing 2012*, 1 (2012), 1–17.

[131] Orini, M., Bailón, R., Mainardi, L., and Laguna, P. Synthesis of HRV signals characterized by predetermined time-frequency structure by means of time-varying ARMA models. *Biomedical Signal Processing and Control 7*, 2 (2012), 141–150.

[132] Orini, M., Bailón, R., Mainardi, L., Laguna, P., and Flandrin, P. Characterization of dynamic interactions between cardiovascular signals by time-frequency coherence. *IEEE Transactions on Biomedical Engineering 59*, 99 (2012), 663–673.

[133] Orini, M., Laguna, P., Mainardi, L., and Bailón, R. Assessment of the dynamic interactions between heart rate and arterial pressure by the cross time–frequency analysis. *Physiological Measurement 33*, 3 (2012), 315–331.

[134] Pagani, M., Mazzuero, G., Ferrari, A., Liberati, D., Cerutti, S., Vaitl, D., Tavazzi, L., and Malliani, A. Sympathovagal interaction during mental stress. a study using spectral analysis of heart rate variability in healthy control subjects and patients with a prior myocardial infarction. *Circulation 83*, 4 Suppl (1991), II43–51.

[135] Pallas-Areny, R., Colominas-Balague, J., and Rosell, F. The effect of respiration-induced heart movements on the ECG. *IEEE Transactions on Biomedical Engineering 36*, 6 (1989), 585–590.

[136] Pan, J., and Tompkins, W. A real-time QRS detection algorithm. *IEEE Transactions on Biomedical Engineering 32*, 3 (1985), 230–236.

[137] Patton, D. J., Triedman, J. K., Perrott, M. H., Vidian, A. A., and Saul, J. P. Baroreflex gain: characterization using autoregressive moving average analysis. *American Journal of Physiology - Heart and Circulatory Physiology 270*, 4 (1996), H1240–H1249.

[138] Pattyn, N., Migeotte, P.-F., Neyt, X., Van den Nest, A., and Cluydts, R. Comparing real-life and laboratory-induced stress reactivity on cardio-respiratory parameters: Differentiation of a tonic and a phasic component. *Physiology and Behavior 101*, 2 (2010), 218–223.

[139] Paul, G., Elam, B., and Verhulst, S. J. A longitudinal study of students' perceptions of using deep breathing meditation to reduce testing stresses. *Teaching and Learning in Medicine 19*, 3 (2007), 287–292.

[140] Penzel, T., Kantelhardt, J. W., Grote, L., Peter, J.-H., and Bunde, A. Comparison of detrended fluctuation analysis and spectral analysis for heart rate variability in sleep and sleep apnea. *IEEE Transactions on Biomedical Engineering 50*, 10 (2003), 1143–1151.

[141] Petersen, O. H. *Lecture Notes: Human Physiology.* Lecture Notes Series - Blackwell Scientific Publications. Wiley, 2006.

[142] Piepoli, M., Sleight, P., Leuzzi, S., Valle, F., Spadacini, G., Passino, C., Johnston, J., and Bernardi, L. Origin of respiratory sinus arrhythmia in conscious humans: an important role for arterial carotid baroreceptors. *Circulation 95*, 7 (1997), 1813–1821.

[143] Pompe, B., Blidh, P., Hoyer, D., and Eiselt, M. Using mutual information to measure coupling in the cardiorespiratory system. *IEEE Engineering in Medicine and Biology Magazine 17*, 6 (1998), 32–39.

[144] Porges, S. Cardiac vagal tone: a physiological index of stress. *Neuroscience and Biobehavioral Reviews 19*, 2 (1995), 225–233.

[145] Porges, S. W. The polyvagal perspective. *Biological Psychology 74*, 2 (2007), 116–143.

[146] Porta, A., Baselli, G., Lombardi, F., Montano, N., Malliani, A., and Cerutti, S. Conditional entropy approach for the evaluation of the coupling strength. *Biological Cybernetics 81*, 2 (1999), 119–129.

[147] Porta, A., Baselli, G., Rimoldi, O., Malliani, A., and Pagani, M. Assessing baroreflex gain from spontaneous variability in conscious dogs: role of causality and respiration. *American Journal of Physiology - Heart and Circulatory Physiology 279*, 5 (2000), H2558–H2567.

[148] Porta, A., Bassani, T., Bari, V., Pinna, G. D., Maestri, R., and Guzzetti, S. Accounting for respiration is necessary to reliably infer Granger causality from cardiovascular variability series. *IEEE Transactions on Biomedical Engineering 59*, 3 (2012), 832–841.

[149] Porta, A., Bassani, T., Bari, V., Tobaldini, E., Takahashi, A., Catai, A. M., and Montano, N. Model-based assessment of baroreflex and cardiopulmonary couplings during graded head-up tilt. *Computers in Biology and Medicine 42*, 3 (2012), 298–305.

[150] Porta, A., and Faes, L. Assessing causality in brain dynamics and cardiovascular control. *Philosophical Transactions of the Royal Society A: Mathematical, Physical and Engineering Sciences 371*, 1997 (2013), 20120517.

[151] Porta, A., Guzzetti, S., Montano, N., Pagani, M., Somers, V., Malliani, A., Baselli, G., and Cerutti, S. Information domain analysis of cardiovascular variability signals: evaluation of regularity, synchronisation and co-ordination. *Medical and Biological Engineering and Computing 38*, 2 (2000), 180–188.

[152] Reyes del Paso, G. A., Langewitz, W., Mulder, L. J., Roon, A., and Duschek, S. The utility of low frequency heart rate variability as an index of sympathetic cardiac tone: a review with emphasis on a reanalysis of previous studies. *Psychophysiology 50*, 5 (2013), 477–487.

[153] Ritz, T. Studying noninvasive indices of vagal control: The need for respiratory control and the problem of target specificity. *Biological Psychology 80*, 2 (2009), 158–168.

[154] Ritz, T., and Dahme, B. Implementation and interpretation of respiratory sinus arrhythmia measures in psychosomatic medicine: Practice against better evidence? *Psychosomatic Medicine 68*, 4 (2006), 617–627.

[155] Ritz, T., Thöns, M., and Dahme, B. Modulation of respiratory sinus arrhythmia by respiration rate and volume: stability across posture and volume variations. *Psychophysiology 38*, 5 (2001), 858–862.

[156] Rosch, P. J. The quandary of job stress compensation. *Health and Stress 3* (2001), 1–4.

[157] Rosenblum, M., Pikovsky, A., Kurths, J., Schäfer, C., and Tass, P. A. Phase synchronization: from theory to data analysis. *Handbook of Biological Physics 4* (2001), 279–321.

[158] Rosenblum, M. G., Cimponeriu, L., Bezerianos, A., Patzak, A., and Mrowka, R. Identification of coupling direction: application to cardiorespiratory interaction. *Physical Review E 65*, 4 (2002), 041909.

[159] Rosengren, A., Hawken, S., Ôunpuu, S., Sliwa, K., Zubaid, M., Almahmeed, W. A., Blackett, K. N., Sitthi-amorn, C., Sato, H., and Yusuf, S. Association of psychosocial risk factors with risk of acute myocardial infarction in 11 119 cases and 13 648 controls from 52 countries (the interheart study): case-control study. *The Lancet 364*, 9438 (2004), 953–962.

[160] Saul, J., Berger, R., Chen, M., and Cohen, R. Transfer function analysis of autonomic regulation. II. Respiratory sinus arrhythmia. *American Journal of Physiology - Heart and Circulatory Physiology 256*, 1 (1989), H153–H161.

[161] Schäfer, C., Rosenblum, M. G., Abel, H.-H., and Kurths, J. Synchronization in the human cardiorespiratory system. *Physical Review E 60*, 1 (1999), 857–870.

[162] Schleifer, L. M., Ley, R., and Spalding, T. W. A hyperventilation theory of job stress and musculoskeletal disorders. *American Journal of Industrial Medicine 41*, 5 (2002), 420–432.

[163] Schölkopf, B., Smola, A., and Müller, K. R. Nonlinear component analysis as a kernel eigenvalue problem. *Neural Computation 10*, 5 (1998), 1299–1319.

[164] Schreiber, T. Measuring information transfer. *Physical Review Letters 85*, 2 (2000), 461–464.

[165] Schulz, S., Adochiei, F.-C., Edu, I.-R., Schroeder, R., Costin, H., Bär, K.-J., and Voss, A. Cardiovascular and cardiorespiratory coupling analyses: a review. *Philosophical Transactions of the Royal Society A: Mathematical, Physical and Engineering Sciences 371*, 1997 (2013), 20120191.

[166] Schumacher, A. Linear and nonlinear approaches to the analysis of RR interval variability. *Biological Research for Nursing 5*, 3 (2004), 211–221.

[167] Schumann, A. Y., Kantelhardt, J. W., Bauer, A., and Schmidt, G. Bivariate phase-rectified signal averaging. *Physica A: Statistical Mechanics and its Applications 387*, 21 (2008), 5091–5100.

[168] Seidel, H., and Herzel, H. Modelling heart rate variability due to respiration and baroreflex. In *Modelling the Dynamics of Biological Systems*. Springer, 1995, pp. 205–229.

[169] Sharma, H., Sharma, K. K., and Bhagat, O. L. Respiratory rate extraction from single-lead ecg using homomorphic filtering. *Computers in Biology and Medicine 59* (2015), 80–86.

[170] Silverthorn, D., Johnson, B., Ober, W., Garrison, C., and Silverthorn, A. *Human Physiology: An Integrated Approach*. Pearson Education, 2013.

[171] Singh, D., Vinod, K., and Saxena, S. C. Sampling frequency of the RR interval time series for spectral analysis of heart rate variability. *Journal of Medical Engineering and Technology 28*, 6 (2004), 263–272.

[172] Sloan, R., Shapiro, P., Bagiella, E., Boni, S., Paik, M., Bigger Jr., J., Steinman, R., and Gorman, J. Effect of mental stress

throughout the day on cardiac autonomic control. *Biological Psychology 37*, 2 (1994), 89–99.

[173] Soufer, R., Jain, H., and Yoon, A. J. Heart-brain interactions in mental stress-induced myocardial ischemia. *Current Cardiology Reports 11*, 2 (2009), 133–140.

[174] Speca, M., Carlson, L. E., Goodey, E., and Angen, M. A randomized, wait-list controlled clinical trial: the effect of a mindfulness meditation-based stress reduction program on mood and symptoms of stress in cancer outpatients. *Psychosomatic Medicine 62*, 5 (2000), 613–622.

[175] Stefanovska, A. Cardiorespiratory interactions. *Nonlinear Phenomena in Complex Systems 5*, 4 (2002), 462–469.

[176] Stein, P., and Kleiger, R. Insights from the study of heart rate variability. *Annual Review of Medicine 50* (1998), 249–261.

[177] Strauss-Blasche, G., Moser, M., Voica, M., McLeod, D., Klammer, N., and Marktl, W. Relative timing of inspiration and expiration affects respiratory sinus arrhythmia. *Clinical and Experimental Pharmacology and Physiology 27*, 8 (2000), 601–606.

[178] Suess, W. M., Alexander, A. B., Smith, D. D., Sweeney, H. W., and Marion, R. J. The effects of psychological stress on respiration: a preliminary study of anxiety and hyperventilation. *Psychophysiology 17*, 6 (1980), 535–540.

[179] Suykens, J. A. K., Van Gestel, T., De Brabanter, J., De Moor, B., and Vandewalle, J. *Least squares support vector machines*. World Scientific Pub. Co., Singapore, 2002.

[180] Taelman, J., Vandeput, S., Vlemincx, E., Spaepen, A., and Van Huffel, S. Instantaneous changes in heart rate regulation due to mental load in simulated office work. *European Journal of Applied Physiology 111*, 7 (2011), 1497–1505.

[181] Tarvainen, M. P., Ranta-aho, P. O., and Karjalainen, P. A. An advanced detrending method with application to HRV analysis. *IEEE Transactions on Biomedical Engineering 49*, 2 (2002), 172–175.

[182] Task Force of The European Society of Cardiology and The North American Society of Pacing and Electrophysiology. Heart rate variability: Standards of measurement, physiological interpretation, and clinical use. *European Heart Journal 17*, 3 (1996), 354–381.

[183] Thayer, J. F., Åhs, F., Fredrikson, M., Sollers III, J. J., and Wager, T. D. A meta-analysis of heart rate variability and neuroimaging studies: implications for heart rate variability as a marker of stress and health. *Neuroscience and Biobehavioral Reviews 36*, 2 (2012), 747–756.

[184] Thayer, J. F., and Lane, R. D. Claude bernard and the heart–brain connection: Further elaboration of a model of neurovisceral integration. *Neuroscience and Biobehavioral Reviews 33*, 2 (2009), 81–88.

[185] Thayer, J. F., Yamamoto, S. S., and Brosschot, J. F. The relationship of autonomic imbalance, heart rate variability and cardiovascular disease risk factors. *International Journal of Cardiology 141*, 2 (2010), 122–131.

[186] Tiinanen, S., Kiviniemi, A., Tulppo, M., and Seppänen, T. RSA component extraction from cardiovascular signals by combining adaptive filtering and PCA derived respiration. In *Proc. of the 37th Annual Computing in Cardiology* (2010), pp. 73–76.

[187] Tiinanen, S., Tulppo, M., and Seppanen, T. Reducing the effect of respiration in baroreflex sensitivity estimation with adaptive filtering. *IEEE Transactions on Biomedical Engineering 55*, 1 (2008), 51–59.

[188] Tiinanen, S., Tulppo, M., and Seppänen, T. RSA component extraction from heart rate signal by independent component analysis. In *Proc. of the 36th Annual Computers in Cardiology* (2009), pp. 161–164.

[189] Toledo, E., Akselrod, S., Pinhas, I., and Aravot, D. Does synchronization reflect a true interaction in the cardiorespiratory system? *Medical Engineering and Physics 24*, 1 (2002), 45–52.

[190] Vaishnav, S., Stevenson, R., Marchant, B., Lagi, K., Ranjadayalan, K., and Timmis, A. D. Relation between heart rate variability early after acute myocardial infarction and long-term mortality. *The American Journal of Cardiology 73*, 9 (1994), 653–657.

[191] Van Diest, I., Verstappen, K., Aubert, A. E., Widjaja, D., Vansteenwegen, D., and Vlemincx, E. Inhalation/exhalation ratio modulates the effect of slow breathing on heart rate variability and relaxation. *Applied Psychophysiology and Biofeedback 39*, 3–4 (2014), 171–180.

[192] Vandeput, S. *Heart rate variability: linear and nonlinear analysis with applications in human physiology.* PhD thesis, Faculty of Engineering, KU Leuven, 2010.

[193] Vandeput, S., Widjaja, D., Aubert, A. E., and Van Huffel, S. Adaptation of the autonomic heart rate regulation in astronauts after spaceflight. *Medical Science Monitor 19*, 1 (2013), 9–17.

[194] Vapnik, V. *The nature of statistical learning theory*. New York: Springer Verlag, 1995.

[195] Varon, C., Montalto, A., Jansen, K., Lagae, L., Marinazzo, D., Faes, L., and Van Huffel, S. Interictal cardiorespiratory variability in temporal lobe and absence epilepsy in childhood. In *Proc. of the 8th Conference of the European Study Group on Cardiovascular Oscillations* (2014), pp. 31–32.

[196] Varon, C., Testelmans, D., Buyse, B., Suykens, J. A., and Van Huffel, S. Sleep apnea classification using least-squares support vector machines on single lead ECG. In *Proc. of the 35th Annual International Conference of the IEEE Engineering in Medicine and Biology Society* (2013), pp. 5029–5032.

[197] Visnovcova, Z., Mestanik, M., Javorka, M., Mokra, D., Gala, M., Jurko, A., Calkovska, A., and Tonhajzerova, I. Complexity and time asymmetry of heart rate variability are altered in acute mental stress. *Physiological Measurement 35*, 7 (2014), 1319–1334.

[198] Vlemincx, E., Taelman, J., De Peuter, S., Van Diest, I., and Van den Bergh, O. Sigh rate and respiratory variability during mental load and sustained attention. *Psychophysiology 48*, 1 (2011), 117–120.

[199] Vlemincx, E., Vigo, D., Vansteenwegen, D., den Bergh, O. V., and Van Diest, I. Do not worry, be mindful: Effects of induced worry and mindfulness on respiratory variability in a nonanxious population. *International Journal of Psychophysiology 87*, 2 (2013), 147–151.

[200] Voss, A., Schulz, S., Schroeder, R., Baumert, M., and Caminal, P. Methods derived from nonlinear dynamics for analysing heart rate variability. *Philosophical Transactions of the Royal Society A: Mathematical, Physical and Engineering Sciences 367*, 1887 (2009), 277–296.

[201] Vrijkotte, T. G., van Doornen, L. J., and de Geus, E. J. Effects of work stress on ambulatory blood pressure, heart rate, and heart rate variability. *Hypertension 35*, 4 (2000), 880–886.

[202] Wibral, M., Lizier, J. T., Vögler, S., Priesemann, V., and Galuske, R. Local active information storage as a tool to understand distributed neural information processing. *Frontiers in Neuroinformatics 8*, 1 (2014).

[203] Widjaja, D., Caicedo, A., Vlemincx, E., Van Diest, I., and Van Huffel, S. Separation of respiratory influences from the tachogram: A methodological evaluation. *PLoS ONE 9*, 7 (2014), e101713.

[204] Widjaja, D., Faes, L., Montalto, A., Van Diest, I., Marinazzo, D., and Van Huffel, S. Information dynamics in cardiorespiratory analyses: Application to controlled breathing. In *Proc. of the 36th Annual International Conference of the IEEE Engineering in Medicine and Biology Society* (2014), pp. 6353–6356.

[205] Widjaja, D., Montalto, A., Vlemincx, E., Marinazzo, D., Faes, L., and Van Huffel, S. Information dynamics in cardiorespiratory time series during mental stress testing. In *Proc. of the 8th Conference of the European Study Group on Cardiovascular Oscillations* (2014), pp. 23–24.

[206] Widjaja, D., Montalto, A., Vlemincx, E., Marinazzo, D., Van Huffel, S., and Faes, L. Cardiorespiratory information dynamics during mental arithmetic and sustained attention. *PLoS ONE* (submitted).

[207] Widjaja, D., Orini, M., Vlemincx, E., and Van Huffel, S. Analysis of cardiorespiratory dynamics during mental stress using (partial) time-frequency spectra. In *Proc. of the 40th Annual Computing in Cardiology* (2013), pp. 105–108.

[208] Widjaja, D., Orini, M., Vlemincx, E., and Van Huffel, S. Cardiorespiratory dynamic response to mental stress: A multivariate time-frequency analysis. *Computational and Mathematical Methods in Medicine 2013* (2013), 451857.

[209] Widjaja, D., Taelman, J., Vandeput, S., Braeken, M. A., Otte, R. A., Van den Bergh, B. R., and Van Huffel, S. ECG-derived respiration: Comparison and new measures for respiratory variability. In *Proc. of the 37th Annual Computing in Cardiology* (2010), pp. 149–152.

[210] Widjaja, D., Van Diest, I., and Van Huffel, S. Extraction of direct respiratory influences from the tachogram using multiscale principal component analysis. In *Proc. of the 7th International Workshop on Biosignal Interpretation* (2012), pp. 299–302.

[211] Widjaja, D., Van Diest, I., and Van Huffel, S. Extraction of direct respiratory influences from the tachogram using multiscale principal component analysis. *International Journal of Bioelectromagnetism, Special Issue on Biosignal Processing and Interpretation II 15*, 1 (2013), 97–101.

[212] Widjaja, D., Vandeput, S., Taelman, J., Braeken, M. A., Otte, R. A., Van den Bergh, B. R. H., and Van Huffel, S. Accurate R

peak detection and advanced preprocessing of normal ECG for heart rate variability analysis. In *Proc. of the 37th Annual Computing in Cardiology* (2010), pp. 533–536.

[213] Widjaja, D., Vandeput, S., Van Huffel, S., and Aubert, A. E. Cardiovascular autonomic adaptation in lunar and martian gravity during parabolic flight. *European Journal of Applied Physiology* (2015), accepted.

[214] Widjaja, D., Varon, C., Caicedo Dorado, A., Suykens, J., and Van Huffel, S. Comparison of algorithms for single lead ECG-derived respiration. In *Proc. of the 10th Belgian day on Biomedical Engineering* (2011), p. 85.

[215] Widjaja, D., Varon, C., Caicedo Dorado, A., Suykens, J., and Van Huffel, S. Application of kernel principal component analysis for single lead ECG-derived respiration. *IEEE Transactions on Biomedical Engineering 59*, 4 (2012), 1169–1176.

[216] Widjaja, D., Varon, C., Testelmans, D., Buyse, B., Faes, L., and Van Huffel, S. Separating respiratory influences from the tachogram: methods and their sensitivity to the type of respiratory signal. In *Proc. of the 41st Annual Computing in Cardiology* (2014), pp. 609–612.

[217] Widjaja, D., Varon Perez, J., Caicedo Dorado, A., and Van Huffel, S. An improved ECG-derived respiration method using kernel principal component analysis. In *Proc. of the 38th Annual Computing in Cardiology* (2011), pp. 45–48.

[218] Widjaja, D., Vlemincx, E., and Van Huffel, S. Multiscale principal component analysis to separate respiratory influences from the tachogram: Application to stress monitoring. In *Proc. of the 39th Annual Computing in Cardiology* (2012), pp. 277–280.

[219] Widjaja, D., Vlemincx, E., and Van Huffel, S. Stress classification by separation of respiratory modulations in heart rate variability using orthogonal subspace projection. In *Proc. of the 35th Annual International Conference of the IEEE Engineering in Medicine and Biology Society* (2013), pp. 6123–6126.

[220] Willemen, T., Van Deun, D., Verhaert, V., Vandekerckhove, M., Exadaktylos, V., Verbraecken, J., Huffel, S., Haex, B., and Vander Sloten, J. An evaluation of cardio-respiratory and movement features with respect to sleep stage classification. *IEEE Journal of Biomedical and Health Informatics 18*, 2 (2013), 661–669.

[221] Willemsen, G., Ring, C., McKeever, S., and Carroll, D. Secretory immunoglobulin a and cardiovascular activity during mental arithmetic: effects of task difficulty and task order. *Biological Psychology 52*, 2 (2000), 127–141.

[222] World Health Organization. *Global status report on noncommunicable diseases 2010.* World Health Organization, 2011.

[223] Yasuma, F., and Hayano, J. Respiratory sinus arrhythmia: why does the heartbeat synchronize with respiratory rhythm? *Chest 125*, 2 (2004), 683–690.

[224] Yildiz, M., and Ider, Y. Model based and experimental investigation of respiratory effect on the HRV power spectrum. *Physiological Measurement 27*, 10 (2006), 973–988.

[225] Zhang, J., Yu, X., and Xie, D. Effects of mental tasks on the cardiorespiratory synchronization. *Respiratory Physiology and Neurobiology 170*, 1 (2010), 91–95.

[226] Zhao, L., Reisman, S., and Findley, T. Derivation of respiration from electrocardiogram during heart rate variability studies. In *Proc. of the 21st Annual Computers in Cardiology* (1994), pp. 53–56.

[227] Zucker, T. L., Samuelson, K. W., Muench, F., Greenberg, M. A., and Gevirtz, R. N. The effects of respiratory sinus arrhythmia biofeedback on heart rate variability and posttraumatic stress disorder symptoms: A pilot study. *Applied Psychophysiology and Biofeedback 34*, 2 (2009), 135–143.

Curriculum vitae

Devy Widjaja was born in Asse on September 17, 1986. She obtained her Bachelor degree in Electrical Engineering (minor Mechanical Engineering) at the KU Leuven in 2008. Next, she started a Master in Biomedical Engineering, option Biomedical Information Technology, at the KU Leuven and obtained her degree, magna cum laude, in July 2010. Her master thesis on the effect of stress on the cardiorespiratory system in pregnant women, was carried out under the supervision of Prof. dr. ir. Sabine Van Huffel.

Since September 2010, she has been working as a PhD researcher in STADIUS at the Department of Electrical Engineering (ESAT) of the KU Leuven under the supervision of Prof. dr. ir. Sabine Van Huffel, resulting in this thesis. She received a PhD grant from the Agency for Innovation by Science and Technology in Flanders (IWT Vlaanderen) in 2010. Her research interests include biomedical signal processing for cardiovascular and respiratory signals, with special attention to the interaction between cardiorespiratory signals in applications of mental stress and reduced gravity. She was nominated for several paper awards and was invited as keynote speaker at "Cardiology meets Physics and Mathematics" in March 2015, in Zakopane, Poland. In 2014, she was awarded the Amelia Earhart Fellowship by Zonta International.

Publication list

Papers in international journals

1. **Widjaja D**, Varon C, Caicedo Dorado A, Suykens JAK, Van Huffel S. Application of Kernel Principal Component Analysis for Signal Lead ECG-Derived Respiration. *IEEE Transactions on Biomedical Engineering*, vol. 59, no. 4, Apr. 2012, pp. 1169-1176. (Finalist of the best paper award at the IEEE-EMBS Benelux chapter 2013)

2. **Widjaja D**, Van Diest I, Van Huffel S. Extraction of Direct Respiratory Influences from the Tachogram using Multiscale Principal Component Analysis. *International Journal of Bioelectromagnetism, Special Issue on Biosignal Processing and Interpretation II*, vol. 15, no. 1, Jan. 2013, pp. 97-101.

3. Vandeput S, **Widjaja D**, Aubert AE, Van Huffel S. Adaptation of the Autonomic Heart Rate Regulation in Astronauts after Spaceflight. *Medical Science Monitor*, vol. 19, no. 1, Jan. 2013, pp. 9-17.

4. Matic V, Perumpillichira JC, **Widjaja D**, Jansen K, Naulaers G, Van Huffel S, De Vos M. Heart Rate Variability in Newborns with Hypoxic Brain Injury. *Advances in Experimental Medicine and Biology*, vol. 789, May 2013, pp. 43-48.

5. **Widjaja D**, Orini M, Vlemincx E, Van Huffel S. Cardiorespiratory Dynamic Response to Mental Stress: a Multivariate Time-Frequency Analysis. *Computational and Mathematical Methods in Medicine, Special Issue on New Trends on Noninvasive Assessment of Autonomic Nervous System through Signal Processing*, vol. 2013, Dec. 2013, pp. 1-12.

6. **Widjaja D**, Caicedo A, Vlemincx E, Van Diest I, Van Huffel S. Separation of Respiratory Influences from the Tachogram: a Methodological Evaluation. *PLoS ONE*, vol. 9, no. 7, Jul. 2014, pp. e101713.

7. Van Diest I, Verstappen K, Aubert AE, **Widjaja D**, Vansteenwegen D, Vlemincx E. Inhalation/exhalation Ratio modulates the Effect of Slow Breathing on Heart Rate Variability and Relaxation. *Applied Psychophysiology and Biofeedback*, vol. 39, no. 3-4, Dec. 2014, pp. 171-180.

8. **Widjaja D**, Vandeput S, Van Huffel S, Aubert AE. Cardiovascular Autonomic Adaptation in Lunar and Martian Gravity during Parabolic Flight. Accepted in *European Journal of Applied Physiology*, Jan. 2015.

Papers submitted to international journals

9. Braeken MAKA, Jones A, Otte RA, **Widjaja D**, Van Huffel S, Van den Bergh BRH. Anxious Women do not show the Expected Decrease in Cardiovascular Stress Responsiveness at the End of Pregnancy. To be revised for *Biological Psychology*.

10. **Widjaja D**, Montalto A, Vlemincx E, Marinazzo D, Faes L, Van Huffel S. Cardiorespiratory Information Dynamics during Mental Arithmetic and Sustained Attention. Submitted to *PLoS ONE*.

11. De Cooman T, Goovaerts G, Varon C, **Widjaja D**, Willemen T, Van Huffel S. Heart Beat Detection in Multimodal Data Using Automatic Signal Type Recognition. Submitted to *Physiological Measurement, focus issue on Detection of Heart Beats in Multimodal Data*.

Papers in proceedings of international conferences

12. **Widjaja D**, Taelman J, Vandeput S, Braeken MAKA, Otte RA, Van den Bergh BRH, Van Huffel S. ECG-Derived Respiration: Comparison and New Measures for Respiratory Variability, in *Proc. of the 37th Annual Computing in Cardiology (CinC 2010)*, Belfast, Northern Ireland, Sep. 2010, pp. 149-152.

13. **Widjaja D**, Vandeput S, Taelman J, Braeken MAKA, Otte RA, Van den Bergh BRH, Van Huffel S. Accurate R Peak Detection and Advanced Preprocessing of Normal ECG for Heart Rate Variability Analysis, in *Proc. of the 37th Annual Computing in Cardiology (CinC 2010)*, Belfast, Northern Ireland, Sep. 2010, pp. 533-536.

14. Taelman J, Vandeput S, **Widjaja D**, Braeken MAKA, Otte RA, Van den Bergh BRH, Van Huffel S. Stress during Pregnancy: Is the Autonomic

Nervous System influenced by Anxiety?, in *Proc. of the 37th Annual Computing in Cardiology (CinC 2010)*, Belfast, Northern Ireland, Sep. 2010, pp. 725-728.

15. **Widjaja D**, Varon C, Caicedo A, Van Huffel S. An improved ECG-Derived Respiration Method using Kernel Principal Component Analysis, in *Proc. of the 38th Annual Computing in Cardiology (CinC2011)*, Hangzhou, China, Sep. 2011, pp. 45-48.

16. Eykens H, **Widjaja D**, Vanderperren K, Taelman J, Braeken MAKA, Otte RA, Van den Bergh BRH, Van Huffel S. Phase-Rectified Signal Averaging for the Quantification of the Influence of Prenatal Anxiety on Heart Rate Variability of Babies, in *Proc. of the International Conference on Bio-inspired Systems and Signal Processing (BIOSIGNALS 2012)*, Vilamoura, Portugal, Feb. 2012, pp. 163-168.

17. Aerts W, Joosen P, **Widjaja D**, Varon C, Vandeput S, Van Huffel S, Aubert AE. Heart Rate and Blood Pressure Variability under Moon, Mars and Zero Gravity Conditions during Parabolic Flights, in *Proc. of the Joint Life Science Meeting 'Life in Space for Life on Earth'*, Aberdeen, United Kingdom, Jun. 2012, pp. 1-6.

18. **Widjaja D**, Van Diest I, Van Huffel S. Extraction of Direct Respiratory Influences from the Tachogram using Multiscale Principal Component Analysis, in *Proc. of the 7th International Workshop on Biosignal Interpretation (BSI2012)*, Como, Italy, Jul. 2012, pp. 299-302.

19. **Widjaja D**, Vlemincx E, Van Huffel S. Multiscale Principal Component Analysis to Separate Respiratory Influences from the Tachogram: Application to Stress Monitoring, in *Proc. of the 39th Annual Computing in Cardiology (CinC2012)*, Krakow, Poland, Sep. 2012, pp. 277-280.

20. Joosen P, Aerts W, Varon C, **Widjaja D**, Vandeput S, Aubert AE, Van Huffel S. Effect of Posture on the Cardiorespiratory System using Canonical Correlation Analysis, in *Proc. of the 39th Annual Computing in Cardiology (CinC2012)*, Krakow, Poland, Sep. 2012, pp. 269-272.

21. Lucchini M, **Widjaja D**, Varon C, Jansen K, Van Huffel S. Phase-Rectified Signal Averaging to Evaluate ANS Development in Premature Infants, in *Proc. of the International Conference on Bio-inspired Systems and Signal Processing (BIOSIGNALS 2013)*, Barcelona, Spain, Feb. 2013, pp. 203-208.

22. **Widjaja D**, Vlemincx E, Van Huffel S. Stress Classification by Separation of Respiratory Modulations in Heart Rate Variability using Orthogonal

Subspace Projection, in *Proc. of the 35th Annual International Conference of the IEEE Engineering in Medicine and Biology Society (EMBC 2013)*, Osaka, Japan, Jul. 2013, pp. 6123-6126. (Finalist of the IEEE-EMBC 2013 student paper competition)

23. **Widjaja D**, Orini M, Vlemincx E, Van Huffel S. Analysis of Cardio-Respiratory Dynamics during Mental Stress using (Partial) Time-Frequency Spectra, in *Proc. of the 40th Annual Computing in Cardiology (CinC2013)*, Zaragoza, Spain, Sep. 2013, pp. 105-108.

24. **Widjaja D**, Montalto A, Vlemincx E, Marinazzo D, Faes L, Van Huffel S. Information Dynamics in Cardiorespiratory Time Series during Mental Stress Testing, in *Proc. of the 8the Conference of the European Study Group on Cardiovascular Oscillations (ESGCO 2014)*, Trento, Italy, May 2014, pp. 23-24.

25. **Widjaja D**, Faes L, Montalto A, Van Diest I, Marinazzo D, Van Huffel S. Information Dynamics in Cardiorespiratory Analyses: Application to Controlled Breathing', in *Proc. of the 36th Annual International Conference of the IEEE Engineering in Medicine and Biology Society (EMBC 2014)*, Chicago, USA, Aug. 2014, pp. 6353-6356.

26. Faes L, **Widjaja D**, Van Huffel S, Nollo G. Investigating Cardiac and Respiratory Determinants of Heart Rate Variability in an Information-Theoretic Framework, in *Proc. of the 36th Annual International Conference of the IEEE Engineering in Medicine and Biology Society (EMBC 2014)*, Chicago, USA, Aug. 2014, pp. 6020-6023.

27. **Widjaja D**, Varon C, Testelmans D, Buyse B, Faes L, Van Huffel S. Separating Respiratory Influences from the Tachogram: Methods and their Sensitivity to the Type of Respiratory Signal, in *Proc. of the 41th Annual Computing in Cardiology (CinC2014)*, Cambridge, USA, Sep. 2014, pp. 609-612.

28. De Cooman T, Goovaerts G, Varon C, **Widjaja D**, Van Huffel S. Heart Beat Detection in Multimodal Data Using Signal Recognition and Beat Location Estimation, in *Proc. of the 41th Annual Computing in Cardiology (CinC2014)*, Cambridge, USA, Sep. 2014, pp. 257-260. (Winner in phase II and third in phase III, of the CinC Challenge 2014)

Abstracts in proceedings of (inter)national conferences

29. Braeken MAKA, Otte RA, **Widjaja D**, Vandeput S, Taelman S, Van Huffel S, Van den Bergh BRH. Mental Stress and Heart Rate Variability during the First Pregnancy Trimester, in *Developmental Psychobiology*, vol. 52, no. 7, Nov. 2010, p. 695.

30. **Widjaja D**, Taelman J, Vandeput S, Braeken MAKA, Otte RA, Van den Bergh BRH, Van Huffel S. Influence of Stress and Anxiety on the Autonomic Nervous System during Pregnancy, in *Proc. of the 9th Belgian Day on Biomedical Engineering*, Brussels, Belgium, Nov. 2010, p. 93.

31. **Widjaja D**, Varon C, Caicedo Dorado A, Van Huffel S. Comparison of Algorithms for Single Lead ECG-Derived Respiration, in *Proc. of the 10th Belgian Day on Biomedical Engineering*, Brussels, Belgium, Dec. 2011, p. 85.

32. **Widjaja D**, Vandeput S, Van Huffel S, Aubert AE. Gravity effects on heart rate variability during partial G-parabolic flights, in *Proc. of 19th IAA Humans in Space Symposium (HIS2013)*, Cologne, Germany, Jul. 2013.

33. **Widjaja D**, Vlemincx E, Van Diest I, Van Huffel S. Separation of Respiratory Modulations from the Tachogram for the Classification of Mindfulness, in *Proc. of International Society for the Advancement of Respiratory Psychophysiology Meeting 2013 (ISARP2013)*, Leuven, Belgium, Sep. 2013.

34. **Widjaja D**, Vandeput S, Bersenev E, Van Huffel S, Aubert AE. Alterations in Autonomic Cardiovascular Control elicited during Parabolic Flight in the Mars500 Crew', in *Proc. of the XIVth Conference on Space Biology and Aerospace Medicine*, Moscow, Russia, Oct. 2013.

35. **Widjaja D**, Vandeput S, Van Huffel S, Aubert AE. Autonomic Cardiovascular Adaptation during Parabolic Flight in the Mars500 Crew, in *Proc. of the 13th Belgian Day on Biomedical Engineering*, Brussels, Belgium, Nov. 2014.

36. De Cooman T, Goovaerts G, Varon C, **Widjaja D**, Van Huffel S. Heart Beat Detection in Multimodal Data Using Signal Recognition and Beat Location Estimation, in *Proc. of the 13th Belgian Day on Biomedical Engineering*, Brussels, Belgium, Nov. 2014.



FACULTY OF ENGINEERING SCIENCE
DEPARTMENT OF ELECTRICAL ENGINEERING
STADIUS CENTER FOR DYNAMICAL SYSTEMS, SIGNAL PROCESSING AND DATA ANALYTICS
Kasteelpark Arenberg 10, box 2446
B-3001 Heverlee
devy.widjaja@esat.kuleuven.be